LIVE-LOAD MODELS FOR DESIGN AND FATIGUE

EVALUATION OF HIGHWAY BRIDGES

by

JOSEPH C. DAVIS

A Dissertation submitted to the

Graduate School-New Brunswick

Rutgers, The State University of New Jersey

in partial fulfillment of the requirements

for the degree of

Doctor of Philosophy

Graduate Program in Civil and Environmental Engineering

written under the direction of

Dr. Hani H. Nassif

and approved by

‒‒‒‒‒‒‒‒‒‒‒‒‒‒‒‒‒‒‒‒‒‒‒‒‒‒‒‒‒‒‒

‒‒‒‒‒‒‒‒‒‒‒‒‒‒‒‒‒‒‒‒‒‒‒‒‒‒‒‒‒‒‒

‒‒‒‒‒‒‒‒‒‒‒‒‒‒‒‒‒‒‒‒‒‒‒‒‒‒‒‒‒‒‒

‒‒‒‒‒‒‒‒‒‒‒‒‒‒‒‒‒‒‒‒‒‒‒‒‒‒‒‒‒‒‒

New Brunswick, New Jersey

October, 2007

ABSTRACT OF THE DISSERTATION

Live-Load Models For Design and Fatigue Evaluation of Highway Bridges

by JOSEPH C. DAVIS

Dissertation Director:

Dr. Hani H. Nassif

New load design factors and models are introduced to account for site-specific live-load demands in the state of New Jersey. Live-load for highway bridges is highly site specific. The current AASHTO LRFD design specifications provide a notional design truck to which load factors are applied. These strength design factors were calibrated using reliability theory to provide a consistent level of safety for various spans and bridge types. The original calibration was done using a small sample of data from decades ago. Truck weights and volumes have significantly increased, reducing the level of safety of highway bridges designed today.

Live-load is quantified using an extensive weigh-in-motion (WIM) database for the state of New Jersey as well as instrumentation at a bridge located in the heart of Port Newark, NJ. An integrated system combines a WIM system to measure truck loads and a data logger to capture the strains and deflections. This, first of its kind, system provides a complete picture of bridge behavior. The WIM data collected include all of the

parameters needed to quantify truck loading: gross and axle weights, axle spacings, classification, counts, speeds, lane, etc. The bridge response includes parameters such as: strains and deflections.

Information on truck loads are used to develop load effect envelopes for various span lengths. The load effects are then extrapolated using Normal probability paper to predict the maximum expected levels for the full service life of 75 years. The effect of other distributions, various measurement durations, and truck multiple presence is also studied. Based on the analysis of moment and shear envelops for various spans, it was found that the current load factors must be increased to maintain the level of safety that the code dictates. A new load model is proposed to provide a more uniform bias for New Jersey trucks.

Fatigue load effects are studied in terms of effective truck weights, truck dimensions, and multiple presence in comparison with current evaluation procedures. Experimental load and response data from the instrumented bridge along with computer models is used to study the effect of truck weight, volume, and multiple presence of the fatigue life. Statistical techniques developed by the automotive industry are applied to short experimental measurements to predict a fatigue load profile that would be expected if measurement extended to a much longer duration. The rainflow extrapolation techniques utilize Extreme Value Theory and non-parametric smoothing methods to render a future prediction of the rainflow counted stress cycle matrix. The effect of measurement duration, seasonality, and truck multiple presence on fatigue life prediction is studied.

DEDICATION

To my wife Karen, who has so graciously supported me. I Love You.

ACKNOWLEDGEMENTS

TABLE OF CONTENTS

LIST OF FIGURES

xiii

LIST OF TABLES

CHAPTER 1

INTRODUCTION

Highway bridges in the United States are subject to ever increasing truck weights and volumes. At the same time, many transportation agencies are experiencing budget shortfalls. New methods for design and evaluation are needed to compensate for an increased demand on highway infrastructure in the coming years. In addition, evaluation methods are needed to direct maintenance funding to the most vulnerable structures.

Currently highway bridge design is governed by the American Association of State Highway Transportation Officials (AASHTO) Load and Resistance Factor Design (LRFD) Bridge Design Specifications (2004). The two design parameters: load and resistance are described by statistical random variables based on reliability theory. The code is calibrated to assure a consistent and uniform level of safety for many different types of bridges. The previous design philosophy of Allowable Stress Design (ASD) did not consider variability in loads or resistance; designs were based on arbitrarily chosen safety factors. A later manifestation in the 1970's, Load Factor Design (LFD) addressed variation in live load, but neglected variation of other loads.

The LRFD design specifications include provisions for four design limit states: ultimate strength, serviceability, fatigue and fracture, and extreme events. To date, only

the ultimate limit state has been calibrated to provide consistent levels of safety. The live-load models and applied load factors are based on truck survey data sampled in the 1970s in Ontario, Canada. The live-load effects, specifically moments and shears, were extrapolated using Further assumptions were made to compensate for lack of available information.

Today, with the proliferation of truck measurement systems such as weigh-in-motion, vast amounts of data are available to verify the code design assumptions and update the load factors to assure a consistent level of safety. This study utilizes a vast database of weigh-in-motion (WIM) data to revisit the LRFD code assumptions in terms of load factors for the strength limit state and fatigue evaluation procedures. New load factors based on site specific live-loads for New Jersey are proposed. Current fatigue evaluation procedures are tested using the site specific WIM data. One particular site, the Doremus Avenue Bridge, offers both truck live-load information and bridge response as part of a long-term structural health monitoring program.

1.1   Research Significance

A wealth of truck weigh-in-motion data is currently available to describe the truck population. Truck weights and volumes are highly site specific and may exceed the design values specified in the design code. In addition, trucks weights and volumes have increased since the original load factor calibration. There is a need to update the current calibration factors to reflect the heavy truck traffic seen today. There is also a need to verify the current code assumptions given more available data.

Along with an increase in truck volumes and weights comes additional fatigue damage. This study evaluates the effectiveness of the current fatigue load model in

predicting fatigue damage and remaining life. New extrapolation techniques are also introduced to replace current simplistic methods.

1.2 Objectives

The main objective of this study is to evaluate the current live-load and fatigue-load models and recommend a new models to reflect the increasing weight of the truck population. New extrapolation techniques utilizing extreme value theory and rainflow extrapolation are applied to load spectra. New models that incorporate the statistical scatter of the data to predict future load demands based on short-term measurements are developed.

1.3 Organization of the Thesis

The thesis contains seven chapters. This chapter serves as an introduction of the thesis outlining the problem statement and statement of objectives.

Chapter two presents a brief introduction on past and current design code methodologies and calibration procedures. Related techniques for future load prediction and extrapolation are also discussed

Chapter three provides background on the reliability theory that forms the basis for the current code philosophy, methods for prediction future load effects, and detailed calibration procedures.

Chapter four describes the experimental program developed to capture live-load information and simultaneous bridge response for a newly constructed LRFD-designed bridge. Both controlled load testing and long-term monitoring were conducted. A description of the sensors, systems, and tests done is also provided. Descriptions for the

numerous weigh-in-motion (WIM) system locations in two states that were considered as part of this study are also given. Methods used to analyze bridges, specifically, the beam-line, semi-continuum, and grillage methods, are introduced and verified with field measurements.

Chapter five presents statistics used to describe the live-load spectra including: truck volumes and weights, permit configurations, and vehicle superposition for the main study site with comparisons to WIM sites throughout New Jersey and California. The mean maximum observed and maximum design life load effects (simple moments, simple shears, and negative moments for various span lengths) are compared between all sites. A parametric study to examine the effects of: choice of statistical distribution, sample duration, and inclusion of permit vehicles in data on the maximum design load prediction is also given in this chapter.

Chapter six presents the study of live load data with respect to fatigue damage. The effectiveness of the current code provisions is studied in relation to the fatigue design vehicle configuration and weight. Further analysis is given on the effect of multiple presence of trucks on fatigue loading. Finally, a procedure based on WIM data is proposed for use in identifying regions where extreme fatigue loading may occur.

Chapter seven contains the summary and conclusions of this thesis.

CHAPTER 2

LITERATURE REVIEW

2.1   Bridge Design Codes

The current design philosophy of Load and Resistance Factor Designed (LRFD) was introduced by AASHTO in 1994 (AASHTO 1994). The new code specifications replaced the allowable stress method (ASD) and load factor design (LFD) given in the AASHTO 1992 code (AASHTO 1992). The AASHTO 1992 code was the result of over fifty years of changes and adaptations that resulted in inconsistencies in safety levels for different span and bridge materials (Nowak 1995). The present code methodology involves the use of reliability theory to achieve uniform safety levels for different materials and span lengths in addition to taking statistical variability of loads and resistance into account.

2.1.1   Allowable Stress Design (ASD)

Earlier design procedures used Allowable Stress Design (ASD). The ASD philosophy was developed to address the needs of steel bridge designers (Barker and Puckett 1997). The same basic principles of resistance being greater than load existed. The design requirement was formulated in terms of a fraction the yield strength of the material, hence allowable stress. If the allowable stress was required to be less than half

of the yield strength of material, then the safety factor, *SF*, of the design was 2. ASD

came into use when truss and arch bridges were popular. Members were designed to be

pin connected (statically determinate), making structural analysis simple yet accurate. In

truss bridges each members was subject to either uniform tension or compression forces,

with no bending or shear. The required area for any member was therefore the

anticipated load divided by the allowable stress. Later bridges were built using statically

indeterminate connections and beams to resist bending forces. At this time, the ASD was

adapted to evaluate the force effects in terms of moment. Assumptions that sections

remain planar and responses were linear allowed for this adaptation. Instead of a

required area, a required section modulus, S_x, was used. The required section modulus

was simply the expected bending moment divided by the allowable stress in bending.

Throughout the years following its adoption, ASD was found to be inadequate in

many design scenarios. ASD had no direct way of accounting for member residual

stresses for newly developed thin walled sections (wide flange shapes). The original

ASD procedures had been sufficient for the simple rod and bars used to construct trusses

and arches. Adjustments were introduced to compensate for residual stresses in ASD.

ASD also had a shortcoming with regard to combined load effects. In steel beams

bending and shear usually act together according to the Von Mises theorem. Since ASD

was based solely on yield stress of material samples, there was no way to account for

stress interaction. A more logical definition of the allowable stress would be needed to

account for interaction of stresses.

Since ASD was based on the material properties of steel, there existed many

shortcomings relating to the use of other materials. Concrete, for example, is a non-linear

non-homogenous material whose properties and strength change with time. Furthermore, the design of concrete at ultimate is much more reliable than design at intermediate states where material properties and strengths are more variable. Realizing the limitations of ASD, concrete and other material designers have moved to strength design procedures for increased consistency.

Loads applied to structures have a high variability in terms of intensity and duration; however, ASD does not recognize that different types of loads have different levels of uncertainty. For example, live loads and wind forces have different levels of certainty compared with dead loads, yet all are treated equally under ASD. Fixed values for design loads are given in specification and codes.

The level of safety in terms of probability is not known in ASD, since safety factors are chosen by judgment and experience. Therefore, incremental increases in safety cannot be done.

Barker and Puckett (1997) summarize the limitations of ASD for use designing modern structures:

(1)   The resistance concepts are based on elastic behavior of isotropic, homogeneous materials

(2)   It does not embody a reasonable measure of strength, which is a more fundamental measure of resistance than allowable stress

(3)   The safety factor is applied only to resistance. Loads are considered to de deterministic

(4)   Selection of a safety factor is subjective, and it does not provide a measure of reliability in terms of probability of failure

2.1.2   Load and Resistance Factor Design (LRFD)

In order to incorporate the variability of loads into the design, AASHTO adopted the Load Factor Design philosophy in 1992, but kept the allowable stress design procedures. All materials were assigned the same level of reliability resulting in inconsistent levels of safety. There remained a need to quantify uncertainty in material strength and capacity prediction methods (mechanics)

In 1994 AASHTO adopted the Load and Resistance Factor Design, LRFD, approach (AASHTO 1994). The major innovation of the new code was incorporate reliability analysis. Structural performance is now measured in terms of a probability of failure or reliability index. The code provisions were designed to achieve a uniform safety index for different spans and materials. In LRFD, the resistance, Q, is multiplied by a statistically based reduction factor, φ, whose value is equal to or less than 1.0, and the loads are multiplied by a statistically based load factor, γ, whose value is usually greater than 1.0. The basic form of the LRFD design equation (Nowak 1995) is given as:

$$\phi R_n \geq \sum \gamma_i Q_i \hspace{3cm} \textbf{Eq. 2.1}$$

where φ = resistance factor, R_n = nominal (design) resistance, γ_i = load factor for given load type, and Q_i = nominal (design) load component. The load and resistance factors of Eq. 2.1 must be calibrated such that a target safety index is achieved. The resistance factor, φ, accounts for uncertainties for the following parameters: material properties, design assumptions that predict strength, workmanship, quality control, and consequence of failure (Barker and Puckett 1997). The load factor, γ_i, is chosen to account for uncertainties in the following: magnitudes, arrangements, and combinations of loads (Barker and Puckett 1997).

2.1.2.1   Calibration of the LRFD Load and Resistance Factors

The choice of load and resistance factors is done after a formal calibration procedure as outline by Nowak (1995):

(1)   Selection of representative bridges: About 200 structures were selected from various geographical regions of the United States. For each selected bridge, load effects were calculated. Load carrying capacities were also evaluated.

(2)   Establishment of statistical database for load and resistance parameters: available data on loads, including truck survey and weigh-in-motion (WIM) data were used for modeling live load. A numerical procedure was developed to simulate the dynamic bridge behavior to compensate for lack of dynamic bridge data. Statistical data for resistance include: material tests, component tests, and field measurements. Numerical procedures were developed to simulate the behavior of large structural systems.

(3)   Development of load and resistance models: Loads and resistance are treated as random variables. Their variation is described by cumulative probability distribution functions (CDF) and correlations. CDFs for loads were derived using the available statistical database (step 2). The live load model includes the multiple presence of trucks in one lane and in adjacent lanes. Multilane reduction factors were calculated for wider bridges. The dynamic load was modeled for single trucks and two trucks die-by-side. Resistance models were developed for girder bridges. The variation of the ultimate strength was determined by simulations

(4)   Development of reliability analysis procedures: Structural performance is measured in terms of reliability and probability of failure. Reliability is measured in terms of reliability index β, calculated by using an iterative procedure. The developed load

and resistance factors (step 3) are part of the reliability analysis procedure.

(5)   Selection of target reliability index: Performance of existing bridges was evaluated to determine whether their reliability level is adequate. The target reliability index β_T was selected to provide a consistent and uniform safety margin for all structures.

(6)   Calculation of load and resistance factors: Load factors γ are calculated so that the factored load has a predetermined probability of being exceeded. Resistance factors, φ, are calculated so that the structural reliability is close to the target value β_T.

2.1.2.2   Load Models

Loads acting on bridges include: dead load, live load, dynamic impact, environmental loads (i.e. wind, earthquake, temperature, water pressure), and special loads (collision forces) (Nowak 1995). Nowak reviewed the mean to nominal weights (bias) and variation (COV) for various structural components (dead loads). Included in the study were weights of both structural components (concrete, steel, etc.) and non-structural components (asphalt, railings, etc.). It was found that factory-made components (structural steel, precast concrete, etc.) had a mean to nominal ratio of 1.03 and COV of 0.08. Field constructed components were found to have a mean to nominal ratio of 1.05 and COV of 0.10. Therefore, field constructed components have more variability and the corresponding load factor should be greater than factory-made components.

Live load on bridges is mainly due to trucks. The AASHTO 1992 design code used a design model known as HS-20 for Highway Semi-trailer weighing 20 tons (US customary units) (AASHTO 1992). The design model consists of three components:

the HS-20 truck (consisting of three axles of weights 8k, 32k, 32k with a first axle spacing of 14 feet and variable last axle spacing of 14 to 30 feet, chosen to maximum load effect), lane load of 640 pounds per lineal foot, and military loading consisting of two 24k axles spaced 4 feet apart. Nowak (1995) found that the HS20 load model was inadequate to represent the heavy truck traffic being observed on interstate highways. The actual moments and shears from the heaviest observed heavy vehicles ranged from 1.5 to 1.8 times the moments and shears using HS20.

Nowak proposed a new load model to provide a more consistent moment and shear ratios across different span lengths. The new load model was named HL-93 for Highway Loading adopted in 1993. The new model consisted of the original HS20 truck with a superimposed lane load of 640 pounds per lineal foot. A tandem load (two 24k loads spaced 4 feet apart) with superimposed lane load (640 pounds per lineal foot) was introduced for shorter spans.

2.1.2.3   Multiple Load Effects

The case of more than one loaded lane usually controls the design of bridges. Nowak conducted simulations of truck weights and multiple presence (multipresence) frequencies to determine the maximum expected load during a 75-year design life. It was found that in a side-by-side occurrence, each truck was estimated to weigh 85% of the mean maximum 75-year single truck weight. It was estimated that for a highway site with average daily truck traffic (ADTT) of 1000 trucks per day the load effect due to one, two, three, and four lanes loaded would be 1.20, 1.00, 0.85, and 0.60 times the 75-year truck load, respectively.

2.1.2.4   Dynamic Load Amplification

The ratio of dynamic deflection to static deflection due to motion of a truck is referred to as dynamic impact amplification, or impact. Dynamic impact is influenced by three factors: road roughness, bridge dynamics (natural period of vibration), and vehicle dynamics (suspension type and condition). Simulations indicated that the impact is less than 0.17 for a single truck and less than 0.12 for two trucks, for all spans. Nowak proposed a single dynamic load factor of 0.33 for all spans. The impact factor is applied only to the truck load effect, not the uniform lane load.

2.2   Fatigue Evaluation

 2.2.1   Background

Fatigue is a mode of failure whereby a crack develops and propagates within metal under loads that are less than the design ultimate strength of the structure. The ASTM definition: "The process of progressive localized permanent structural change occurring in a material subjected to conditions which produce fluctuating stresses and strains at some point or points and which may culminate in cracks or complete fracture after a sufficient number of fluctuations" (ASTM E206-62T).

Fatigue failures were noted by engineers as early as 1829 (Munse 1990). This phenomenon was studied in conveyor chains used in coal mines by Albert in 1837 (Schutz 1996). A more notable researcher in fatigue was Wohler. He developed deflection gages for in-service monitoring to study why railcar axles were failing in 1858. He developed one of the earliest "safe-life" approaches to fatigue design, stating that if

bearings were designed for 200,000 miles of service, then the fatigue life of the axles

should be designed likewise (Schutz 1996).

2.2.2   The S-N Diagram

The fatigue resistance of a structure depends on the loading level (stress range) and

the frequency of loading. The relationship between stress ranges and loading cycles is

often shown using a S-N or Wohler plot, Figure 2.1 (Munse 1990).
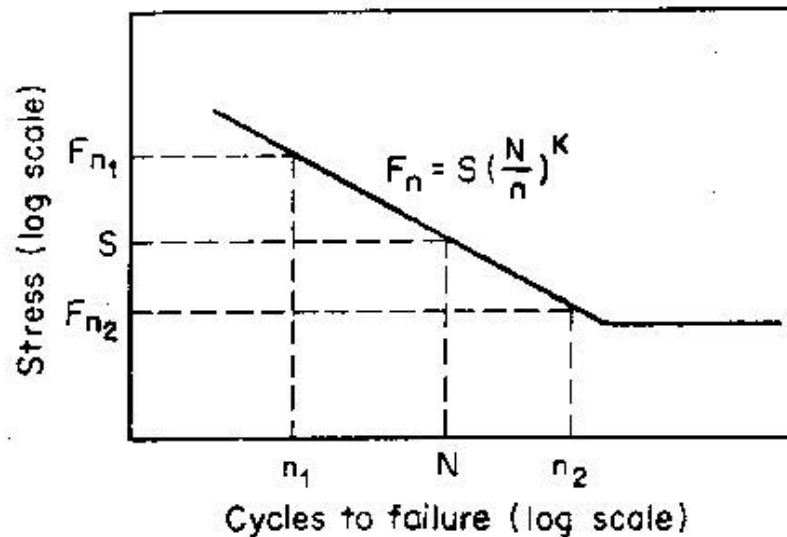
Figure 2.1 S-N Diagram

The scale of the S-N plot is log-log to show the ultimate number of cycles to

failure, often greater than 2,000,000. Additionally, the horizontal line to the right of the

abscissa represents the stress level of infinite life. At this level the metal element can

theoretically endure an infinite number of cycles without propagating a fatigue crack.

The S-N curves vary by type of metal and also by geometry of the element. For example, notched or corroded elements will fail under much lower loads and a fewer number of cycles.

2.2.3   Rainflow Cycle Counting

There are a variety of cycle counting methods available. The goal of each method is to best describe the effects of variable amplitude loading in terms of discrete cycles which can be compared to constant amplitude test data (Bannantine 1990). Rainflow cycle counting, as specified in ASTM, identifies closed hysteresis loops from the loading spectrum. The original rainflow method was first described by Matsuishi and Endo in 1968. Cycles are defined by the same way that rain falls from pagoda roofs. The stress history is rotated vertically, such that time increases downward. The primary cycles are extracted and the process is repeated for the minor cycles. The following rules are applied to control the counting procedure:

1. To eliminate the counting of half cycles, the strain-time history is rearranged to begin at the largest strain value. More complex procedures have been developed to eliminate this requirement (Downing 1982).

2. A flow of rain is begun at each strain reversal in the history and is allowed to continue to flow unless:

   a. The rain began at a local maximum point (peak) and falls opposite a local minimum point greater than that from which it came.

   b. The rain began at a local minimum point (valley) and falls opposite a local minimum point greater (in magnitude) than that from which it came.

   c. It encounters a previous rainflow.

The following example illustrates the rainflow counting method for a sample complex loading as shown in Figure 2.2. The procedure is started at each reversal:

1. Rain flows from point A over points B and D and continues to the end of the history since none of the conditions for stopping rainflow are satisfied.

2. Rain flows from point B over point C and stops opposite point D, since both B and D are local maximums and the magnitude of D is greater than B (rule 2a).

3. Rain flows from point C and must stop upon meeting the rain flow from point A (rule 2c).

4. Rain flows from point D over points E and G and continues to the end of the history since none of the conditions for stopping are satisfied.

5. Rain flows from point E over point F and stops opposite point G, since both E and G are local minimums and the magnitude of G is greater than E (rule 2b).

6. Rain flows from point F and must stop upon meeting the flow from point D (rule 2c).

7. Rain flows from point G over point H and stops opposite point A, since both G and A are local minimums and the magnitude of A is greater than G (rule 2b).

8. Rain flows from point H and must stop upon meeting the rainflow from point D (rule 2c).
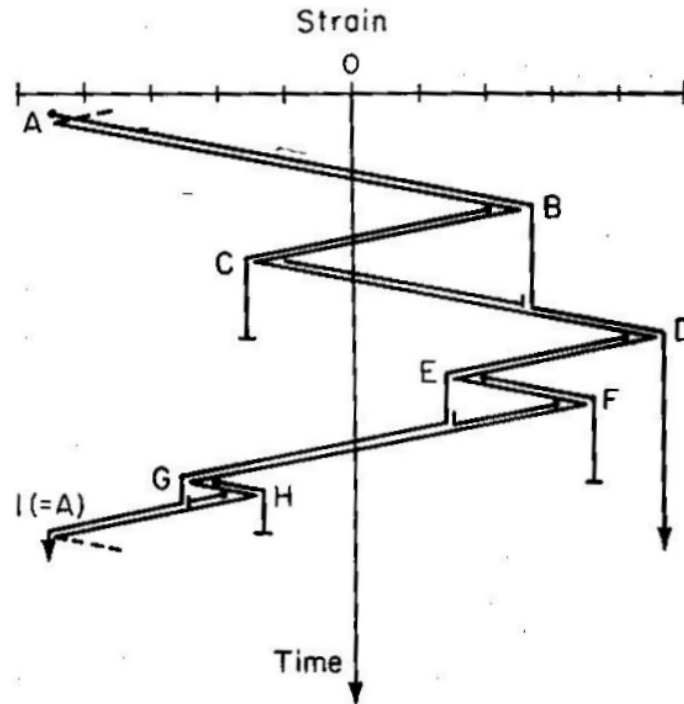
Figure 2.2 Rainflow counting example (Bannantine 1990)

The following closed hysteresis loops are computed from Figure 2.2: A-D-A, B-C-B, E-F and G-H. The resulting rainflow table is compact compared to the much larger stress history. Thus, a very lengthy time history is equivalently described in a matrix of values.

Rainflow counting can be accomplished in a variety of forms, some examples include: range only, range-mean, and to-from. In range only counting, only the range of the cycle is kept. The range-mean method contains the basic range of the cycle in addition to the mean value of the min and max. Finally, the to-from rainflow matrix, contains the starting and ending point of every cycle. Therefore, with a to-from matrix, information about a cycle's origin and terminus are maintained. Information about load switching from tension to compression is also preserved. Figure 2.3 shows a typical to-from rainflow matrix for the stresses of a steel highway bridge.
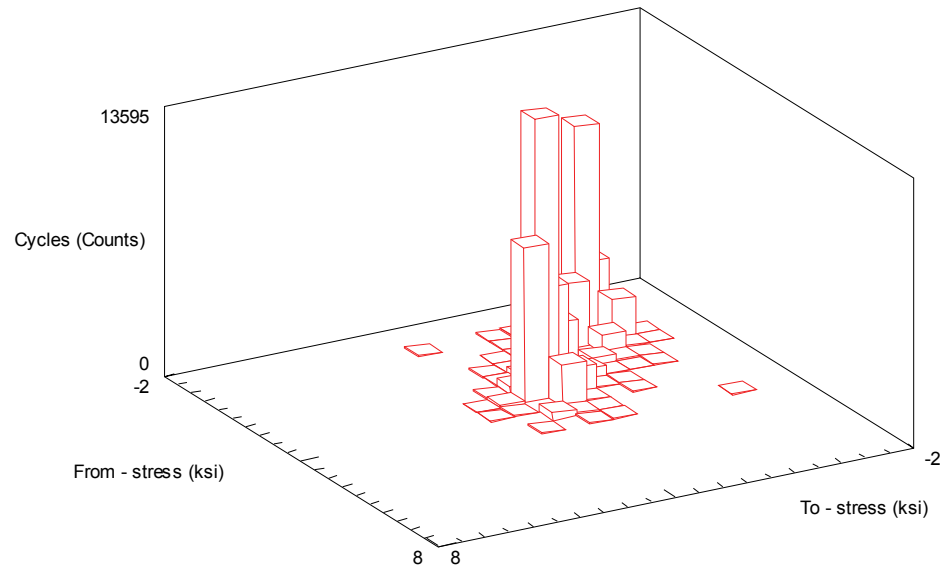
Figure 2.3 To-From rainflow matrix.

The shape of the to-from rainflow matrix describes the nature of the fatigue loading. All cells along the diagonal are zero since a cycle cannot originate and terminate at the same value. Clusters of high cycles describe the dominant stress ranges. Typically in mechanical engineering the clusters represent duty cycle loads of machinery. For example, separate clusters for loaded and unloaded vehicles would be present. Values are typically higher near the diagonal and dissipate further out. The value of the stress range increases with the distance from the diagonal. The range of the stress is not immediately evident from a to-from matrix, but can be easily calculated. As an example, consider the stress cycles shown in Figure 2.4. Cycle r-c would be recoded as "to 5 from 3", while cycle p-v would be recorded as "to 2 from 6".
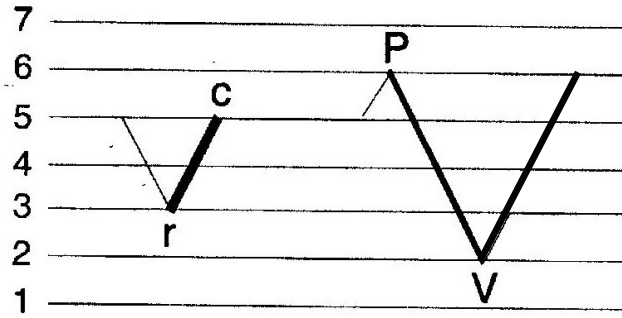
Figure 2.4 Cycle counting example (Socie 2001).

2.2.4   Effective Stress

The effective stress, also nominal stress, of a load history is defined as a stress that causes the same amount of fatigue damage as the actual load history for the given number of cycles. The equation, Miner's Law (root mean cube stress), is given as:

$$S_r = (\sum f_i S_{ri}^3)^{1/3}$$

Eq. 2.1

where: f_i = fraction of stress ranges at level i, S_{ri}=the stress range magnitude of interval i, and S_r = effective stress range. Extensive laboratory testing has proven Miner's Rule is applicable to bridge members (Schilling 1978). When calculating the effective stress, a minimum sufficient number of cycles should be present to avoid falsely high effective stresses from a few high range cycles.

There is no consensus among fatigue researchers as to how to calculate the effective stress from an observed experimental record. Field data includes many low range stress cycles due to sensor noise and vibration. These minute cycles cause a negligible contribution to the fatigue damage. Rainflow processing modes within data acquisition systems offer a lower threshold below which cycles are omitted. The choice threshold has an influence on the value of the effective stress. Since effective stress is

calculated as a root-mean-cube weighted average, a large number of minute stress cycles causes a significant drop in the calculated effective stress. Shenton et al. (2006) studied the effect of lower threshold on the effective stress outcome. The choice of lower cutoff caused the calculated effective stress to vary from 0.88ksi to 3.02ksi. Fisher et al. (1998) recommends taking a lower cutoff such that the number of observed stress cycles approximately equals the average daily truck traffic at the bridge location.

2.2.5   Cumulative Damage Estimation

Multiple laboratory tests of specimens subject to repeated loading cycles at constant amplitudes are used to generate these S-N curves. However, the loading patterns of actual structures contain random variable amplitude stress cycles. Therefore, a means to find an equivalent damage accumulation is needed. The linear cumulative damage rule, or the Palmgren-Miner Rule, herein referred to as Miner's Rule, is used to relate variable amplitude behavior to constant amplitude behavior (Miner 1945). The failure criterion is defined as when the damage reaches unity. Miner's Rule, in its simplest form, is given as:

$$\sum_i \frac{n_i}{N_i} = \frac{n_1}{N_1} + \frac{n_2}{N_2} + \frac{n_3}{N_3} + ... = 1$$

Eq. 2.2

where: n_i = number of stress cycles at level σ_i, N_i = number of stress cycles to produce failure at σ_i

The damage caused by a load history is not immediately clear from the number of cycles or the maximum stress range. In other words, the most damaging load history is not necessarily the one with the highest number of cycles. The most damaging load

history is most likely the history that contains a large number of mid-to-high range cycles (Socie and Pompetzki 2004). Therefore it is critical that the cumulative damage method be applied to normalize each load history for comparison.

2.2.6 Fatigue of Bridge Structures

The current design provisions for highway bridges are set forth in the American Association of State Highway Officials (AASHTO) Load and Resistance Factor Design (LRFD) Specifications (AASHTO 2004). The current methodology was the recommendation of Moses, Schilling, and Raju as part of the NCHRP Report 299, "Fatigue Evaluation Procedures for Steel Bridges" (Moses, et al 1987). The principle inputs for fatigue design are the average daily truck traffic, percentage of truck traffic, and connection detail category. A fatigue design truck is specified for calculation of stresses. The gross weight and axle spacing is chosen such that the fatigue damage caused by the design truck is similar to that of the actual truck population. The NCHRP Report 299 also gives provisions for calculating a site specific fatigue truck. The gross weight of the design truck is calculated from the root-mean-cube effective gross weight of the truck population. The distribution of gross vehicle weights has been shown to be greatly site specific (Laman 1996). Therefore, a more accurate assessment of fatigue remaining life can be accomplished with local truck weight distributions.

$$W_{equ} = \left(\sum_i f_i W_i^3 \right)^{1/3}$$ **Eq. 2.3**

where f_i=fraction of gross weights within interval i and W_i = midwidth of interval i. The current fatigue design truck consists of two 32-kip axles that are 30 feet apart (Figure 2.5). In order to calculate the member stresses due to the design truck, lateral distribution factors for fatigue are specified. The distribution factors for static design of the members

assume an ultimate load condition which produces the maximum load effect. Fatigue

damage, however, is an accumulated damage caused by single truck passages. Therefore,

the most likely distribution is chosen for fatigue design, whereas, the most severe is

chosen for the static ultimate strength limit state.
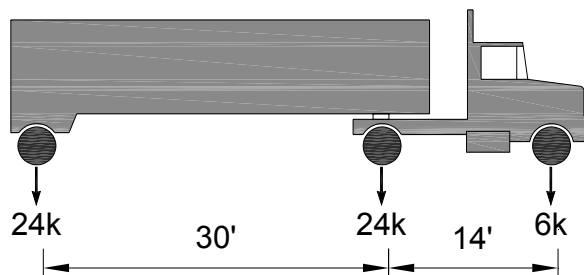
Figure 2.5 AASHTO LRFD Fatigue Design Truck (AASHTO 2004)

The stresses caused by the fatigue truck passage are used to determine the design

stress range for fatigue.   Depending on the bridge span, the number of cycles caused by a

truck is determined. For shorter spans, the design truck shows two distinct peaks,

whereas, for longer spans there is one overall peak (Schilling 1984).

Another important consideration in fatigue design is impact or dynamic load

amplification. The impact factor used for fatigue is an effective impact factor (Moses

1987). The stress range is amplified not the peak stress. The effective impact factor

represents typical bridges with normal road roughness. Factors of 1.10 and 1.10-1.13 for

smooth and rough surfaces, respectively, were chosen for the current design provisions

(Moses 1987).

The current code, as with the previous AASHTO code, and the American

Welding Society (AWS) code, specify detail categories for welded and bolted

connections (Table 2.1). The categories are denoted by letter and include: A, B, B', C,

D, D', E, and E'. Category A details include rolled beam sections and are considered the

most fatigue resistant details. Category E', however, are the most susceptible to fatigue

damage and include longitudinally loaded fillet-welded attachments.

The fatigue design is based on a single lane loaded. Therefore, the average daily

truck traffic is used for determination of fatigue loading. Multiple truck loading is

considered rare (Moses 1987). Special provisions are given for cases when multiple

truck situations may occur. For example, bunching of trucks may occur on a bridge near

traffic signals or uphill on a two or more lane bridge. For these cases, a 15% increase in

fatigue truck weight is prescribed.

2.2.7   Current Fatigue Design Equations

The fatigue limit state as defined in the AASHTO LRFD code is given as:

$$\eta\gamma(\Delta f) \leq \varphi(\Delta F)_n \qquad \textbf{Eq. 2.4}$$

where: η=1.0, and φ=1.0. The fatigue resistance is defined as:

$$(\Delta F)_n = \left(\frac{A}{N}\right)^{\frac{1}{3}} \geq \frac{1}{2}(\Delta F)_{TH} \qquad \textbf{Eq. 2.5}$$

for which: N=(365)(75)n(ADTT)$_{SL}$ and where: A=detail category constant, n=number

of stress range cycles per fatigue truck passage, (ADTT)$_{SL}$=single-lane ADTT, and

($\Delta F)_{TH}$=constant-amplitude fatigue threshold (AASHTO 2004 6.6.1.2.5).
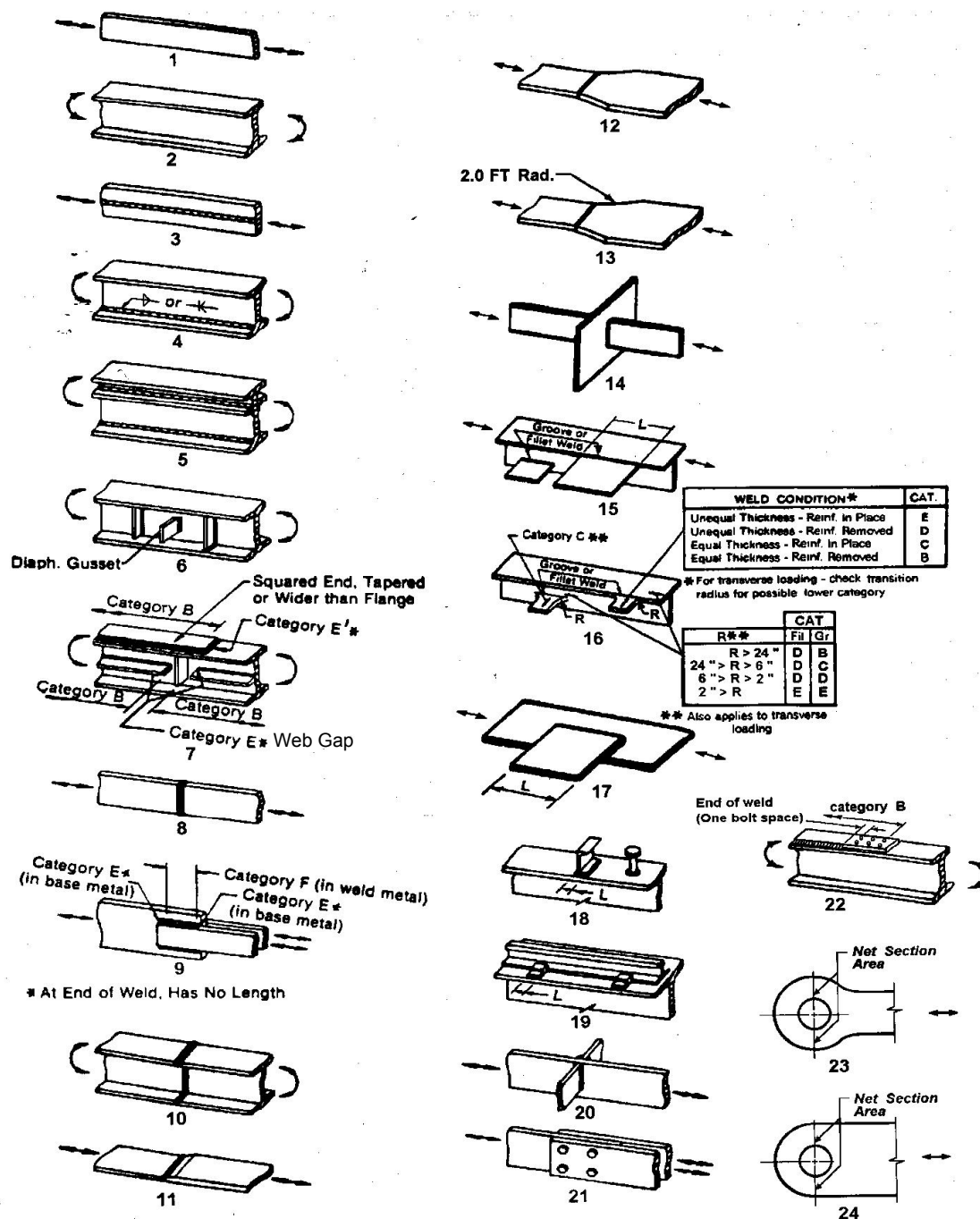
Figure 2.6 Fatigue design details (AASHTO 2004)

Table 2.1 Fatigue detail constant, A, by category x10^7

Detail Category	Constant, A, x 10^8
A	250.0
B	120.0
B'	61.0
C	44.0
C'	44.0
D	22.0
E	11.0
E'	3.9

Table 2.2 Constant amplitude fatigue threshold by category

Detail Category	Threshold (ksi)
A	24.0
B	16.0
B'	12.0
C	10.0
C'	12.0
D	7.0
E	4.5
E'	2.6

2.2.8   Current Remaining Life Estimation

In 1985, NCHRP Project 12-28, "Fatigue Evaluation Procedures for Steel Bridges", was initiated. The goal of the principle investigators: Moses, Schilling, and Raju, was to develop fatigue design procedures that more accurately reflect fatigue loading conditions. Probabilistic techniques were employed to ensure consistent levels of reliability. Also included in the recommendations was a means for evaluating existing bridges. A quantitative means of assessing remaining life was developed. Additionally, there were guidelines for engineers to develop site specific fatigue design loads and account for future traffic volumes. New factors for load distribution, impact, truck superposition, and cycles per truck were introduced. Factors were developed to represent

the typical or average effect of truck loading. Fatigue design was differentiated from static (ultimate) limit state design. Whereas, exceeding the ultimate limit state would result in structural collapse, exceeding the fatigue limit state would simply result in shortened life of a structural component. Corrective actions could be taken to extend the life or replace the structure before serious damage occurred. The end result of the shift from ultimate to a more tolerant limit state would be a more realistic, cost efficient design philosophy

The basis for the material properties needed in fatigue design were developed from laboratory testing of bridge elements. The tests conducted by Keating and Fisher (1985) were done for different samples at constant amplitude stress ranges. The cycles to failure were plotted on a representative SN curve. There was significant scatter the data; therefore, the allowable stress ranges were defined as two standard deviations below the mean stress. The current design SN curves approximate the lower 95 percent confidence limits from test results. The mean SN curves, therefore, provide a higher number of cycles.

There has been extensive work done on field testing of bridges to determine remaining fatigue life. For the most part, the investigator installs strain gages to key fatigue prone detail locations on a bridge structure and monitors strain/stress levels for a given period of time. The cumulative damage is calculated based on Miner's Rule, and along with the ADTT for the location, the fatigue life is calculated based on the recommendations of Moses et al, 1987. The remaining fatigue life is simply the total life less the current service life of the structure.

Hahin, South, Mohammadi, and Polepeddi (1993) applied the new fatigue evaluation procedures proposed by Moses, et al. to numerous bridges in Illinois. The experimental program consisted of instrumenting fifteen representative steel bridges with strain gages and monitoring stresses at critical details over a 3 to 8 hour period. Stresses cycles were collected using rainflow techniques. Stress cycles below 0.5 ksi were discarded as noise and were considered a negligible contribution to fatigue damage. Short term data were linearly extrapolated to a 24-hour period. Miner's Rule of linear damage accumulation was used along with fatigue strength coefficients and exponents based on the Munse et al, 50% mean data for structural details, given by:

$$N = c(S)^m$$
<div style="text-align:right">**Eq. 2.6**</div>

where S=stress range (ksi); c=fatigue strength coefficient; m=fatigue strength exponent; and N=number of cycles to major crack formation or failure. The daily damage caused by truck traffic was computed. Traffic information was provided by Illinois Department of Transportation as far as truck volumes. No indication was made of the truck weight distributions or superposition. Stress cycles were linearly projected by multiplying the daily data out to 25 years. No consideration was made with regard to variability of the stress cycles. The authors, however, do make provisions to account for truck volume and weight increases by compounding the number of cycles annually and increasing the stress magnitudes, respectively. The authors conclude that increasing the truck weights by 10% once and the truck volume 5% annually, fatigue damage is 4.5 times greater than with no volume or weight change over 25 years. The study is comprehensive with regard to the number of structures instrumented, however, little is known about the truck load spectra. Furthermore, only 3-8 hours of monitoring at 3-4 superstructure locations was conducted

for each site. Additional monitoring is needed to verify the assumption that the short test

durations represent a typical day of loading. Additional gage locations could also be

added to determine load distributions for use in computer modeling of similar structures.

A subsequent study by Mohammadi, Guralnick, and Polepeddi (1998)

incorporated more probabilistic treatment of fatigue damage. A beta distribution is

assumed for the stress range, a Weibull distribution for the fatigue resistance (Ang and

Tang 1975). Different fatigue reliability target levels of 97.7% and 99.9% for redundant

and non-redundant members, respectively. The bridge is said to have failed in fatigue

when the sum of the Miner's Rule has reached unity. The authors express the expected

damage as a statistical term:

$$E(D) = \int_0^{S_{max}} \frac{\overline{n}}{N(s)} f(s) ds \qquad \textbf{Eq. 2.7}$$

where S is the stress range expressed as a continuous random variable with f(s) as a

probability density function, and ň=average number of cycles for all ranges, given by:

$$\overline{n} = \frac{c}{\int_0^{S_{max}} S^m f(s) ds} \qquad \textbf{Eq. 2.8}$$

where c and m are empirical constants (Ang and Munse 1975). Finally the fatigue

reliability is expressed using Ang and Munse's (1975) equation:

$$L(n) = \exp\left\{ -\left[\frac{\overline{n}}{n} \Gamma(1+\alpha) \right]^{1/\alpha} \right\} \qquad \textbf{Eq. 2.9}$$

in which L(n)=fatigue reliability, Γ=gamma function, $\alpha = \Omega^{1.08}$, Ω=uncertainty of fatigue

life (0.54 for sections with cover plates), and n=total number of cycles. A traffic growth

factor is implemented similar to the Hahin (1993) paper and fatigue lives computed.

Results are similar to the 1993 paper. Again, no consideration was made to with regard to the truck weight distributions.

Nowak, Nassif, and Frank (1993) published the findings of a fatigue evaluation of a steel bridge. The bridge under study was instrumented to determine the remaining fatigue life. Strain gages were installed such that fatigue critical members were monitored. Additionally, all girders in one span were instrumented to determine the load distribution. This was found to be crucial to understanding the actual vs. assumed load distribution. Analytical results showed high stresses in the exterior girders, making those members most fatigue critical. However, the measured stresses were much less than the calculated stresses. Sensors indicated that the connection of the floor beams to the exterior girder was behaving like fixed moment connection. Furthermore, the floor beam was responding as a beam fixed against rotation but undergoing a relative displacement between the supports at the exterior and first interior girders.

After instrumenting the structure, the authors conducted test runs with a calibration truck of known weight. Knowing the truck gross weight and axle weight distribution is key when comparing the experimental to analytical results. Bridge stress range data was collected continuously using rainflow techniques for two weeks. Meanwhile, the traffic was recorded for 24 hours using a video camera. The video was later reviewed to determine the truck volumes and superposition (multiple presence). It was found that the ADTT was 11,334 in both directions, less than 10% of trucks used the left-most lane, and that approximately every 20th to 25th truck is on the bridge simultaneously with another truck moving side by side in the same direction. In a similar

manner to Hahin et al (1993), a minimum stress threshold of 0.5 ksi was used to eliminate possible signal noise error.

Information on truck volumes from the opening of the bridge as well as projections 20 years into the future was given. A full fatigue life assessment could now be done. Given the historical load data, the authors calculated the fatigue damage accumulated up to the time of testing and extrapolated 20 years into the future, considering traffic volume growth. The authors concluded that despite a 25% increase in truck volumes, the bridge would be free of major fatigue cracking for at least 30 additional years. The Nowak et al (1993) fatigue study provided a more complete analysis given the calibration runs and information on truck superposition. The distribution of truck weights would have made the study more comprehensive and provided an opportunity for computer simulation of stress cycles. This paper provides an important contribution to the state of the art for fatigue study of bridges by proposing the following major steps:

1. Review the available drawings. Identify fatigue prone components and details on the basis of experience. Special attention should be paid to distortion-induced fatigue

2. Perform analysis to determine the load spectra for main girders (load distribution factors) and fatigue-prone details.

3. Instrument the bridge and take WIM measurements. Measure stress ranges under normal traffic flow.

4. Verify the accuracy of analytical girder distribution factors by comparing with the measured load distribution.

5. Verify the calculated stress ranges by comparison with measured values.

6. Establish the cumulative distribution functions for stress range.

7. Estimate the fatigue resistance of the critical components and details.

8. Evaluate the fatigue performance of critical components by comparison of load and resistance.

9. Estimate the remaining fatigue life.

Laman and Nowak (1996) examined the truck weight distribution and stress response of five bridge sites in Michigan. The goal was to show the site specific nature of truck loads and develop a representative fatigue load model. The bridges were instrumented with strain gages and a Weigh-in-Motion system. For each site, a truck of known weight was used to calibrate the sensors. Strain cycles were collected for a period of up to 3 weeks per site using the rainflow method. The authors recommend the use of weigh-in-motion systems as opposed to weigh station data for gathering truck weight distributions. It was found that the heaviest trucks were traveling on busy interstate highways far away from weigh stations (Laman 1996). The truck weight distribution was found to be strongly site specific. The difference between the highest and the lowest median value was approximately 40% and the variation for the extreme GVW values was 100%. The equivalent truck weight was ranged from 62.4k to 78k for the five locations. It was found that between 40% and 80% of the truck population were 5-axle trucks. Furthermore, vehicle with 3 and 4 axles were configured similar to 5-axle vehicles. When the vehicles of similar configurations are grouped together they represent between 55% and 95% of the truck population. The effect of span length on the number of cycles was also investigated. The number of cycles is much higher for shorter span bridges.

This means that a bridge with a 15 to 30 ft span may experience 2 or more stress cycles per truck passage, accelerating the fatigue damage. The primary conclusion of the study was the proposal of two fatigue design trucks: one three axle truck and a 4 axle truck. The fatigue damage would be assessed based on the fraction of 11-axle trucks and all other trucks by applying the 4 axle and 3 axle models respectively. The primary contribution of this study was that truck weight distributions are strongly site specific. The truck records collected during the field monitoring were later entered into a simulation to determine the actual fatigue damage. The final fatigue models were also simulated across the bridges and compared to the actual truck fatigue. A comprehensive fatigue damage study includes the distribution of vehicle weights and types.

2.2.9   Forecasting Remaining Fatigue Life

As stated in the AASHTO 2004 code, if the factored design stress range of a member is below the constant amplitude threshold as specified in Table 2.2, the member is said to have infinite fatigue life. Additionally, if the stress range is found to be entirely in compression, a fatigue check is not required. The code specifies a basic procedure and more refined procedures for estimating remaining life. The remaining life in years corresponding to the factored stress range, R_sS_r, is given as:

$$Y_f = \frac{fK \times 10^6}{T_aC(R_sS_r)^3} - a \qquad \text{Eq. 2.10}$$

in which T_a is the estimated lifetime average daily truck volume, C is the cycles per truck passage, a is the present age of the bridge in years, K is the detail constant, and f is a factor to account for the difference between the mean and allowable SN curves.

2.2.10   Distortion Induced Fatigue

Fatigue cracking may also develop as a result of out-of-plane distortions between girder flanges and stiffeners. Distortion induced stresses cause cracking very early into service of bridges with vulnerable details (Fisher 1990). The resulting stresses can be as high was 30 ksi in the web gap. Distortion prone details are often the result of designers desire to avoid welding transverse stiffeners to tension flanges. Another example are the gusset plates welded to tension portions of webs to connect lateral bracing members. The cause of distortion is often unanticipated secondary bending or vibration of lateral bracing (Moses 1987). Distortion induced fatigue is difficult to model since it depends heavily on the specific detail and loading conditions. Therefore, this type of fatigue cracking is not easily predicted using the current code provisions. Field testing must be done to measure out-of-plane displacements and stress concentrations at vulnerable details.

2.3   Forecasting Future Effects

Forecasting future occurrences has long been studied in regard to wind and flood engineering. Structures such as building must be designed to resists the maximum wind forces that may occur during the service life. Likewise, bridges and buildings must be designed safely above the elevation of the maximum expected flood levels. In order to arrive at a prediction, historical data is analyzed and a statistical distribution is assumed. Given the properties of the fitted distribution, future effects or extrapolations are determined.

2.3.1   Probability Paper

The underlying statistical distribution of observed data may be found empirically by plotting the data on probability papers. The scale of these special probability papers is proportioned to match the standard variate of the given distribution. The most common probability paper is for the Normal or Gaussian distribution. Probability papers can be construction for other distributions such as: Gumbel, lognormal, exponential, etc.

Nowak (1999) used the Normal Probability Paper (NPP) during the calibration for the load factors of the AASHTO LRFD Bridge design specifications (AASHTO 2004). Truck load effects, including simple moment, simple shear, and two-span continuous negative moment, were plotted using NPP in terms of a bias to the notional HS20 load model. It was found that the upper tail of the distribution plotted as a straight line in the NPP scale, indicating a good fit to the normal distribution. Thereafter, the future load effects were determined by linearly extrapolating the upper tail to the 75-year level.

2.3.2   Extreme Value Theory

The study of extreme values, or Extreme Value Theory (EVT), has become increasingly popular in recent years. Applications have been found in many disciplines within and outside engineering. For example, for portfolio management in the insurance industry, risk assessments for financial markets, and for traffic prediction in telecommunications networks (Coles 2001). EVT has also been applied to the field of alloy strength prediction (Tryon and Cruse 2000), ocean wave modeling (Dawson 2000, Brodktorb 2000), memory cell failure (McNulty et al. 2000), wind engineering (Harris, 2001), management strategy (Dahan and Mendelson 2001), biomedical data processing (Roberts 2000), assessment of meteorological change (Thompson et al. 2001), non-linear beam vibrations (Dunne and Ghanbari 2001) and food science (Kawas and Moreira 2001). Furthermore, EVT was used by Gindy (2004) to determine the maximum expected deflection during the design life of bridges.

The objective of EVT is to quantify the stochastic behavior of a process at unusually large or small levels sometimes more extreme than has ever been observed (Coles 2001). For example, a telecommunications tower is to be constructed to withstand the maximum wind gust expected during its 100-year service life. Wind data for this site may be available for a much shorter durations, say 25 years. EVT provides a framework that enables extrapolations of short-term observed data to longer periods needed for structural design.

2.3.3   Rainflow Extrapolation

The problem of fatigue life prediction is well studied in the automotive engineering. Data collection is expensive and time consuming. Therefore, only a short

period of measurement is practical. Long term predictions are made from the short term

data. Often, engineers perform fatigue analysis on a short term load history that is

repeated until failure to determine the fatigue life. Aspects of loading, such as load level

and count variability, that would occur in longer tests are lost (Socie 2001). Rainflow

cycle counting has long been used in fatigue analysis to quantify load levels and number

of cycles in an efficient form. Rainflow data, in the form of a "to-from" matrix,

maintains the variability of test data and allows realistic extrapolation to longer time

periods. The "to-from" matrix is essentially a tally of the cycle minima and maxima.

The cycle starting and peak information is kept along with the corresponding frequency.

Information about load chronology is lost; however, long term fatigue damage is

independent of load sequence. The cumulative damage is computed using a linear

damage rule such as Miner-Palmgren.

The first description of rainflow matrix manipulation was given by Cacko (1993).

The operational loading in terms of stress cycles and mean stress levels are represented in

a rainflow matrix. Stress cycles in the rainflow matrix are classified as being continuous

or discontinuous. These parts are to be considered separately and recombined by

superposition after analysis. The continuous part is simulated by reconstructing a time

history given the distribution and power spectral density defined by the rainflow data.

The discontinuous part represents a non-stationary process, such as rare but extreme

loading events. Three parameters describe discontinuous events: (1) average frequency

of events, (2) average time delay between events, and (3) typical geometric shape of

events. Discontinuous events are modeled as a Poisson process where the continuous and

discontinuous components are superimposed. The difficulty of verifying rainflow

extrapolations is addressed. Verification of continuous process for common stress cycles is possible using distribution parameters (mean, variance, and probability density). Verification of extreme or discontinuous event is more difficult since there is no exact definition of the extremes. Cacko (1993) offers valuable framework for the use of rainflow matrices to describe fatigue loadings, but does not offer a clear methodology for extrapolating and interpreting the results.

Dressler (1996) was among the earliest to describe, so called, rainflow extrapolation. The "to-from" rainflow matrix is described by a two dimensional probability distribution. Rainflow histograms have arbitrary shapes; therefore, they may only be described by nonparametric methods. Kernel estimators are used to estimate the probability density. One challenge noted was the choice of kernel estimators to describe data density. Scaling the estimator may result in strong weight given to data near the estimation point or broad estimation may neglect the nearby points and offer a good overall description. To solve this dilemma, adaptive bandwidth kernels are used based on how much data is in the neighborhood of the point being considered. A framework for time history construction from an extrapolated rainflow matrix is proposed. The extrapolated rainflow matrix is used to randomly generate an expected time history based on the probability of cycle occurrence. This method is then used to determine the load levels corresponding to a 99th percentile extreme user. Engineers then use this data to design components to withstand a severe user based on the measurement of several average users.

Johannesson and Thomas (2001) analyzed load data from automobile suspensions systems during test track loops using rainflow extrapolation. A vehicle was driven

around a test track. Drivers were instructed to repeat identical laps. The rainflow matrices showed variability, but also similarities in the load cycles. None of the time histories were identical because of inherent differences in each loop. Procedures are given to combine multiple rainflow matrices from different users to determine the extreme user rainflow matrix. Rainflow extrapolation techniques similar to Dressler (1996) are used to determine the cycle counts for longer periods. A novel approach for extrapolation is proposed using a hybrid method of statistical extreme value theory and kernel smoothing. The extreme loads are modeled using an asymptotic expression based the Poisson convergence of upper level crossings. The remainder is estimated using kernel smoothing techniques. It was found that the shape of a limiting rainflow matrix can be described as the number of loops (test trials) goes to infinity. In other words, at some point during long-term loading, the shape of the rainflow matrix stabilizes and only the counts are increasing.

Traditional extrapolation for fatigue lifetime involves short term measurement of stress cycles and linear extrapolation or growth factor extrapolation. One example of this method is Mohammadi (1993). However, linear extrapolation assumes that the short term record is typical of the site and may be duplicated until the fatigue life of the structure is consumed.

CHAPTER 3

RELIABILITY AND PREDICTION MODELS

The parameters of load and resistance in engineering are subject to a great degree of uncertainty. A designer must consider the expected use of a structure and, to the best of his or her ability, anticipate the various loads that will act on it. The demand on a structure, the loads, and the resistance, capacity, are not fully known. Therefore, they must be expressed as random variables. Perfection in nature or design is nearly impossible. Every engineering quantity has an inherent variability and cannot be expressed as a single value or point. They are described by statistical functions based on observed and/or extrapolated data. Given the scatter of a random variable, absolute certainty in design cannot be guaranteed. In other words, a structure designed properly using certified materials maintains a certain non-zero probability of failure.

Structural design is simplified using assumptions and idealizations to fit more complex mechanics. These assumptions are imperfect, but when used within their limitations, allow the engineer to design structures that are reasonable safe. The exact safety level is chosen based the acceptable level of risk that society allows (Nowak and Collins 2000). Design codes and specifications account for these sources of uncertainty and levels of risk using a reliability-based methodology.

Consider the case of a reinforced concrete beam. There exist uncertainties both natural and human. The anticipated loads are given in a design code including design simplifications, for example, the Whitney Stress Block (Nawy 2005). The material properties are specified with a built-in level of safety. The designer is endorsed by a state agency to ensure competency. Despite these factors, natural variation within the loads and materials, human error in design or construction, and uncertainty in the design assumptions may contribute to failure. A reliability based design code uses the measure of variability in loads, materials and methods to arrive a specific load amplification and material resistance reduction factors to assure a consistent level of safety.

When designing durable structures such as highway bridges that are expected to have a service life of at least 75-years, information is needed about future loads. Therefore, extrapolation techniques must be applied to a short period of measurement to predict the load level at the design life. Prediction, whether applied to live load spectra, wind velocities, flood severity, or other natural phenomena, involved a great deal of uncertainty especially at longer future return levels. Despite the uncertainty an answer is needed. Diligence and care must be taken when extrapolating to future periods, as the answer is both critical to the design of the structure, and more importantly, nearly impossible to verify. However, robust statistical techniques have been developed and tested on various natural phenomena. Furthermore, the extreme values tend to exhibit defined patterns of behavior that aid in extrapolation.

This chapter introduces the reliability theory including the background of the current Load and Resistance Factored Design (LRFD) for highway bridges, sources of uncertainty, and prediction methods.

3.1   Sources of Uncertainty

Ang and Tang (1984) describe several sources of uncertainty in engineering practice:

(1) Uncertainty associated with randomness. Most parameters in reality are unpredictable. In other words, the repetition of a test or action will always produce a different result. Some observed values will be more frequent than others. The relationship between the magnitude and frequency of occurrence defines the statistical distribution of the variable. Often, histograms are constructed to determine the underlying distribution from observed data. A statistical distribution is then chosen to best describe the shape of the histogram. The fit, or lack of, will contribute to the next example of uncertainty associated with modeling.

(2) Uncertainty associated with imperfect modeling and estimation: error and uncertainty may be introduced when inferences are made based on limited or biased data. Additional uncertainty is added from the use of idealizations and simplifications to describe reality. Further, probability distributions and predictions introduce additional uncertainty, especially if the observed data only "suggests" a particular distribution.

In engineering decisions must be made based on incomplete, imperfect data, and/or imperfect models. Conservatism can be built into the designs of structures by applying choosing to design for the worst possible scenario of extreme loads and weakened resistance. This is impractical and results in designs that are too costly to build. On the other hand, a design based on the lowest cost will not provide the desired level of safety

or durability. Procedures must be enacted that account for the trade offs between cost and levels of performance. The precise level of safety or performance is not a single value, rather it is chosen based on the acceptable level of failure that society dictates. This is the essence of reliability.

3.2   Failure in Engineering

The failure of an engineered structure is not necessarily a catastrophic collapse. Failure is typically defined as when a structure fails to perform as designed. Limit states are defined in the code include: (1) ultimate and (2) serviceability limit states. Ultimate limit states involve the load carrying capacity of the structural members to resist loads in various forms including: compression, tension, flexural bending, shear, buckling and torsion (Barker and Puckett 1997). Exceeding the strength limit state implies that the structure is loaded beyond the threshold of its original design. This may involve yielding, buckling, fracture, etc. at an extreme load level at some instantaneous point in time. Therefore, the extreme combination of loads need only occur at a single point in time during the life of the structure. The AASHTO LRFD Strength-I criteria is a typical example of an ultimate limit state (AASHTO 2004). A load model is provided such that, when factored, represents the most severe load that the bridge should see during its 75-year service life.

The serviceability limit state, on the other hand, describes a set of secondary failure criteria that may occur over a short period of time (less than the design life) or have some cumulative development. Examples of serviceability failures include: excessive deflection, vibration, cracking, and fatigue. These failures occur at service load levels during the lifetime of the structure and represent durability and maintenance concerns.

For example, the AASHTO LRFD Service-III limit state describes the limit state for prestressed concrete members to control cracking of the bottom section and exposure of the prestressing strands to corrosive elements (AASHTO 2004).

3.3   Random Variables

Each load or material parameter takes on its own distribution of values. Typically, each can be described by a probability density function, PDF, which follows a defined mathematical function. When a random variable can be described by a function, various aspects can easily be determined such as mean, standard deviation, and future value predictions. The following is a collection of the most common distributions in structural engineering.

3.3.1   Normal Random Variables

The normal or Gaussian distribution, which can be used to describe most naturally occurring phenomena (Ang and Tang 1975), is the most common used in structural engineering reliability. The probability density function, PDF for the standard normal variable **Z** is:

$$\phi(z) = \frac{1}{\sqrt{2\pi}} \exp\left[-\frac{1}{2}(z)^2\right] = f_Z(z) \qquad \text{Eq. 3.1}$$

Where, **Z,** the normal variate is expressed in terms of the mean, **μ**, and standard deviation, **σ**:

$$z = \frac{x - \mu_x}{\sigma_x} = \left(\frac{1}{\sigma_x}\right)x + \left(\frac{-\mu_x}{\sigma_x}\right) \qquad \text{Eq. 3.2}$$

The standard normal is a special case of the normal random variable where the mean is equal to zero and the standard deviation is equal to one. A cumulative probability function, CDF and PDF for the standard normal is shown in Figure 3.1. The most significant feature of the normal distribution is the fact that probability above and below the mean is equal to one-half. This aspect is most visible in the CDF of Figure 3.1b where the CDF intersects the ordinate at 0.5.

Often, the inverse of the normal CDF is calculated to obtain the standard variate, Z, corresponding to a given probability. There is no closed mathematical solution for the inverse normal. Fortunately, most common spreadsheet applications contain the numerical approximation for Z as given in Eq. 3.3. Before access to computers, the inverse standard normal was obtained from the reference tables of statistical texts (Ang and Tang 1975). An approximation of Z can be calculated from the following equation for probabilities equal to or less than 0.5 (Nowak and Collins 2000):

$$z = \Phi^{-1}(p) = -t + \frac{c_0 + c_1 t + c_2 t^2}{1 + d_1 t + d_2 t^2 + d_3 t^3} \qquad \textbf{Eq. 3.3}$$

Where:

$$t = \sqrt{-\ln(p^2)} \qquad \textbf{Eq. 3.4}$$

And where:

$$c_0 = 2.515517$$
$$c_1 = 0.802853$$
$$c_2 = 0.010328$$
$$d_1 = 1.432788$$
$$d_2 = 0.189269$$
$$d_3 = 0.001308$$

For probabilities greater than 0.5, Z is calculated for a probability of p' = (1 - p) since the normal distribution is symmetric about the mean at zero.

3.3.2 Lognormal Distribution

A distribution can be described as being lognormal if the natural logarithm of X, $\ln(X)$, is normal is normal. The variance and mean, respectively, are given as follows:

$$\sigma^2{}_{\ln(x)} = \ln\left(V_x^2 + 1\right) \qquad \text{Eq. 3.5}$$

$$\mu_{\ln(x)} = \ln(\mu_x) - \frac{1}{2}\sigma^2{}_{\ln(x)} \qquad \text{Eq. 3.6}$$

Since the lognormal is related to the normal distribution, the probabilities associated with the lognormal variate can be found in the standard normal probability table. The standard variate of the lognormal distribution is:

$$S = \frac{\ln(x) - \mu_{\ln(x)}}{\sigma_{\ln(x)}} \qquad \text{Eq. 3.7}$$

The resulting PDF for the lognormal distribution is given as:

$$f_x(x) = \frac{1}{x \cdot \sigma_{\ln(x)}} \phi\left(\frac{\ln(x) - \mu_{\ln(x)}}{\sigma_{\ln(x)}}\right) \qquad \text{Eq. 3.8}$$

Further discussion of the shape and extremal behavior of the lognormal distribution will be given in terms of the probability papers and predictions.
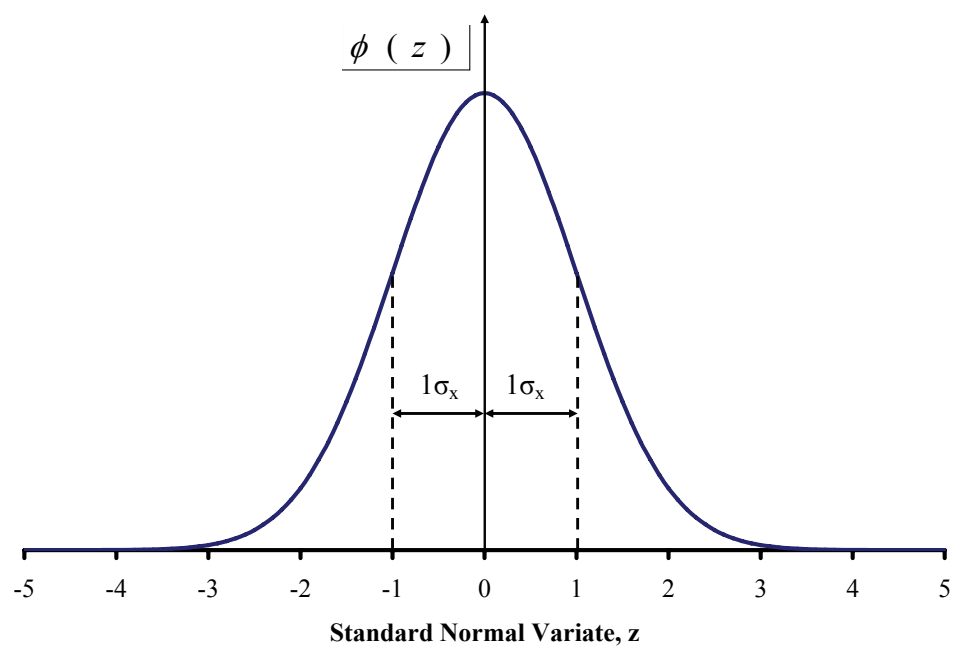
(a)
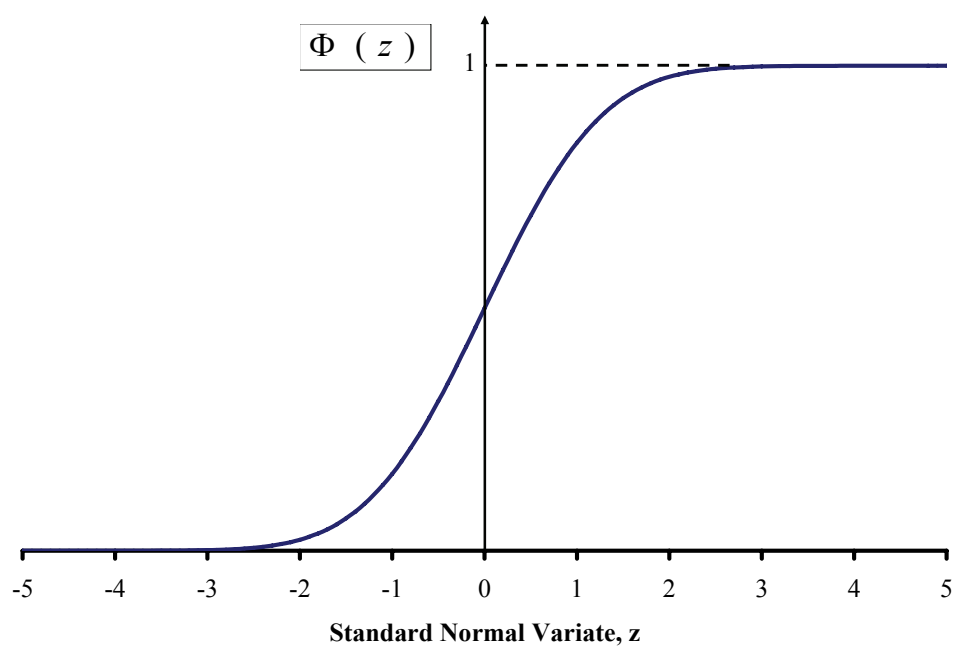
(b)

Figure 3.1 Standard Normal PDF (a), and CDF (b)

3.4   Reliability Theory

As mentioned previously, reliability principles are built into the design code to ensure a consistent safety level for different materials and types of loads. The following is an introduction to the quantification and application of random variables used to describe the statistical nature of random variables. Nowak and Collins (2000) and Ang and Tang (1975, 1984) provide comprehensive introduction to the study of random variables in engineering.

In general, safety in design is defined as having a quantity of capacity or resistance, **R**, beyond than the loading demand, **Q**. This surplus capacity is defined as the safety margin or safety factor. The performance of a structure can be described by a limit state function $g(X_1, X_2, ... X_n)$, where X_i are various parameters such as compressive strength of concrete, yield strength of steel, Young's Modulus, moment of inertia, etc. The function is defined as the loading minus the resistance, or:

$$g(R, Q) = R - Q$$

<div align="right">**Eq. 3.9**</div>

The function can take on three possible results:

$$g(\mathbf{X}) > 0 \quad \text{Safety}$$

$$g(\mathbf{X}) = 0 \quad \text{Threshold between safety and unsafe}$$

$$g(\mathbf{X}) < 0 \quad \text{Failure}$$

The precise amount of reserve capacity, or the result of Eq. 3.9, is the margin of safety or probability of failure.

PDF

Resistance, R

Load Effect, Q

R < Q

X
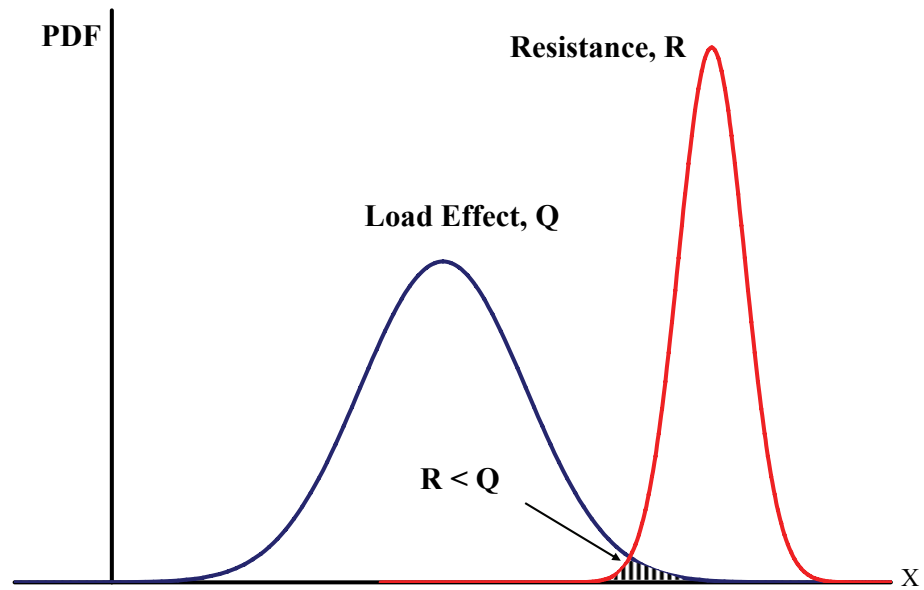
Figure 3.2 Probability density functions for load, Q, and Resistance, R. (Nowak and Collins, 2000)

PDF

$G(R,Q)=R - Q$

Probability of
Failure

Mean, μ_G

0

X
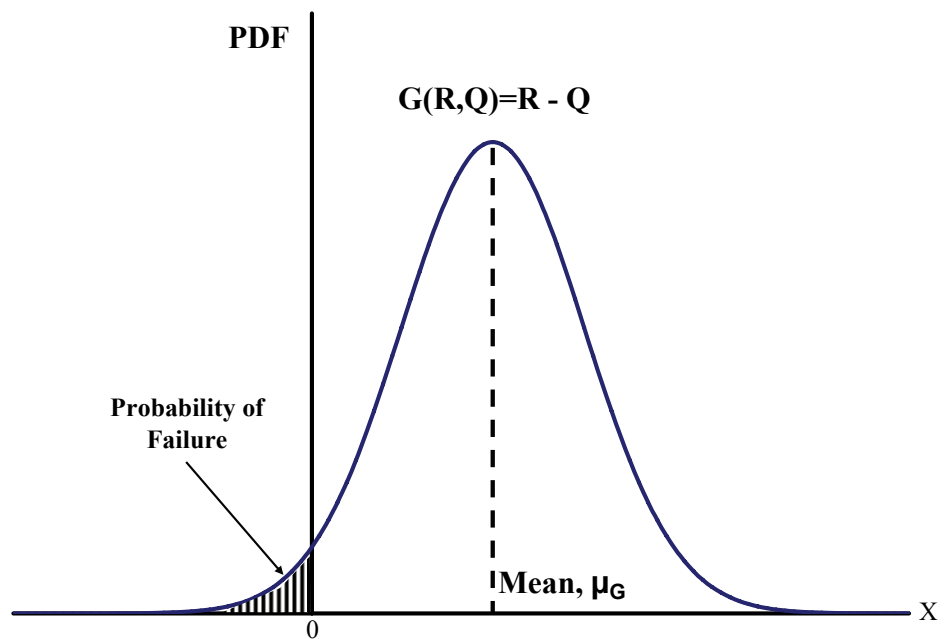
Figure 3.3 Performance function, G, showing failure region left of the ordinate (Nowak and Collins 2000)

3.4.1   Extreme Type II (Gumbel Distribution)

The family of extreme value distributions, including the Gumbel, are used to describe extremes that occur infrequently but with large magnitudes. Typically, the Gumbel can be used to describe wind speeds, flood levels, ocean wave intensity, etc (Coles 2001). The CDF and PDF (Nowak and Collins 2000) of this variable are given as:

$$F_x(x) = e^{-e^{-\alpha(x-u)}}$$
<div align="right">Eq. 3.10</div>

$$f_x(x) = \alpha \cdot e^{-e^{-\alpha(x-u)}} \cdot e^{-\alpha(x-u)}$$
<div align="right">Eq. 3.11</div>

Where: u is the largest characteristic value and $1/\alpha$ is a measure of dispersion.

The standard variate of the Gumbel distribution can be determined by solving the following function for s:

$$p = F_s(s) = e^{-e^{-s}}$$
<div align="right">Eq. 3.12</div>

<div align="right">Eq. 3.13</div>

$$\text{Solving for s, } \quad s = \ln\left(\frac{1}{\ln\left(1/p \right)} \right)$$

Where, s is the standard Gumbel variate and p is the plotting position defined as m/(1+N), where m is the order of the data point when the data is sorted ascending, and N is the total number of observed data points.

3.5   **Extreme Value Theory**

Extreme Value Theory (EVT) as the name implies deal with extreme and rare phenomena that are rare yet significant. The most common applications in terms of Civil Engineering are to describe physical phenomena with a long return period such as ocean

waves, flooding, wind speeds, earthquakes, hurricanes, etc. Regardless of the specific

application, the basic focus of EVT is the following: to find an extreme distribution to

predict future levels of occurrence of physical phenomena long into the future.

According to the application extreme events may occur at very low or very high levels.

At these levels most every physical phenomena exhibits extreme behavior since the

probability of occurrence decreases rapidly for more extreme events. For the purposes of

bridge engineering, there is a need to determine the extreme occurrence of live-load that a

structure is likely to encounter during its 75 to 100 year service life. The following is a

brief introduction to the fundamentals of Extreme Value Theory.

Coles (2001) provides a complete introduction to the fundamentals of EVT. The

following theorems and statistical distributions lay the framework for EVT.

3.5.1 Asymptotic Models

The asymptotic model forms the cornerstone of EVT. The model is based on the

statistical behavior of the following:

$$M_n = \max\{X_1, X_2, ..., X_n\}$$

Eq. 3.14

where X_1, X_2, …,X_n, is a sequence of independent random variables having a common

distribution function F. The value of X_i is usually represented in terms of engineering

units as measured on a regular time-scale, i.e., hourly, monthly, yearly values. M_n

represents the maximum of the process over n time units of observation. If n is the

number of observations in a year, then M_n corresponds to the annual maximum value. In

theory the distribution of M_n can be derived exactly for all values of n such that:

$$\Pr\{M_n \leq z\} = \Pr\{X_1 \leq z, ..., X_n \leq z\}$$
$$= \Pr\{X_1 \leq z\} \times ... \times \Pr\{X_n \leq z\}$$
$$= \{F(z)\}^n$$

Eq. 3.15

However, the theory is not useful in practice since the distribution of observed data

points, F, is unknown. It may be possible to estimate F from observed data using

statistical techniques then to substitute the estimate into Eq. 3.15. Error in the estimation

of F can be substantially propagated for F^n. One alternative is to look for approximate

models for F^n, which can be estimated on the basis of the extreme data only (the upper

tail). This is similar to approximating the distribution of sample means by the normal

distribution, according to the central limit theorem.

The behavior of F^n as $n \to \infty$ is now considered. The variable Mn is normalized to

avoid upper and lower limit degeneration. The new normalized variable is:

$$M_n^* = \frac{M_n - b_n}{a_n}$$

Eq. 3.16

Where $a_n > 0$ and b_n is real. Proper choices of a_n and b_n will stabilize the location and

scale of M_n^* as n increases. Distributions for M_n^* are then sought using appropriate

choices for a_n and b_n.

3.5.2   Extremal Types Theorem

The range of limit distributions for M_n^* is given by the Extremal Types Theorem.

If there exist sequences of constants $\{a_n > 0\}$ and $\{b_n\}$ such that:

$$\Pr\{(M_n - b_n)/a_n \leq z\} \to G(z) \quad n \to \infty$$

Eq. 3.17

where G is a non-degenerate distribution function, then G belongs to one of the following

families:

I: $G(z) = \exp\left\{-\exp\left[-\left(\dfrac{z-b}{a}\right)\right]\right\}, -\infty < z < \infty;$ Eq. 3.18

II: $G(z) = 0, z \leq b;$ Eq. 3.19

$G(z) = \exp\left\{-\left(\dfrac{z-b}{a}\right)^{-\alpha}\right\}, z > b;$

III: $G(z) = \exp\left\{-\left[-\left(\dfrac{z-b}{a}\right)^{\alpha}\right]\right\}, z < b$ Eq. 3.20

$G(z) = 1, z \geq b$

for parameters $a > 0$, b and, in the case of families II and III, $\alpha > 0$. The theorem in Eq.

3.17 essentially states that the rescaled sample maxima $(M_n - b_n) / a_n$ converge in

distribution to a variable having a distribution within one of the families I, II, and III.

These three classes of distributions are known as extreme value distributions, where I, II,

and III formally known as the Gumbel, Fréchet, and Weibull families, respectively. Each

family has a location and scale parameter, b and a, respectively. The Fréchet and Weibull

families have a shape parameter α.

The Extremal Types Theorem stated in Eq. 3.17 implies that when M_n can be

stabilized with suitable sequences $\{a_n\}$ and $\{b_n\}$ the corresponding normalized variable

M_n^* has a limiting distribution that must be one of the three types of extreme value

distributions. The three types of extreme value distributions are only applicable as limits

for the distribution M_n^*, not the population distribution F. This is an application of the

central limit theorem as it applies to extremes.

3.5.3   Generalized Extreme Value Distribution (GEV)

The Gumbel, Fréchet, and Weibull families of distributions can be combined into a more general form, the Generalized Extreme Value (GEV) distribution:

$$G(z) = \exp\left\{ -\left[1 + \xi\left(\frac{z - \mu}{\sigma} \right) \right]^{-1/\xi} \right\},$$

Eq. 3.21

valid over the range $\{z : 1 + \xi(z - \mu)/\sigma > 0\}$, where the parameters satisfy $-\infty < \mu < \infty$, $\sigma > 0$, and $-\infty < \xi < \infty$. The model has three parameters: a location parameter, μ; a scale parameter, σ; and a shape parameter, ξ. The type II and type III classes of extreme value distributions are given for the cases of when $\xi > 0$ and $\xi < 0$, respectively. The Gumbel family is given when $\xi \rightarrow 0$, which gives:

Eq. 3.22

$$G(z) = \exp\left\{ -\exp\left\{ -\left(\frac{z - \mu}{\sigma} \right) \right\} \right\}, -\infty < z < \infty.$$

The most important step in the use of extreme value distributions is the choice of parameters, especially the shape parameter, ξ. The data must be used to find the best shape factor. There is no need to select a particular family of extreme value distributions; only the parameters must be chosen.

3.6   Normal Probability Paper (NPP)

One method of plotting observed data independent of a chosen distribution is to plot the data on a probability paper or scale. The horizontal axis has a scale equal to the

units of the given data, for example, stresses, moment, or loads. The vertical axis corresponds to the standard variate for which the paper was developed.
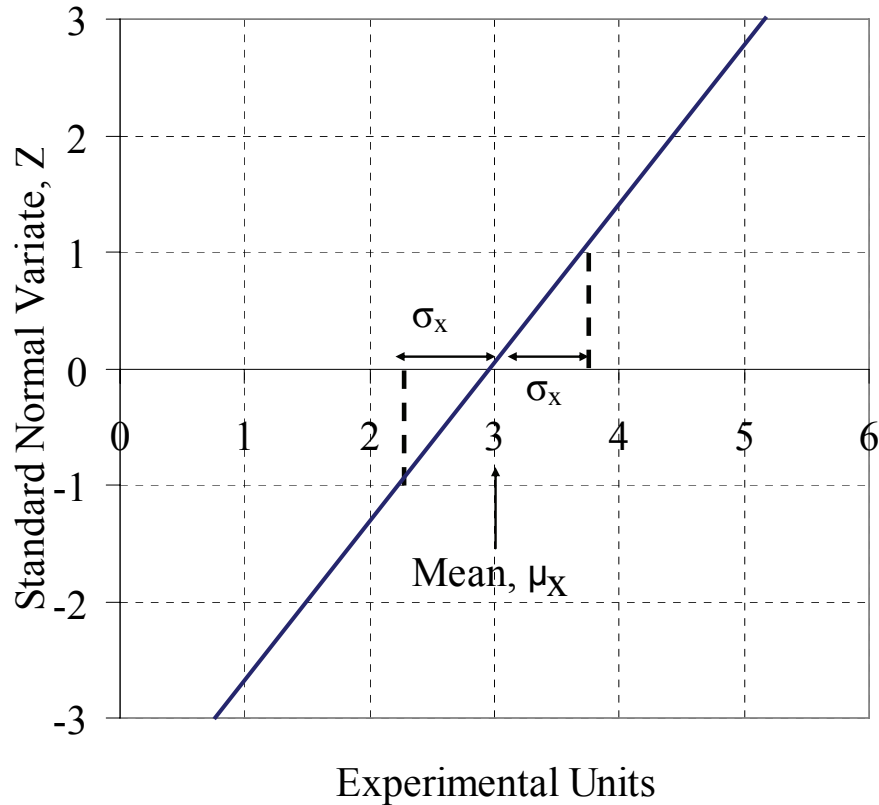
Figure 3.4 Normal Probability Paper with associated mean and standard deviation shown

Figure 3.4 shows a typical normal probability paper. The vertical scale is the standard normal variate, Z. Recall from Eq. 3.2 that, Z, can be expressed as a function of X plus a constant related to the mean and standard deviation. Therefore, a straight line on the normal probability paper represents a perfect normal distribution. The following procedure describes the construction of normal, or any other probability paper for that matter (Ang and Tang 1975):

(1) Sort the observed data (having N data points) in ascending order from least to greatest

(2) Assign an index, m, starting at 1 for the lowest value, and N for the greatest

value to each data point

(3) Assign a cumulative probability to each data point, where $p = m/(N+1)$. The

domain of the probability ranges from zero to one: $0 < p < 1$.

(4) Using a spreadsheet function, for example NORMSINV(p), available in the

most popular brand of spreadsheet applications, calculate the standard normal

variate also called the inverse standard normal $Z(p)$, or alternatively, using Eq.

3.3 and Eq. 3.4. Another alternative would be to use commercially available

probability paper.

(5) Finally, create an XY scatter plot where the x-values are the observed data in

the original engineering units, and the y-values are the calculated standard

normal variate, Z.

Data with any underlying distribution may be plotted on normal probability paper.

However, data that does not appear linear on the NPP scale indicates that the data does

not follow a normal distribution. In this case, other probability papers may be attempted

to find a suitable linearity. For the case when the NPP plot of the observed data is linear,

a specific normal distribution can be found and described by parameters of the mean, μ_x

and standard deviation, σ_x. From Figure 3.4, the mean is determined graphically as the

intersection of the plot and the abscissa, corresponding to a Z equal to zero, in this

example the mean is 3 (expressed in native units). The corresponding cumulative

probability at the mean is 0.5. Recall that the standard normal distribution, as shown in

Figure 3.1b, contains an equal amount above and below the mean. Therefore, the NPP

mean can be thought of as a median value. The sample standard deviation can also be

determined graphically from the plot in Figure 3.4, as the X-value corresponding to a Z

value of plus or minus 1, in other words:

$$\text{Sample mean, } \overline{X} = Z(0) \qquad\qquad \textbf{Eq. 3.23}$$

$$\text{Sample Std. Deviation, } s_x = Z(1) \text{ or } s_x = Z(-1) \qquad \textbf{Eq. 3.24}$$

Where, Z(x) is described by Eq. 3.2 and is in the form of Z=AX+B, where it represents a

linear fit to the NPP plotted data.

The highest Z value on the vertical axis represents a return level equal the duration

over which the data was collected. If the observed data fits a linear function within the

NPP scale, levels of the observed parameter can be estimated for future return levels not

present in the data. For example if data was sampled over a period **T**, and **N** data points

were observed, the corresponding variate, **Z**, of the greatest observed value would be

$\Phi^{-1}(p_0)$, where p_0=N/(N+1). Therefore the **Z** value at a return period equal to twice the

sample duration would be: $\Phi^{-1}(p_2)$, where p_2=2N/(2N+1). Values of the variate for

different number of data points and associated probabilities are given in Table 3.1 and

Table 3.2. Note that the variate is not sensitive to change although the number of

observations increases tremendously. This characteristic facilitates the prediction of

future levels far beyond the initial sample period.

Table 3.1 Values of Z given number of observations

N	p=N/(1+N)	Z=Φ⁻¹(p)
10	0.9	1.335
100	0.99	2.330
1,000	0.999	3.091
10,000	0.9999	3.719
100,000	0.99999	4.265
1,000,000	0.999999	4.753
10,000,000	0.9999999	5.199
100,000,000	0.99999999	5.612
1,000,000,000	0.999999999	5.998
10,000,000,000	0.9999999999	6.361

Table 3.2 Number of observations given the variate, Z

N (Approx.)	p=N/(1+N)	Z=Φ⁻¹(p)
6	0.8	1
44	0.98	2
741	0.999	3
31,574	0.99997	4
3,488,555	0.9999997	5
1,013,594,635	0.999999999	6

To illustrate the prediction procedure, consider the following example. All trucks

passing on a particular road are weighed. Over an observation period of 2 weeks, 10,000

trucks are weighed. Say that the 75-year truck weight needs to be estimated. The

cumulative probability associated with the greatest recorded weight is 10,000/10,001 or

0.9999. The corresponding variate would be 3.719. Assuming that the NPP plotted data

exhibits a clear linear trend; the future value would correspond to the intersection of the

linear extension of the data trend with a future variate level. Given that 10,000 trucks

traveled the road within 14 days, the average daily truck traffic (ADTT) is

10,000/14=714 trucks per day. The number of trucks in 75-years, assuming all other

factors constant, would be:

$$N_{75Year} = \left(\frac{10,000 trucks}{14 days}\right) \cdot 365 \frac{days}{year} \cdot 75 years = 19553571$$

<div align="right">**Eq. 3.25**</div>

And the corresponding standard normal variate would be:

$$\Phi^{-1}(p_{75}) = \Phi^{-1}\left(\frac{19553571}{19553571+1}\right) = 5.323$$

<div align="right">**Eq. 3.26**</div>

Now the 75-year truck weight could be estimated by extending the NPP linear plot to a Z-value of 5.323 and reading the corresponding weight from the abscissa.

3.7 Code Calibration

There are several methods to calibrate a design code. Codes can be calibrated by judgment, fitting to older codes, reliability, or any combination of these methods (Barker and Puckett, 1997). Calibration by judgment entails an iterative process whereby the calibration is tested through performance. If failure occurs, the code factors are increased. If the code parameters are found to be good, then no change is made. This method provides an inconsistent margin of safety because parameters that do not lead to failure will not be adjusted and will remain over-conservative. Furthermore, parameters that are based on long return periods such as floods or earthquakes may not be conservative enough since the limit state has not been reached yet.

Calibration by fitting entails matching the parameters of some previous code or guideline. This is done when there is a change in code format or philosophy. The new code factors are adjusted to achieve a similar designs and performance as in the previous code. The main motivation of this method is to maintain consistency between previous designs and new designs to maintain the industry standard.

Calibration by fitting ensures that designs done by the new code are similar to existing designs. Essentially the code parameters are adjusted to achieve similar designs for the past and present codes. Though simple, it's inconsistent in terms of margins of safety. The new code will mirror the previous code and any excessive margins of safety will be carried on in the new code.

Finally, the new code may be calibrated using reliability theory. Reliability theory is a more formal process that eliminates much of the historical code legacies by replacing them with more logical and rational methods. The formal process for calibrating code factors for load and resistance are (Barker et al., 1991):

(1) Compile the statistical database for load and resistance parameters

(2) Estimate the level of reliability inherent in the current design methods of predicting structural capacities

(3) Observe the variation of the reliability levels with different span lengths, dead to live load ratios, load combinations, types of bridges, and methods of calculating strengths

(4) Select a target reliability index based on the margin of safety within the current designs

(5) Calculate load and resistance factors consistent with the selected target reliability index and consider experience and judgment with the results.

The calibration of the current AASHTO LRFD Design Specifications was done by Nowak as part of NCHRP Project 12-33 (Nowak 1999). The work defines the procedure for determining load and resistance factors for the new LRFD code. The work included the development of load models, resistance models, reliability analysis procedures, selection of target reliability indices, and calculation of load and resistance factors for the new code.

Bridge loads include dead load, live load (static and impact), environmental loads (temperature, wind, and earthquake), and other loads (collision, braking forces, concrete shrinkage, etc) (Nowak 1999). The most common types of loads are dead and live loads. For the most part, dead loads are easily determined and consistent, as indicated by their lower load amplification factor. Live loads that consist of random truck traffic and impact are much more difficult to quantify. Live loads vary by site, over time, and no two vehicles are exactly the same. Therefore, statistical distributions and models are developed to describe live loads. Live loads depend on the following parameters: fraction of traffic that are trucks (ADTT), span length, truck weight, axle loads, axle spacing, position of the vehicle, truck superposition or mutlipresence, girder spacing, and stiffness of the structural members (Nowak and Hong 1991).
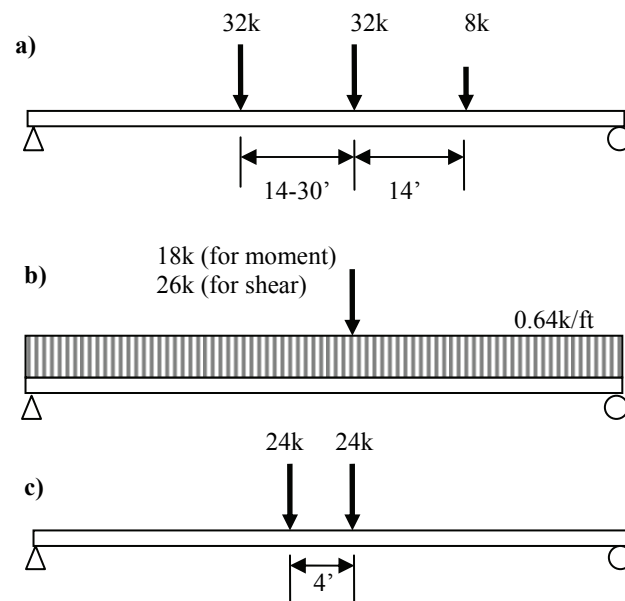
Figure 3.5 Design live-load models in AASHTO 1989: a) Standard HS20 truck, b) HS20 Lane Loading, and c) Military Loading

The load effects are given in terms of simple moment, simple shear, negative moment on two continuous spans, continuous positive moment, and continuous shear. Using the available, trucks are passed over an influence line to determine their load effects on various span lengths. The load effect is represented in terms of a bias factor, or the ratio of the effect compared to some nominal value (design truck model). The nominal load models from the original AASHTO design code are given in Figure 3.5 (AASHTO 1989). A new load model was developed for the AASHTO LEFD Design code with the goal of producing more uniform bias for load effects over different span lengths. The new load model is shown in Figure 3.6.
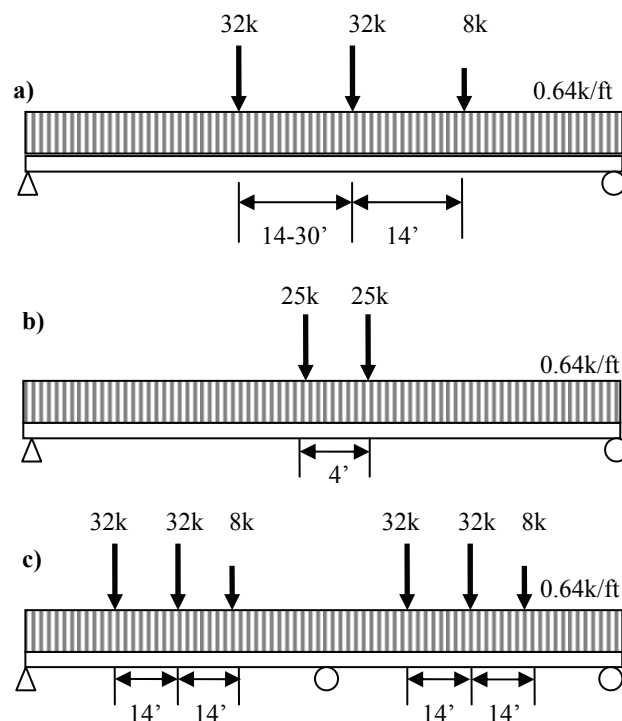
Figure 3.6 HL-93 Design Live Load Model for the AASHTO LRFD Code: a) Truck and Uniform Load, b) Tandem and Uniform Load, c) Alternative Load for Negative Moment 9 (reduce to 90%)

3.7.1 Ontario 1975 Truck Survey Data

Truck load statistics can be measured from three possible sources: permanent weigh-in-motion data, static weigh stations, or police enforcement records. Weigh-in-motion systems measure truck weights surreptitiously without alerting drivers. As such, WIM data remains the most reliable source of unbiased truck weight data. When weight data is sourced from enforcement agencies such as weigh stations or police citations, the information generally represents only overweight vehicles or other violations. Further, drivers who realize that weight enforcement is in effect may avoid the checkpoint altogether, resulting in a biased dataset. Data that most accurately reflects the truck population is an essential input for any load factor calibration.

With the evolution of truck weighing technology since the 1970s, the amount of available truck weight data grew steadily into a large resource for the engineering community. The Ontario Ministry of Transportation utilized weigh-in-motion systems to conduct a truck weight survey in 1975 in advance of the OHBDC 1979 calibration (Nowak and Lind 1979). Other surveys contributed to the WIM database and were completed in 1979, 1980-1981, 1982, and 1988.

The Ontario Truck Survey data collected in 1975 is referred to as the Ontario-75 data. The Ontario-75 data contains 9250 truck records that represent the heavy truck population of the general population sampled. (Agarwal and Wolkowicz 1976). The Ontario-75 data was used by Nowak and Hong (1991) to develop a live load model as part of the AASHTO LRFD code calibration (Nowak 1995). The data was run over beam influence lines to obtain simple moments, simple shears, and negative moments for spans ranging from 30 to 200 feet. The maximum load effects for each truck were represented

in terms of ratios to the nominal HS20 load model of the current code at that time,

AASHTO 1989 (Figure 3.5). The maximum load effect was based on the governing load

case of the following from Figure 3.5: (a) HS20 design truck, (b) single point load and

distributed lane load, and (c) the military tandem load. The governing design values for

the HS20 load model in terms of maximum simple moment, simple shear and negative

moment are given in Table 3.5. The HS20 standard truck loading typically controls up to

a span length of 140 feet for simple moment and 120 feet for simple shear. For longer

spans the standard lane loading, consisting of a single point load (18k for moment, 26k

for shear) and 0.64 k/ft distributed load, controls the design.

The maximum load effects (simple and negative moment, and simple shear) were

calculated for each Ontario-75 truck record and plotted on normal probability paper,

NPP. The mean bias values for the observed data ranged from 1.12 to 1.76, 1.24 to 1.67,

and 0.83 to 1.73 for mean maximum simple moment, simple shear, and negative moment,

respectively. The data for each span were then extrapolated using the properties of the

normal distribution on the normal probability paper. The 75-year maximum load effects

were reported as ranging from 1.65 to 2.10, 1.49 to 1.93, and 0.92 to 1.93 for simple

moment, simple shear, and negative moment, respectively.

Since the survey data represented only heavy trucks an assumption had to be

made to relate the sample to a more general sample set. Also the time duration was

needed to calculate the normal variate corresponding to the 75-year return level which is

needed for extrapolation. To make this adjustment, it was assumed that the heavy survey

truck data represented the upper twenty percent of a two week sample on a typical

interstate highway. Therefore the average daily traffic, ADT, would be assumed to be

5000 vehicles per weekday. Since the truck population was assumed to account for the upper twenty percent of the traffic, the average daily truck traffic (ADTT) was assumed to be 5000 divided by 5, or 1000 trucks per weekday. Typical values for the normal variate, **Z,** by the number of samples is given in Table 3.1. For example, the ADTT for the Ontario-75 data is 1000 trucks per day. The variate for a one day period is $\Phi^{-1}(1/1001)$, or 3.091. The expected number of trucks in the entire 75-year design life of a bridge would therefore be 1000 multiplied by 260 weekdays per year multiplied by 75 years, or 19.5×10^6 trucks. The 75-year normal variate would then be $\Phi^{-1}(1/(N+1))$, or 5.322.

To account for load effects due to multiple trucks, assumptions had to be made regarding the frequency of truck mutlipresence, and the corresponding weights. The frequency of mutlipresence events (Table 3.3) were based on limited bridge WIM studies conducted by Nowak, Nassif, and Defrain (1993). For the case of both side by side and following the correlation of the truck weights were assumed based on three levels: (1) no correlation (ρ=0), (2) partial correlation (ρ=0.5), and (3) full correlation (ρ=1.0). The correlation of weights is summarized in Table 3.4.

The side by side case represents the case of two trucks in adjacent lanes where the longitudinal distance between the front axles is less than six feet (Nowak et al, 1993). The side-by-side often controls the design since two lanes contribute load to a single girder. As given in Table 3.3, it was assumed that one out of every fifteen trucks (6.67%) will be involved in a side by side event. Within the cases of side by side, it was assumed that 1/30 (3.33%) side by side events or 1/450 (0.22%) total trucks would contain two fully correlated trucks. Using the correlation definitions in Table 3.4, the case of two

fully correlated side by side trucks is defined as two 2-month trucks traveling in adjacent lanes over a bridge. Given the Ontario-75 data, a 2-month truck corresponds to a simple moment ratio of 1.80*HS20 on a 120ft simple span. In other words, 1/450 trucks on the highway will occur such that two 130-kip trucks are side by side. Given a site with an ADTT of 1000, such as the Ontario-75, this would mean that about 67 side-by-side events would be expected per day with 2 fully correlated heavy truck events occurring per day.

Table 3.3 Summary of LRFD Calibration Multipresence assumptions (Nowak 1999)

Loaded Lanes	Frequency of Following	Following $\rho=0.5$	Following $\rho=1.0$	Headway
Single Lane	1/50	1/150	1/500	Less than 100 ft
Loaded Lanes	**Frequency of Side-by-side**	**Side-by-side $\rho=0.5$**	**Side-by-side $\rho=1.0$**	**Transverse Distance btw. Trucks**
Two Lanes	1/15	1/150	1/450	4 ft.

Table 3.4 Load parameters for two lane conditions (Nowak 1999)

Loaded Lanes	Correlation	Lane	N	Z	Time
One		L_1	20,000,000	5.33	75 years
Two	r = 0	L_1	1,5000,000	4.83	5 years
		L_2	1	0.00	Average
	r = 0.5	L_1	150,000	4.36	6 months
		L_2	1,000	3.09	1 day
	r = 1.0	L_1	50,000	4.11	2 months
		L_2	50,000	4.11	2 months

Table 3.5 Governing HS20 Design Values for Simple Moment, Simple Shear, and Continuous Negative Moment

Span Length (ft)	Governing Simple Moment (k-ft)	Governing Simple Shear (k)	Governing Two-Span Cont. Neg. Moment (k-ft)
10	80	32	43.68
20	160	41.6	123.16
30	282.1	49.6	192.29
40	449.8	55.2	266.56
50	627.9	58.5	373.21
60	806.5	60.8	495.85
70	985.6	62.4	634.49
80	1164.9	63.6	789.13
90	1344.4	64.5	959.77
100	1524	65.3	1146.4
110	1703.6	65.9	1349
120	1883.3	66.4	1567.6
130	2063.1	67.6	1802.3
140	2242.8	70.8	2052.9
150	2475.1	74	2319.4
160	2768	77.2	2602
170	3077.1	80.4	2900.6
180	3402.1	83.6	3215.2
190	3743.1	86.8	3545.7
200	4100	90	3892.5
210	4473	93.2	4255.1
220	4862	96.4	4633.7
230	5267	99.6	5028.3
240	5688	102.8	5439
250	6125	106	5865.6
260	6578	109.2	6308.2
270	7047	112.4	6766.8
280	7532	115.6	7241.5
290	8033	118.8	7732
300	8550	122	8238.6

Table 3.6 Comparison of Simple Moments for HS20 and HL93 Load Models

Span (ft)	AASHTO HS20 Simple Moment k-ft	AASHTO LRFD HL93 Simple Moment k-ft	Ratio HL93/HS20
10	80	88	1.10
20	160	232	1.45
30	282.1	397	1.41
40	449.8	578	1.29
50	627.9	820	1.31
60	806.5	1088	1.35
70	985.6	1372	1.39
80	1164.9	1672	1.44
90	1344.4	1988	1.48
100	1524	2320	1.52
110	1703.6	2668	1.57
120	1883.3	3032	1.61
130	2063.1	3412	1.65
140	2242.8	3808	1.70
150	2475.1	4220	1.70
160	2768	4648	1.68
170	3077.1	5092	1.65
180	3402.1	5552	1.63
190	3743.1	6028	1.61
200	4100	6520	1.59
210	4473	7028	1.57
220	4862	7552	1.55
230	5267	8092	1.54
240	5688	8648	1.52
250	6125	9220	1.51
260	6578	9808	1.49
270	7047	10412	1.48
280	7532	11032	1.46
290	8033	11668	1.45
300	8550	12320	1.44

The following case contains two trucks traveling the same lane. The distance from the last axle of the leading truck to the first axle of the following truck is defined as the headway and limited to a maximum of 100 feet. As given in Table 3.3, based on the data observed by Nowak et al., 1/50 trucks are followed by a truck with a headway distance less than 100 feet. It was also assumed that 1/500 trucks is involved in a fully correlated following event. For the Ontario data, 20 following events would be expected

per day with 2 fully correlated following events. The fully correlated event would

contain two trucks each weighing 130 kips following within a headway distance of less

than 100 feet. The moments and shears for the following case were based on simulations.

The simulation parameters included: truck configuration, weight, headway distance, and

frequency of occurrence. The minimum headway for any simulation case was 15 feet.

This limit was imposed to represent stopped truck traffic on the bridge with vehicles

bumper-to-bumper.

Overall, it was found that for single lane loading, the maximum moment was

governed by a single truck up to a span of 100 ft and by two following truck for longer

spans. For two-lane loading, the case of two fully correlated side-by-side trucks

controlled for all spans. The newly proposed load model, HL-93 (for Highway Loading

adopted in 1993), shown in Figure 3.3, was shown to provide a more consistent bias

compared to the HS20 load model (Figure 3.5).

3.7.2   Statistical Characteristics of Ontario-75 Data

The Ontario-75 data was collected by the Ontario Ministry of Transportation with

the intent of collecting heavy truck information. Therefore, the data is biased toward the

heavy side. The account for this bias, Nowak, assumed that the data represented the

upper twenty percent of the overall truck data. The details of the original Ontario-75

data are given in Table 3.7 and Figure 3.7 (Nowak and Hong 1991).

As given in Table 3.7, the dominant truck type for the Ontario-75 data is a five

axle truck with an average weight of 72.7 kips and COV of 15%. The data mirrors the

composition of most highways, in that; the most common truck type is Class 9 or five-

axle trucks. The shape of the overall gross vehicle weight histogram in Figure 3.7a

represents the probability density function, PDF, of the normal distribution as illustrated

in Figure 3.1a. The normal shape is important when plotting the data in normal

probability paper, since the prediction depends on the fit of the data to the normal

distribution.

Table 3.7 Load statistics for the Ontario 1975 Truck Survey Data (Agarwal and Wolkowicz 1976)

Axles	Count	Average Weight (k)	Std. Dev. Weight (k)	COV	Max Weight (k)	Average Length (ft)
2	23	28.9	4.4	0.15	35.6	14.1
3	1200	46.3	7.0	0.15	66.4	19.0
4	559	54.4	9.0	0.17	73.3	41.9
5	5515	72.7	10.6	0.15	117.5	45.9
6	1327	96.8	12.6	0.13	128.2	49.8
7	277	116.7	13.0	0.11	146.8	56.2
8	309	118.6	13.8	0.12	140.9	58.8
9	32	121.9	10.9	0.09	143.8	59.4
10	3	113.3	22.6	0.20	127.9	58.5
Overall	9245	74.5	21.1	0.28	146.8	43.4

3.7.3   Load Effect Envelopes of the Ontario-75 Data

The following section deal with the load effects for moments and shears as

reported by Nowak in the calibration of the LRFD Code. The truck records from the

Ontario-75 dataset were applied to influence lines to determine simple moments, simple

shears, and negative moments at various spans. The load effects were then extrapolated

to the 75-year expected levels using Normal Probability Paper, NPP. The load effect

ratios to the HS20 load model are given in Table 3.8
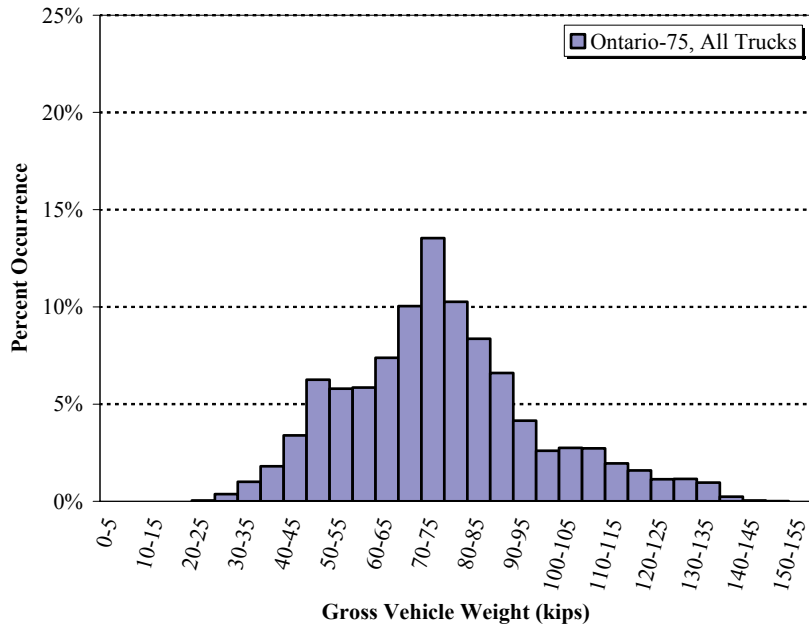
(a)
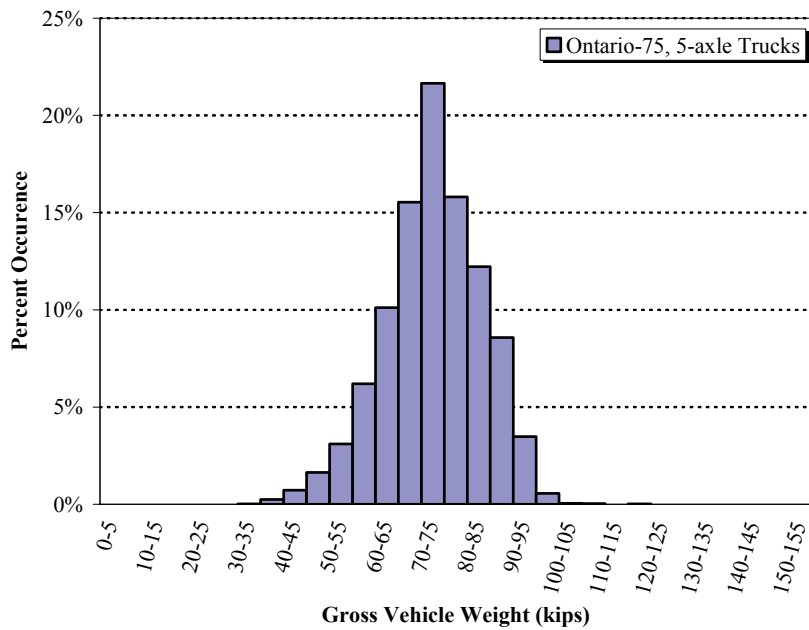
(b)

Figure 3.7 Gross vehicle weight frequency histogram for Ontario 1975 truck survey data: (a) for all trucks and (b) for 5-axle trucks (Agarwal and Wolkowicz 1976)

Table 3.8 Maximum 75-year load effects for Ontario-75 Data (Nowak 1999)

Span Length (ft)	Maximum 75-yr Simple Moment Ratio to HS20	Maximum 75-yr Simple Shear Ratio to HS20	Maximum 75-yr Neg. Moment Ratio to HS20
10	1.65	1.62	1.55
20	1.68	1.52	1.60
30	1.72	1.49	1.77
40	1.74	1.51	1.93
50	1.75	1.56	1.85
60	1.79	1.62	1.67
70	1.83	1.70	1.53
80	1.89	1.78	1.40
90	1.94	1.85	1.33
100	2.00	1.90	1.27
110	2.05	1.93	1.22
120	2.08	1.93	1.18
130	2.10	1.91	1.14
140	2.10	1.87	1.10
150	2.07	1.83	1.07
160	2.03	1.80	1.03
170	1.98	1.75	1.00
180	1.94	1.70	0.97
190	1.88	1.65	0.94
200	1.82	1.60	0.92

Additionally, the original Ontario-75 data was analyzed to replicate the findings of the NCHRP 368 LRFD Calibration. First, the original procedures outlined in the calibration were mirrored to reproduce the results (Figure 3.8). Then, these verified procedures would be replicated using the more recent WIM data to perform a site-specific calibration for New Jersey. The original calibration work was done using simple spans ranging from 10 to 200 feet. The current site specific calibration will include spans up to 300 feet to account for longer spans now commonly used. Advancements in construction materials, including high strength concrete and high performance steel, make longer spans possible now than were common when the original code calibration was performed.

(a) Simple Moment

(b) Simple Shear
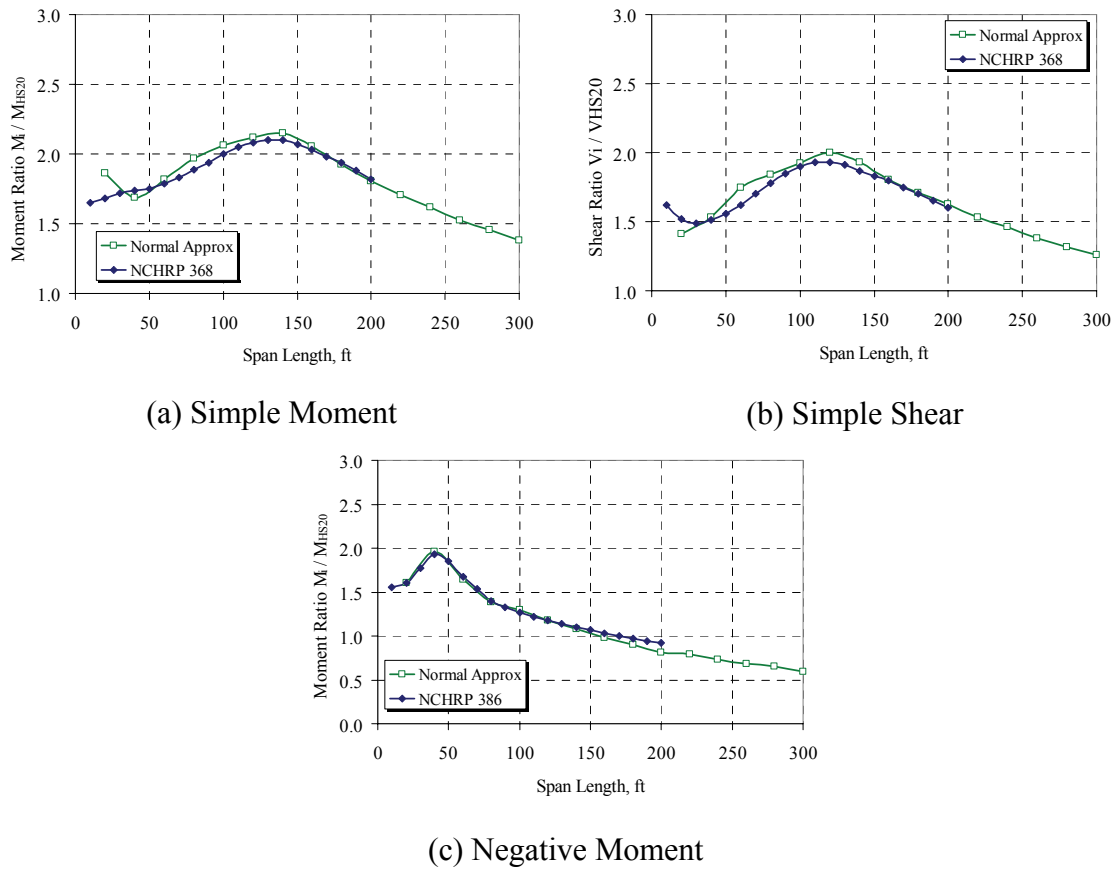
(c) Negative Moment

Figure 3.8 75-year extrapolated load effect comparison: original LRFD Calibration (Nowak 1999) and reproduced results, (a) simple moment, (b) simple shear, and (c) negative moment

The differences in the 75-year load effect extrapolations shown in Figure 3.8 between the original LRFD calibration and the reproduced results relate to the subjective nature of the original extrapolations. The current reproduction uses a spreadsheet application with linear regression curve fitting functions.

3.8   Fatigue Load Description

3.8.1   Rainflow Representation for Fatigue

Several formats are available for representing rainflow counted stress cycles. The two main output parameters in rainflow cycle counting are: (1) stress level and (2) the corresponding number of cycles.

3.8.1.1   Rainflow Histogram

The most common and simplest representation of rainflow results is a two-dimensional histogram. A typical rainflow histogram for Span 3 Girder 9 of Doremus Avenue Bridge is given in Figure 3.9 and Table 3.9. The histogram shown represents about 6 months of stress cycles at this location. The x-axis gives the stress cycle bins. The y-axis is the number of counted cycles in the corresponding bin. The range (width) of each bin is defined as the channel minimum and maximum bounds divided by the number of bins specified in the rainflow data parameters. The minimum, maximum, and number of bins or the Doremus Avenue Data logger were 0 ksi, 6 ksi, and 36, respectively. Therefore the width of each bin is (6 - 0) / 36, or 0.167 ksi. The x–axis labels in Figure 3.9 are the midpoint of each bin.

The rainflow histogram in Figure 3.9 shows that the majority of stress cycles are below 1.4 ksi. There is a secondary peak at about 2.1 ksi, indicating that there is a bimodal distribution within the truck population. As will be shown later in Chapter 5, the truck weight distribution for Doremus Avenue is bimodal, meaning that there are two distinct populations: loaded and unloaded. Cycles above 3 ksi were observed but do not appear on the rainflow histogram due to the relative scale. These cycles are shown the in

the rainflow data in Table 3.9. There were 21 cycles observed above 6 ksi. The exact

magnitude of these cycles is unknown since the maximum range of the system was set to

6 ksi. While these cycles are highly damaging, overall they contribute little to the total

damage.
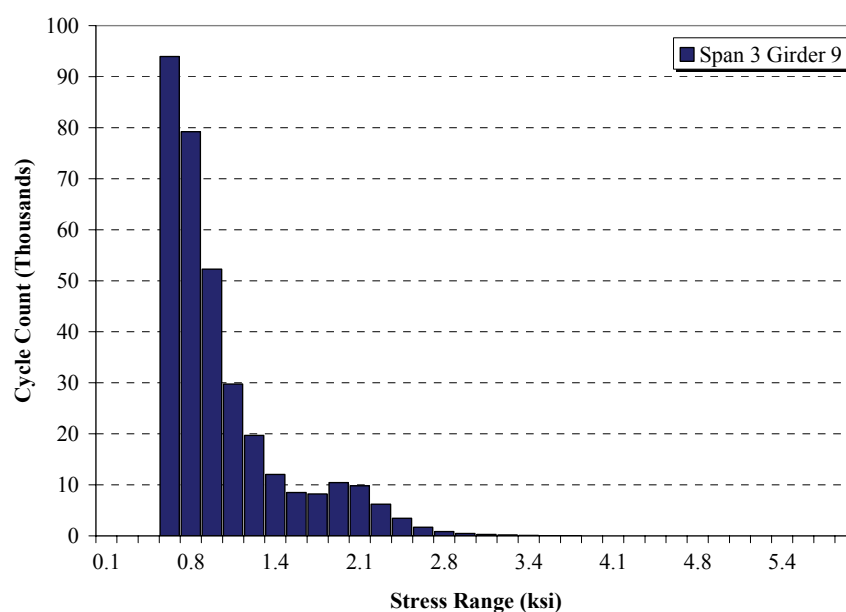
Figure 3.9 Rainflow histogram for Span 3 Girder 9 of Doremus Ave. Bridge

Table 3.9 Rainflow histogram detailed stress cycle information

Stress Range ksi (midpoint)	Number of Cycles	Stress Range ksi (midpoint)	Number of Cycles
0.08	(omitted)	3.08	265
0.25	(omitted)	3.25	150
0.42	(omitted)	3.42	89
0.58	93978	3.58	40
0.75	79210	3.75	24
0.92	52273	3.92	9
1.08	29760	4.08	7
1.25	19665	4.25	16
1.42	12046	4.42	8
1.58	8490	4.58	7
1.75	8214	4.75	4
1.92	10437	4.92	4
2.08	9822	5.08	11
2.25	6196	5.25	13
2.42	3412	5.42	7
2.58	1692	5.58	9
2.75	839	5.75	6
2.92	457	6.00+	21

3.8.1.2   Rainflow Matrix (3D Histogram)
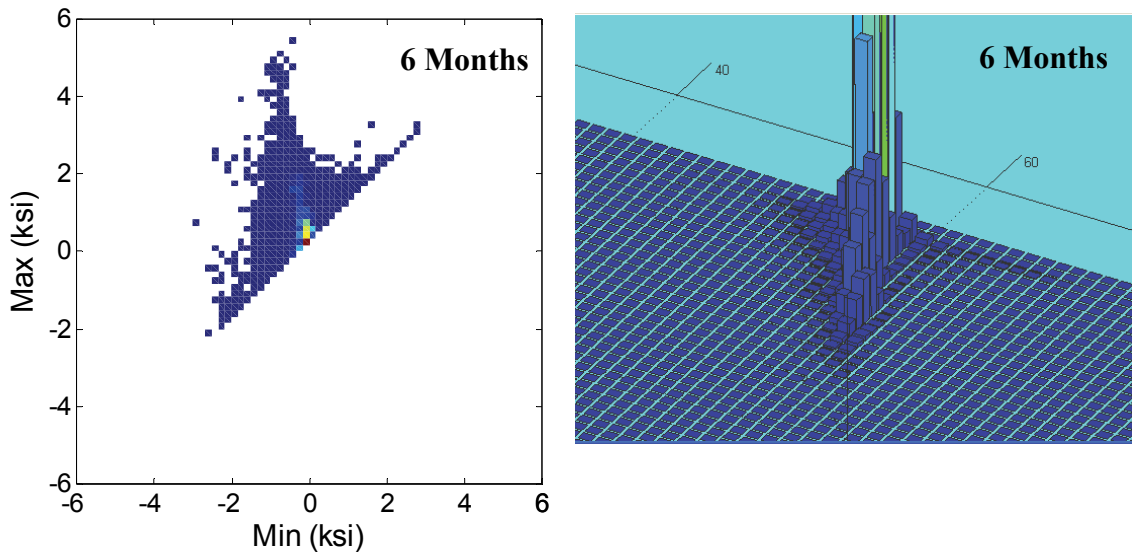
Figure 3.10 Rainflow matrix for Span 3 Girder 9 of Doremus Avenue Bridge.

3.8.2   Rainflow Extrapolation

Traditional extrapolation for fatigue lifetime involves short term measurement of stress cycles and linear extrapolation or growth factor extrapolation. One example of this method is Mohammadi 1993. However, linear extrapolation assumes that the short term record is typical of the site and may be duplicated until the fatigue life of the structure is consumed.

Rainflow extrapolation as described by Socie (2001) has the ability to model the statistical properties of load spectra to a long time period given a short period of measurement. Extrapolation, unlike repetition, can reveal extremes that are not present in test data, but are likely to occur within longer periods. Accounting for load variability enables an engineer to better estimate the fatigue life of a structure given limited test data.

It should be noted that rainflow extrapolation only considers modeling of the load

(Johannesson 1998). That is, only damage that occurs prior to crack formation.

Dressler et al. (1996) describes rainflow extrapolation simply as "estimating a

rainflow matrix corresponding to longer measurement periods or a larger set of customers

from a single original rainflow matrix assembled from short term measurements or a

smaller set of customers." Basically, a loading record for a given short length of time can

be approximated by a two dimensional rainflow function instead of a discrete matrix.

Non-parametric estimation is used to describe the two dimensional rainflow matrix.

Kernel estimators are convenient in this application. The probability distributions of

local areas of the histogram are described. Adaptive kernel bandwidths describe the

influence of nearby data on the local distribution. Thus, areas of high data density can be

estimated independently of sparsely populated areas. The probability density of a two

variate normal distribution $N(0|\Sigma)$ with mean 0 and covariance matrix Σ is given by

$$k(u,v) = \frac{1}{2\pi\sqrt{\det\Sigma}} e^{-\frac{1}{2}(u,v)\Sigma^{-1}\binom{u}{v}} \qquad \text{Eq. 3.1}$$

In which is the covariance matrix is given by

$$\Sigma = \frac{1}{2}\sigma^2 \begin{pmatrix} \lambda^2+1 & \lambda^2-1 \\ \lambda^2-1 & \lambda^2+1 \end{pmatrix} \qquad \text{Eq. 3.2}$$

the value of σ^2 is chosen to best describe all points in a region of the matrix. Regions are

generally groups of data of similar magnitude. In the case of the rainflow matrix, data in

common sub-diagonals contain data of equal stress range. Data within these sub-

diagonals are grouped together during the kernel averaging process. A low value of σ^2

(Figure 3.11a) will more heavily weight points near to the cluster center but offer little

averaging in the less populated regions. A high σ^2 (Figure 3.11b) provides good overall

averaging while poorly describing dense regions.   The variation, σ^2, should be chosen to best fit both the local data and distant data within the neighborhood of the data cluster (Figure 3.12).

a) Low smoothing factor   b) High smoothing factor
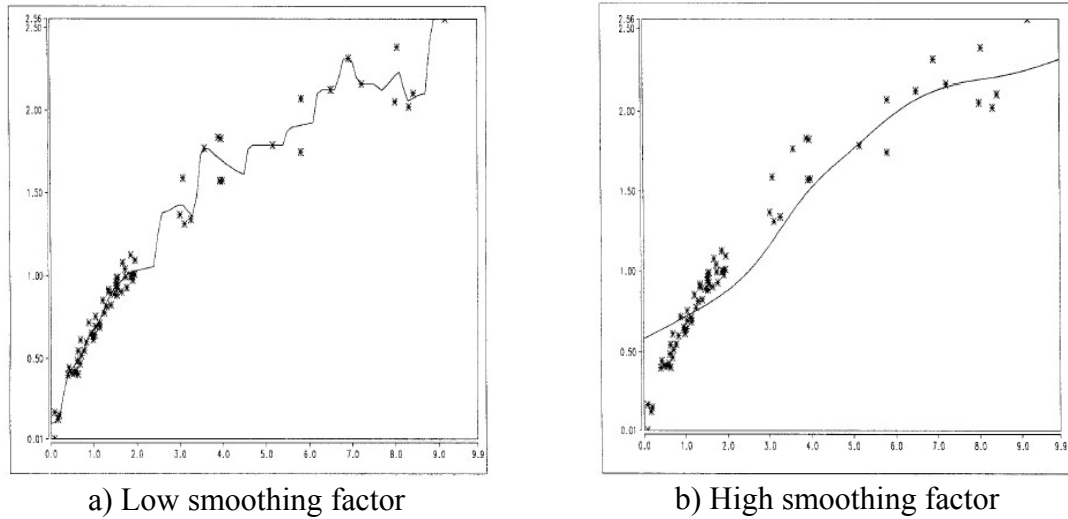
Figure 3.11 Choice of smoothing factor (Dressler, et al. 1996)

Dressler (1996) offers a graphical method to estimate the parameters of the covariance matrix. The value of λ is analogous to the shape of a ellipse for $\lambda \in (0,1)$. The contour lines of the kernel describe ellipses where the major axis is parallel to the sub diagonals and λ is the ratio between the major and minor axes.
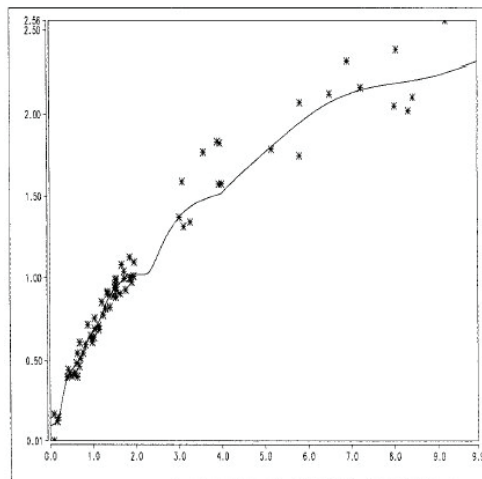
Figure 3.12 Optimal choice of smoothing factor (Dressler, et al. 1996)

Rainflow matrices from different test runs may also be combined to assess variability under different scenarios. Matrices of test repetitions will show similar shape, but vary slightly in mean and extremes. Multiple matrices from tests can be combined to determine the x% most extreme case. The rainflow matrix for a set of test track drivers could be combined to determine the 99th percentile most extreme driver for vehicle design purposes. The extrapolation would save the expense of monitoring multiple in service vehicles for long periods of time. In a test run the principle variables are the test track, vehicle, and driver. The random process is mainly defined by the driver and track. The rainflow matrix contains two parts: one common to all tests due to track conditions and one due to driver behavior. This done by computing the average rainflow matrix R_M given as:

$$R_M(i, j) = \frac{1}{N} \sum_{k=1}^{N} R_k(i, j)$$

Eq. 3.3

and a relative deviation matrix R_D:

$$R_D(i, j) = \frac{1}{R_M(i, j)} \sqrt{\frac{1}{N-1} \sum_{k=1}^{N} (R_k(i, j) - R_M(i, j))^2}$$

Eq. 3.4

Elements of the individual rainflow matrices are strongly influenced by the other elements within the matrix. Therefore, a covariance matrix is also needed to conduct rainflow averaging. The covariance matrix is given as:

$$K[i, j] = \text{cov} \begin{pmatrix} (D_1(R_1), ..., D_m(R_1)) \\ ... \\ (D_1(R_n), ..., D_m(R_n)) \end{pmatrix}$$

Eq. 3.5

where R is the individual matrix and D(R) is the damage associated with that matrix. The damage vectors, such as $(D_1(R_1), ..., D_m(R_1))$, represent the influence of the driver for a

given track. The index of the damage matrix, *m*, represent the damage regions of the

rainflow matrix R. Each matrix is divided into clusters of elements with similar

variability. Clusters of low variability represent mechanical effects from the track that

have little to do with the driver. Highly variable clusters are due to driver behavior.

Damage within a cluster is calculated using Miner's Rule of linear damage. The problem

of finding the distribution of a distribution is now reduced to a manageable size.

Rainflow extrapolation as described by Socie (2001) has the ability to model the

statistical properties of load spectra to a long time period given a short period of

measurement. Extrapolation, unlike repetition, can reveal extremes that are not present in

test data, but are likely to occur within longer periods. Accounting for load variability

enables an engineer to better estimate the fatigue life of a structure. It should be noted

that rainflow extrapolation only considers modeling of the load (Johannesson 1998).

That is, only damage that occurs prior to any material cracking is modeled.

3.8.3   Limiting Rainflow Matrix

Johannesson and Thomas (2001) contribute to the field of rainflow extrapolation

with the introduction of a limiting rainflow matrix. The limiting RFM is defined as the

matrix that would result as the number of load cycles goes to infinity. The limiting RFM,

G, is defined as:

$$\mathbf{G} = (g_{ij})_{i,j=1}^{n} \qquad\qquad \text{Eq. 3.6a}$$

where

$$g_{ij} = \lim_{z \to \infty} \frac{E[f_{ij}]}{z}$$

Eq. 4.6b

assuming that a limit exists, and where the elements f_{ij} of F_z are the number of rainflow

cycles , in a time z, with a minimum in class i and maximum in class j. Several

techniques for estimating G from a measured RFM are given:

1. Estimate a model for the load, and calculate the limiting shape of the RFM.

2. Estimate the limiting shape of the RFM by applying some smoothing technique

   on F_x.

3. Model only the RFM for large cycles (those causing the most damage). Model

   the remaining part by some other technique from 1 or 2.

It is only possible to calculate an exact solution for the limiting RFM for loads that follow

certain models, such as the Markov structure. The approach in this study follows the

third point above.

The process of rainflow extrapolation is now a task with two major parts:

calculating a limiting RFM for large amplitude cycles and for small cycles. For the case

of large amplitude cycles it is assumed that the times of up-crossings of high and of low

levels converge to two independent Poisson processes. The asymptotic expression for the

limiting cumulative RFM is

$$\mu(u,v) \approx \frac{\mu(u)\mu(v)}{\mu(u) + \mu(v)}$$

Eq. 3.7

where u is an extremely low level and v is an extremely high level, the $\mu(u)$ is the

expected level up-crossing intensity. The expression given in Equation 3.7 is valid for

large cycles. The expected level up-crossing intensity $\mu(u)$ is not known but can be

estimated from test measurements. The level crossing intensity is extrapolated for high

and low levels using the generalized Pareto distribution. The remaining part of the limiting RFM is estimated using a kernel smoothing technique. The two parts are joined and the result is the estimate of the limiting RFM.

Treatment of extreme events involves extrapolation of the level crossing intensities. When extrapolation the rainflow matrix for a measured signal, the up-crossing intensity is not known, and must be estimated from the data. For high and low level crossings the intensity can be extrapolated by parametric shape such as generalized Pareto distribution (GPD) as described by extreme value theory. The peaks over threshold (POT) method of extreme value theory is utilized for the extrapolation. Several reasons for choosing the GPD include: (1) attraction to a GEV is equivalent to POT convergence GPD, (2) the maximum of a Poisson distributed number of independent GPD variables has a GEV distribution, and (3) the GPD is threshold stable, i.e. the exceedences or GPD variables gives a GPD, with he same shape parameter, but with a different scale parameter. The last two properties are unique to the GPD versus all other distributions. The use of the GPD requires the estimation of two parameters: (1) shape parameter, k, where $-\infty < k < \infty$ and (2) scale parameter, σ, where $\sigma > 0$. There are several methods that can be used to estimate these parameters: (1) Pickands' method, (2) method of moments, (3) method of probability weighted moments, and (4) maximum likelihood method. The authors found that the maximum likelihood was the best estimator.

Besides shape and scale parameters, a threshold must also be chosen for peak over threshold extrapolation. A threshold must be chosen to be high enough to provide a good fit to the GPD, but still give enough exceedences to get an accurate estimate. The choice

of optimum threshold is a difficult problem in extreme value theory. Several techniques are suggested to identify the appropriate threshold: (1) trial by judgment with diagnosis using quantile-quantile plots, (2) minimization of mean square error (MSE) of a given diagnostic plot, (3) rule of thumb, such as mean plus two standard deviations, (4) choose a threshold that represents a given fraction of the data, such as 20%, or (5) threshold such that there are $\sqrt{N}$ exceedences, where N is the number of stress cycles.

The estimated RFM for anytime in the future can be built by inserting cycles by their respective probabilities as given by the limiting RFM. Cycles which are greater in severity than those observed will be generated. Thus a more representative description of future load conditions is given.

3.8.4 Wave Analysis for Fatigue and Oceanography (WAFO) Toolkit

Brodtkorb, et al. (2000) have developed a MATLAB toolkit for the statistical analysis of random waves and loads. The package contains routines for cycle counting, extrapolation of rainflow matrices, cumulative damage calculation, Kernel density estimation, and extreme value analysis. Tools for estimation of random ocean wave spectral density and extreme wave prediction are also included. For fatigue analysis Markov models are used to model the sequence of turning points by a Markov chain.

To illustrate the process of rainflow extrapolation the WAFO developers included sample data sets and a tutorial. Figure 3.13 shows a sample generated time history of stress for a fictitious structure based on the Markov chain loading pattern. The simulated loading is used to verify the accuracy of the extrapolation method, since the limiting FRM of a Markov load has an exact solution. The load pattern resembles a two phase load, one loaded cycle and one unloaded cycle, such as a truck suspension system.
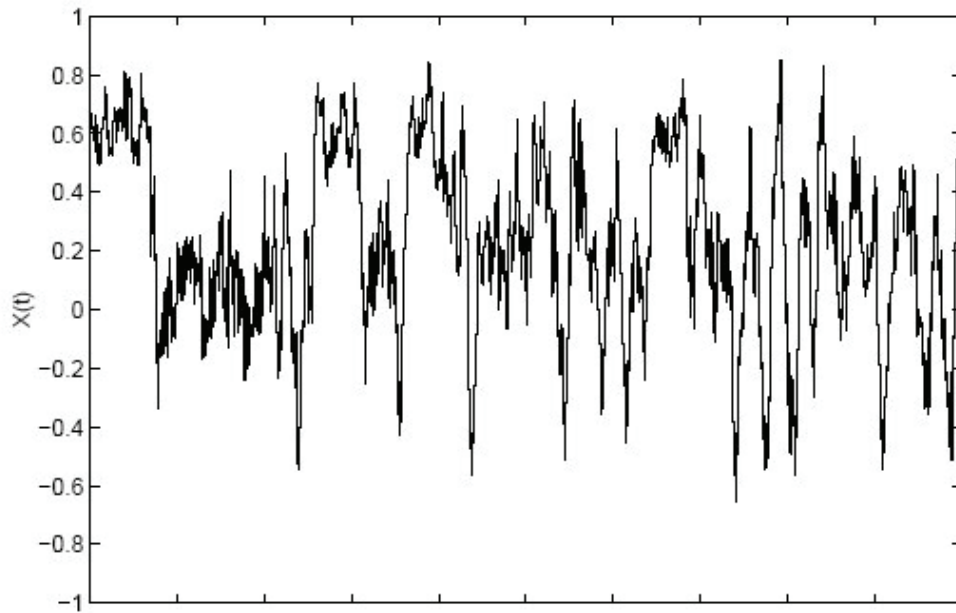
Figure 3.13 Sample time history (Brodtkorb 2000).

Given the time history, rainflow counting procedures are used to decompose the record into discrete stress cycles. These cycles are organized in the to-from RFM shown in Figure 3.14. The dots represent the actual counted cycles from the time history.   Note that the higher value cycles are fewer and are located further from the diagonal. A dense cluster of low range cycles can be seen near the diagonal. The contour lines in Figure 3.14 represent the iso-lines of the estimated rainflow density function.
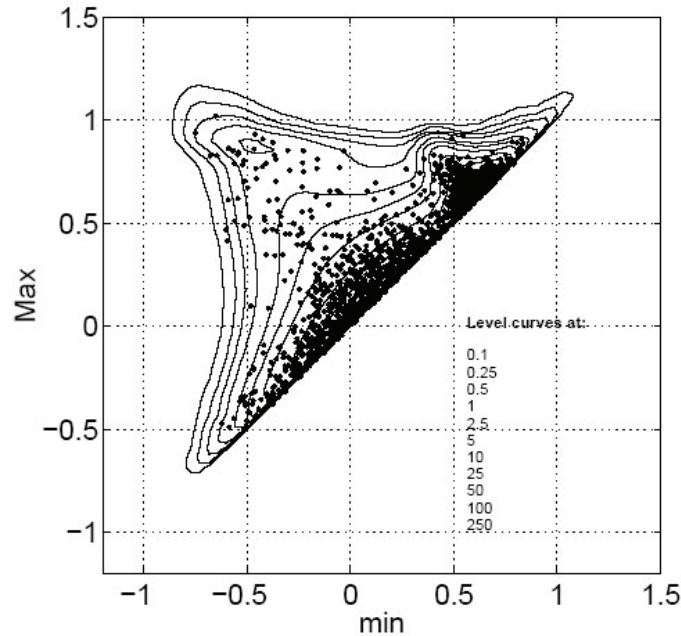
Figure 3.14 Calculated To From rainflow matrix for the load given in Figure 3.13 (Brodtkorb 2000).

The WAFO routine also contains plotting applications to visualize rainflow calculations. One important aspect of rainflow extrapolation is smoothing. Kernel smoothing is used as a non-parametric estimator of the data for low level cycles. The adaptive bandwidth, h, is selected to achieve representative smoothing with regard to a Markov model RFM. The sensitivity of the RFM shape due to the adaptive bandwidth is illustrated in Figure 3.15. As seen in Figure 3.15a, a low value of h provides very little smoothing of the RFM, while a very large value over generalizes the RFM (Figure 3.15f). The degree of smoothing is chosen such that the observed RFM resembles the shape of the Markov model RFM.
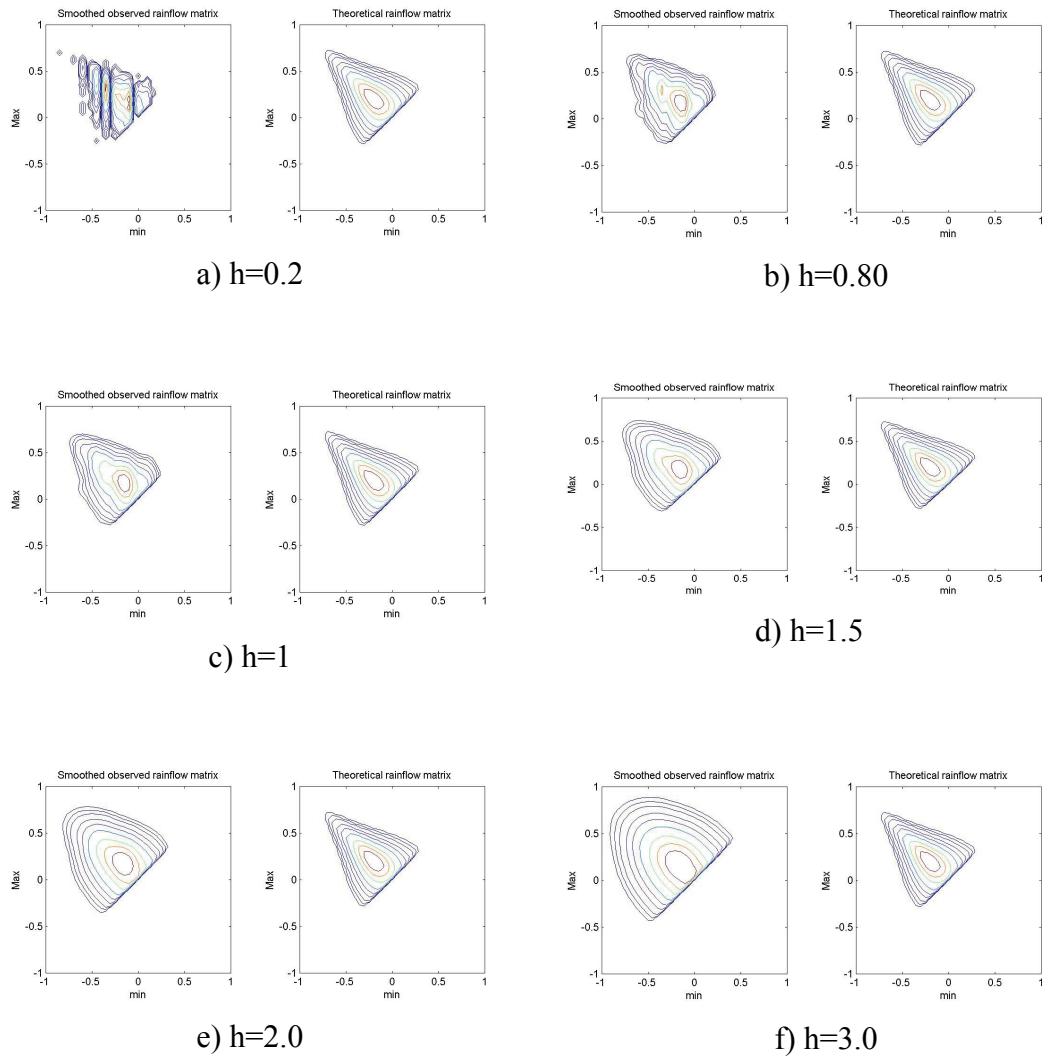
Figure 3.15 Comparison of RFM shapes with variation in smoothing constant, h (Brodtkorb 2000).

3.8.4.1   Rainflow Reconstruction

After the rainflow matrix is extrapolated to the desired future duration rainflow reconstruction techniques are used to build a representative time history. The method, first proposed by Khosrovaneh and Dowling (1990) with later work by Dressler et al. (1997), serves to produce a time history that has similar fatigue damage as the extrapolated rainflow matrix. The reconstructed time history is then used to develop

fatigue testing sequences for prototypes. The test sequences replicate the damage that would be expected during the deign life of the sample. Basic rules are governing the insertion of cycles are imposed. Each reconstruction is different yet contains the same fatigue damage (Figure 3.16). The purpose of reconstruction is to identify the extreme loads which would be expected for longer service durations or more extreme cases. In the case of long term fatigue damage, the exact order of load cycle is not important. The damage is based on the amplitude and frequency of load cycles.
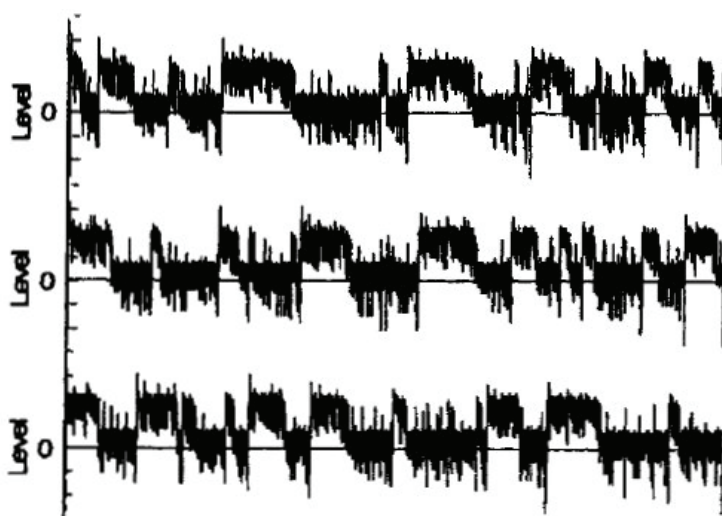
Figure 3.16 Sample reconstructed load histories (Socie 2001).

A methodology is needed to predict the remaining fatigue life of bridge structure details based on a short period of measurement. Inherent variability of the daily number and magnitude of cycles must be included to accurately reflect the loading conditions. Simple linear forecasting is limited. Current life prediction estimations are based on general assumptions of truck weight and volumes. More detailed estimations, which use field data, rely on linear extrapolations of stress cycles to estimate fatigue life.   Site

specific information about truck volumes, multiple presences, and gross vehicle weights are needed for statistical simulation of traffic loading. Likewise, the actual load distribution and stresses are needed to fully understand the structural response. Unlike the strength limit state that requires the maximum future load effect, the fatigue load prediction centers on the mean effect. Fatigue damage accumulates over a wide range of stress levels. Predicting the maximum load during the design life of a bridge will not aid in fatigue life prediction. A method that accounts for the statistical variation of both stress cycles and truck loads provides a more comprehensive estimation of fatigue life.

The time history for a short period of measurement can be represented in the form of a two-dimensional rainflow matrix (RFM). This rainflow matrix can then be processed to generate a two-dimensional probability distribution. A new RFM for any time, N, in the future is generated. The damage for this new RFM can be computed using linear cumulative damage rules, such as the Palmgren-Miner Rule. The flowchart in Figure 3.17 outlines the rainflow extrapolation procedure. In a similar fashion, the truck load records from a weigh in motion system can be used in a simulation to model the live load. The truck load and geometric data are simulated using Monte Carlo techniques and processed with a bridge model. The simulated time histories are decomposed into a two-dimensional RFM. The same rainflow extrapolation procedure is applied and the damage from extrapolated test data and simulation are compared.
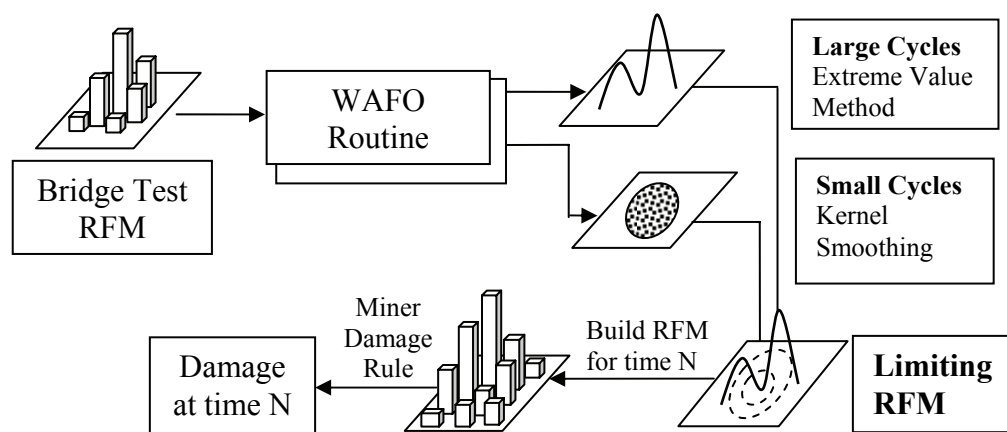
Figure 3.17 Flowchart of rainflow extrapolation procedure

CHAPTER 4

FIELD TEST SETUP AND STRUCTRUAL HEALTH MONITORING

A comprehensive experimental program was developed to measure the live load and their effects on bridge structures. The experimental study is focused on the newly constructed Doremus Avenue Bridge, New Jersey's first LRFD designed bridge. Controlled live load testing and long-term structural monitoring were performed to evaluate the performance of the LRFD design specifications. Other field studies for response were conducted on area bridges to include the effect of different site specific loads and bridge configurations.

Information about the type and distribution of live loads beyond the single case study at Doremus is also important. For this purpose weigh-in-motion data from over 80 sites in New Jersey is studied for regional and temporal changes in live loads. In all, more than 100 million truck records were included in the live load studies contained herein. Live load parameters such as: truck volumes, types, gross weight, axle spacing, axle weights, truck superposition all contribute to the live load spectra that affects the design of highway bridges. The data contained in this study will aid designers by providing guidance on the maximum load effects for which durable and safe bridges are to be built to resist.

4.1 The Doremus Avenue Bridge

The Doremus Avenue Bridge is a composite steel slab-on-girder construction (Figure 4.1 and Figure 4.2). As part of the field investigation, all ten girders of the 3-span continuous unit were instrumented to measure strains, overall span deflections, bridge vibrations, and truck weights. Controlled live load testing was performed at milestones during the construction. These include: (1) Phase I: completion of the first five girder, two lane, structure (Figure 4.1), (2) Phase II: completion of the final ten-girder superstructure (Figure 4.2). Various loading patterns, including single, following, and side-by-side, using heavily loaded 5-axle trucks are considered during controlled testing. These results would be used to verify computer models for later use in simulation. Bridge response due to normal truck traffic is continuously monitored and recorded for long term (5 years) evaluation of the bridge.
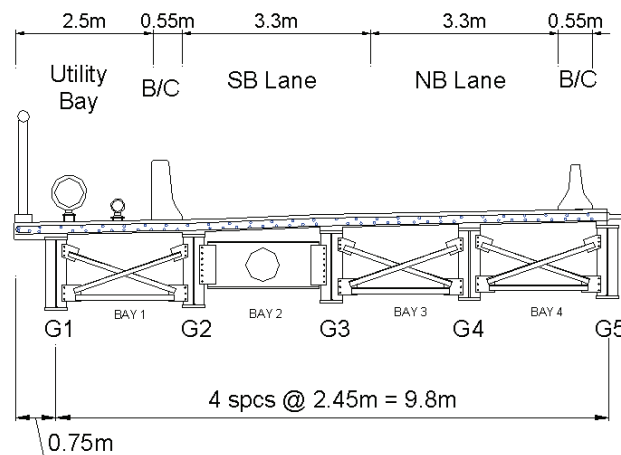
Figure 4.1 Cross sectional view of the partial Doremus Ave Bridge (Stage I)
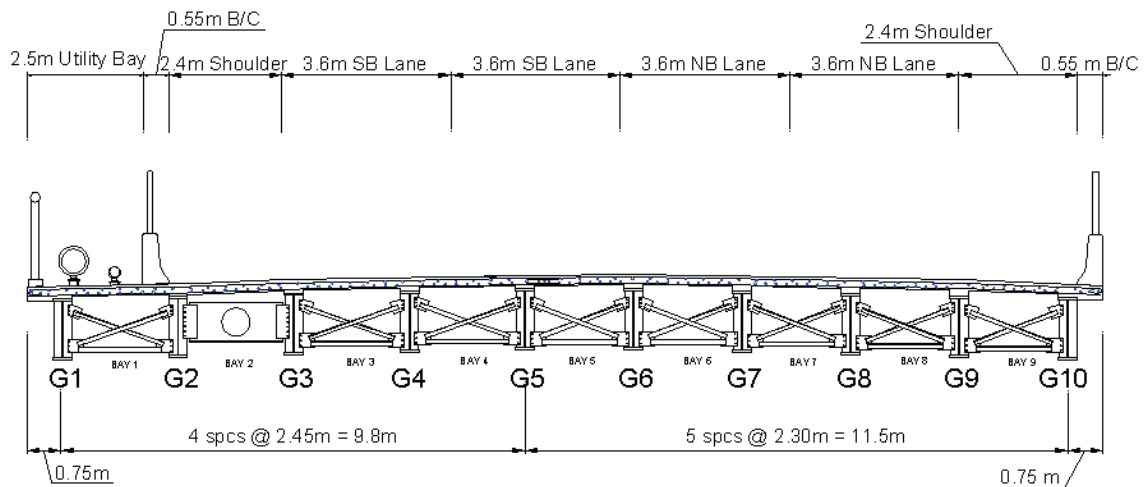
Figure 4.2 Cross sectional view of the completed Doremus Ave Bridge (Stage II)

4.1.1 Bridge Description

The Doremus Avenue Bridge was selected as the central case study in this research. The bridge is New Jersey's first LRFD design, over the Oak Island Rail Yards in Newark, New Jersey. It provides the primary north and south access along the City of Newark's waterfront industrial area east of the NJ Turnpike and also serves as a major access to and from the shipping terminals located in Port Newark and Port Elizabeth. It serves all modes of transportation: sea, rail, road, and air (Newark Liberty International Airport), as is shown in Figure 4.3. These interconnections result in an area of high truck volume and a high percentage of heavy trucks, rendering this site ideal for a live load fatigue study.

The Doremus Avenue Bridge was anticipated to be a national test bed for the implementation of the LRFD design specifications. As such, the construction contract included provisions for the equipment and its installation. For the purpose of fatigue

monitoring, two main systems were designed: the long term strain monitoring system, or
Fatigue System, and the weigh-in-motion System (WIM).
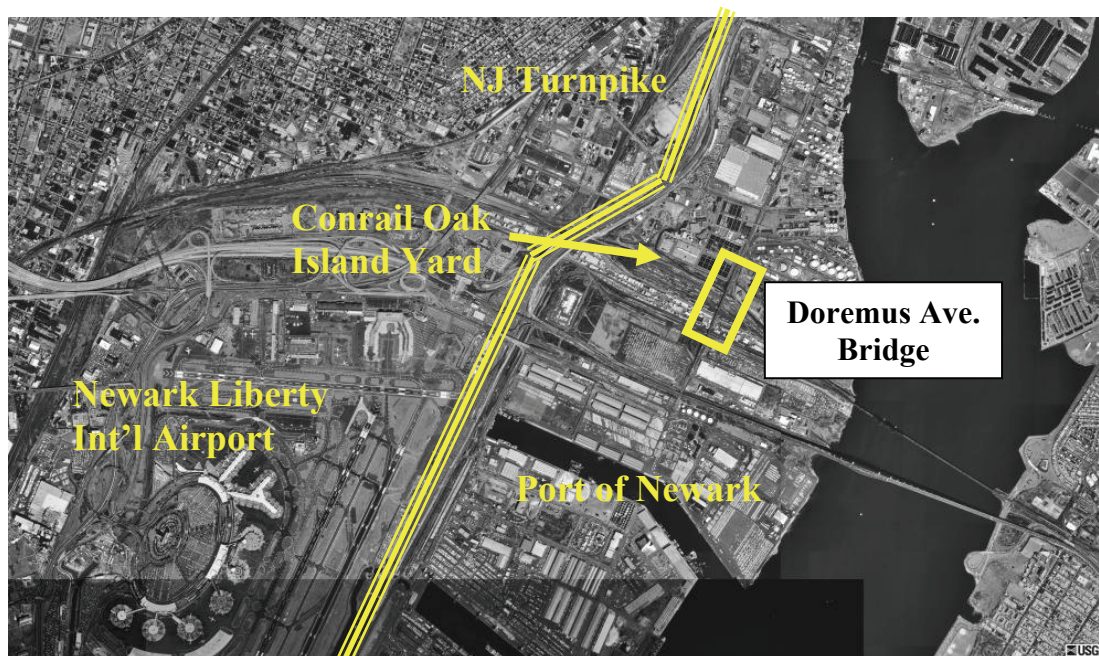
Figure 4.3 Aerial photo of Port Newark with Doremus Ave Bridge highlighted (Microsoft 2005)

The Doremus Avenue Bridge is a $31 million bridge replacement project and is
the first project (ground-breaking, July 2000) of Phase I (of three) of the Portway
International/Intermodal Corridor program. This program is a billion dollar, decade-long
project that includes the phased development of related roadway improvement projects
designed to improve the efficiency of truck movements between New Jersey's Newark-
Elizabeth air and seaport complex and other intermodal service centers. The program
focuses on a 17-mile corridor that runs from Union and Essex counties in the south to
Hudson and Bergen counties in the north. Currently, the regional road network supports
10,000 trucks movements from the port each day with 2.5 million twenty-foot equivalent

units (TEUs) of intermodal containers. Freight volume is expected to reach 5.3 million

TEUs with 21,000 truck movements per day in 2015 (NJDOT Portway).

The Federal Highway Administration (FHWA) in conjunction with the U.S.

Environmental Protection Agency has also selected the Portway program as one of the

projects nationwide to be included in the Environmental Streamlining Pilot Program.

This program is aimed at finding new means to streamline and accelerate the delivery of

transportation improvements while achieving better environmental protection.
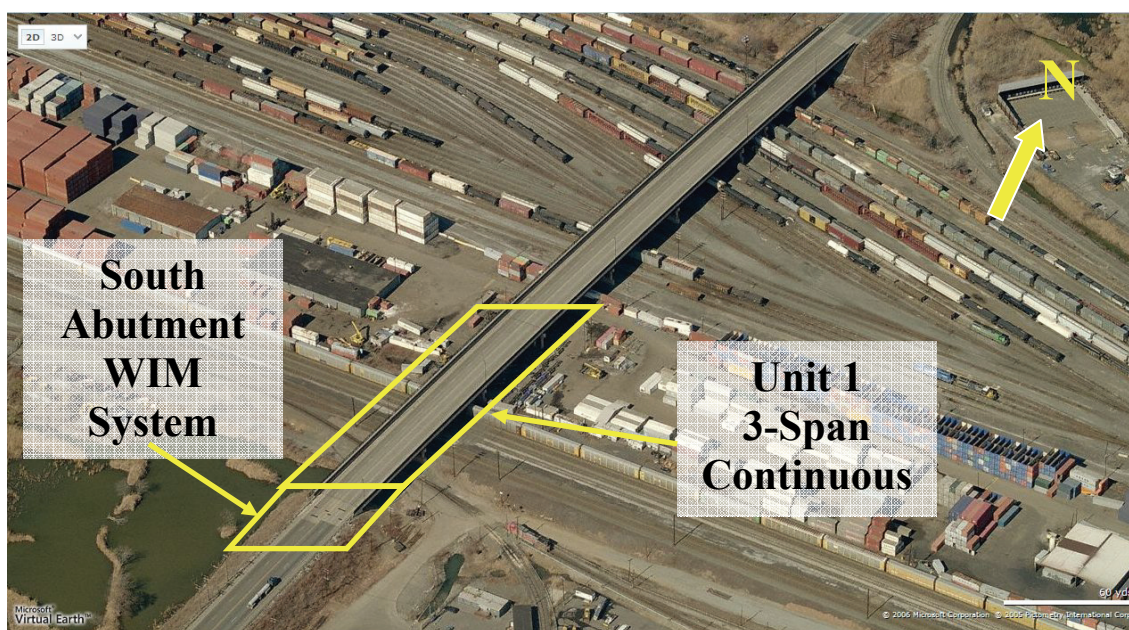
Figure 4.4 Aerial view of the Doremus Avenue Bridge, south abutment with WIM system shown in lower left corner. (Microsoft 2007)

The former bridge, originally built in 1918, was functionally obsolete and

structurally deficient (NJDOT-website). Its two lanes had an average daily traffic (ADT)

of over 8,300 vehicles, with over 40% of the total consisting of trucks. The bridge spans

over thirty-three (33) active rail tracks. This rail yard is one of the busiest yards east of

the Mississippi River. The original structure was built with a clearance to satisfy the

railroad car height of that time; however, at some point the bridge was raised to accommodate larger rail cars. The retrofit was accomplished by simply jacking up the superstructure and placing the spans on blocks as seen in Figure 4.5 (right). The resulting inconsistent pier heights and uneven spans led to higher impact forces on the bridge and a decrease in ride quality.

Figure 4.5 The new Doremus Avenue Bridge (left) and the original bridge (right)

4.2   Instrumentation

A wide variety of sensors and equipment were used to study the effect of live load on bridges. The following section describes the instruments, their function, and the basis for their choice in this study.

4.2.1   Strain Transducers

A total of 53 Bridge Diagnostics, Inc. (BDI 2001) full bridge strain transducers were installed to the top and/or bottom flanges of the steel superstructure.   Figure 4.7 shows the installation scheme for the strain transducers. The layout was designed to capture a full ten-girder cross section within each of the three spans at the maximum positive moment position. Complete girder lines are also instrumented along Girders 4 and 8 in all three spans at intermediate locations. Additionally, at one cross frame location between girders 2 and 3 of Span 1 each of the four struts of a cross frame are instrumented. During load testing all 53 gages plus one additional unattached gage, called a dummy gage, are connected to the STS data acquisition system. The dummy gages are connected to detect any electromagnetic interference that may be present during the test. If there is a noise signal in the gages, the dummy gage can be referenced to verify that the noise is EMI, and not a true strain.

The BDI gages consist of a full Wheatstone bridge circuit with four small strain gages encased in a rugged aluminum frame (Figure 4.6b). All BDI gages were wired to an equipment box located at Pier 2 at ground level using 5 conductor shielded cable. The use of shielded cable is crucial for field testing to reduce EMI or signal noise. The demountable BDI gages were attached to the bridge onto threaded studs driven into the

steel flange using a Hilti® powder actuated tool (Figure 4.6). Alternatively, the gages

may be clamped to the girder flange. Installation on the top of the bottom flange was

favored by the railroad administration to prevent any obstructions that would compromise

overhead clearance.

(a)
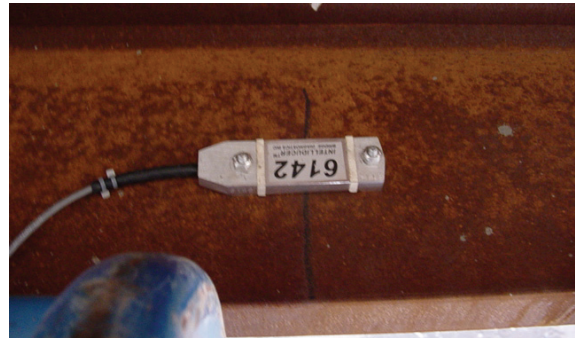
(b)
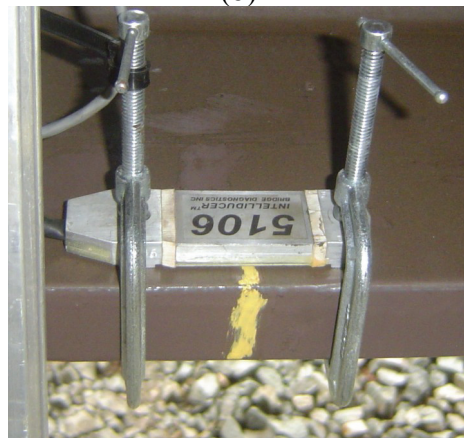
(c)

Figure 4.6 Strain transducer installation: (a) studs are shot into girder flange, (b) the gage is tightened on the studs, and (c) alternate installation with clamps
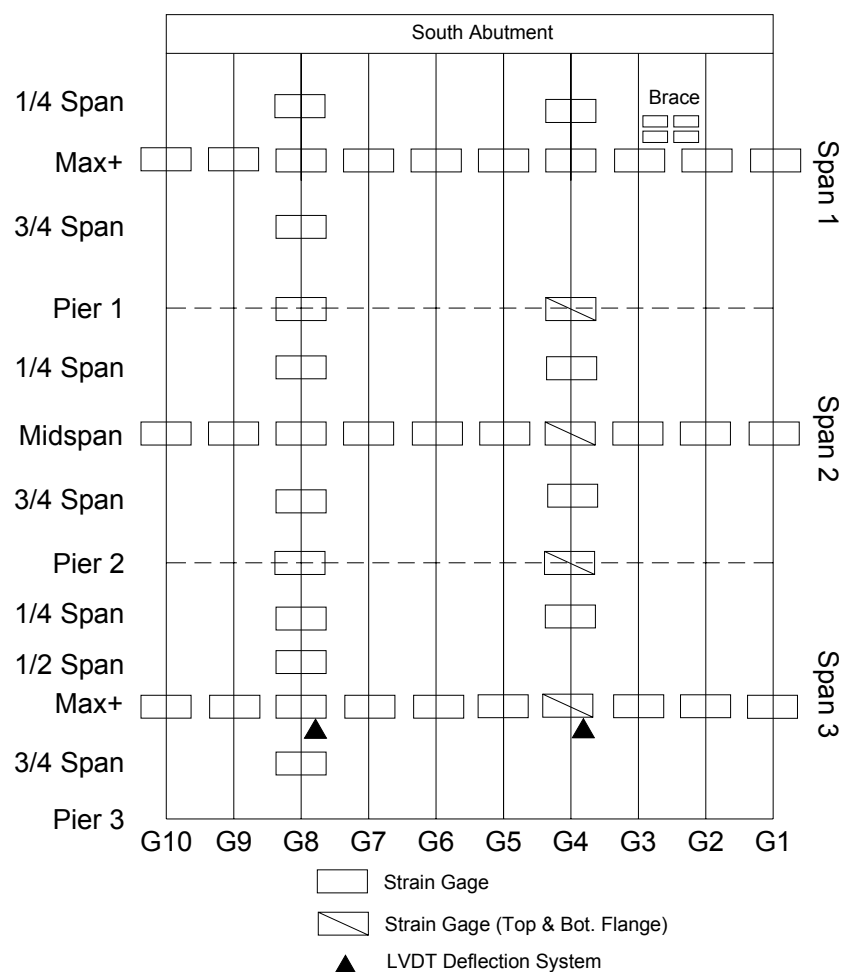
Figure 4.7 Strain transducer installation scheme at Doremus Avenue. A total of 53 gages and 2 LVDTs are installed.

Positions of maximum positive bending moment, negative moment (over pier locations), and one cross frame were instrumented. The instrumentation scheme was designed to achieve sections of full instrumentation across all ten girders and throughout all spans along two girder lines (Figure 4.7).

All gages were sampled during the live load testing of the bridge. Only 22 strain gages and 2 LVDTs were monitored continuously for long-term monitoring purposes.

4.2.2   Linear Variable Differential Transformers

Measurement of bridge deflection is often difficult due to large superstructure clearances and obstacles underneath the deck. During load testing portable equipment such as the Laser Doppler Vibrometer may be setup under the deck to measure deflection. However, this equipment can only be used for a short period of time and only measures a single point under the deck. To overcome these limitations an LVDT (linear variable differential transformer) and reference cable were used at several locations on the Doremus Avenue Bridge. These locations include: Span 3 along Girder 4 and Girder 8 at the maximum positive moment location. Over Piers 2 and 3, steel mounting blocks were epoxied to the diaphragms. A 1/8" diameter aircraft cable was strung between the Piers 2 and 3 through cross braces. One end was fastened directly to the mounting block while the other end was attached to a turnbuckle and to a mounting block. The cable was pulled taught. The LVDTs were mounted on an adjustable platform and attached to the reference cable with a saddle. Each LVDT was hardwired back to the main data logger enclosure at Pier 2. The LVDT piston was frictionless with no spring return such that no force was imparted on the cable when the girder deflected.

The accuracy of the LVDT reference cable system was verified during multiple controlled load testing sessions (Nassif et al. 2005). A Laser Doppler Vibrometer was installed to measure deflection at the same point where the LVDT was fixed to the girder. Both instruments were sampled during different test truck configurations. The Laser and LVDT systems reported nearly identical displacements in all tests, proving that the LVDT reference cable system is an accurate, less expensive, and practical way to measure bridge displacement.

The LVDT system has one major disadvantage: tension change with temperature. Daily and seasonal temperature fluctuations cause the cable tension to change; therefore, changing the cable height over time. The absolute position of the cable is not important since a zero point is calculated every hour by the data logger. However, if the cable sags too far, it may exceed the LVDT range and the displacement cannot be measured. To reduce temperature effects, a high resistance spring was added to the cable at one end.
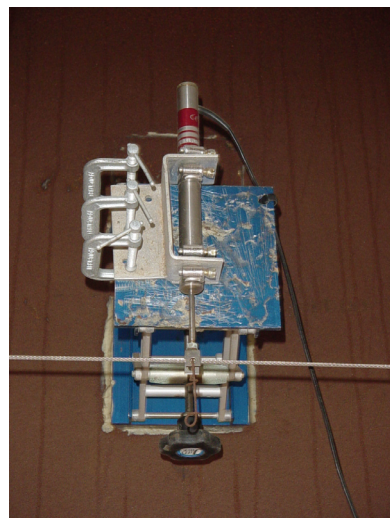
(a)
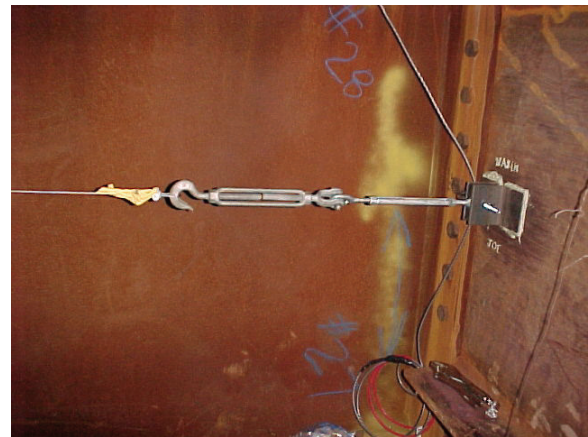
(b)

(c)

(d)

Figure 4.8 LVDT Reference Cable displacement system: (a) LVDT located at maximum moment location, (b & c) cable mounted at piers, (d) cable parallel to girder.

4.2.3   Laser Doppler Vibrometer

The Laser Doppler Vibrometer (LDV), manufactured by Polytec PI, is a non-contact sensor that measures displacement and velocity of a remote point up to 200 meters away. The LDV uses laser interferometetry to measure vibration as opposed to simple signal time delay. A change in the distance between the laser head and the reflective target will produce a Doppler shift in the light frequency that is decoded into displacement and velocity. The system is composed of three parts: 1) the helium neon Class II laser head, 2) the decoder unit, and 3) the reflective target attached to the structure. The laser head is mounted to a tripod that is positioned underneath the target. The reflective target, typically retro-reflective tape, provides a stronger signal compared to the plain bridge components. The signal strength is read on a scale on the laser head. A tripod is adjusted to maximize the signal prior to a test run. Typically, the laser will take 5-10 minutes to relocate and iterate to a good position. Figure 4.9 shows the LDV as setup for a test on the Turnpike Delaware River Bridge.

Figure 4.9 Laser Doppler Vibrometer for non-contact deflection measurement at a distance up to 300 feet.

4.2.4   Permanent Weigh-in-Motion (WIM)

All of the sensors described earlier were used for detecting the bridge live load or long term response. Knowing the bridge response provides important information about the bridge performance, however, the applied loads are also needed in order to verify computer models and perform simulations. Moreover, the data obtained from these sensors must be verified that the readings had no interference. A weigh-in-motion (WIM) system was used to detect the live load (truck loads) traveling on the bridge. A WIM system, as opposed to a static scale, is designed to weigh a passing vehicle traveling at normal traffic speed. The WIM system layout for Doremus Ave is shown in Figure 4.10.

There are three main technologies that are used for weighing trucks on highways: a piezoelectric (piezo) axle sensor, a single load cell, and bending plates. Piezo sensors are the least expensive and the most widely used of the three. The single load cell sensor

is the most expensive and the most accurate. The sensor uses a dynamic rated (fatigue rated) load cell to measure the load. The load cell is embedded in the pavement underneath a steel plate. As the vehicle passes over the steel plate, the plate compresses onto the load cell that registers the load to the WIM system. The bending plate consists of a thick steel plate with gages attached to measure the flexural strains. Bending plates are more expensive than piezo sensors and are more difficult to install, but they provide a longer service life. Regardless of the sensor involved, calibration is needed before these devices produce useful data.
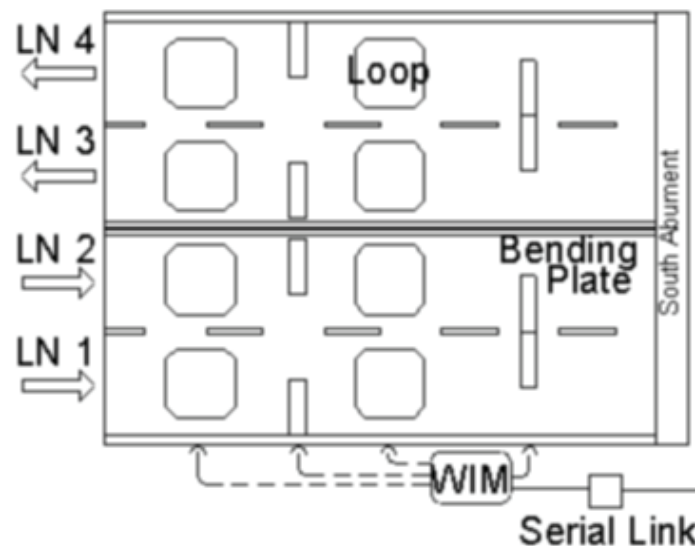
Figure 4.10 WIM System Configuration at the Doremus Avenue South Approach

4.2.4.1 Piezo WIM sensors

Although the piezoelectric is the cheapest sensor of the three types but it is the least accurate as well as the least durable. The sensor is about 10 feet in length (other lengths are available depending on the application) and about 1/2-in wide. When a vehicle passing over the sensor, an electrical signal is generated from the sensor and sent to a WIM system. The signal magnitude is compared to a calibration value and a weight

is calculated. There are two classes of piezo axle sensors: Class 1 and Class 2. Class 1

sensors are manufactured with a higher precision for weighing axles, while Class 2

sensors are produced to only detect axles.

The piezo sensors may be installed either permanently or temporarily. The

method of installation will depend on the application and the expected service life. The

permanent installation is illustrated in Figure 4.11. The procedure includes (ref IRD or

MSI manual): (1) ensure that proper traffic control is in effect, (2) layout sensor and loop

locations, (3) cut a 3/4" x 1" deep x 10 foot long slot in the road for each sensor, (4) clear

the slot of any debris or moisture, (5) place the sensor into the slot with alignment tabs,

(6) fill the slot with epoxy and level off, and (7) run the cables to the WIM system

location.

4.2.4.2   Bending Plate WIM Sensors

The bending plate system, used in this project, uses strain gages installed on steel

plates to measure the load. A strain gage is attached to a steel plate embedded in the

roadway. As the steel plate bends, a signal is transmitted to the WIM system, which then

converts the signal into load. The system is cheaper than the single load cell system, but

provides equivalent accuracy. To improve the accuracy, two sensors needed to be

installed per lane such that the right and left side of the vehicle could be measured. The

WIM record contains individual axle weights and axle spacing for each side of the

vehicle. Further, the WIM system is programmed to compare the right and left weights

and make a determination as to the accuracy of the measurement. For a typical vehicle,

the weights of each side of an axle should be similar within a given tolerance. If there is

a large difference, the WIM system will flag the record and include an error code in the

record. In addition, for the system to determine the speed and the vehicle, two inductive loops need to be installed so that the WIM system can distinguish one vehicle from another.

(a) Step 1-cutting slots for piezo sensors and loops

(b) Step 2-clean out slots

(c) Step 3 – Place piezo sensor into slot

(d) Step 4 – Fill slot with epoxy & level off

Figure 4.11 Permanent Piezo WIM installation procedure

Eight bending plates and inductive loops, two in each lane, were installed on the south approach slab of the Doremus Avenue Bridge. A staggered bending plate setup, shown in Figure 4.12, was used such that the two bending plates in each lane could detect the left and right wheels of each axle. The two inductive loops in each lane were spaced 16 feet apart leaving sufficient distance to calculate the speed of the vehicle. The WIM system was installed in a stainless steel electrical enclosure located on the east of the approach slab. The data from the WIM system was also transmitted to a fatigue data acquisition system located on Pier 2, about 100 meters to the north.
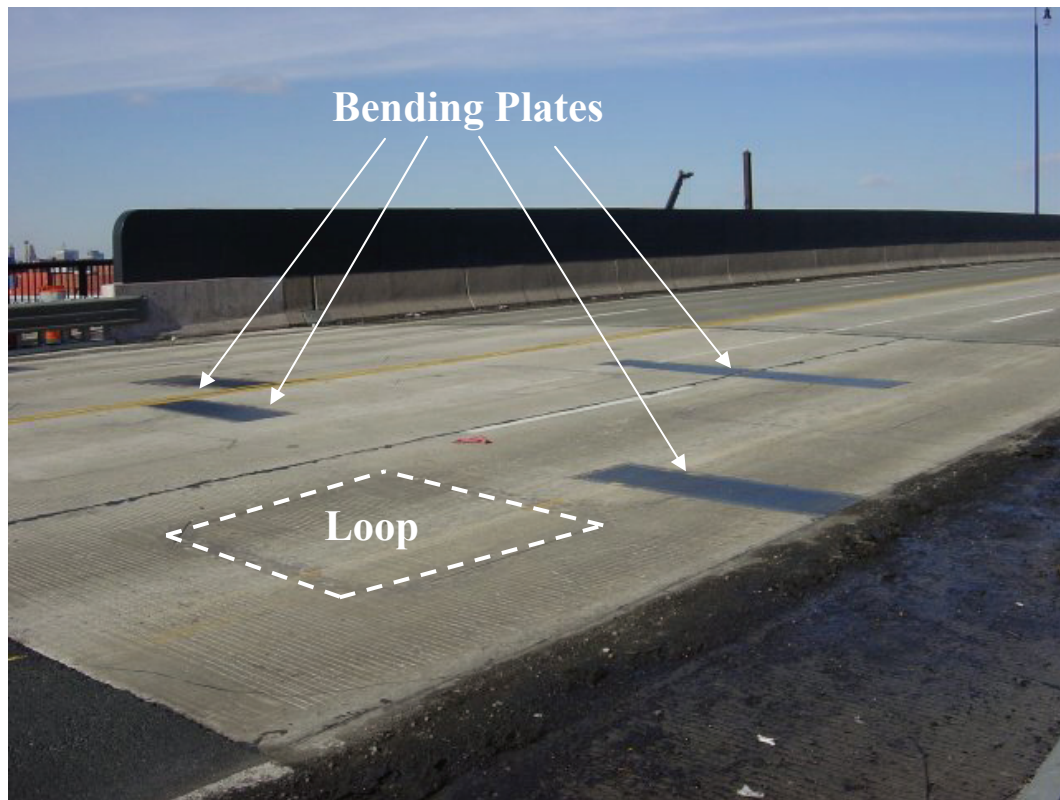
Figure 4.12 Installed bending plates and inductive loops on the Doremus Avenue approach slab

4.2.4.3   Inductive Vehicle Detection Loops

In addition to axle sensors, inductive vehicle detection loops are also recommended to detect vehicle presence in the lane. The axle sensors are limited in their ability to differentiate between separate vehicles traveling close. For example, if two 5-axle trucks are traveling closely in the same lane over a WIM instrumented lane without an inductive loop, the system may read the event as a single 10-axle truck. If the lane had been outfitted with inductive loops, the gap between the trucks would have been detected and the system would register two separate vehicles. An inductive loop functions the same way as a metal detector to detect gaps between vehicles. A loop is composed of a single cable placed into a square slot in the center of a lane. The cable extends from the WIM data logger unit to the lane, where it is wound several times within the slot, creating a series of cable "loops", and returned to create a circuit. An electrical potential is then added to the wire and held constant. As a large metal object passes over the loop, the voltage in the cable is changed according to the principle of electrical induction, allowing the WIM system to detect the presence of a vehicle. Since inductive loops do not make contact with vehicle wheels they are much more durable than axle sensors. Loops are often used in situations where vehicle speed or presence are the only parameters desired, such as traffic volume counting or vehicle detection for actuated traffic signals.

4.2.5   Portable Weigh-in-Motion Systems

Portable weigh-in-motion testing is becoming increasing popular among transportation agencies or researchers as a tool for enforcement and design. The systems are simple to install and operate, and allow the sampling of trucks away from established WIM sites to detect regional variations in truck volumes or weights. Short-term sampling may also be done in advance of bridge construction to allow designers to consider the

actual truck volumes and weights. Such information in the form of average daily truck

volumes is vital to any fatigue design calculation. Portable studies may also be done to

check for illegally overloaded trucks that pose a danger to load restricted bridges.

Two portable systems were used to sample site-specific truck data in this study:

(1) WIM-TRS, manufactured by PAT America of Evanston, IL (Figure 4.13a) and (2)

TCC-540 WIM, made by International Road Dynamics of Saskatoon, Alberta, Canada

(Figure 4.13b). Both systems are compact, portable, and include internal batteries that

allow them to operate unattended for up to 2 months.

(a)   (b)

Figure 4.13 Portable weigh-in-motion systems: (a) PAT America WIM-TRS and (b) IRD TCC-540 WIM

Two types of sensors are typically connected to the portable WIM system to

collected traffic information: (1) up to 8 piezo axle sensors, (2) up to 4 inductive loops,

and (3) up to 4 pneumatic tube counters. The latter is used exclusively for speed and axle

counting applications and cannot determine vehicle weight. Axle sensors and inductive
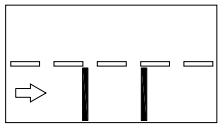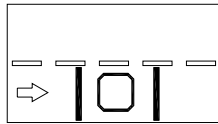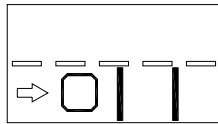
loops are installed in a Piezo-Loop-Piezo, or P-L-P, configuration in each lane. Table 4.1

shows these and other configurations, including Piezo-Piezo (P-P), that are possible. IRD

recommends the installation of inductive loops along with axle sensors to detect gaps

between vehicles and allow the system to differentiate between separate closely

following vehicles (Ref IRD). Piezo sensors alone may be installed in each lane,

however, a maximum vehicle length variable must be specified to allow the system to

close the record after a last axle has been read. This compensation has been found to be

reliable in studies involving highways with average speeds greater than 50 MPH.

4.2.6   Temporary WIM Sensor Installation

For short-term traffic monitoring, there is no need to make the installation of the

axle and loop sensors permanent. Typically, bituthane tape composed of fabric strip with

an asphaltic binder and an internal pocket for sensor placement is used. The installation

procedure using the temporary tape is as follows (IRD 2005): (1) prepare the sensors by

cutting bituthane tape to length, warm the tape with a portable gas torch, (2) ensure

proper traffic control is in effect and that all crew members are following safety

guidelines for highway work, (3) upon traffic closure, enter lane and clear the roadway of

any loose debris and moisture, (4) mark the layout of the sensors, (5) adhere the pocket

tape to the roadway, (6) slide the piezo axle sensors into the pocket tape, and (7) secure

and run the sensor cables back to WIM system location.

Table 4.1 WIM sensor installation configurations per lane (IRD 2005)

Sensor Configuration	Notation	Description
	P-P	Piezo-Piezo
	P-L-P	Piezo-Loop-Piezo
	L-P-P	Loop-Piezo-Piezo
	L-P-L	Loop-Piezo-Loop
	L-P-P-L	Loop-Piezo-Piezo-Loop
	L-P-L-P	Loop-Piezo-Loop-Piezo

If temporary loops are required, the loops are pre-assembled ahead of time by laying out the loops cables and encasing them in bituthane tape. IRD recommends a minimum number of cable revolutions based on the area that the loop encloses (IRD 2005). Typically, seven revolutions are needed to attain an adequate signal as a vehicle passes. Install the pre-assembled loop unit in the same manner as the piezo axle sensors, run the two cable leads back to the WIM system and connect to the appropriate terminal.

4.2.7   Portable WIM System Calibration

Each time piezo sensors are installed they must be calibrated, even if the same sensors were previously calibrated at another site. The reason for recalibration is that the piezo signal depends on a number of factors (IRD ref): (1) pavement dynamic modulus, (2) temperature, (3) speed of traffic, and (4) length of cable run from sensor to WIM system. Calibration of the portable WIM system is relatively simple. Only the piezo axle sensors need to be calibrated, the loops are self-calibrated when the WIM is initialized. Calibration is accomplished by passing a vehicle of known weight over the piezo sensors at typical highway speed and adjusting the WIM output to match the static scale weight. While knowing the individual axle weights is optimum, it is not required for calibration. Calibration is accomplished after the following procedure: (1) ensure that all sensors are connected and properly functioning by checking the sensor diagnostic screen on the WIM, (2) then obtain a certified scale receipt containing the truck gross weight (or axle weights), (3) begin passing the vehicle over the WIM instrumented lane at highway speed, (4) after the vehicle passes and a reading is produced, calculate a new calibration factor by taking the ratio of the reading to the known weight, (5) continue making passes and adjusting the calibration factor, and (6) when two or more consecutive runs produce a weight near the static scale weight, calibration is complete.

Calibration is typically accomplished in 5 to 7 runs. Additional runs may be needed if the vehicle dynamic effect over the sensor is high. The system accounts for dynamic by taking the readings from the two sensors and averaging them to arrive at the gross and axle weights. In service verification and auto-calibration routines are available within the WIM system.   The weight of the front (steering) axle of a 5-axle tractor trailer

(Class 9) is independent of the payload and averages about 9 to 10 kips. To verify the calibration, check the front axle of Class 9 vehicles as they pass the WIM system. If the average weight is near 9 kips, then the calibration is good. If not, there are auto-calibration routines programmed in the WIM system to sample Class 9 trucks and adjust the calibration to match the 9k front axle weight.

The calibration of piezo axle sensors is not permanent. Changes in temperature and age of the sensor will contribute to drift. WIM data should be evaluated for accuracy by applying the concepts in the FHWA Traffic Monitoring Guide (FHWA 2001). The procedures discussed in the report will be applied to field data and given in the results section to follow.
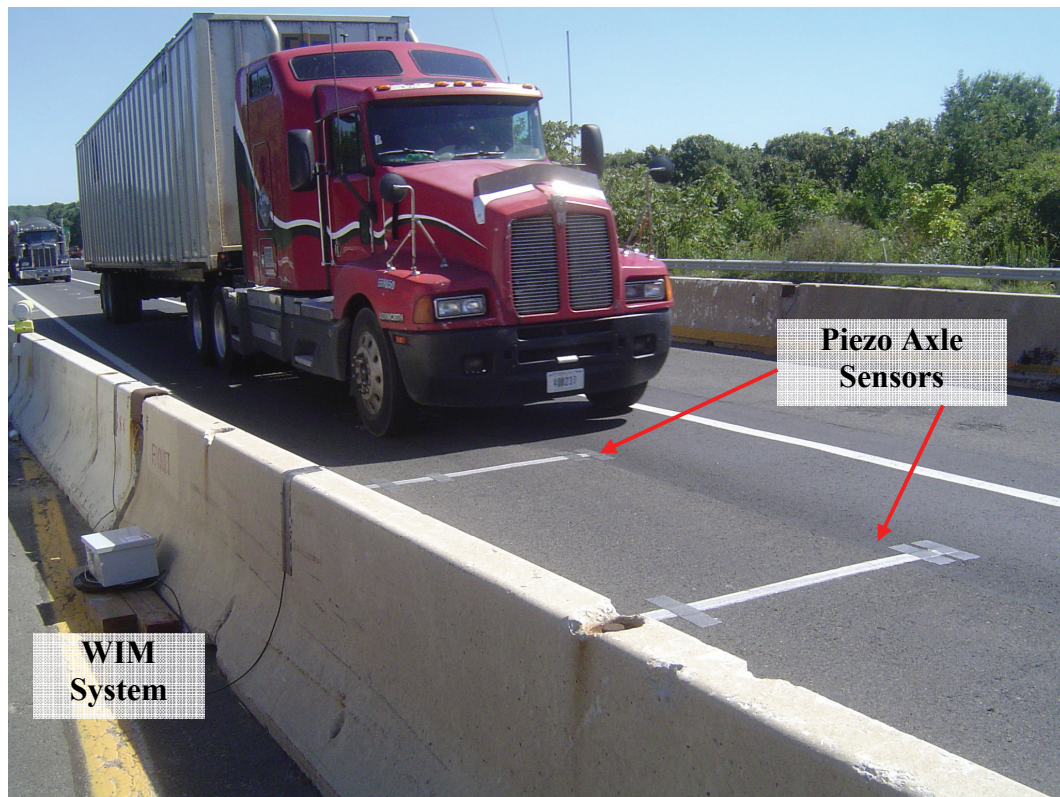
Figure 4.14 Typical portable WIM sensor layout with Piezo-Piezo configuration as installed on NJ Turnpike PA Extension (September 2006)

4.2.7.1   PAT America TRS-WIM

The PAT TRS-WIM is a multifunctional traffic sampling system. The main unit consists of the CPU board, WIM board, Loop board, and Pneumatic tube board and battery in a hardened metal case. The system can be programmed entirely from the LCD display built into the front panel or interfaced to a notebook PC through a serial port. A configuration and data utility software package were provided by the manufacturer. Various configuration parameters such as: site ID, site layout, sensor calibration factors, number of lanes, and filtering options can be specified. Furthermore, the system allows detailed data to be collected for each vehicle, or as a simple count for each class of vehicles. Data for site specific live load studies must be collected for each vehicle and include individual axle load, spacing, and other truck information. Data is collected and stored in the proprietary data format (binary) and must be extracted to a readable format using the product software. The timestamp of each vehicle is stored to the nearest second, which will limit the applicability of this system for more advanced live load analysis.

More recently, the study of truck superposition is become increasing important among researchers and transportation agencies (Nowak, Nassif, DeFrain 1993). In order to determine the cases of superposition, also called multi-presence, the vehicle time of arrival or timestamp must have a resolution of at least one-hundredth of a second. This point will be further illustrated when dealing with specific cases of multi-presence but the following is a brief illustration of this issue. For example, consider than the site being studied has two instrumented lanes. If two trucks approach the WIM system at nearly the same time in adjacent lanes, each traveling at 50 MPH, an event of superposition has

occurred. However, if the truck timestamps are stored to the nearest second, the position

uncertainty of the two trucks is:

$$\Delta x = \pm Speec_i \cdot \Delta t_{precision} = \pm 50 \frac{mi}{hr} \left(\frac{5280 ft}{mile} \right) \left(\frac{hr}{3600s} \right) \cdot 1s = 73 ft \qquad \textbf{Eq. 4.1}$$

4.2.7.2   IRD TCC-540WIM Portable WIM system

The International Road Dynamics TCC-540WIM contains all of the features of

the PAT TRS-WIM, with one exception, the timestamp is further refined. The TCC-

540WIM has the ability to store the vehicle time of arrival to the nearest one-hundredth

of a second allowing for measurement of vehicle multi-presence statistics. As shown in

Eq. 4.1, a whole second timestamp leads to a position estimation uncertainty of 73 feet at

highway speeds. The IRD system memory was programmed to store an additional data

string for the decimal seconds. Although every WIM system has the capability to

measure seconds with a resolution of 1/1000 sec, few until recently, stored the final

timestamp with such a resolution. The rationale relates to the memory capabilities. With

many sites having thousands of truck passages per day the extra two digits of data would

add to the memory demand and limit the overall number of records that could be stored.

4.2.8   The Fatigue System

The CR9000 Data logger, or Fatigue System, is designed to monitor the bridge

response of heavy truck loads passing over the bridge (Figure 4.16). The system is

programmed to record a time history for the passage of each heavy truck, as specified, by

gross vehicle weight and class. In addition, the system continuously collects hourly

rainflow stress cycle counts for each channel (ASTM 1985). There are 24 input channels that are designed for connecting 22 strain transducers and 2 LVDTs[1]. The 22 strain transducers are strategically located at fatigue critical sections. The LVDTs measure the deflection relative to a taut steel wire strung from pier to pier. Strain and deflection data are collected at 100 samples per second to capture the full dynamic effect of truck passages.

4.2.8.1   Rainflow Cycle Counting

A means of viewing the overall stress envelope of the bridge is needed for fatigue analysis. The heaviest trucks may not impose the most damage. The time history data captures only the heaviest loading events based on a WIM system trigger. A method of quantifying all of the stress ranges in the bridge in a compact format is needed. The rainflow method, ASTM E1049, evaluates the time history data and separates it into discrete stress ranges (ASTM 1985). The number of times a stress cycle of various ranges occurs is recorded in tabular format. Rainflow counting is needed to estimate the cumulative fatigue damage of bridge elements due to repetitive stress cycles. The fatigue system continuously stores strain and deflection readings in a ring buffer. The ring buffer is a 60-second record of all strain and deflection channel readings that is continuously overwritten with the newest data. Rainflow algorithms process the data from the buffer in real-time, counting the number and magnitude of stress cycles. Every hour the rainflow histograms are stored to permanent memory (flash cards) and reset to zero.

Hourly rainflow data is recorded for each of the 22 stress channels; covering ranges of 1 to 10 ksi at 1ksi increments. Each stress range cycle is tabulated into one of

---

[1] Linear Variable Differential Transducer (LVDT) an electronic device that measures displacement due to change in voltage.

ten categories or bins. For example, the 4 ksi bin contains all stress ranges between 4.0 and 4.99 ksi. Any stress range equal to or greater than 10 ksi is tabulated in the last bin. Hourly cycle data is useful for identifying periods of peak traffic and the respective stress cycles.
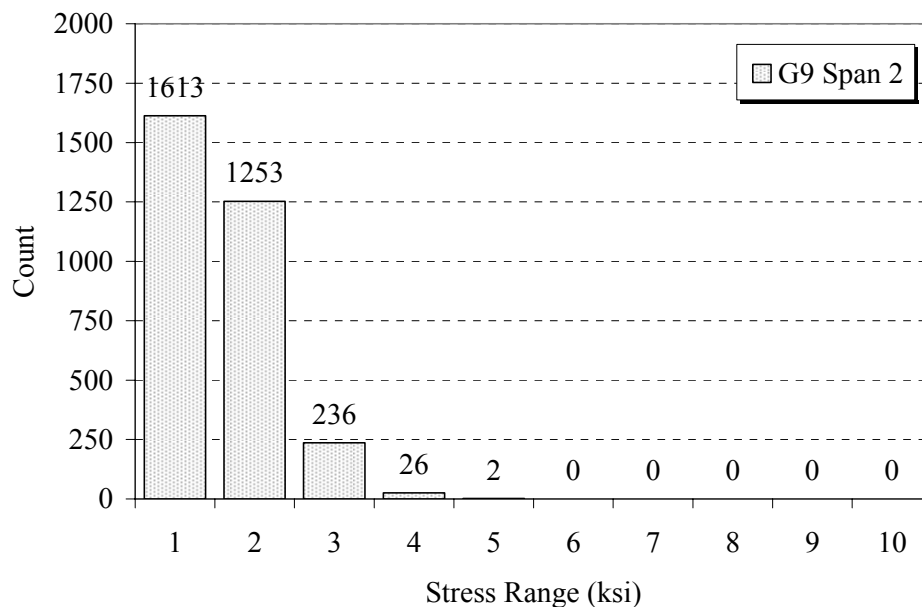
Figure 4.15 Typical daily rainflow histogram for Girder 9 Span 2 of Doremus Ave. Bridge

4.2.8.2   WIM System Trigger

One critical feature of this system is a data buffer that continuously monitors the strains and deflections of the bridge even when there is no load present. Therefore, when an exiting heavy truck is registered at the weigh-in-motion (WIM) system, the fatigue system is activated to capture the bridge response.
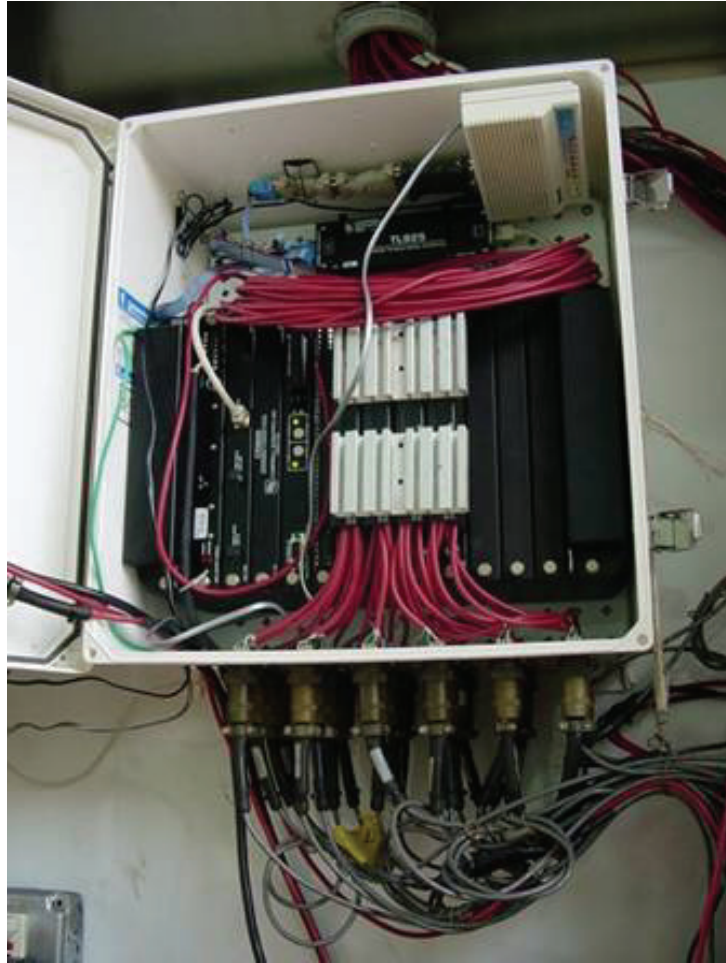
Figure 4.16 The Fatigue System shown monitors 22 strain and 2 deflection channels.

As previously mentioned, the main triggering mechanism for the Fatigue System is the text output of the WIM system. The flexibility of the CR9000 Data logger allows for specific categorized triggers. A listing of the gross vehicle weight and class triggers for the Doremus Avenue Bridge is shown in Table 4.2. The trigger values are chosen to limit the recorded data to heavy load events. Different truck configurations affect the stress induced on the bridge, therefore the GVW triggers differ by class. A schematic of the WIM and Fatigue system is shown in Figure 4.18. A flowchart illustrating the trigger mechanism is given in Figure 4.19.

Table 4.2 Trigger values by class for the Fatigue System at Doremus Ave.

FHWA Vehicle Class	Gross Weight (kips)
1 to 6	55
7	66
8	77
9	88
10 to 15	100

Soon after the WIM system identifies a truck, a comma-delimited ASCII text string is transmitted via a serial connection to the Fatigue System. This string, 125 characters in length, contains all relevant truck information as shown in Figure 4.17 and Table 4.3. For example, the record shown in Figure 4.17 is for a Class 9 truck traveling in lane 4, weighing 80.7 k, crossing the bridge on October 5, 2005 at 5:35:53.33 AM.

<4, ,10, 5, 5, 6,36,53,33, 1087, 5, 9, 807, 542, 348,146, 43,278, 39, , , , , 94,190,158,207,158, , , , >

Figure 4.17 Typical WIM ASCII Truck information string
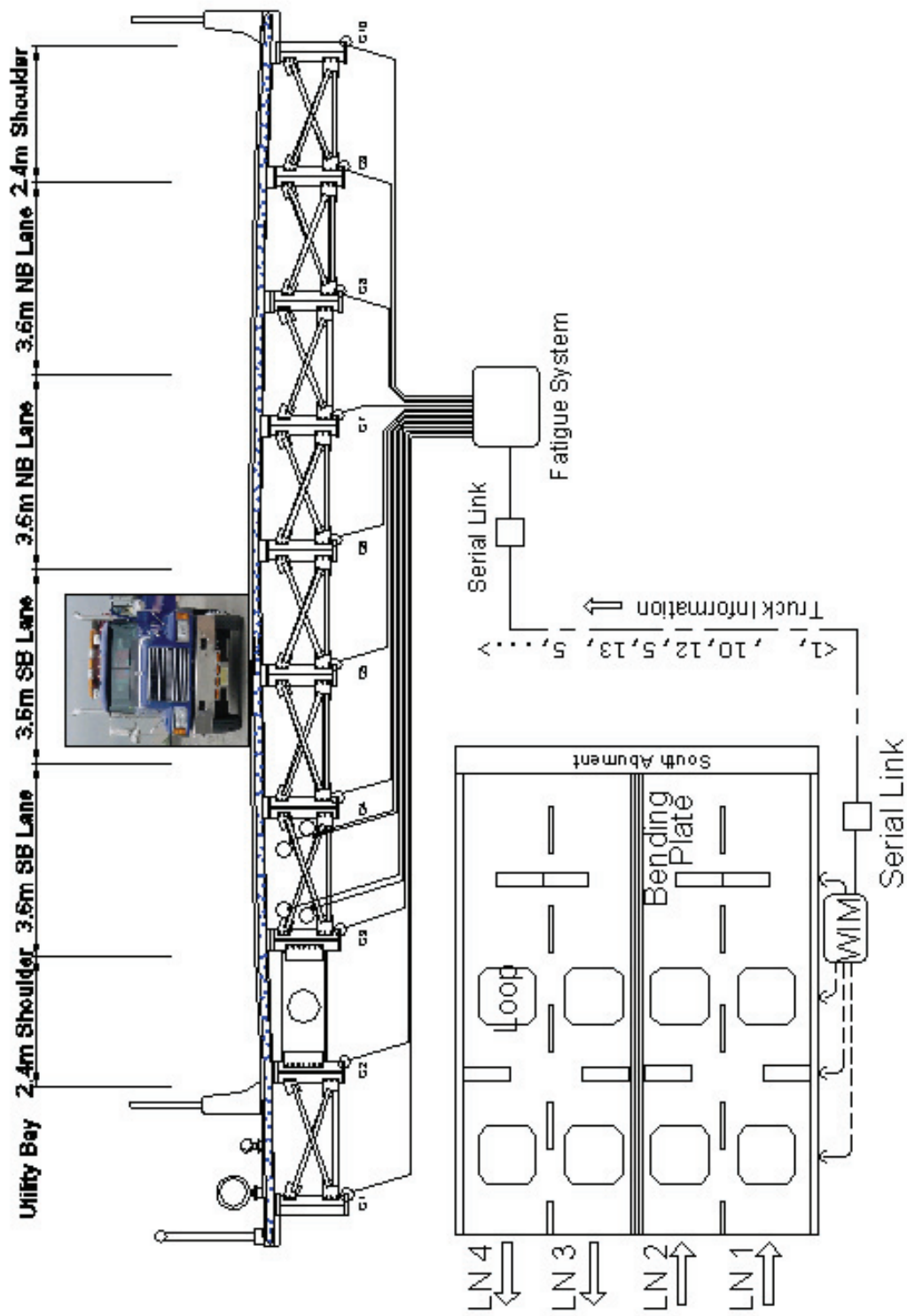
Figure 4.18 Doremus Avenue WIM and Fatigue System Layout including data link.
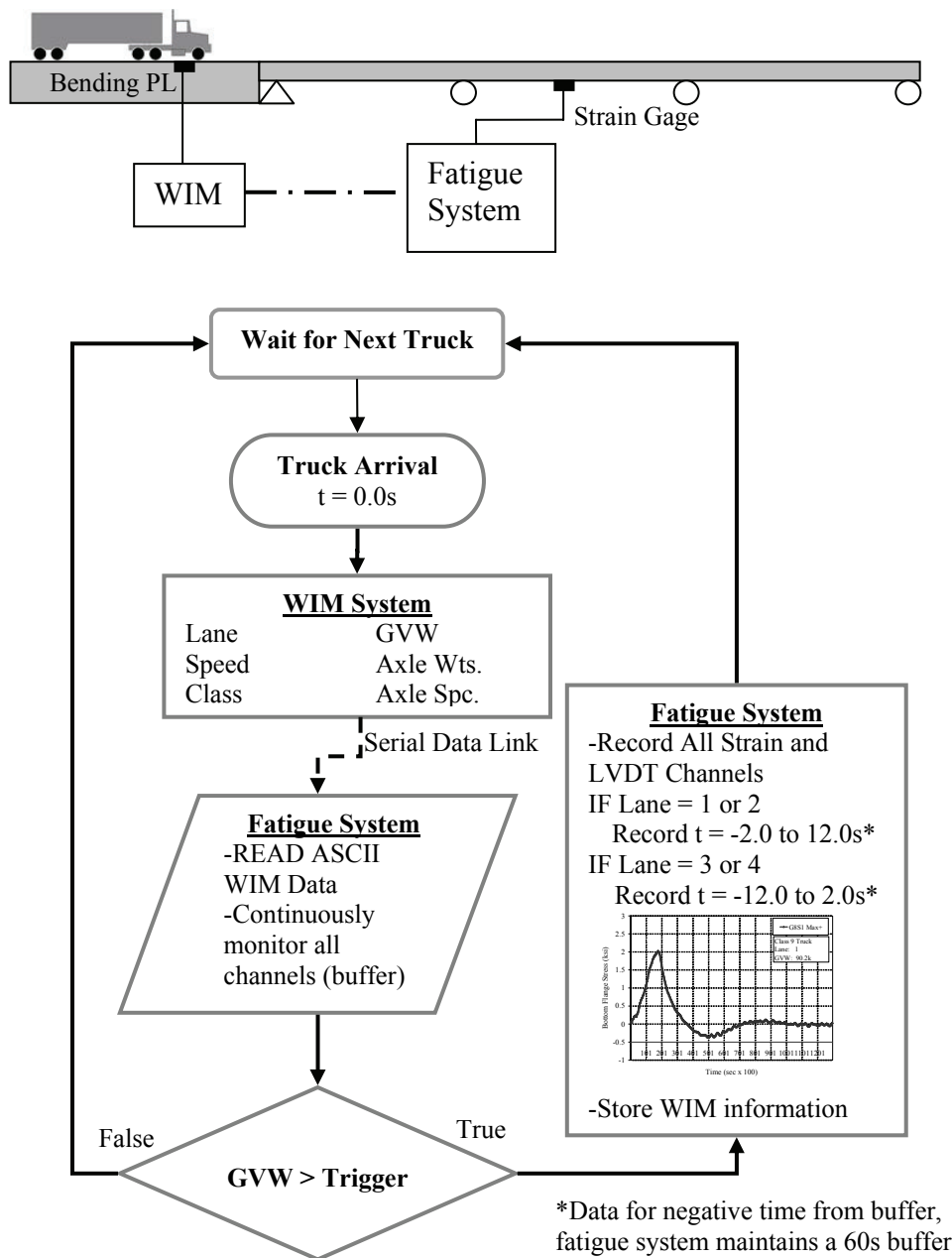
Figure 4.19 Flowchart of Fatigue System trigger from WIM system

The information in the ASCII string is formatted for memory efficiency. All of the ASCII WIM data is represented without decimals. For example, the GVW of a truck weighing 80.7k would be stored 807. This reduces the need to additional memory allocation for the decimal places of each parameter.

Table 4.3 WIM ASCII Truck information field labels

Data Field	Units / Comment
Lane	
Lane Direction	(Optional)
Month	Two Digits
Day	Two Digits
Year	One Digit
Hour	24-Hour Time
Minute	
Second	
Hundredth of Sec.	
Vehicle Number	Starts from 1 daily.
Number of Axles	
Class	
Gross Weight	x10, kips
Length	x10, feet
Speed	x10, MPH
Axle Spacing 1-2	x10, feet
…Axle Spc 8-9	x10, feet
Axle Weight 1-2	x10, feet
…Axle Weight 9	x10, feet

The truck information file is transmitted from the WIM system located on the south approach of the bridge to the Fatigue system located centrally underneath the structure. The signal is received by a Serial I/O Interface connected to the Fatigue System. This unit scans the serial channel continuously for incoming signals from the WIM. When an ASCII string is received, the serial interface relays the signal to a data logger input channel. The string is then separated into the fields shown in Table 4.3.

The Fatigue System evaluates the values of the "Class" and "Gross Vehicle Weight" fields to determine if a trigger condition has been met. If the weight exceeds the preset threshold shown in Table 4.2, the time history of the stresses and deflections are recorded. The pre-trigger data buffer of the Fatigue System compensates for the time needed to transmit and process the ASCII WIM string, typically 1 second. An extended pre-trigger is provided for Lanes 3 and 4 since the truck is weighed after crossings the bridge. The pre-trigger allows the fatigue system to capture readings for trucks that have already left the bridge. Strain and deflection data for the trigger vehicle is retrieved from the ring buffer and stored to permanent memory.

4.2.8.3   Time History Data

When a trigger condition is met, the system records stress and deflection time histories at a rate of 100 records per second. From the WIM ASCII string, the lane of travel and direction are known. For the northbound lanes, the data is collected one second before and eleven seconds after the fatigue system determines that there is a heavy truck present. On the other hand, for the southbound lanes, all of the data is post-triggered since the vehicle passes over the bending plate as it exits the bridge. The readings for all channels are monitored continuously, when a trigger event occurs a complete time history is stored. A typical time history record (Figure 4.20) is about 360 KB and contains 12,000 lines of data for each sensor. Additionally, the WIM vehicle number is added to the record to later identify the corresponding trigger vehicle.
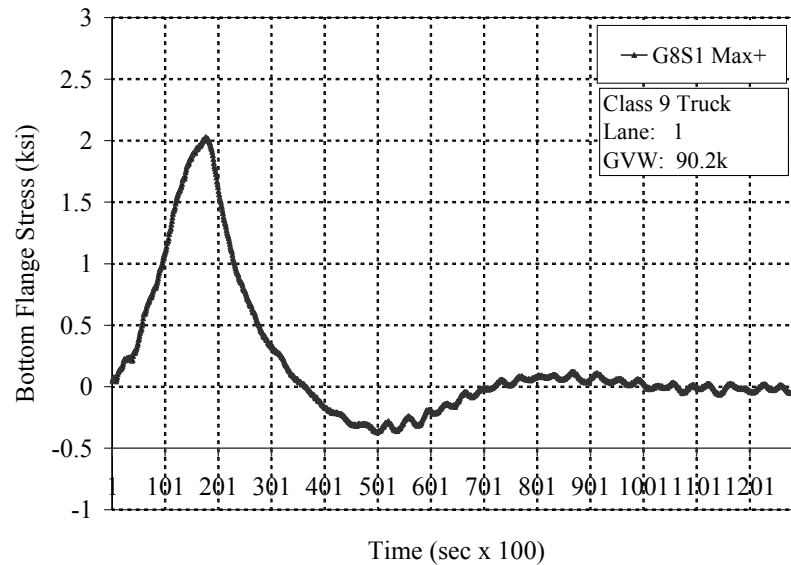
Figure 4.20 Typical time history stress record for Doremus Avenue Bridge

To compensate for signal drift and temperature induced stresses, a zeroing algorithm was developed. The system checks if the bridge is unloaded by monitoring the strain channels conditions. Every ten minutes, if no load is present, the strain gages and LVDTs are zeroed. Therefore, the strain and deflection readings represent the net effect of live load, not the temperature or sensor drift. Long-term loading effects such as concrete creep, thermal expansion/contraction, or settlement are not measured by this system.

4.2.8.4   WIM Data Storage

Once used to trigger the Fatigue System, the incoming WIM ASCII text string is stored to a separate record in the permanent memory. During post-processing, the time histories and WIM trigger record are searched using a FORTRAN program to locate the truck information. It was determined during trial runs that including the WIM trigger information in the time history was impractical.   Since the ASCII WIM data string is

concise, all data received from the serial link is stored within the Fatigue System. This allows comparison of live loads with not only trigger events, but general rainflow histograms.

4.2.9 Other Data Acquisition Systems

There are a number of other systems that were used to measure bridge response. These systems and their respective features are discussed in the following sections.

4.2.9.1 Structural Testing System (STS)

The STS system is a modular data acquisition system manufactured by Bridge Diagnostics Inc., Boulder CO. The system consists of a main processing unit that samples data, junction boxes, and strain transducers. The strain transducers are mounted to structural elements with clamps or bolted to epoxied tabs. Each sensor and junction box has a unique identification number and a microchip that allows it to be identified and located within the system. The sensor calibration factors are stored in the configuration files and applied automatically. The main advantage of the STS system is a random wiring capability. Sensors can be moved within the system and instantly identified independent of channel number. The STS as installed on Doremus included 64 sensors sampled at 100 Hz. Longer sampling durations require use of a different system along with a rain flow algorithm to reduce data requirements. The STS system is programmed and controlled with a notebook computer and powered with standard AC power or 12VDC vehicle power. The STS is highly reliable and rugged.

(a)   (b)
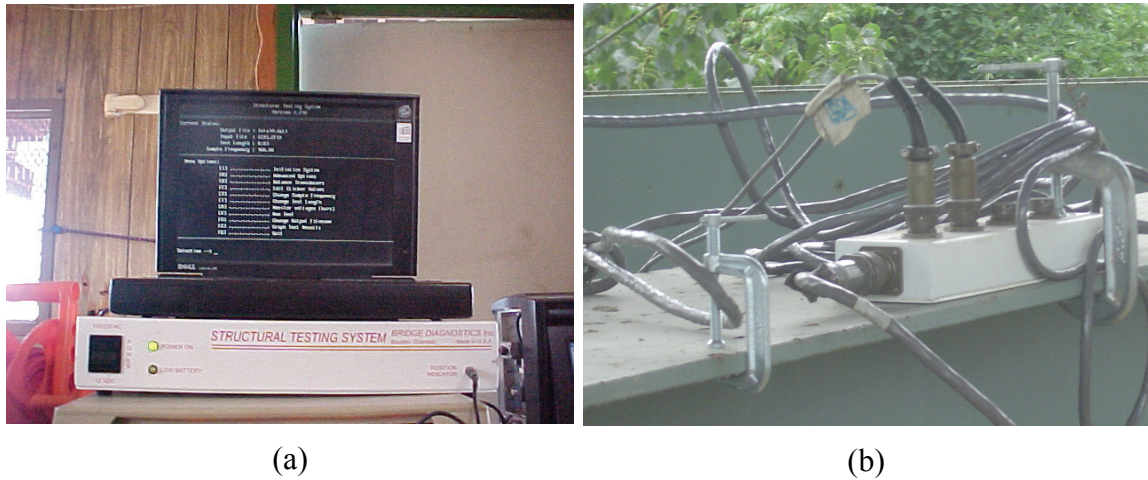
Figure 4.21 Structural Testing System: (a) main unit and (b) modular junction box

A typical test procedure consists of connecting the strain transducers to the

structural members, the strain transducers were connected to a junction box which in turn

is connected with a master cable to the main STS unit. The system is initialized and all

sensors are balanced to zero. Each test is assigned an automatic file number and the test

is initiated using a trigger button. Upon completion of the test, data is downloaded from

the STS unit to a notebook computer. The STS data files contain information such as

date, time, duration, sensor ID numbers, and strain data in ASCII text format.

4.2.9.2   MegaDac High Speed Data Acquisition System

The MegaDac is a data acquisition system manufactured by the now defunct

Optim Electronic Corporation. The Laser Doppler Vibrometer (LDV), accelerometers,

tape switches, and LVDT reference cable system were connected to the MegaDec for

load testing. The AC3415AC data acquisition system can connect to 48 channels and

sample at an overall rate of up to 25,000 Hz. Therefore it is ideal for dynamic testing

with a large number of sensors. Each sensor is connected to a satellite junction box

where the appropriate excitation voltages and configurations are set. Each junction box

handles up to 8 channels and is then connected to a channel board within the main unit.

The system interfaces with a notebook computer through a GPIB board via a USB cable.

The main advantage of the MegaDac is the large number of sensors and high sampling

rate. The overall disadvantage is that the system is cumbersome, not rugged, and

consumes a great deal of power.

(a)   (b)
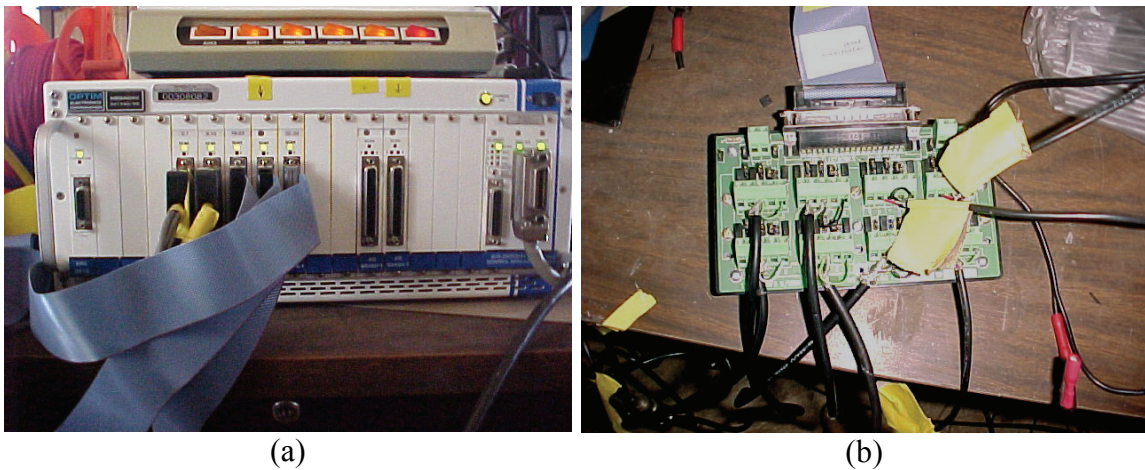
Figure 4.22 MegaDac system, (a), and modular junction box, (b)

4.2.9.3   SoMat eDaq

The SoMat eDaq is a compact portable data acquisition system designed primarily

for use in vehicle monitoring. The eDaq memory is provided by a modular PCMCIA

card that can be expanded. The unit can be programmed to take real time data, rainflow

tables, or intermittent burst records. The system boards are stacked and additional

channels can be added in the form of layers. The eDaq is primarily used with the Laser

Doppler Vibrometer, as a substitute for the Megadac data acquisition system when a

smaller number of channels is needed.

4.2.9.4   SOMAT 2100 Data Acquisition System

The SOMAT 2100 is a compact field data acquisition system with many of the same features as the Campbell CR9000 but in a scaled down unit. The system is powered, for up to 4 weeks, using 12-volt deep cycle batteries. Communication with the system is accomplished using either a serial cable or a Free Wave wireless radio transceiver. The system modules, or layers, are interchangeable for different field testing setups. BDI strain transducers are connected to 12-bit analog modules. The sampling rate for field testing was 100 Hz to capture the full dynamic effects of truck passages. A rainflow data mode was used to record the stress cycles continuously during the test period. Additionally, trigger values of stress were set to initiate a 4 second time history record known as burst history. Using the burst history, extreme truck load events could be seen in their entirety to verify large stress cycles and calculate load distribution factors. Other effects such as dynamic load amplification can be seen in the burst history.

The SOMAT 2100 does not have the capability to zero the channels during test runs. Therefore, temperature effects can be seen in the burst history records. These can be ignored since live load effects occur over a relatively short period of time compared to temperature effects. Furthermore, rainflow histograms only record the net live load stress cycles.

Figure 4.23 SoMat FCS2100 Data Acquisition System shown within protective enclosure

The main advantages of the FCS2100 are: small profile makes field installation simple, low power consumption, easy programming, very rugged and water resistant. The included Test Control Software is simple to program and features icon driven programming commands.

4.3   New Jersey Weigh-in-Motion Database

The New Jersey Department of Transportation has installed over 80 weigh-in-motion sites throughout the state to monitor long term trends in truck volumes and weights. The locations of these sites are shown in Figure 4.25 and described in Table 4.4. Each circle represents one WIM system which includes one or more instrumented lanes, a WIM data logger, and a permanent enclosure. The data from these sites is used for

pavement design, long-term freight planning, and enforcement. The functional

classification of the sites ranges from two lane country roads, to urban arterials, to major

interstate highways. The duration of available data varies by site depending on the

installation date. Typically about five years of data is available for the sites, with some

having as much as 13 years of continuous data.

Most of the NJWIM sites employ permanently installed piezo strip axle sensors.

These sensors are installed in slots cut into the roadway and filled with weather resistant

epoxy. A typical installation procedure is illustrated in Figure 4.11. First, slots are cut

into the asphalt wearing surface, the sensors are placed and aligned, and the sensor is

encased in epoxy. According to the manufacturer (IRD 2005) these sensors are rated for

over two million equivalent single axle loads (ESALS), a measure of the number of

equivalent 18k axle loads per truck. A typical five axle Class 9 (5-axle) vehicle exerts

1.2 ESALS per passage (FHWA 2001).
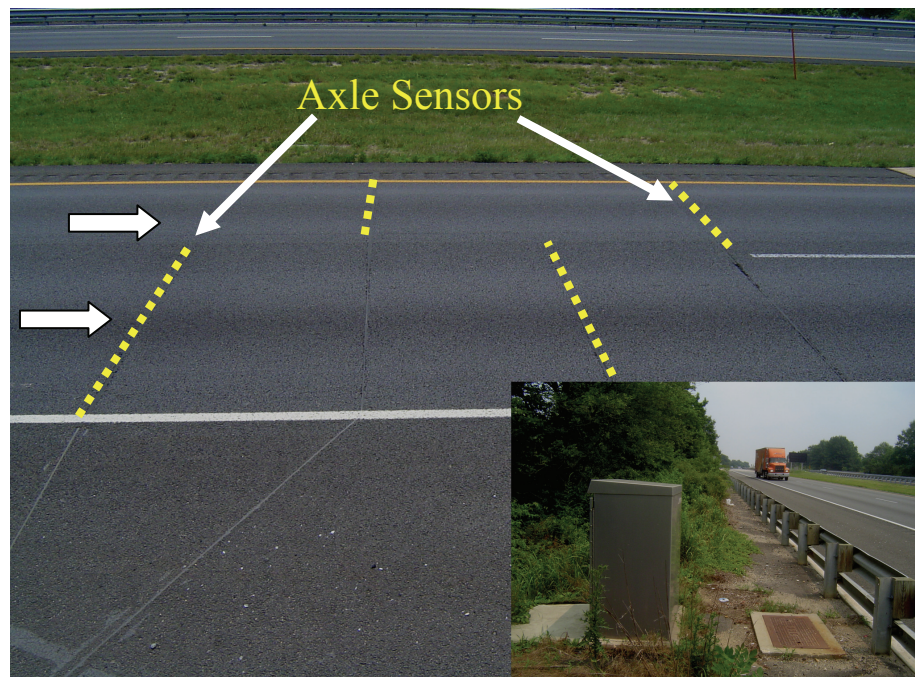
Figure 4.24 Sensor configuration for NJ WIM Site 195 (approaching traffic shown in insert)
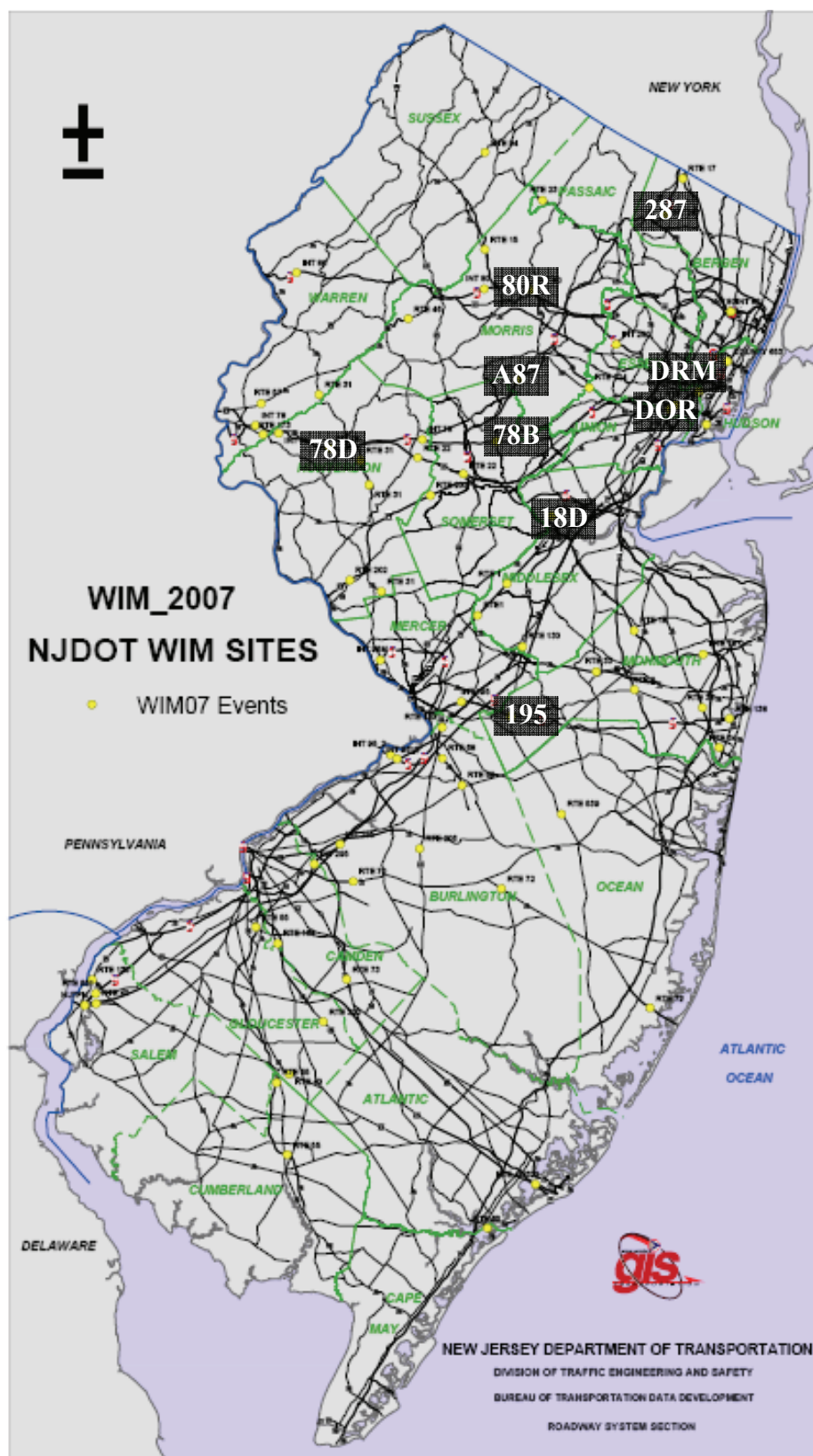
Figure 4.25 Selected New Jersey WIM Sites shown in rectangles (NJDOT 2007)

Table 4.4. Description and Location for NJWIM Sites (NJDOT)

ROUTE	LANES	MILEPOST	MUNICIPALITY	COUNTY	SITENAME	CONFIGURATION
Co-539	NB/SB(2)	29.3	PlumsteadTwp.	Ocean	539	(L-P-L-P)
Co-551	NB/SB(2)	6.8	UpperPittsgroveTwp	Salem	C51	(L-P-P-L)
Co-653	NB(2)	2.6	SecaucusTown	Hudson	CLR	(L-P-P-L)
DoremusAve	NB/SB(2)	2.3	NewarkCity	Essex	DRM	(L-P-L-P-L)
I-195	EB/WB(4)	4.0	HamiltonTwp.	Mercer	19B	(L-P-P-L)
I-195	EB/WB(4)	10.2	UpperFreehold	Monmouth	195	(L-P-P-L)
I-280	WB(3)	5.1	RoselandBoro	Essex	280	(L-P-P-L)
I-287	NB(3)	31.7	HardingTwp	Morris	A87	(L-P-P-L)
I-287	NB/SB(4)	61.7	FranklinLakesBoro	Bergen	287	(L-P-P-L)
I-295	NB/SB(6)	35.7	CherryHillTwp	Camden	I2C	(L-P-L-P)
I-295	NB/SB(6)	39.6	Mt.LaurelTwp	Burlington	295	(L-P-L-P)
I-78	EB/WB(6)	25.7	ReadingtonTwp.	Hunterdon	78D	(L-P-L-P)
I-78	WB(4)	34.5	BernardsTwp.	Somerset	78B	(L-P-L)
I-80	EB(6)/WB(6)	66.2	S.Hackensack	Bergen	SHE/SHW	(L-P-L-P-L)
NJ-124	EB/WB(4)	7.6	SummitCity	Union	124	(L-P-L-P-L)
NJ-138	EB/WB(4)	2.6	WallTownship	Monmouth	138	(L-P-L-P-L)
NJ-15	NB/SB(4)	7.1	JeffersonTwp	Morris	015	(L-P-P)
NJ-168	NB/SB(3)	1.3	GloucesterTwp	Camden	168	(L-P-P)
NJ-18	NB/SB(4)	16.0	ColtsNeckTwp	Monmouth	18B	(L-P-L-P-L)
NJ-18	NB/SB(4)	26.6	MarlboroTwp	Monmouth	018	(L-P-L-P)
NJ-18	NB(3)/SB(2)	44.6	PiscatawayTwp	Middlesex	18D	(L-P-L-P-L)
NJ-23	NB/SB(4)	23.8	WestMilfordTwp	Passaic	23	(L-P-L-P-L)
NJ-31	NB/SB(2)	13.0	EastAmwellTwp	Hunterdon	31B	(L-P-L-P-L)
NJ-31	NB/SB(4)	26.4	ReadingtonTwp.	Hunterdon	31D	(L-P-L-P-L)
NJ-31	NB/SB(2)	40.4	WashingtonTwp	Warren	31C	(L-P-L)
NJ-33	EB/WB(5)	23.5	ManalapanTwp	Monmouth	033	(L-P-P-L)
NJ-34	NB/SB(4)	0.6	WallTownship	Monmouth	034	(L-P-L-P-L)
NJ-34	NB/SB(4)	5.7	WallTownship	Monmouth	34B	(L-P-L-P)
NJ-55	SB(2)	27.4	VinelandCity	Cumberland	55C	(L-P-L)
NJ-55	NB(2)/SB(2)	57.9	DeptfordTwp	Gloucester	552	(L-P-P)
NJ-68	NB/SB(2)	2.4	SpringfieldTwp	Burlington	068	(L-P-P)
NJ-68	NB/SB(4)	7.0	MansfieldTwp	Burlington	68A	(L-P-L)
NJ-72	EB/WB(2)	2.1	WoodlandTwp	Burlington	072	(L-P-P-L)
NJ-73	NB/SB(4)	11.9	WinslowTwp	Camden	073	(L-P-P)
NJ-94	NB/SB(2)	33.8	HardystonTwp	Sussex	094	(L-P-L)
NJTPK	NB(2)	0.8	CarneysPointTwp	Salem	NJT	(L-P-P-L)
US-1	NB/SB(6)	12.9	PlainsboroTwp.	Middlesex	001	(L-P-L-P-L)
US-1	NB/SB(4)	18.0	S.BrunswickTwp	Middlesex	01A	(L-P-L-P-L)
US-130	NB/SB(4)	57.0	BordentownTwp	Burlington	13B	(L-P-P-L)
US-130	NB/SB(4)	70.6	CranburyTwp	Middlesex	13A	(L-P-L-P)
US-202	NB/SB(4)	3.5	WestAmwellTwp	Hunterdon	202	(L-P-P)
US-202	NB/SB(4)	19.2	BranchburgTwp	Somerset	02B	(L-P-L-P-L)
US-22	EB/WB(4)	26.6	ReadingtonTwp.	Hunterdon	022	(L-P-P-L)
US-22	EB/WB(4)	32.3	BridgewaterTwp	Somerset	22B	(L-P-P-L)
US-322	EB/WB(4)	27.5	MonroeTwp	Gloucester	322	(L-P-L-P-L)

Where: NB=Northbound, SB=Southbound, L=Detection Loop, P=Piezo Axle Sensor, BP=Bending Plate

Table 4.4 **(Continued)**

ROUTE	LANES	MILEPOST	MUNICIPALITY	COUNTY	SITENAME	CONFIGURATION
US-40	EB/WB(4)	3.0	CarneysPointTwp	Salem	40A	EB:(L-P-L-P-L) WB:(L-P-P-L)
US-40	EB/WB(2)	28.4	FranklinTwp	Gloucester	040	(L-P-P)
US-40	EB/WB(4)	61.6	EggHarborTwp	Atlantic	40B	(L-P-L)
US-46	EB/WB(4)	25.2	MountOliveTwp	Morris	046	(L-P-L-P-L)
US-9	NB/SB(4)	111.8	FreeholdTwp	Monmouth	09A	(L-P-P)
I-295	NB/SB(4)	2.9	CarneysPoint	Salem	I2S	(L-BP-BP-L)
US-130	NB/SB(2)	3.4	PennsGroveBo	Salem	130	(L-BP-BP-L)
NJ-72	EB/WB(4)	25.0	StaffordTwp	Ocean	72B	(L-P-L-P)
US-1&9	SB(7)	48.1	NerwarkCity	Essex	01C	(L-P-L-P-L)
I-78	EB(3)	5.0	GreenwichTwp	Warren	78E	(P-L-P)
I-78	WB(3)	7.9	BetlehemTwp	Hunterdon	78W	(P-L-P)
I-676	NB/SB(4)		CamdenCity	Camden	676	(L-P-L-P-L)
I-80	EB/WB(6)	32.4	Roxbury	Morris	80B	(L-P-L-P)
I-80	EB/WB(8)	38.1	Rockaway	Morris	80C	(L-P-L-P)
I-80	EB(4)/WB(3)	8.3	Knowlton	Warren	80A	(L-P-L-P)
I-95	NB/SB(6)	1.2	Ewing	Mercer	095	(L-P-L-P)
I-95	NB/SB(6)	6.3	LawrenceTwp	Mercer	95B	(L-P-L-P)
NJ-55	NB/SB(4)	37.0	VinelandCity	Cumberland	551	(L-P-L-P)
NJ-57	EB/WB(4)	3.5	GreenwichTwp	Warren	57A	(P-L-P)
NJ-70	EB/WB(2)	10.3	EveshamTwp.	Burlington	551	(L-P-L-P-L)
NJ-173	EB/WB(4)	2.4	GreenwichTwp	Warren	173	(P-L-P)
I-78	EB/WB(6)	14.5	Union	Hunterdon	78A	(L-P-P)
I-95	NB(2)	2.1	Ewing	Mercer	952	(L-BP-L)
NJ-17	SB(3)	25.5	Mahwah	Bergen	017	BendingPlates
NJ-31	NB/SB(4)	30.1	Clinton	Hunterdon	031	(L-P-P)
NJ-52	NB/SB(4)	1.6	OceanCity	CapeMay	052	(L-P-L)
NJ-440	NB/SB(4)	21.4	BayoneCity	Hudson	169	BendingPlates
US-1&9	SB(2)Ex	47.2	NerwarkCity	Essex	01B	(L-P-L-P-L)
US-206	NB/SB(2)	22.0	Southampton	Burlington	206	(L-P-P)

Where: NB=Northbound, SB=Southbound, L=Detection Loop, P=Piezo Axle Sensor, BP=Bending Plate

The following diagrams illustrate the lane layout for NJ WIM Sites. Solid arrows indicate WIM instrumented lanes, empty arrows indicate lane direction for other lanes (not instrumented).
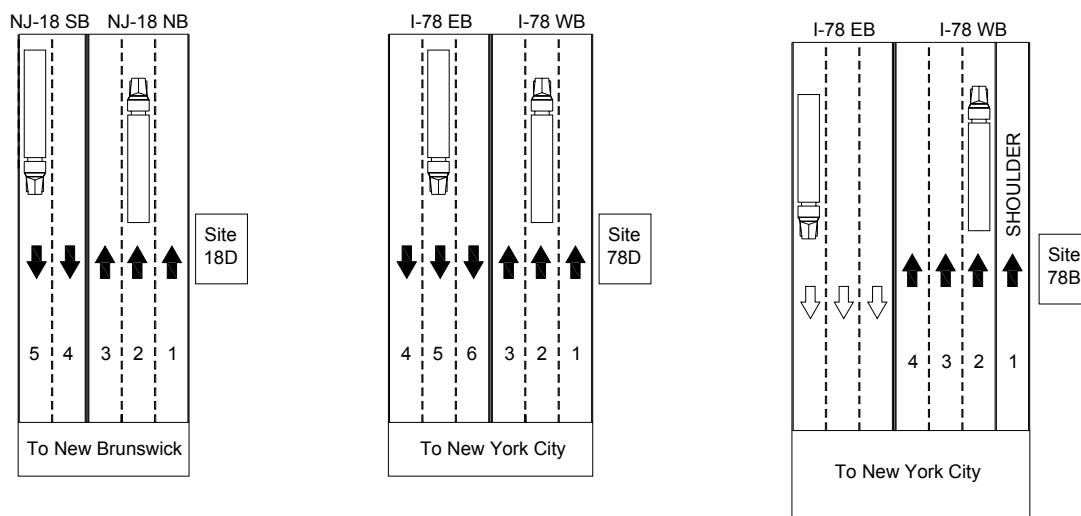
Figure 4.26 WIM System configurations for NJWIM sites 18D (left), 78D (middle), and 78B (right)
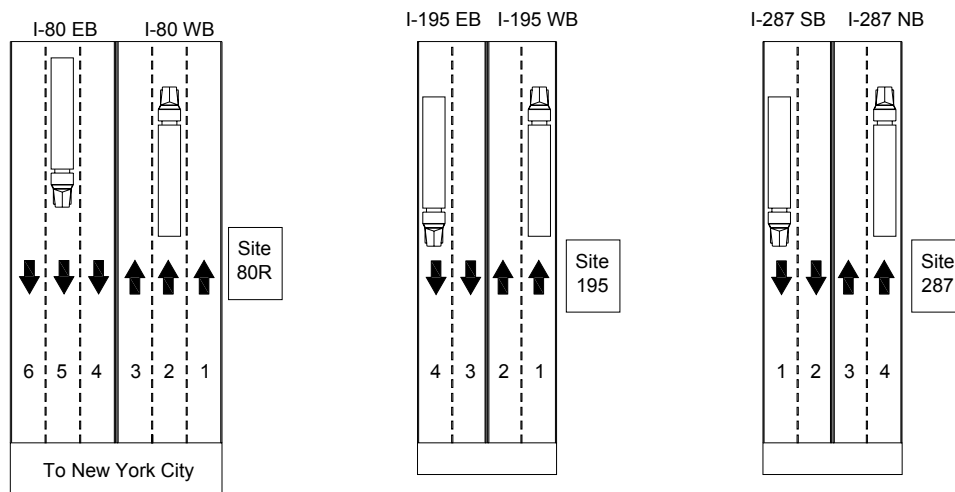
Figure 4.27 WIM System configurations for NJWIM sites 80R (left), 195 (middle), and 287 (right)
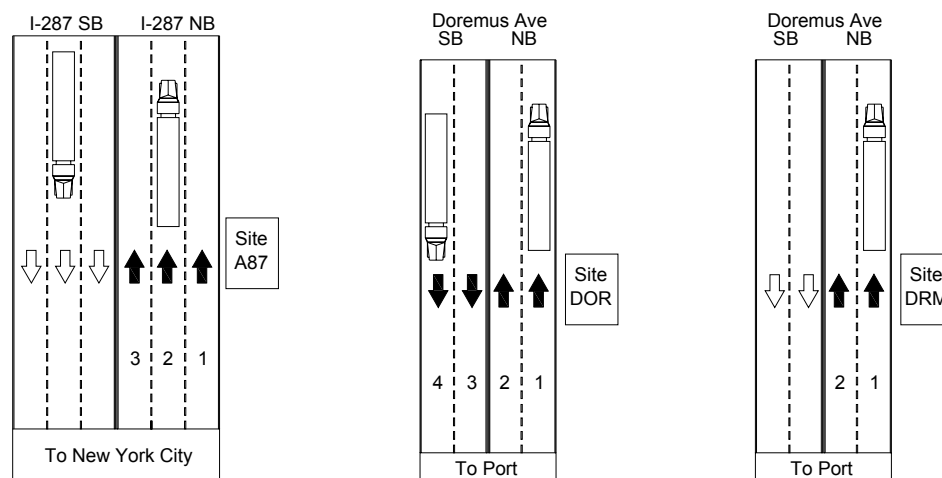
Figure 4.28 WIM System configurations for sites A87 (left), Doremus Avenue Bridge DOR (middle), and (right)

4.4 Other Field Investigation

In addition to the newly constructed Doremus Avenue Bridge, other bridge sites were investigated using similar methodology of measuring the live loads and the bridge response simultaneously. Testing of different types of bridges under site specific load spectra is valuable when studying the effect of live loads. Furthermore, it is important to measure live load spectra in different regions when developing a general load model.

4.4.1   NJ Turnpike Delaware River Bridge

As part of a deck cracking diagnosis and mitigation study for the NJ Turnpike Authority, the Turnpike Delaware River Bridge near interchange 6 in Florence Township, Burlington County was instrumented. The test program included: (1) installation of strain and deflection sensors, (2) controlled live load testing with vehicles of known weight and traffic closure, (3) concrete material testing, (4) portable weigh in motion, and (5) long-term structural monitoring. The portable WIM data obtained at this site is

unique in that there are very few weigh-in-motion sites along the 130-mile NJ Turnpike system. Only the right lane of westbound traffic was instrumented for the WIM study.

The structure of this bridge consists of three different repeating units: (1) simple span plate girder, floor beam, stringer with concrete deck, (2) deep truss, floor beam, stringer with deck, and (3) through-arch truss with suspended simple plate girder spans. The primary focus was on the plate girder and deep truss spans. Demountable BDI strain transducers were clamped to the bottom flanges of the stringers, floor beams, trusses, and plate girders at points of interest, particularly midspan between supports.

Figure 4.29 NJ Turnpike Delaware River Bridge near Interchange 6, Florence Twp., Burlington County.

As part of the controlled live load testing the contractor provided a 3-axle loaded truck and driver. Traffic closure during dynamic and static testing was provided by the NJ State Police. Live load testing was performed to calibrate a finite element model that would later be used to simulate possible mitigation strategies. During testing data from sixteen strain channels and Laser Doppler Vibrometer (one deflection and one velocity channel) were sampled at 100 Hz with two data acquisition systems. Since complete traffic closure even at five minute intervals causes significant traffic congestion, the overall number of controlled tests was limited. Therefore, additional information would need to be gathered during ambient traffic conditions.

To measure the stresses under ambient traffic, with no traffic control or test vehicle, a SoMat FCS2100, field data acquisition system was installed on one of the plate girder spans. A total of six strain channels, battery, wireless communication link, and solar panel were connected to the SoMat. The system was programmed to rainflow count each channel at one hour intervals, creating a separate stress cycle histogram for each hour. A start trigger was also added to the channel underneath the right lane to initiate a burst time history record when a specific stress magnitude was measured. Normally, rainflow histograms are continually tabulating stress cycles. However, when a truck caused a stress in the trigger of more than 3 ksi, a six second burst stress history was recorded and stored along with the timestamp. The timestamp would later allow correlation between WIM data trucks and burst stress events for comparison.
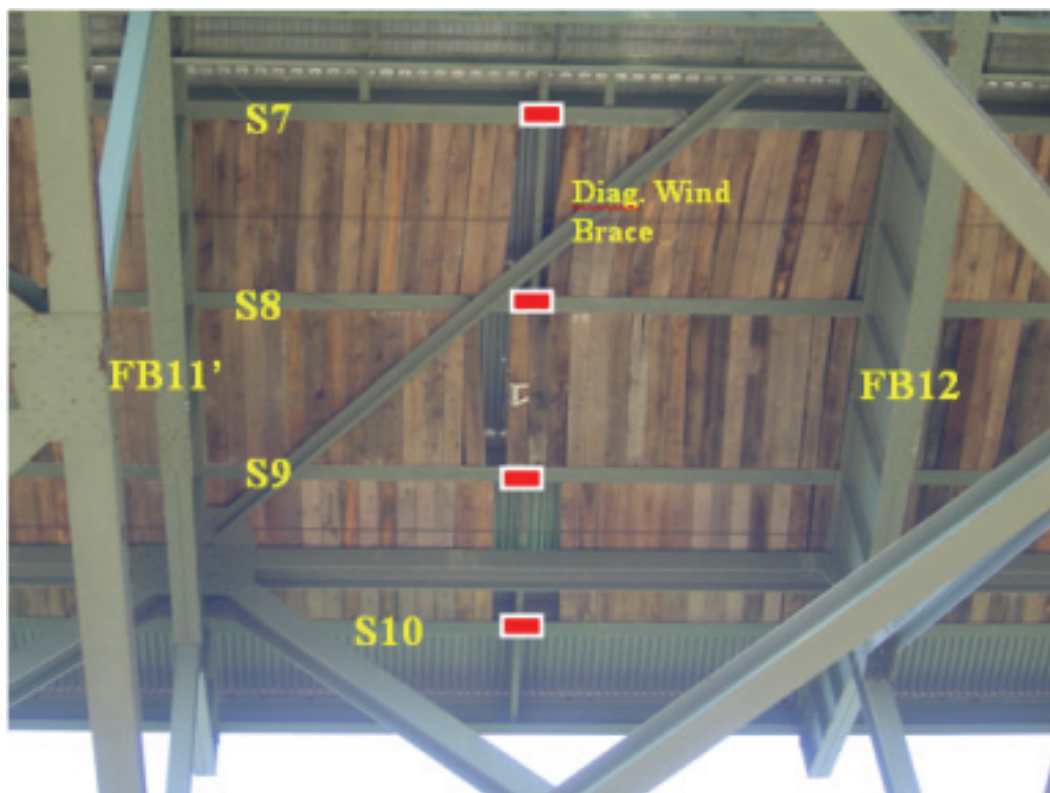
Figure 4.30 Under deck view of NJ Turnpike Delaware River Bridge at Span 26 showing typical sensor locations (rectangles)

A total of 71 controlled live load tests were conducted and 3 months of ambient data collected. Data from this study will give the NJ Turnpike Authority insight into the effect of actual traffic on the highway and allow them to enact measures to reduce the live load effects of adjacent truck traffic on newly poured concrete decks.

4.4.2 Route 18 Over River Road

The Route 18 over River Road Bridge is a three span continuous, 6 girder steel bridge, carrying two lanes (Figure 4.31 and Figure 4.32). At the time of testing, the bridge had been open to traffic for about one year. The plate girders are variable in section along the span with the greatest thickness in the negative moment region over the

piers. The deck is orthogonal with the abutments and the typical girder spacing is 9 ft.

There are 5 sets of intermediate diaphragms within each span.   There are two separate

parallel structures that carry Route 18 over River Road each with three continuous spans

of 35, 45, and 35m. This study focuses on the six-girder southbound structure since the

majority of the northbound traffic exit the highway before being weighed at a permanent

WIM station about 1 mile north of the bridge. The southbound traffic passes through the

WIM station about one mile upstream of the bridge with few trucks exiting prior to

crossing. Additionally, a portable WIM system, axle sensors, and vehicle detection loops

were installed in each of the two lanes to verify the amount of continuous traffic from the

upstream permanent WIM station (Figure 4.31c and Figure 4.32).

(a)

(b)

(c)
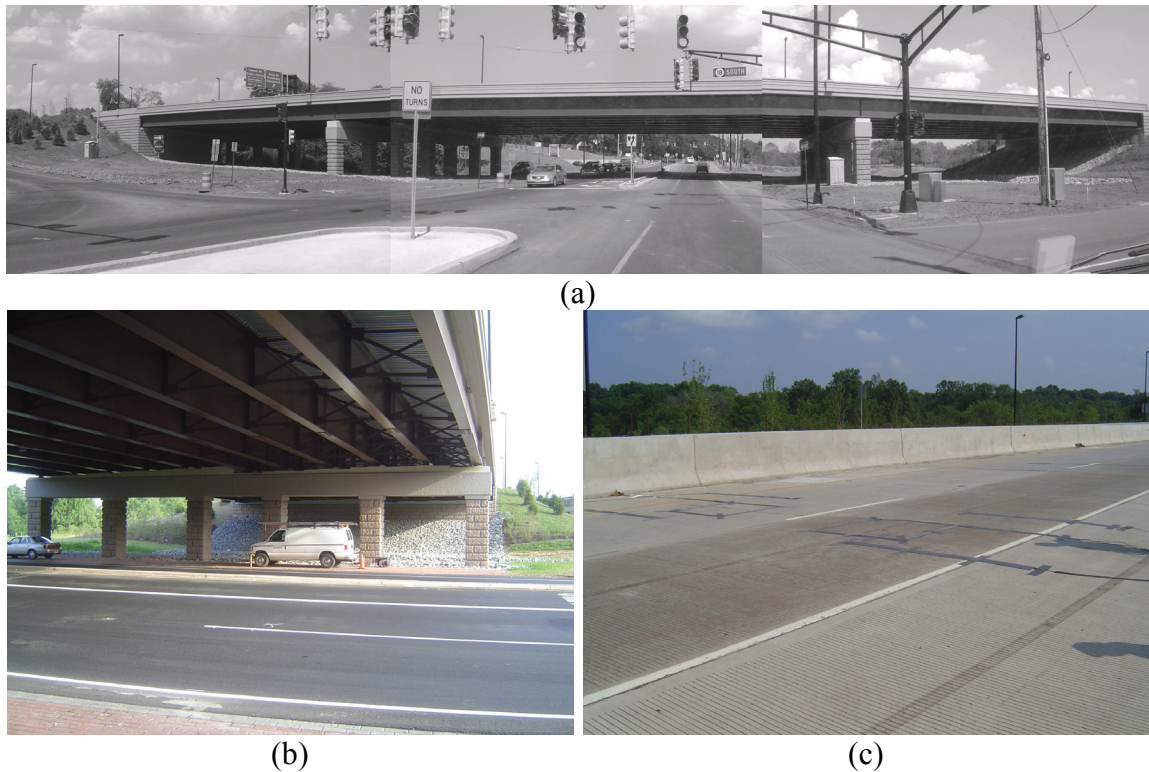
Figure 4.31 Route 18 over River Road Bridge: (a) elevation view, (b) under-deck view, and (c) roadway view with temporary WIM installed

The instrumentation layout in Figure 4.32 shows that strain gages were placed across Span 3 to capture the full bridge response at the maximum moment location. Additionally, a cross frame between girder 3 and girder 4 was instrumented. Only a single gage was installed on the northbound structure. Carry through vibrations were detected on the southbound structure during a northbound truck passage. The two parallel bridges are separated by a one inch gap between the parapets. Construction debris had been lodged in the gap and may have transmitted lateral movement between the bridges. The structures share common piers, but have independent bearings.

The bridge, part of a newly completed three mile Route 18 extension, provides a major link in the local road network between the New Jersey Turnpike in the east and Interstate 287 in the west. The owner, New Jersey Department of Transportation, installed a permanent WIM system about one mile north of the River Road Bridge to monitor truck usage of the new roadway (NJWIM Site 18D). The permanent WIM data and its coordination with bridge response data will be discussed in the results section.
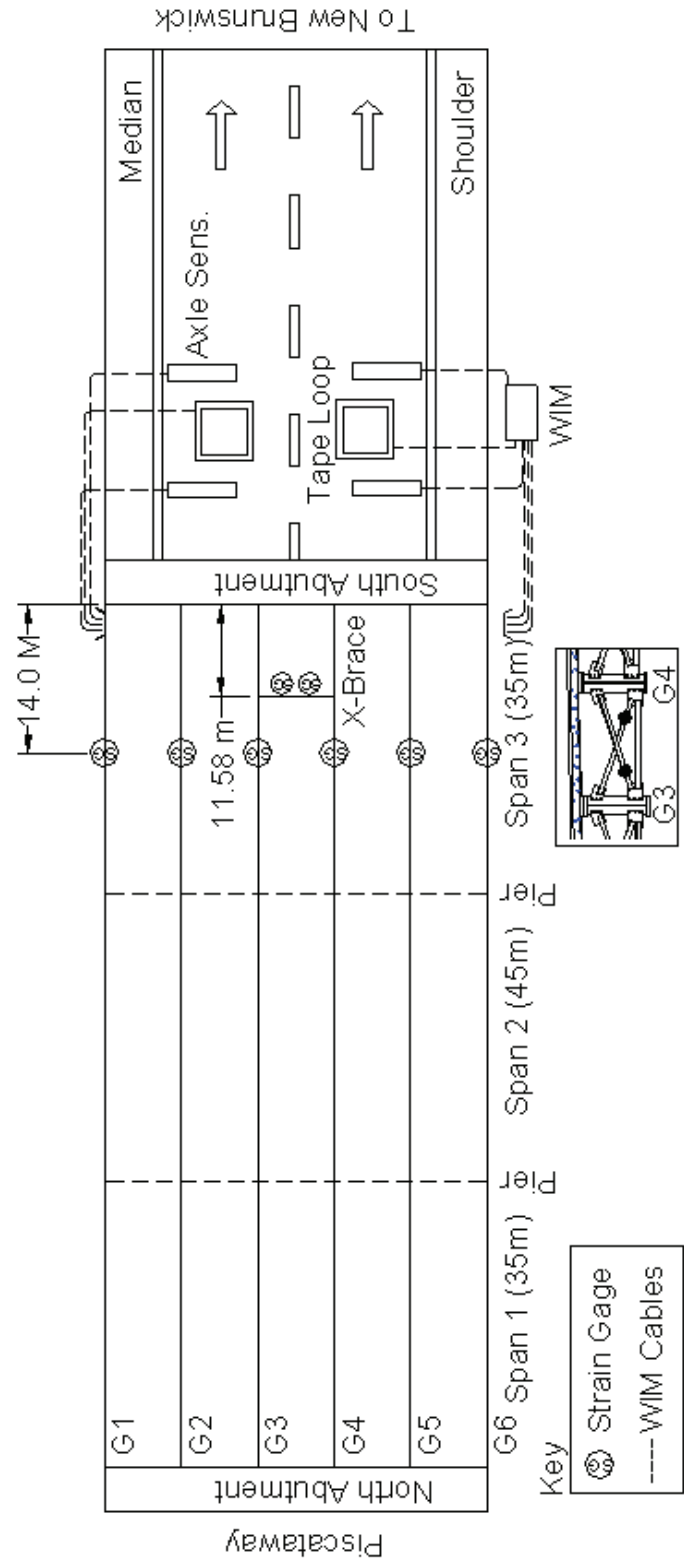
Figure 4.32 Typical portable WIM sensor layout as installed on Route 18 at River Road in July 2005.

4.4.3   Route 23 Over Route 202

The Route 23 over Route 202 Bridge has four simple spans of 16 girders each. The bridge, constructed in 1983, carries 7 lanes over railroad tracks and highway access ramps. Each direction consists of a separate 8 girder structure. The average daily traffic for 2004 was 88,000 vehicles (both directions), with 4% truck traffic. The study span was the 120 ft, second span from the south (Figure 4.33). The south pier is perpendicular to the superstructure, while the north pier is skewed 23 degrees to accommodate a railroad right-of-way. A series of lateral braces connect the outer pair and inner pair of girders. The braces are connected to the girders with a gusset plate welded to the web, 4 inches above the tension flange at transverse stiffener locations. Extensive cracking has developed at the weld toes of the lateral brace connection gussets. A total of 260 gusset weld locations with 89 cracks were noted in a 2004 inspection report. The longest crack length reported was 3.5 inches.

To diagnose the cause of cracking, short term monitoring of member strains was initiated. As Figure 4.33 indicates the primary focus for instrumentation was the lateral bracing members and the girder bottom flanges at the connection locations. A total of ten demountable BDI strain transducers were clamped to the members and connected to a SoMat FCS2100 Field Data acquisition system. Marine deep-cycle batteries, a solar panel, and a wireless communication link were also installed. The structural drawings and recent inspection reports for this bridge were obtained from the New Jersey Department of Transportation for use in planning the instrumentation and checking member stresses.

Rainflow stress cycle tables and burst time history stress data were collected for a period of three weeks. The data indicated that the bridge was subject to relatively low magnitude stress cycles, however, vibration was evident in girders and lateral braces. Hundreds of low amplitude stress cycles on the order of about 0.5 to 1.0 ksi were evident in the lateral braces during each truck passage. Since there were no nearby permanent WIM stations, nor portable WIM system data, truck weights could only be estimated using girder distribution factors and observed girder stresses.
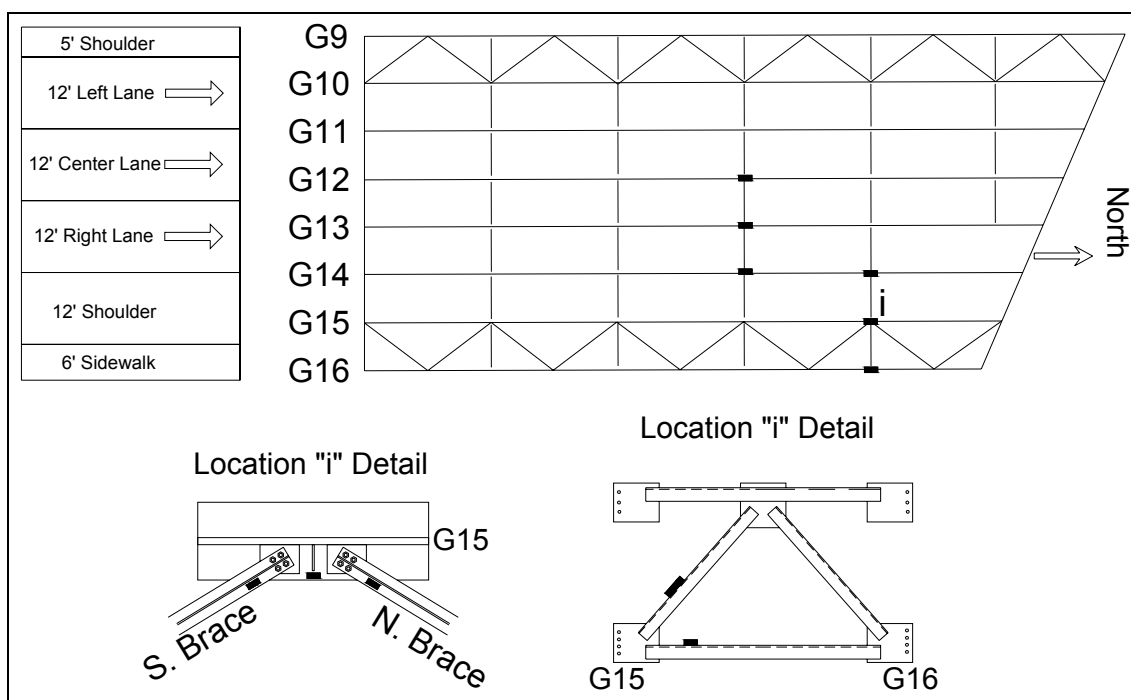
Figure 4.33 Route 23 over Route 202 Span 2 instrumentation plan.

Figure 4.34 Route 202/23 bridge: (a) under deck view of girders and bracing and (b) close-up view of lateral connection plate and cracked web

4.5   Bridge Models

Modeling is used to analyze complex structural systems in some idealized form. Certain assumptions help make the transition from structural reality to computational feasibility. Every structure is idealized in order to facilitate design. The AASHTO bridge design code uses load distribution factors that approximate how much load each element bears. Therein lies the error of design. Often complexity and accuracy are coupled in modeling. The most complex models, such as three-dimensional finite element analysis, offer incredible accuracy but are computationally demanding. Additionally, a great deal of pre-analysis is needed determine the model inputs (i.e. structural connections, and special geometry). The simplest model, a one-dimensional beam, offers the fastest analysis for preliminary design purposes; however, more detailed methods are applied to the final design.

A balance can be found between accuracy and efficiency. Different models use different degrees of idealizations to achieve simplification. A model should be chosen to

best represent the structure with the highest degree of accuracy. More common structures such as slab on girder bridges without skew can be modeled with a high degree of accuracy using less complex models. The level of simplification should be considered when executing numerous simulations. The Monte Carlo technique often demands more than 1000 model runs. Finite element models of a full bridge structure can take as long as 30 minutes per single truck run. Thus, for repetitive simulation a simpler model is needed without excessive loss of accuracy.

4.5.1   Beam Line Analysis

The simplest representation of a bridge is a single beam spanned between two supports. This method is a simplification that may be used to determine the overall moment that different vehicle configurations cause over different spans. Since the moment that any truck causes on a bridge is related to its axle weights and axle spacings, simply choosing the heaviest trucks by overall weight for analysis would not be sensible. A short vehicle will, in fact, induce a higher moment on a beam than a truck of similar weight but with larger axle spacing. Additionally, most truck configurations are designed to pass the FHWA bridge equation, which requires that axle weight and spaces be chosen specifically to reduce the truck effects on bridges.

Simple beam models and influence lines were constructed for simple bending moment, simple span shear force at the support, negative moment on continuous beams, positive bending moment on continuous beams, and shear force on continuous spans. A representation of the simple beam with the applied truck axle loads is shown in Figure 4.35.
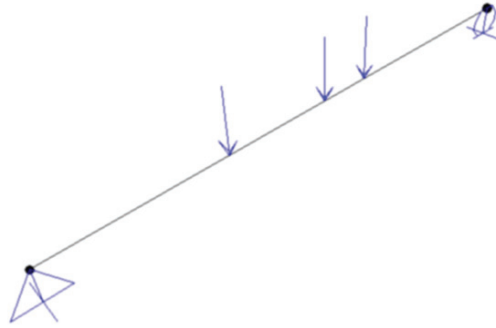
Figure 4.35 Simple beam model shown with applied axle loads

The limitation of the simple beam model for bridges can be appreciated when designing the individual girders. The beam model gives the total moment that a truck will cause for the bridge as a whole. The deck distributes the load to the girders; therefore, no single girder will bear the entire load. Girder distribution factors may be estimated from design equations, simplified analysis, or computer modeling. Furthermore, controlled live load testing can be performed to find the actual girder distribution. Article 4.6.2.2 of the AASHTO LRFD Design Specifications (AASHTO 2004) provides equations for estimating the maximum proportion of total load that will be distributed to a single girder. Eq. 4.2 and Eq. 4.3 show the Imbsen and Associates, Inc. design equation for girder distribution to an interior girder for single and two-lanes loaded as given in the AASTHTO specifications, respectively. The GDF equations for exterior girders with a single and two-lanes loaded are given in Eq. 4.4 and Eq. 4.5, respectively.

$$\text{Interior } GDF_{\sin gle\_lane} = 0.06 + \left(\frac{S}{14}\right)^{0.4} \left(\frac{S}{L}\right)^{0.3} \left(\frac{K_g}{12.0Lt_s^3}\right)^{0.1}$$

Eq. 4.2

Eq. 4.3

$$\text{Interior } GDF_{two\_lane} = 0.075 + \left(\frac{S}{9.5}\right)^{0.6} \left(\frac{S}{L}\right)^{0.2} \left(\frac{K_g}{12.0Lt_s^3}\right)^{0.1}$$

$$\text{Exterior } GDF_{\sin gle\_lane} = 0.06 + \left(\frac{S}{14}\right)^{0.4} \left(\frac{S}{L}\right)^{0.3} \left(\frac{K_g}{12.0Lt_s^3}\right)^{0.1}$$

Eq. 4.4

Eq. 4.5

$$\text{Exterior } GDF_{two\_lane} = 0.075 + \left(\frac{S}{9.5}\right)^{0.6} \left(\frac{S}{L}\right)^{0.2} \left(\frac{K_g}{12.0Lt_s^3}\right)^{0.1}$$

Where, $K_g = n(I + Ae_g^2)$

Where, $n = E_B / E_D$

GDF=proportion of load to most loaded girder

S = transverse girder spacing, ft

L = Span length, ft

K_g = longitudinal stiffness parameter, in^4

t_s = deck thickness, in

I = moment of inertia, in^4

e_g = distance between the centers of gravity of the beam and deck, in

E_B = modulus of elasticity of beam material, ksi

E_D = modulus of deck of beam material, ksi

The limitations of the AASHTO GDF equations are summarized as follows:

$3.5 \le S \le 16.0$

$4.5 \le t_s \le 12.0$

$20 \le L \le 240$

Number of beams ≥ 4

The equations for GDF in the AASHTO LRFD (Eq. 4.2 to Eq. 4.5) have been criticized by the bridge design community for being cumbersome and overly complicated, although accurate (Phuvoravan et al. 2004). The main complaint lies with the longitudinal stiffness parameter, K_g, since it requires that the girder properties be known in order to determine the distribution of moment. Thus an iterative procedure

must be used where the designer assumes the girder properties, finds the moment distribution, and then must return if the section differs from the initial assumption.

4.5.1.1   Beam Analysis Program

A FORTRAN 90 program was developed to calculate the moments of trucks en masse (Nassif 1993). The FORTRAN programming language offers the computational efficiency to handle large volumes of numerical data. A number of additional programs were developed to handle, convert, compute, and process results. Conventional spreadsheet applications lack the capacity and features needed to handle such large datasets.

The main beam analysis program reads the number of axles, axle weights, and axle spaces from a prepared input file. Next, truck information is used to calculate: (1) maximum simple bending moment, (2) maximum simple shear, (3) maximum negative moment on two continuous spans, (4) maximum positive bending moment on two continuous spans, and (5) maximum shear on two continuous spans. For each truck, the maximum moment position is calculated by the absolute maximum moment method. The truck is then applied to the beam model to produce the maximum load effect. A series of HS20 design moments and shears are declared at the start of the program. The maximum load effect for each sample truck is compared to the governing design load effect in the form of a ratio to HS20. Therefore, a ratio of 1.0 would signify an effect equivalent to the design truck. For each load parameter the individual moment or shear ratio is stored to an array to later be converted to a cumulative density function, CDF, on the Normal probability paper, NPP.

The value of the beam analysis program lies in its ability to consider the effect of each truck in an extensive database that sometimes exceeds three million truck per run.

4.5.2   Semi-Continuum Model

The semi-continuum model, developed by Bakht and Jaeger (1985, 1989), assumes a continuous stiffness in the transverse direction of a bridge structure. The model assumptions make it computationally efficient while maintaining accuracy. A typical slab on girder bridge is composed of a reinforced concrete deck set atop parallel primary load carrying girders (Figure 4.36a). The transverse and torisonal stiffnesses are distributed along the bridge by the deck. In the longitudinal direction, the stiffness is discrete and located at the girder positions. This is the basis for the semi-continuum method, where the model contains an infinite number of transverse elements that represent the continuous concrete deck (Figure 4.36b). The discrete longitudinal stiffnesses in the model can be made to coincide with the actual girder locations, making the model more realistic than using an average longitudinal stiffness. Furthermore, the model allows definition of the actual girder stiffnesses. Thus, varying bridge parameters such as interior and exterior girders, barriers, variations in girder section properties can be realistically represented.

Concrete Deck

Girders

(a)

Uniformly Distributed Transverse Stiffness

Longitudinal Elements

(b)

Longitudinal Elements

Transverse Elements

(c)
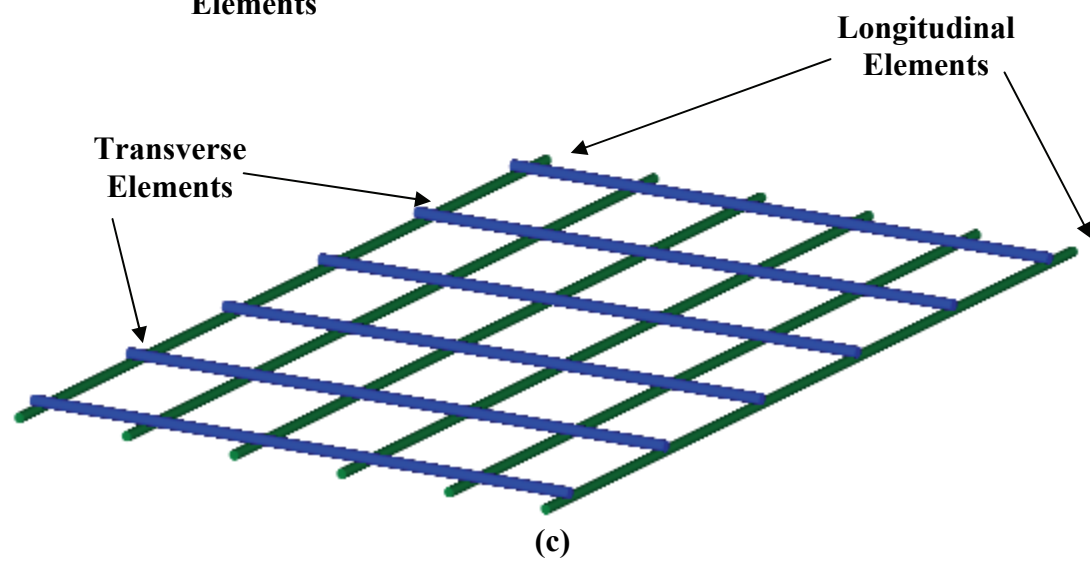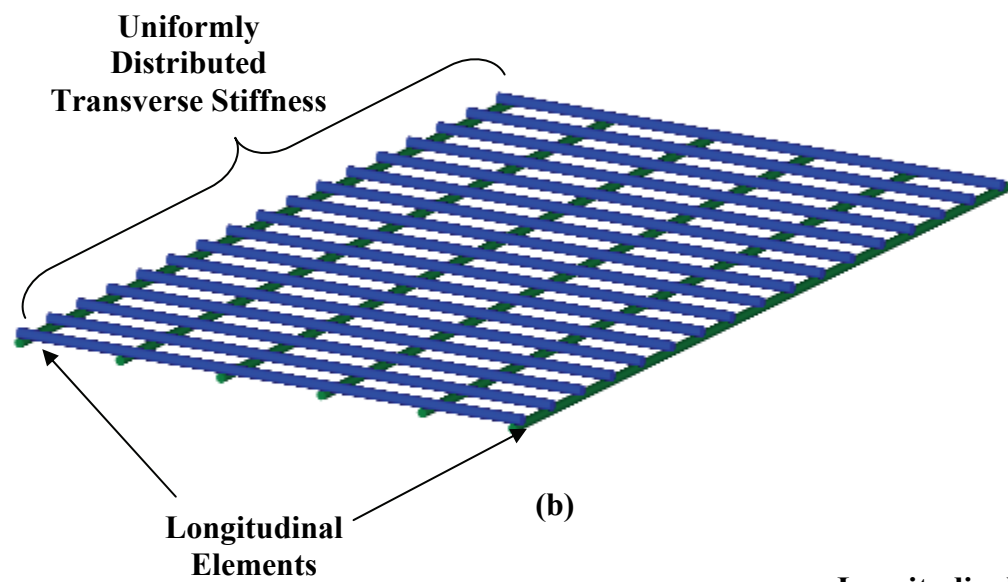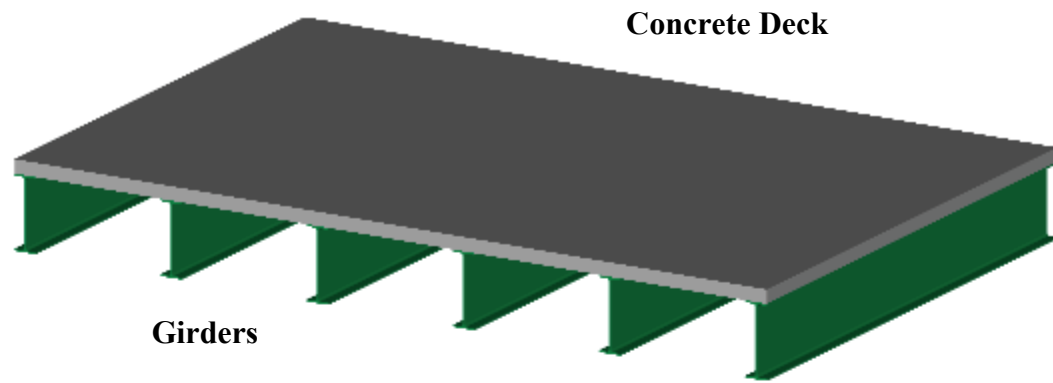
Figure 4.36 Bridge model representations: (a) actual bridge, (b) semi-continuum, and (c) grillage analogy

4.5.2.1 Harmonic Analysis of Beams

The semi-continuum method uses harmonic analysis of externally applied loads along with the continuous representation of the transverse stiffness of a bridge. Overall, this method reduces the number of unknowns and therefore reduces the demand for computations. The applied loads are represented by an infinite summation of continuous functions. For example, the load on a simply supported beam of span length L carrying a distributed load with intensity at a distance x from the support is represented as $q(x)$, the load is expressed in the following form where n is the number of harmonics

$$q(x) = q_1 \sin\left(\frac{\pi x}{L}\right) + q_2 \sin\left(\frac{2\pi x}{L}\right) + \ldots + q_n \sin\left(\frac{n\pi x}{L}\right) + \ldots \quad n = 1,2,3,\ldots \quad \textbf{(4.1a)}$$

The harmonic coefficients are found by multiplying both sides of the above equation by

$\sin\dfrac{n\pi x}{L}$ and noting $\int_{x=0}^{x=L} \sin\dfrac{m\pi x}{L} \sin\dfrac{n\pi x}{L}\,dx = 0$ for any $m \neq n$ and

$\int_{x=0}^{x=L} \sin^2 \dfrac{n\pi x}{L}\,dx = \dfrac{L}{2}$. The coefficients are given by

$$q_n = \frac{2}{L}\int_{x=0}^{x=L} q(x)\sin\left(\frac{n\pi x}{L}\right) dx \quad\quad \textbf{(4.1b)}$$

Some special cases of the above equations include a uniformly constant load and a concentrated load, both of which are discussed below.

For a uniformly distributed load, $q(x) = q$, the coefficients are given by

$$\begin{aligned} n = \text{odd} \quad & q_n = \frac{4q}{n\pi} \\ n = \text{even} \quad & q_n = 0 \end{aligned} \quad\quad \textbf{(4.2a)}$$

The harmonic load is then defined as

$$q(x) = \frac{4q}{\pi}\left(\sin\frac{\pi x}{L} + \frac{1}{3}\sin\frac{3\pi x}{L} + \frac{1}{5}\sin\frac{5\pi x}{L} + ...\right) \qquad \textbf{(4.2b)}$$

A concentrated load, P, at a distance c from the left-hand support, which is discontinuous with respect to the length of the span, is considered as a distributed load of intensity $q(x) = P/2\Delta$ acting over an infinitesimally small section of the beam between $x = (c - \Delta)$ and $x = (c + \Delta)$. The coefficients are found by taking the limit as $\Delta \to 0$ of Equation 4.1b.

$$q_n = \frac{2}{L}\left(\lim_{\Delta \to 0}\int_{c-\Delta}^{c+\Delta}\frac{P}{2\Delta}\sin\frac{n\pi x}{L}\,dx\right) = \frac{2P}{L}\sin\frac{n\pi c}{L} \qquad \textbf{(4.3a)}$$

The load is then defined as

$$q(x) = \frac{2P}{L}\left(\sin\frac{\pi c}{L}\sin\frac{\pi x}{L} + \sin\frac{2\pi c}{L}\sin\frac{2\pi x}{L} + ... + \sin\frac{n\pi c}{L}\sin\frac{n\pi x}{L} + ...\right) \qquad \textbf{(4.3b)}$$

From elementary small-deflection beam theory, the relationships between load $q(x)$, shear force (V_x), bending moment (M_x), slope (θ_x) and deflection (ω) are well defined for a beam with flexural rigidity (EI). These relationships are given by the following set of equations

$$\begin{aligned} q(x) &= EI\frac{d^4\omega}{dx^4} \\ V_x &= -EI\frac{d^3\omega}{dx^3} \\ M_x &= -EI\frac{d^2\omega}{dx^2} \\ \theta_x &= \frac{d\omega}{dx} \end{aligned} \qquad \textbf{(4.4)}$$

Integration of the right-hand side with respect to x of the above equations, yields expressions for the shear force, bending moment, slope and deflection

$$V_x = \frac{2P}{\pi} \sum_{n=1}^{n=\infty} \frac{1}{n} \sin\frac{n\pi c}{L} \cos\frac{n\pi x}{L}$$

$$M_x = \frac{2PL}{\pi^2} \sum_{n=1}^{n=\infty} \frac{1}{n^2} \sin\frac{n\pi c}{L} \sin\frac{n\pi x}{L}$$

$$\theta_x = \frac{2PL^2}{\pi^3 EI} \sum_{n=1}^{n=\infty} \frac{1}{n^3} \sin\frac{n\pi c}{L} \cos\frac{n\pi x}{L}$$ (4.5)

$$w = \frac{2PL^3}{\pi^4 EI} \sum_{n=1}^{n=\infty} \frac{1}{n^4} \sin\frac{n\pi c}{L} \sin\frac{n\pi x}{L}$$

where, *EI* is the flexural rigidity of the beam.

4.5.2.2   Semi-Continuum Program

Bakht and Jaeger have developed a series of FORTRAN programs for the semi-continuum method. The source code was made public by the authors for use in the engineering community. Two versions of the semi-continuum programs are currently available: (1) SECAN, for analysis of simply supported slab on girder bridges with up to ten girders and (2) SECAN2, for continuous bridges with up to ten interior supports. These programs were originally written with limitations to conserve resources when personal computer memory was very expensive. With advances in technology, the programs can be expanded to model an unlimited number of girders.

Input to the program is stored in a file in the same directory as the executable program. The input required includes: (1) number of harmonics for the analysis, (2) number of girders, (3) span length, (4) Elastic and Shear Modulus of the girder material, (5) transverse spacing of girders, (6) moment of inertia and torsional inertia of each individual girder, (7) deck thickness, Elastic and Shear Modulus, (8) number of axles of

the truck load, (9) weights, longitudinal, and transverse location of each axle, and (10) number and location of reference sections for internal girder forces.

Because the FORTRAN source code for the semi-continuum programs was made public, the program can be altered to perform a variety of operations. By constructing a loop within the program code, output for moving loads can be generated. Therefore, the stepped output of truck passages can be directly compared to live load stresses. WIM data provides the input for the truck loads and the semi-continuum program produces outputs of moments and deflections for each increment of the loop. Since the simulation produces a moment or deflection profile for a given reference point as the truck passes, the x-axis must be scaled to coincide with the actual stress history of the truck passage. Further, a unit point load can be applied to the bridge deck in a systematic pattern by incrementing the transverse and longitudinal coordinates to create an influence surface for the bridge.

4.5.2.3 Representing a Variable Girder Section

The primary limitations of the semi-continuum programs used herein are related to the input parameters. Only one value for moment of inertia may be entered per girder. Therefore, if the bridge contains a variable section along the span, such as a cover plate, an approximation must be made for the input value of moment of inertia. Bakht and Jaeger offer suggestions on how to take a weighted average moment of inertia for a variable section girder.

$$i\_effective = I_o + \sum_{r=1}^{n} \Delta I_r \cos \frac{\pi a_r}{L}$$

Eq. 4.6

Where, I_0 is the base moment of inertia of the smallest section, ΔI_r is the incremental change in moment of inertia relative to the base inertia, a_r is the distance to the start of the section from the left hand support, and L is the total span length.

A detailed example of weighted average girder inertia is presented in the following section regarding the input parameters for the Doremus Avenue Bridge which has variable section plate girders.

4.5.2.3.1 Doremus Avenue Variable Plate Girder Analysis

The Doremus Avenue Bridge is the focus of the experimental testing in this work. Doremus Avenue is a newly designed steel plate girder bridge that crosses a rail yard in Newark, NJ. The bridge was designed using the newly adopted LRFD specifications. To economize the design, the bridge was constructed as 3 three-span continuous variable section plate girders. A summary of the variable section dimensions is given in Figure 4.37 and Table 4.5.

Table 4.5 Doremus Avenue Plate Girder Section Dimensions

Section	Section Length (m)	Flange Width (mm)	Top Flange Height (mm)	Bottom Flange Height (mm)	Web Depth d (mm)	Web Thickness tw (mm)
South Abutment						
A	8.35	400	25	30	1200	14
B	27	400	25	55	1200	14
C	5	400	45	55	1200	14
D-Left	4.65	400	70	70	1200	14
Pier 1						
D-Right	7.85	400	70	70	1200	14
E	7	400	45	45	1200	14
F	16	400	25	25	1200	14
G	7	400	45	45	1200	14
H-left	7.15	400	70	70	1200	14
Pier 2						
H-right	5.35	400	70	70	1200	14
I	5	400	45	55	1200	14
J	27	400	25	55	1200	14
K	8.14	400	25	30	1200	14
Pier 3						

When constructing the semi-continuum program input file the dimensional and material properties of the bridge must be found. As mentioned previously, the moments of inertia must be estimated for each of the main girders along the cross section. In a composite slab on girder bridge, as in the case of Doremus Bridge, the moment of inertia of the composite section is used for the input file. The effective flange width according to AASHTO LRFD specifications is calculated to find the width of concrete deck that can contribute to bending resistance. The effective flange width depends on the slab thickness and the transverse girder spacing.
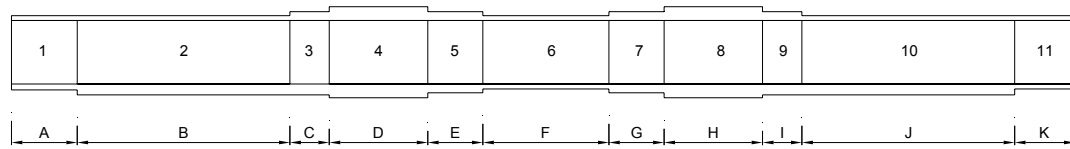
(a)
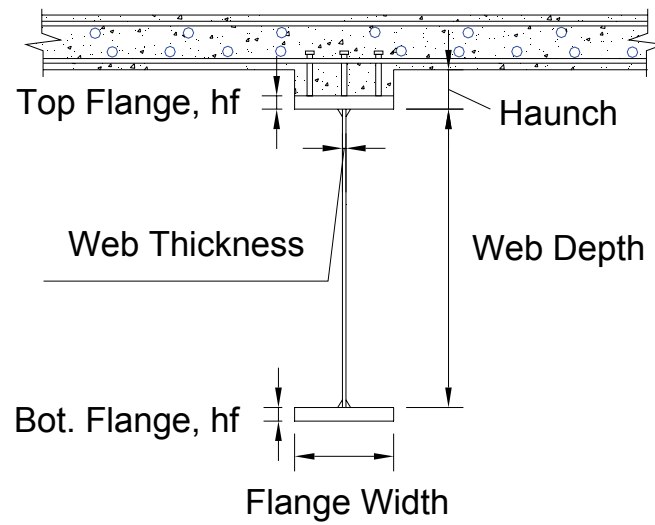
(b)

Figure 4.37 Doremus Avenue Bridge: (a) sections along length, (b) typical plate girder section

After finding the effective flange width, the available concrete deck section is transformed into an equivalent steel section using the modular ratio, n. The modular ratio is taken as the ratio of the Elastic modulus of the girder material (steel) and the Elastic Modulus of the deck material (concrete).
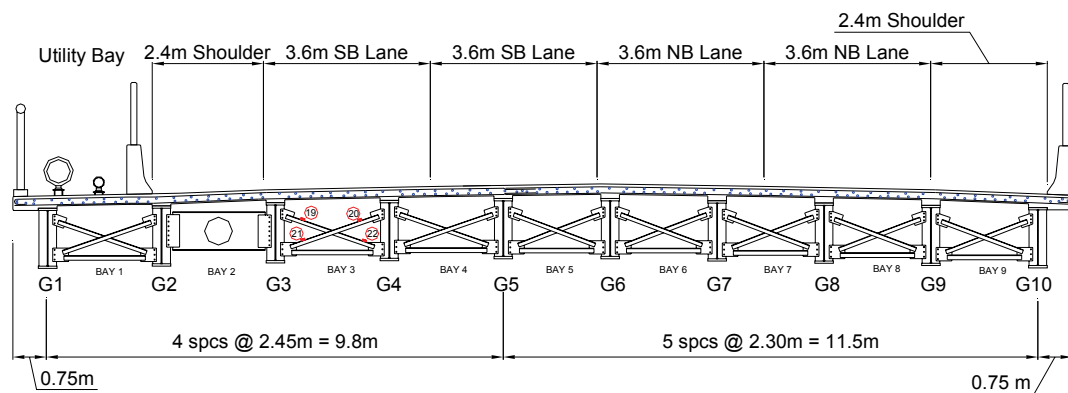
Figure 4.38 Typical cross section of Doremus Avenue Bridge showing travel lanes and plate girders
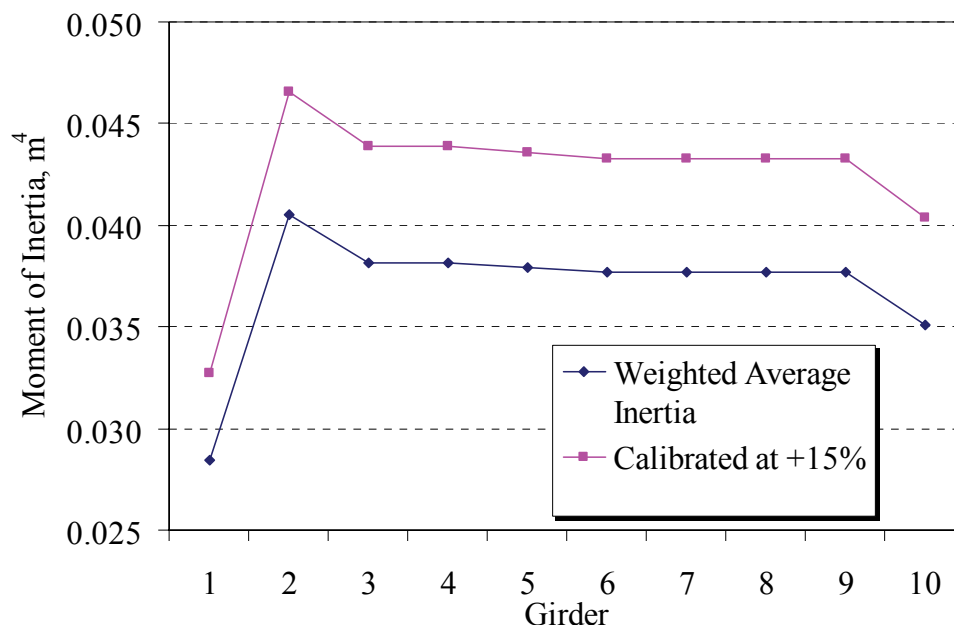
Figure 4.39 Variation of Doremus girder moments of inertia (Girders 1 and 10 are exterior) showing the original and calibrated moments of inertia.

4.6   Model Verification

4.6.1   Controlled Live Load Testing

Numerous controlled live load tests were conducted on the Doremus Avenue Bridge during and after completion of construction. The results were used to calibrate and verify computer models as well as establish the behavior of the bridge prior to service. The construction, and therefore, testing was completed in two phases: (1) Stage I, a five girder bridge that was constructed parallel to the existing bridge and (2) Stage II the completed ten-girder bridge after demolition of the existing bridge.

For each load test the contractor provided loaded five axle trucks with certified weight receipts, drivers, and traffic control. Prior to each test date, equipment and sensors were prepared, cables measured, systems programmed, and sensors installed. On the actual test days, equipment was configured and tested, and the test trucks were

weighed. The drivers were briefed on the test procedure, traffic control was coordinated, and testing was conducted. Traffic was closed for each test, a zero reading for each system was taken as reference, test trucks were rolled into position, readings were taken, and traffic released. Numerous test positions and combinations were done throughout the project. Both static and dynamic tests were performed. Typical test configurations are shown in Figure 4.40 and include: single, side by side, following, and staggered trucks. Static tests were done to maximum the positive bending moment and negative moment. Dynamic tests involved moving trucks along the span at various speeds and configurations.

(a)

(b)

(c)

(d)

Figure 4.40 Controlled load testing of Stage I of Doremus Bridge: (a) single truck, (b) two trucks side-by-side, (c) following trucks, and (d) staggered trucks

During controlled load testing sensors measuring strains, deflections, accelerations, and velocities were sampled. The data was then used to verify and calibrate structural models for further simulations. One of these models, the semi-continuum model, was generated using structural details and material properties. Later the model was verified and calibrated using data from controlled live load tests. The calibrated semi-continuum model was later used to verify truck weights from WIM records and used to perform simulations of truck load effects.

4.6.2   Semi-Continuum Model of Doremus Avenue

A semi-continuum model was constructed for the Doremus Avenue Bridge using the methods and guidelines outlined by the creators (Jaeger and Bakht 1989). The background of the semi-continuum theory and exact detail of the Doremus Avenue model are given in Section 4.5.2. Data from sensors collected during live load data was compared with model output at corresponding locations throughout the bridge. The model data is expressed in terms of moment, shear, and deflection. Output was converted to bending stress using the equation:

$$\sigma = M \cdot c \big/ I$$

<div align="right">**Eq. 4.7**</div>

where σ = bending stress about the major axis (ksi), M = bending moment about the major axis (k-ft), c = distance from bottom flange to centroid of girder/deck section (ft), and I = moment of inertia of section about major axis (ft^4).

The developers of the semi-continuum method recommend using a weighted average moment of inertia to describe a variable section member. The plate girders of the

Doremus Avenue Bridge have variable thickness top and bottom flanges with a constant depth web. The program input for section moment of inertia in the semi-continuum method allows for only a single value per girder. Therefore, the weighted average moments of inertia for each girder were calculated from design plans and written into the input. When calculating member stresses, the location specific moment of inertia is used (Jaeger and Bakht 1989). The moments of inertia for all sensor locations were used to calculate the bending stresses for comparison with load test results.

4.6.2.1   Semi-continuum modeling of design trucks

For reference the code specified design and fatigue trucks were run using the semi-continuum model. The results are used to verify design parameters such as fatigue stress range and maximum stress due to the design truck.

The model results for the AASHTO HS20 design truck and fatigue truck are shown in Figure 4.41 for passage in the northbound right lane (Lane A) of the Doremus Avenue Bridge. The results represent the bottom flange stresses at the maximum positive moment region of Span 3, Girder 9. At this location, the right wheel line of northbound right lane trucks is over Girder 9. The truck enters the bridge from the south abutment and crosses span 1 first. The behavior of the bridge is consistent with the three-span continuous construction where load on Span 1 causes a minor positive stress in Span 3. The maximum bending stress and stress range for the HS20 design truck is 1.92 ksi and 2.18 ksi, respectively. The maximum bending stress and stress range for the Fatigue Truck is 1.24 and 1.43 ksi, respectively.
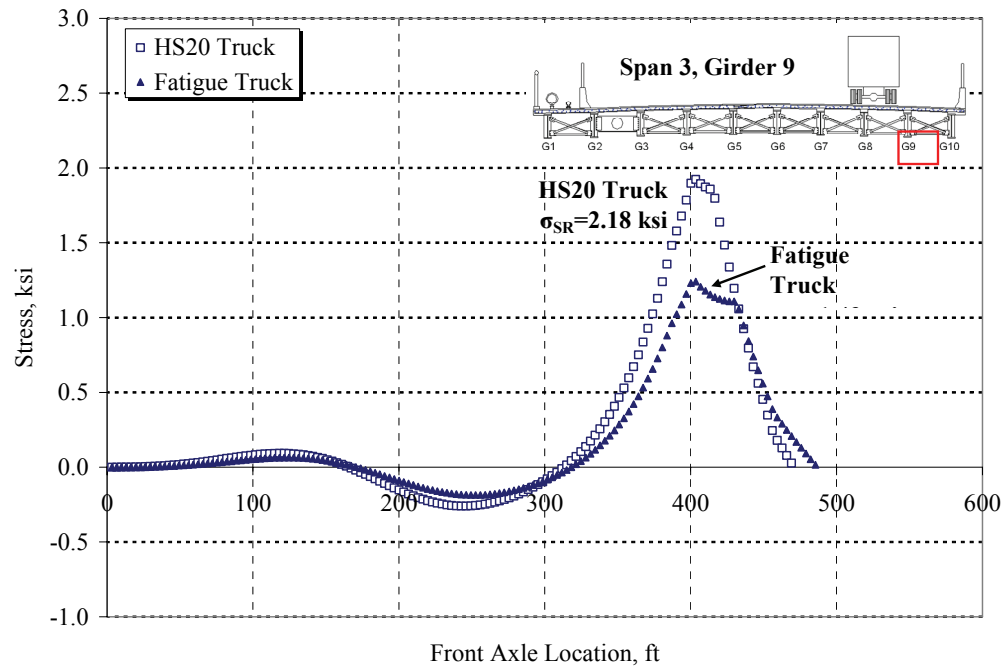
Figure 4.41 Semi-continuum model results for AASHTO HS20 design truck and Fatigue truck.

4.6.2.2   Controlled Load Testing 7/10/2003

Controlled load testing was conducted on July 10, 2003 prior to the opening of the full ten-girder Doremus Avenue Bridge. The testing featured two loaded 5-axle semi-trailers with drivers and traffic control. The truck weight and configurations are given in Figure 4.42 and Table 4.6.
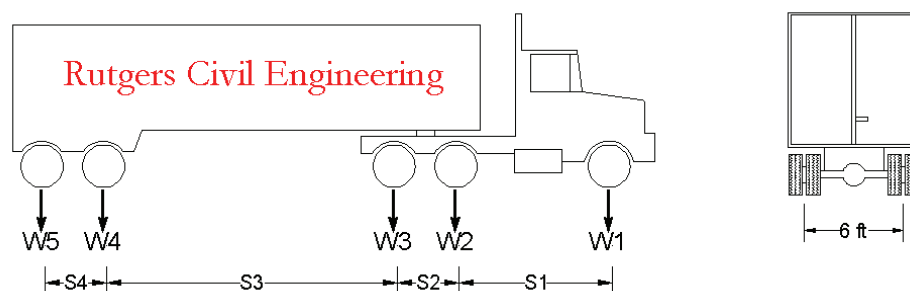
Figure 4.42 Typical test truck configuration

Table 4.6 Doremus Stage II test truck dimensions and axle weights

Truck 1				Truck 2			
W1, k	10.7	**S1, ft**	14.6	**W1, k**	10.3	**S1, ft**	13.3
W2, k	15.7	**S2, ft**	4.6	**W2, k**	13.9	**S2, ft**	4.4
W3, k	15.7	**S3, ft**	23.3	**W3, k**	13.9	**S3, ft**	23.5
W4, k	17.1	**S4, ft**	4.6	**W4, k**	19.3	**S4, ft**	4.5
W5, k	17.1			**W5, k**	19.3		
Total W, k	76.3			**Total W, k**	76.7		
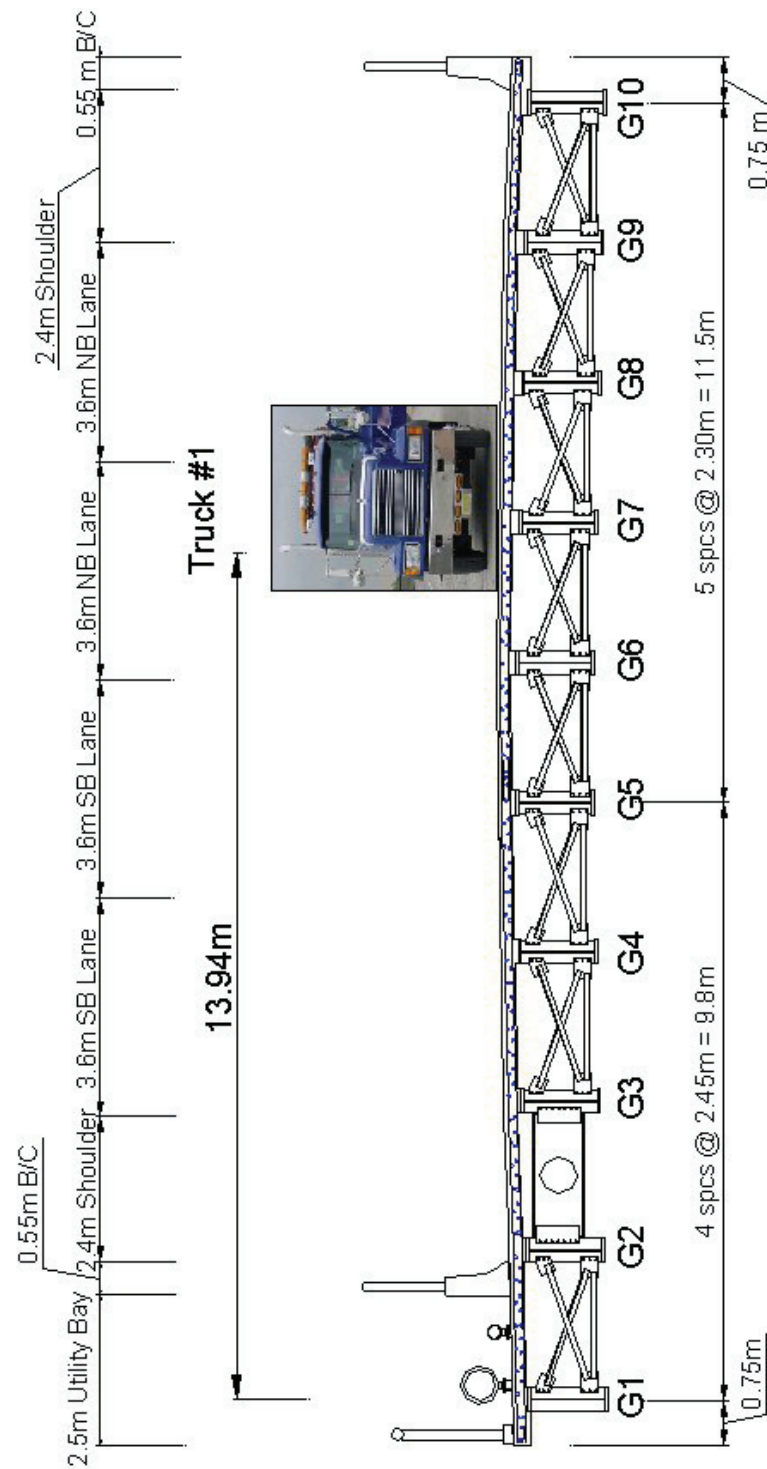
Figure 4.43 Stage II Controlled Load Testing 7/10/2003, Single truck over G7 (Test 18)
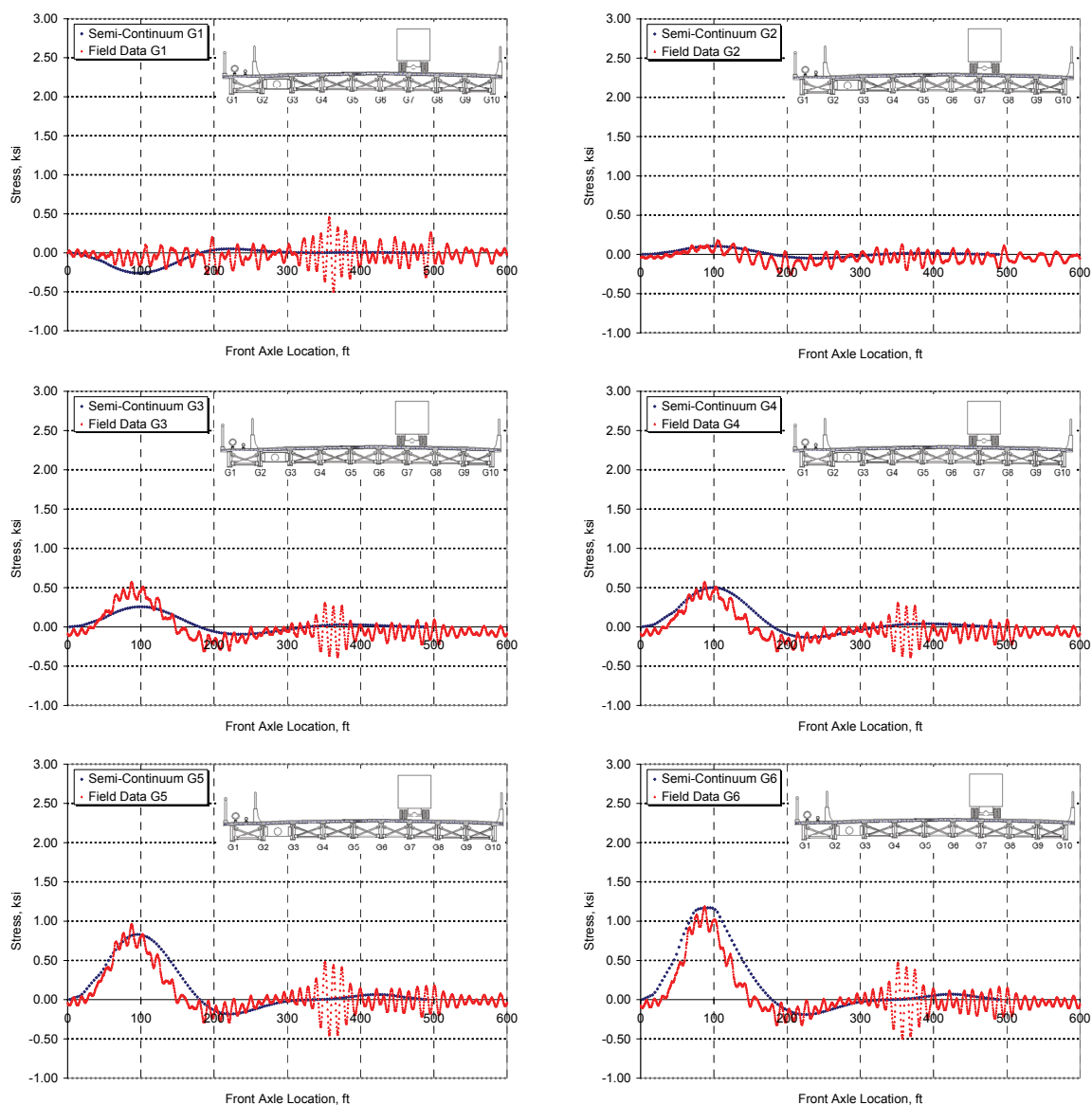
Figure 4.44 Stage II Comparison of Girder Stresses from Load Testing 7/10/2003, Test 18, with a single truck over Girder 7
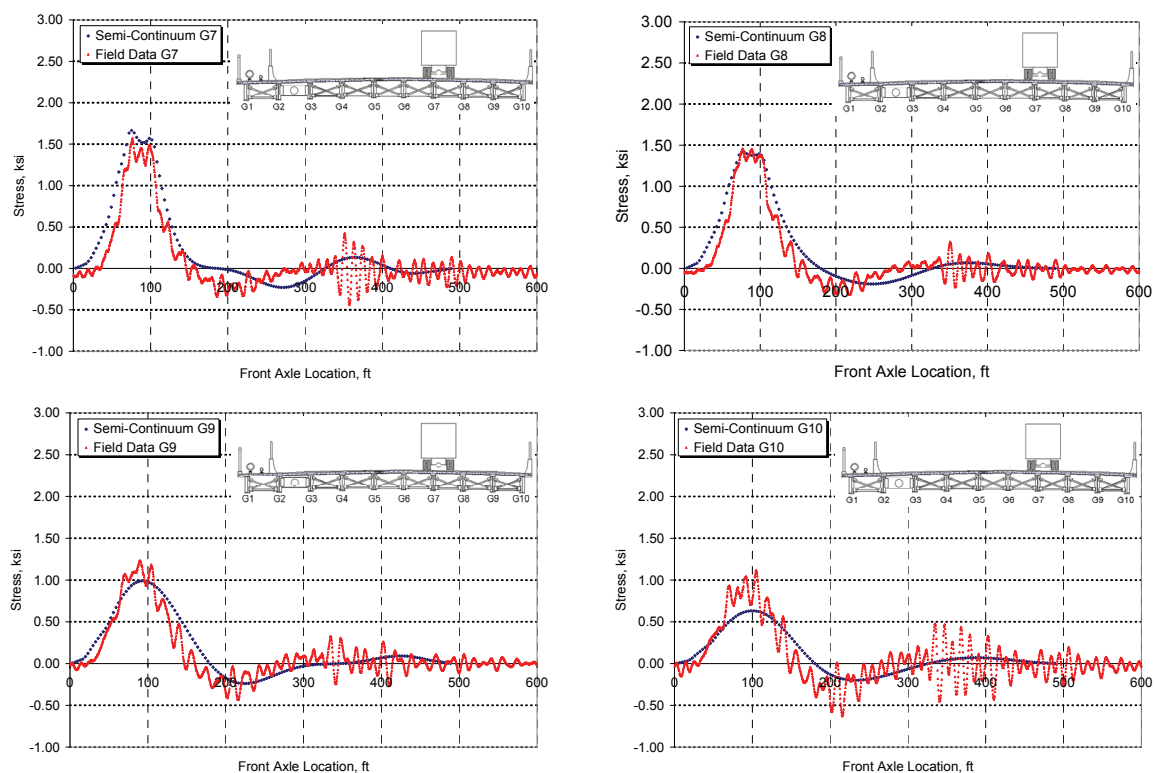
Figure 4.45 Stage II Comparison of Girder Stresses from Load Testing 7/10/2003, Test 18, with a single truck over Girder 7 (Continued)

Figure 4.46 Stage II Controlled Load Testing 7/10/2003, single truck over G7 (Test 18)
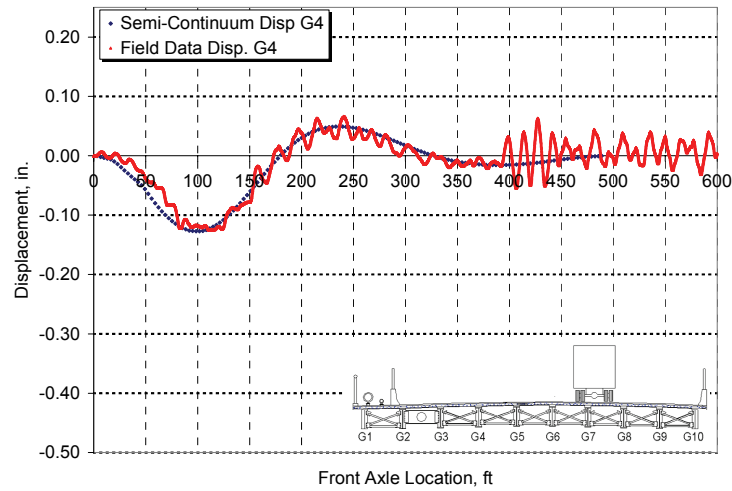
(a) Test 18 Girder 4 Displacement: Semi-continuum model and G4 LVDT
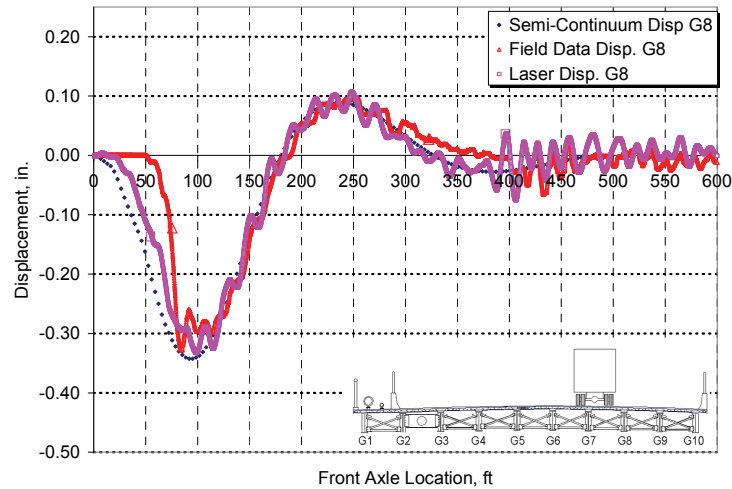
(b) Test 18 Girder 8 Displacement: Semi-continuum model, G8 LVDT, and G8 Laser

Figure 4.47 Stage II Controlled Load Testing, girder displacement comparisons for (a) Girder 4 and (b) Girder 8 (Test 18)
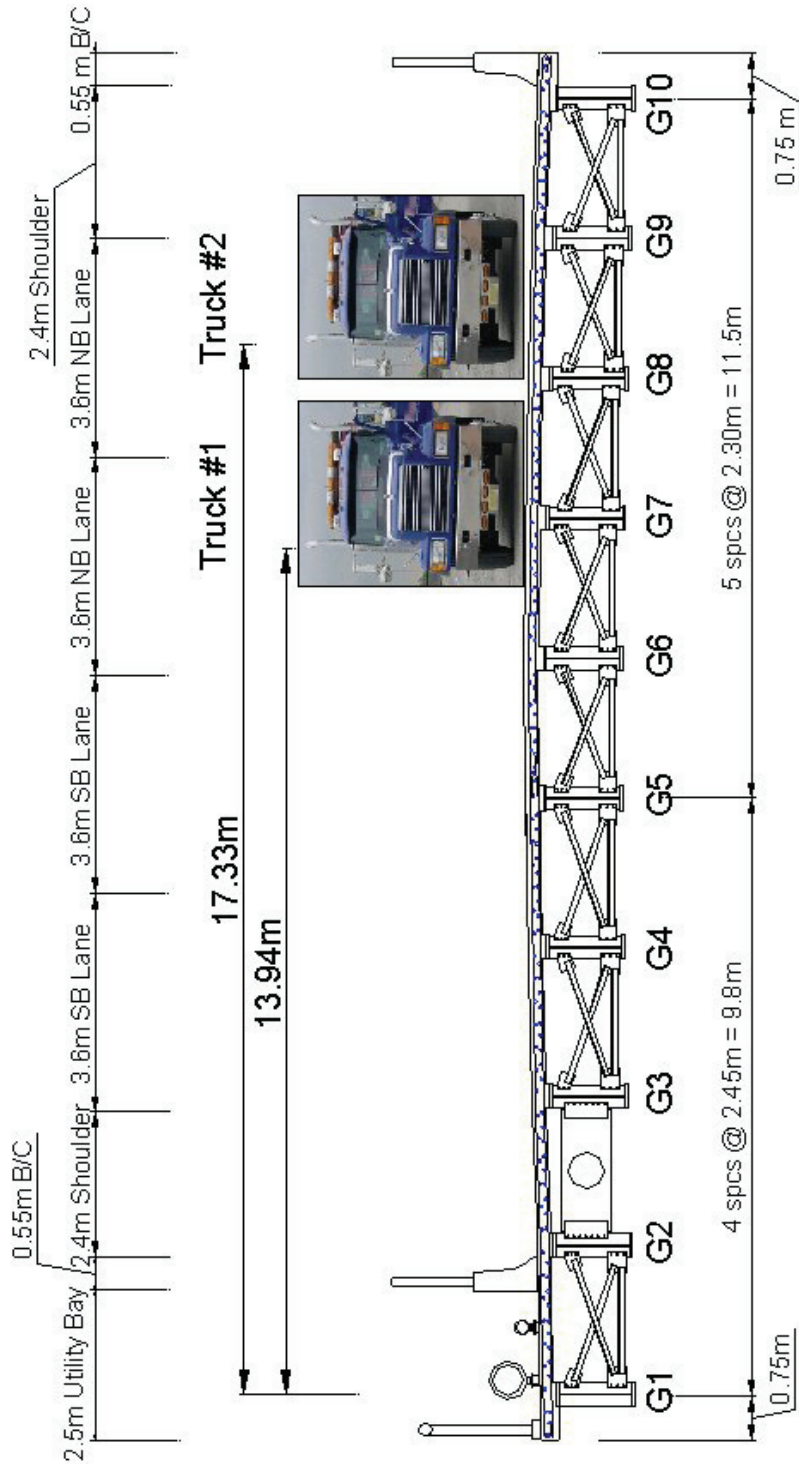
Figure 4.48 Stage II Controlled Load Testing 7/10/2003, 2 trucks side-by-side (Test 23)
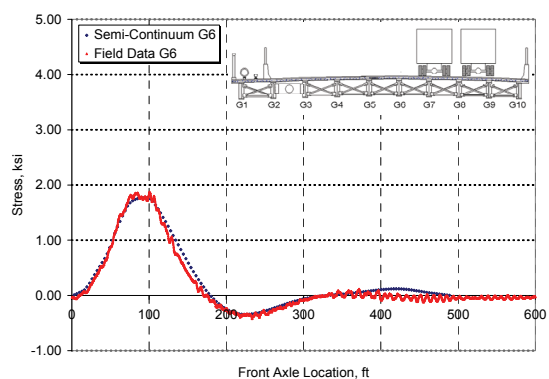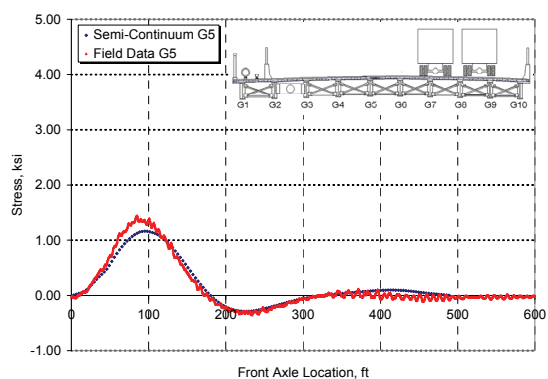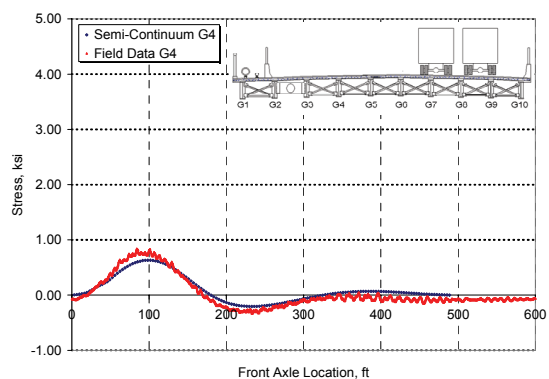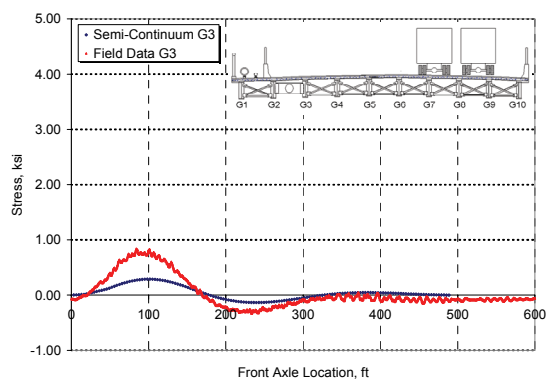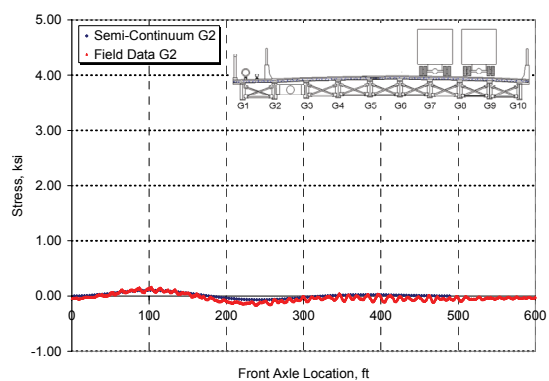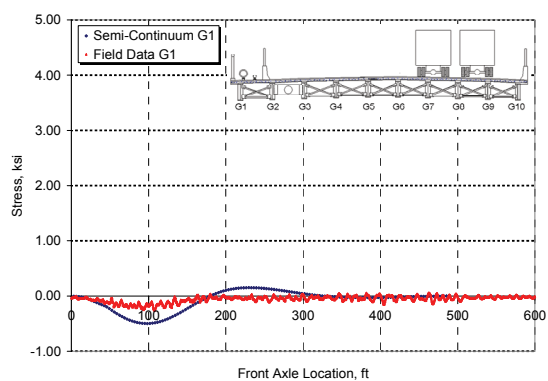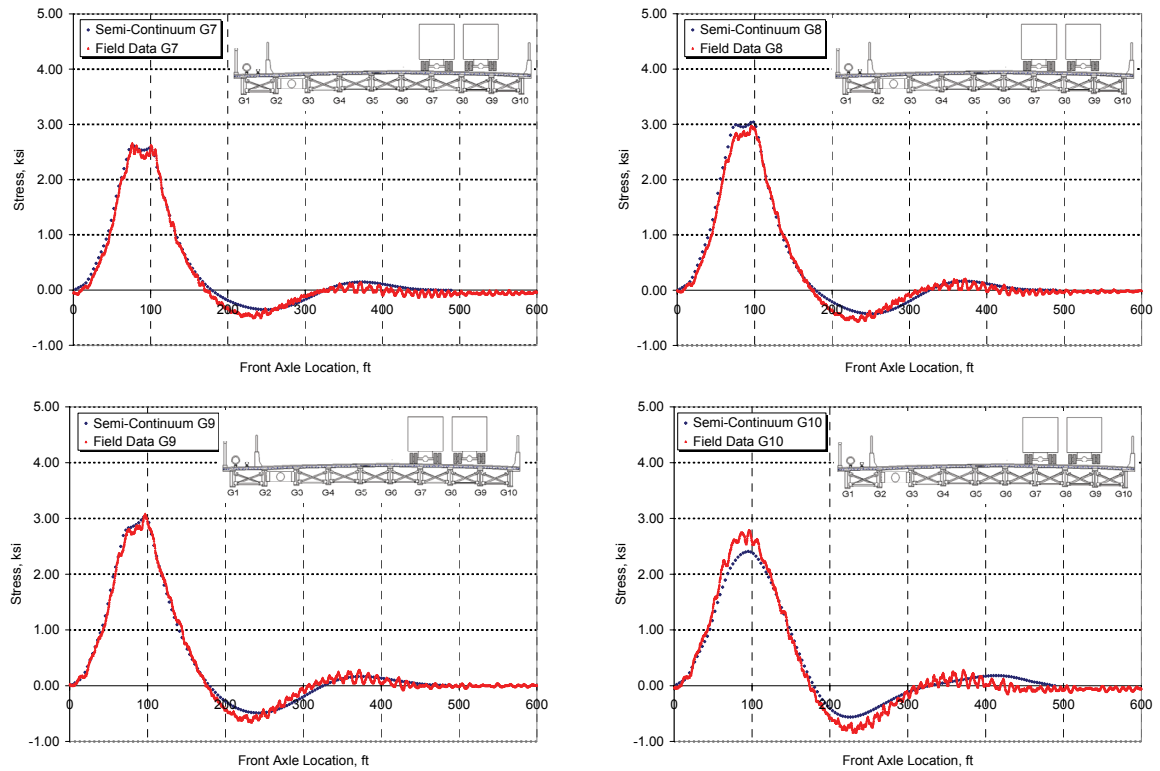
Figure 4.49 Stage II Controlled Load Testing 7/10/2003, two trucks side-by-side (Test 23)
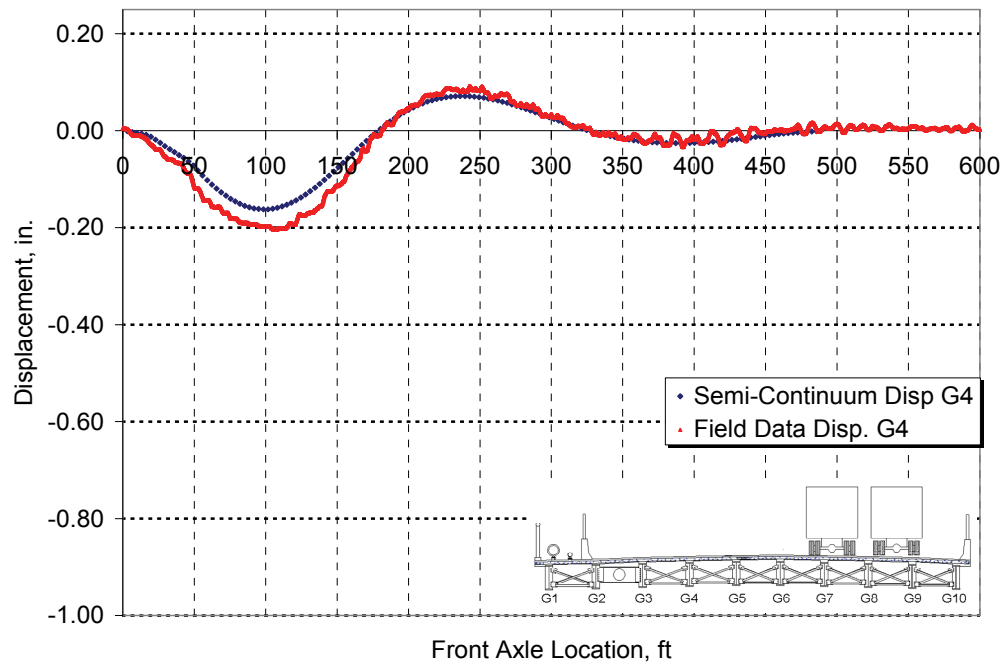
(a) Test 23 Girder 4 Displacement: Semi-continuum model and G4 LVDT
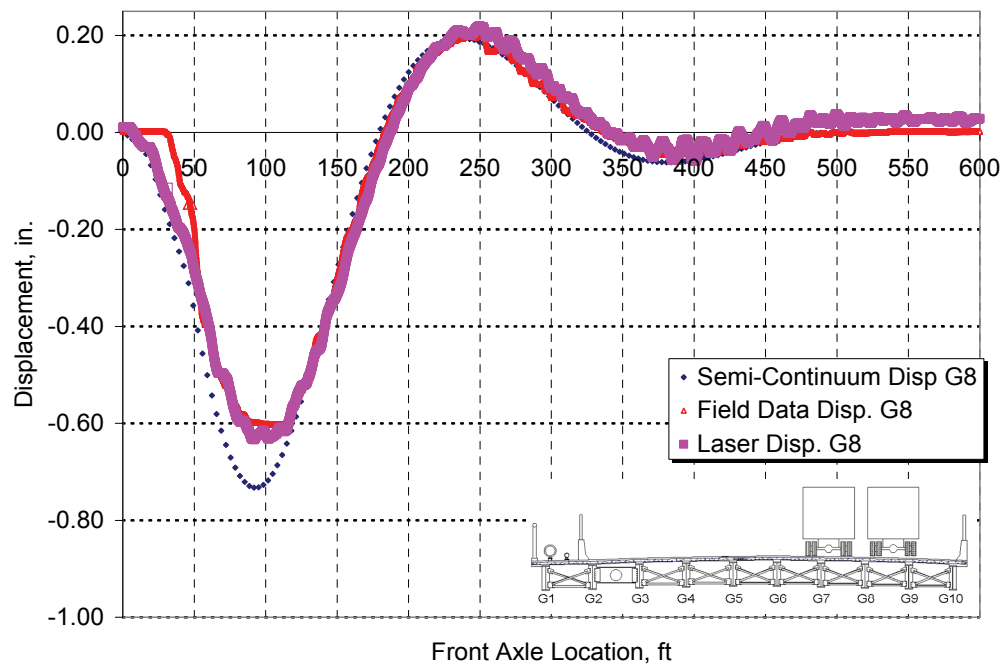
(b) Test 23 Girder 8 Displacement: Semi-continuum model, G8 LVDT, and G8 Laser

Figure 4.50 Stage II Controlled Load Testing, girder displacement comparisons for (a) Girder 4 and (b) Girder 8 (Test 23)

4.6.2.3   Model Verification from WIM and Response Data

Following the initialization of the WIM system at Doremus Avenue truck weight information and bridge response data were collected concurrently to monitor the bridge for a period of five years. Periodically, truck information from the WIM system would be used to predict the bridge response using the calibrated structural models. This process would serve to test the calibration of the WIM data as well as to verify the strain data collected from the girder sensors.

After the passage of each vehicle over the WIM system, a data string is sent to the long term strain monitoring, or Fatigue System, located underneath the bridge at Pier 2. If the truck weight and class satisfy some preset trigger thresholds, the strain system would capture a real-time strain history of the truck passage. Strain transducers installed throughout Unit 1 of the bridge would be sampled at 100Hz and the data stored for future reference.

The data and model predictions for one such triggered event is given in the following figures. The sample designated Truck A121 was recorded because it represents a single truck passage where the weight exceeded the designated threshold for its class. For verification purposes, it is important to consider events involving only one truck on the bridge. The dimensions and weights as reported by the WIM system at the south abutment are given in Figure 4.51. Truck A121 is of special interest since it is overweight, with a gross vehicle weight of 92.6 kips (the NJ legal truck load limit is 80 kips) and it is a Class 9 truck, the most common type of truck. Further, Class 9 vehicles have been used in the past during controlled load testing.

Truck A121 exemplifies a typical Class 9 vehicle. This vehicle type is also referred to as 3S2, where there are three axles in the drive tractor, followed by a semi-trailer with two axles. Some of the common traits of the 3S2 are: (1) steering axle weight of between 10 and 12 kips, here the weight of axle 1 is 8.9k, (2) the spacing of the front axle is typical of the 3S2 type at 17.5 feet., (3) there are two tandems (pairs of closely spaced axles) where the weight of axles 2 & 3 are nearly equal to each other and 4 & 5 are nearly equal to each other. The weight of axles within a tandem are equal due to a common suspension system that parts the load equally.

Truck A121			
W1, k	8.9	S1, ft	17.5
W2, k	20.9	S2, ft	4.3
W3, k	21.5	S3, ft	28.2
W4, k	21.6	S4, ft	3.9
W5, k	19.7		
Total W, k	92.6		
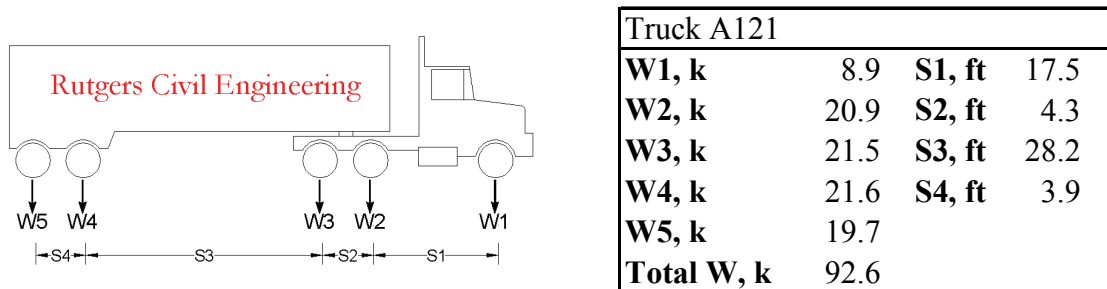
Figure 4.51 Verification truck A121 dimensions and weights from WIM system

For lack of more detailed information, it is assumed that the truck will maintain the measured speed, will remain in the right northbound lane (Lane A) as shown in Figure 4.52, and is traveling in the center of the lane. A lane change is possible to detect from the strain response given a reference strain history from controlled test data. No lane change was detected from the A121 record. In other words, the A121 strain record was comparable to a controlled load test record for a truck that remains in the same lane over the bridge. The position of the left wheel line of Truck A121 relative to Girder 1 is 16.4 meters (Figure 4.52). The truck width of 3S2 is assumed to be 1.83 meters. Therefore the location of the right wheel line relative to Girder 1 is 18.23 meters. The distances of

the wheel lines relative to the leftmost girder are required input for the semi-continuum program.

The recorded strain record and semi-continuum model strains for Truck A121 are given in Figure 4.53 and Figure 4.54. Since the northbound right lane (Lane A) is mostly over Girder 8, the response in this location is expected to be the maximum. This fact is confirmed in Figure 4.53b, where both the field data and the measured response are the maximum at Girder 8. The double peaked shape evident in the model and response is typical for the 3S2 where there are two distinct load units: (1) the first three axles and (2) the trailing tandem axles. The model tends to under predict the stress in the exterior Girder 10. This is typical when modeling girders with composite parapets or barrier curbs. The exact contribution of the parapet is difficult to estimate. Also the contribution of the parapet to the stiffness of the exterior girder also depends on its degree of continuity, or spacing of construction joints. The semi-continuum model may be specifically calibrated to match the girder 10 stiffness. However, girder specific stiffness calibration is not recommended due to user subjectivity. The model used herein was constructed using member properties and an overall 15% increase in stiffness to calibrate the output with controlled load test results.

Figure 4.53 and Figure 4.54 show that the semi-continuum results agree well with the measured bridge response for Truck A121. The WIM system, the strain response, and the model can therefore be deemed accurate in describing the bridge response for this and future trucks. That is, provided that the WIM and strain systems remain in calibration, future truck information may be used as input for the semi-continuum model to compare with the measured response.
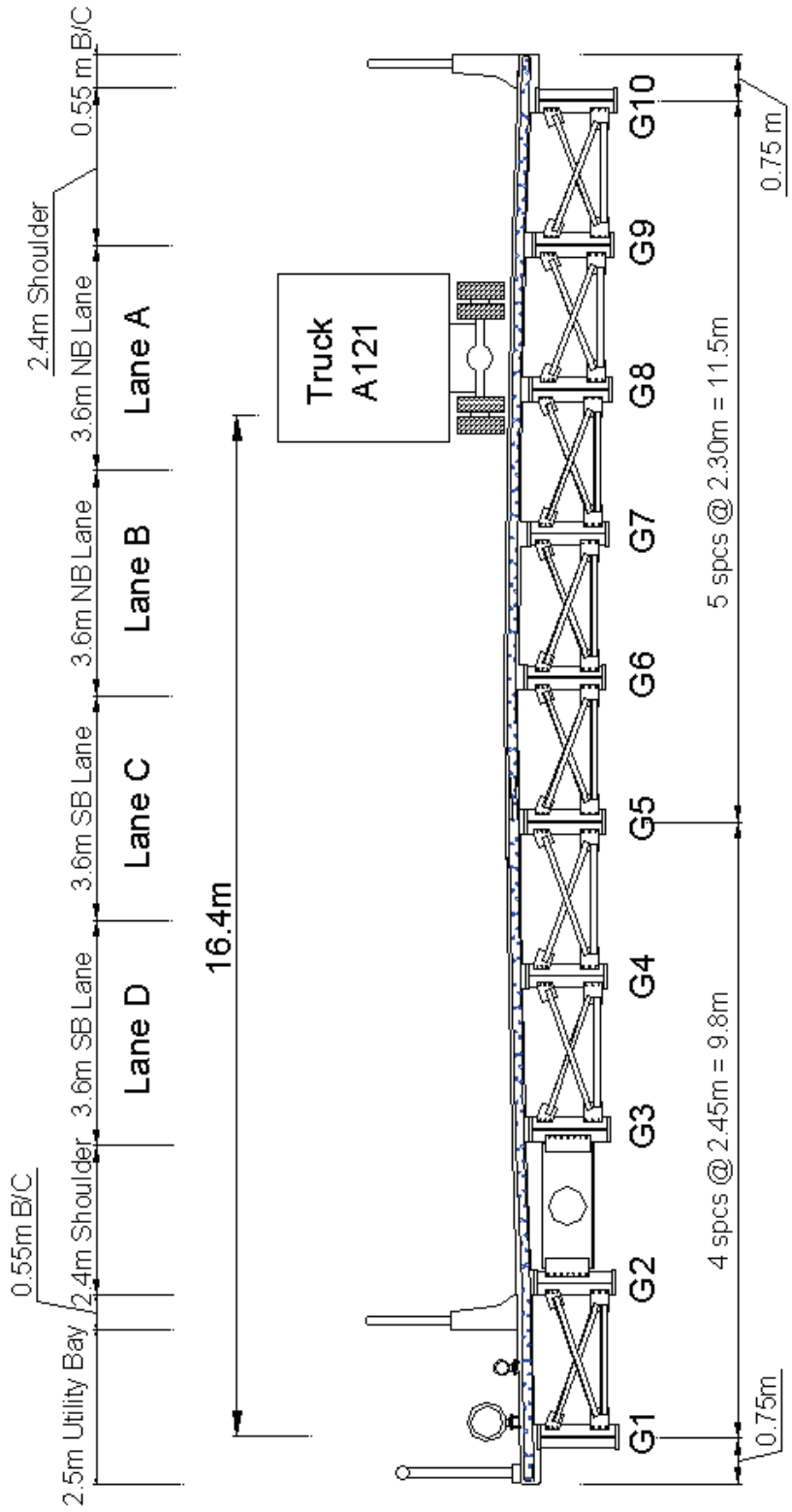
Figure 4.52 Lane position of sampled Truck A121
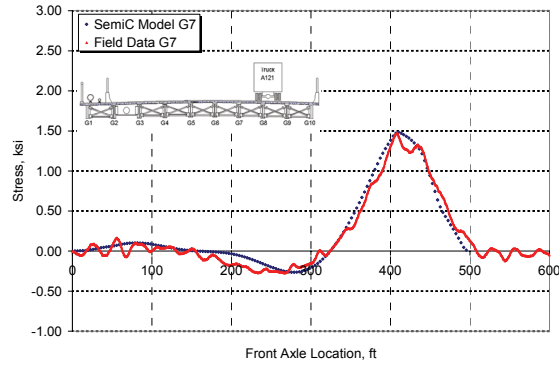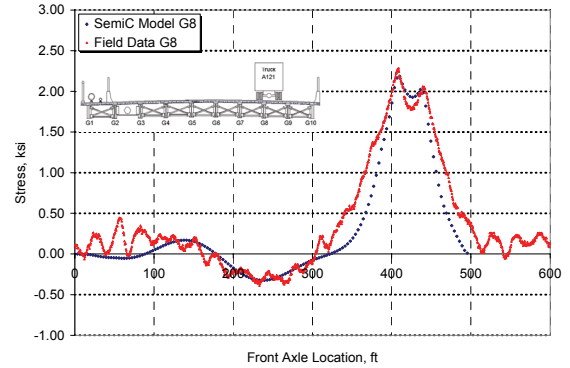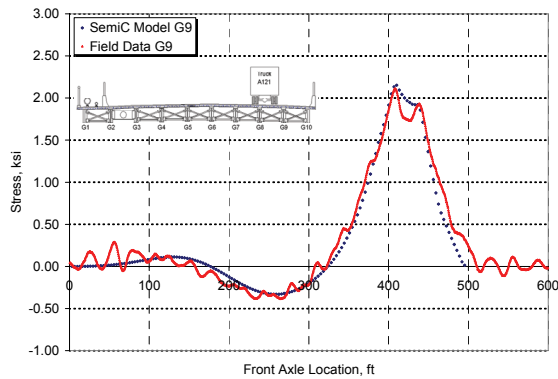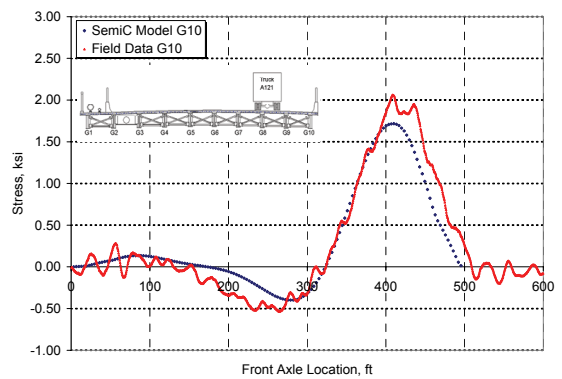
Figure 4.53 Comparison of sampled stresses response and semi-continuum model stresses for sample Truck A121
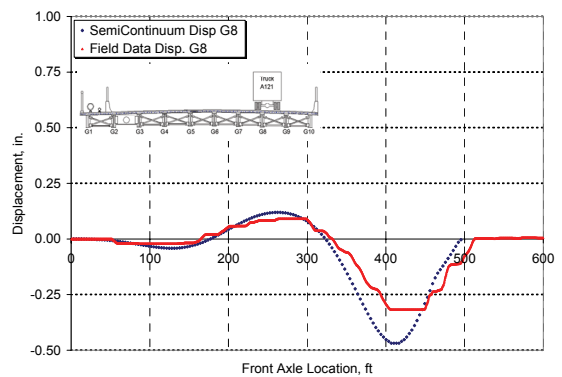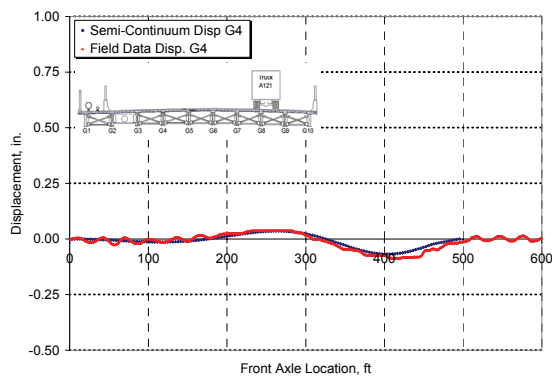
Figure 4.54 Comparison of sampled displacement response and semi-continuum model displacements for sample Truck A121

4.6.3 Semi-continuum Model of Route 18 Over River Road

A small scale test program, similar, to Doremus Avenue Bridge, was carried out on the Route 18 Bridge over River Road is Piscataway, NJ. The purpose was to gather site-specific bridge live-load and response data for a site away from the Port of Newark. Weigh-in-motion and strain gage systems were installed on-site and monitored for a period of two-months. The bridge framing plan and sensor configuration are shown in Figure 4.32. A complete cross section of the bridge was instrumented at the maximum positive moment position of Span 3. Additionally, two sensors were installed on the bottom section of a cross brace between girder 3 and girder 4 near the maximum moment location. A semi-continuum model was developed for Route 18 in the same manner as for Doremus Avenue, using bridge dimensions and material properties to form the model. Later, controlled live-load testing was done using a calibration truck of known weight. The weighted average moment of inertia and bottom centroid distance for Route 18 are given in Table 4.7. Route 18 was proportioned similar to the Doremus Avenue Bridge with variable section plate girders built as a three-span continuous unit. The parapet barriers on Route 18 are placed over Girders 1 and 6, resulting in decreased effective flange width and subsequently, lower moment of inertia.

Table 4.7 Weighted Average Semi-Continuum Model inputs for Route 18 over River Road

Paramter	G1	G2	G3	G4	G5	G6
Wt Avg Inertia, mm4	0.0439	0.0507	0.0507	0.0507	0.0507	0.0425
Wt Avg. C_bot, mm	1236.4	1306.1	1306.1	1306.1	1306.1	1201.2

Controlled live-load testing was done to calibrate the portable weigh-in-motion piezo axle sensors. At the same time, strain and deflection measurements were taken to later calibrate finite element and semi-continuum models. The test truck consisted of a two-axle, six-tire, flatbed truck with crash attenuator. This particular truck was outfitted with additional ballast weight to give it more inertia in the event of vehicle collisions. Federal regulations require such vehicles to protect highway workers from deviant motorists. The truck gross vehicle weight was determined from static scale weight tickets provided by the driver. The overall gross weight of the calibration truck was 22.3 k, with front axle weight of 7.8 and rear axle weight of 14.7k. The axle spacing for this truck was 20.67 ft. Load testing was done under normal traffic conditions. The volume of traffic on Route 18 during the test was minimal. A passenger in the test vehicle radioed the truck location such that testing could be started as the truck approached the bridge. The passenger also noted any additional cars or trucks that were on the bridge with the test vehicle.

During data processing WIM truck records and bridge response were paired using timestamps and truck patterns. When matches were found, the trucks were modeled in semi-continuum to compare the expected with the measured response. Figure 4.55 shows the semi-continuum model output and the observed bridge response from the burst history record for a three axle truck traveling southbound in the right lane of the Route 18 Bridge. The WIM data indicated that the axle weights of the truck were: 12.8k, 15.2k, and 26.3k with axle spacings of 4.6ft and 23.2 feet. The semi-continuum model predicted the Girder 4 stress with less than ten percent error. There is, of course, the possibility of

WIM data errors, nonetheless, the model is a valuable tool for modeling live load effects

on bridges.
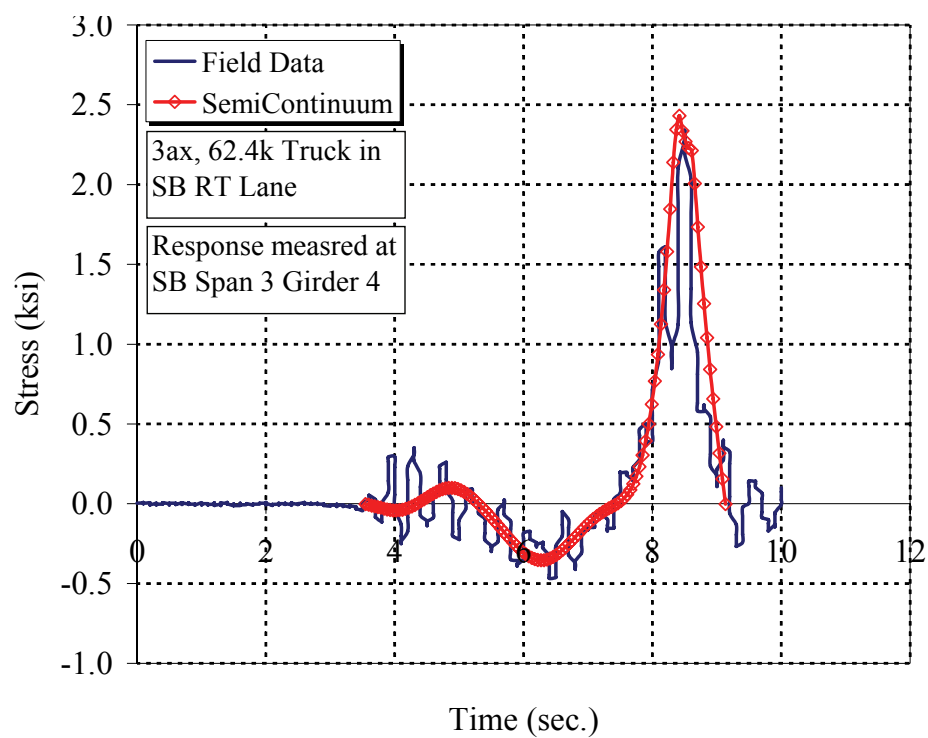
Figure 4.55 Semi-continuum model results shown with observed bridge response for Route 18 over River Road.

CHAPTER 5

LIVE LOAD MODEL

Increasing improvements in material consistency and construction technology have reduced the variability of bridge resistance. However, live load remains a challenging parameter to quantify. A variety of truck configurations, weights, and volumes make prediction of loads difficult. Truck configurations affect bridges differently depending on the span length and girder spacing. Extreme loads are infrequent, but will ultimately control the design. All of these factors combine to form live load spectra. There are two key quantities in load spectra: (1) the loads that will act on the bridge, and (2) the effect of the loads in the form of total moments or shears.

5.1 Analysis of Live Load Data

In order to quantify live load, information about the truck population is needed. Truck loads are known to be highly site specific (Nowak and Laman 1996) and vary from region to region. Live load may also vary for the same highway at different locations. Additionally, live load has seasonal variations, depending on local economic trends. Truck traffic growth is also a factor from one year to the next. Weigh-in-motion data is the primary resource used to quantify the site-specific truck population. WIM systems have become more common and their sensor technology has evolved to a level of

reliability required for long term monitoring. WIM data contains the fundamental

parameters that describe the truck population including: lane, axle weight, axle spacing,

speed, time of arrival, count, classification, length, number of axles, etc. WIM systems

are available from a variety of vendors. Regardless of the manufacturer or particular data

format, all systems provide the same relevant information about the truck traffic. The

following sections provide information on the specific data formats, WIM systems,

sensors, data filters, quality control routines, and data used to analyze the truck

population in this study.

5.1.1   WIM Data Format

WIM data, as collected by the system in the field, is recorded in a proprietary

binary format. In this manner, the data compression makes it possible to store a large

magnitude of truck information for extended durations. The WIM system collects the

traffic information and stores it in daily binary files that are downloaded by the

operations or research personnel on a typical schedule. Once retrieved from the field,

data must be converted from the efficient binary format to a readable ASCII format for

use in spreadsheet or other computer programs. The exact layout of the data is unique to

the manufacturer, but the content is the same across all types of systems. The format for

the data used in this study is given in Figure 5.1.

Field	Parameter
1	Year
2	Month
3	Day
4	Hour
5	Minute
6	Second
7	1/100 sec
8	Violation Code
9	Vehicle Number
10	Lane
11	Speed, MPH
12	FHWA Classification
13	Length, feet
14	Equiv. Single Ax. Ld., ESAL
15	Weight Axle 1
16	Spacing Axle 1-2
17	Weight Axle 2
18	Spacing Axle 2-3
19 to 40	Weights and Spaces Up to Axle 14
41	Custom Code

Figure 5.1 NJDOT WIM data format

In order to describe the truck population in terms of types of vehicles, the Federal Highway Administration (FHWA, 2001) has formulated a classification system (Table 5.1). In this system there are fifteen vehicle classes ranging from Class 1 for motorcycles up to Class 15 for large or unidentified vehicles. Classes 1 and 14 included at the discretion of the transportation agency. A vehicle is classified based on the following parameters: (1) number of axles, (2) length, (3) axle spacing and weights.

The typical vehicle configurations for each class are illustrated in Table 5.2. For example, the most prevalent truck is typically the Class 9.   The Class 9 tractor trailer is also referred to as 3S2, having a three axle drive tractor followed by a 2 axle semi-trailer. This truck type is commonly used for long haul freight operations and container movements. Furthermore, the configuration of the HS20 design truck resembles the 3S2. Classes 5 and 6 are also common but often weigh less than the Class 9. Class 7 trucks are

often bulk material carriers (dump trucks) with a fourth "drop-axle" that can be lowered when there is payload. The motivation for a movable axle is most likely based on toll schedules that asses charges based on number of axles. Therefore, the same vehicle travels empty as a three-axle Class 6 truck and loaded as a four-axle Class 7 truck.

Due to their large volume and little influence on bridge or pavement design, passenger vehicles are often omitted from the WIM data. Therefore, only truck volume is known. Weigh-in-motion sensors are less accurate when measuring the light axles of passenger vehicle or small pickup type trucks.

As each vehicle in a traffic stream passes over the WIM system, the number of axles, length, axle spacing, and axle weights are read to determine its classification. The exact criteria for the FHWA classification scheme are given in ASTM E-1318(02) specifications (ASTM 2002). If the system is unable to classify the truck or there is an error that makes classification not possible, the vehicle is assigned as Class 15. Often Class 15 trucks contain data errors resulting from changes in speed, lane, or excessive dynamic impact. Class 15 trucks may also be the result of inductive loop malfunction. If the loop sensor remains active after the passage of a truck, the system may append more than one truck into a single record. This appended record will be impossible to classify since it contains two separate vehicles.

Table 5.1 FHWA Vehicle Classification System (FHWA 2001)

Class	Type	Description
1	Motorcycles	All two or three-wheeled motorized vehicles. Typical vehicles in this category have saddle type seats and are steered by handlebars rather than steering wheels. This category includes motorcycles, motor scooters, mopeds, motor-powered bicycles, and three-wheel motorcycles. This vehicle type may be reported at the option of the state
2	Passenger Cars	All sedans, coupes, and station wagons manufactured primarily for the purpose of carrying passengers and including those passenger cars pulling recreational or other light trailers
3	Other Two-Axle Four Tire Single Unit Vehciles	All two-axle, four-tire, vehicles, other than passenger cars. Included in this classification are pickups, panels, vans, and other vehicles such as campers, motor homes, ambulances, hearses, carryalls, and minibuses. Other two-axle, four-tire single-unit vehicles pulling recreational or other light trailers are included in this classification. Because automatic vehicle classifiers have difficulty distinguishing class 3 from class 2, these two classes may be combined into class 2
4	Buses	All vehicles manufactured as traditional passenger-carrying buses with two axles and six tires or three or more axles. This category includes only traditional buses (including school buses) functioning as passenger-carrying vehicles. Modified buses should be considered to be a truck and should be appropriately classified
5	Two-Axle, Six Tire, Single Unit Trucks	All vehicles on a single frame including trucks, camping and recreational vehicles, motor homes, etc., with two axles and dual rear wheels
6	Three-Axle, Single Unit Trucks	All vehicles on a single frame including trucks, camping and recreational vehicles, motor homes, etc., with three axles.
7	Four of More Axle Single Unit Trucks	All trucks on a single frame with four or more axles
8	Four of Less Axle Single Trailer Trucks	All vehicles with four or fewer axles consisting of two units, one of which is a tractor or straight truck power unit
9	Five-Axle Single Trailer Trucks	All five-axle vehicles consisting of two units, one of which is a tractor or straight truck power unit
10	Six or More Axle Single-Trailer Trucks	All vehicles with six or more axles consisting of two units, one of which is a tractor or straight truck power unit
11	Five or fewer Axle Multi-Trailer Trucks	All vehicles with five or fewer axles consisting of three or more units, one of which is a tractor or straight truck power unit
12	Six-Axle Multi-Trailer Trucks	All six-axle vehicles consisting of three or more units, one of which is a tractor or straight truck power unit
13	Seven or More Axle Multi-Trailer Trucks	All vehicles with seven or more axles consisting of three or more units, one of which is a tractor or straight truck power unit
14	Not Specified	Custom classification for state use
15	Not Classified or Data Error	Assigned to all records with violation codes pertaining to data errors or vehciles that do not fit any of the above criteria

Table 5.2 Vehicle configurations by vehicle class (FHWA 2001)
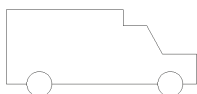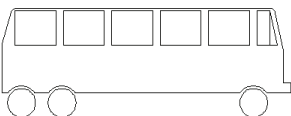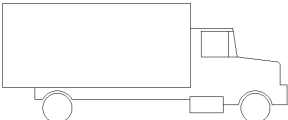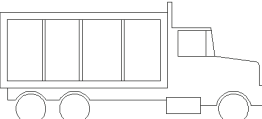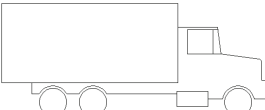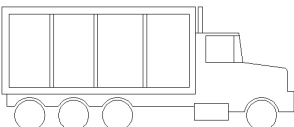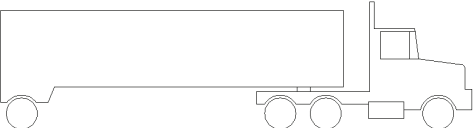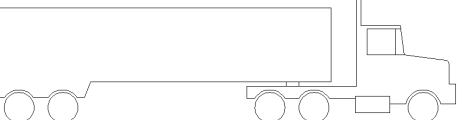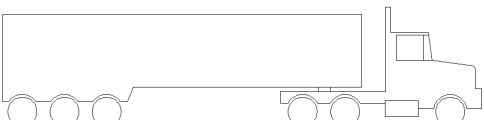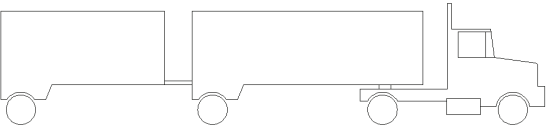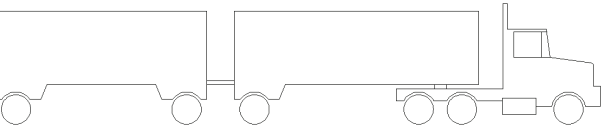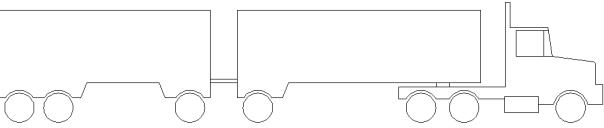
Class	Type	Typical Configuration
1	Motorcycles	
2	Passenger Cars	
3	Other Two-Axle Four Tire Single Unit Vehicles	
4	Buses	
5	Two-Axle, Six Tire, Single Unit Trucks	
6	Three-Axle, Single Unit Trucks	
7	Four of More Axle Single Unit Trucks	
8	Four of Less Axle Single Trailer Trucks	
9	Five-Axle Single Trailer Trucks	
10	Six or More Axle Single-Trailer Trucks	

Table 5.2 **(Continued)**

Class	Type	Typical Configuration
11	Five or fewer Axle Multi-Trailer Trucks	
12	Six-Axle Multi-Trailer Trucks	
13	Seven or More Axle Multi-Trailer Trucks	
14	Not Specified	No Specific Configuration
15	Not Classified or Data Error	No Specific Configuration

5.1.2   Quality Control of WIM Data

Weigh-in-motion data, like any other measured scientific data, must be quality checked before casual use. There are many causes for poor quality WIM data (Southgate 2000):

(1) Suboptimal WIM site choice: rough pavement, road curvature, slowing or accelerating traffic

(2) Settings or Dimensions: inaccurate sensor location, improper installation, wrong settings

(3) Time out settings too long: the system is adding closely following trucks together as a single record

(4) Calibration Drift over time: electronics tend to loose their calibration set point over time

(5) Temperature: Piezo sensors use the impulse of the axle loads to load. At higher temperatures the asphalt is softer and offers less resistance thereby reducing the sensor reading.

There are several methods to check for WIM data quality as well as adjust the data to bring it back into calibration. Auto-calibration functions are built into most systems. These functions use the relationship of the first or steering axle to the gross weight of a typical five axle tractor trailer (Class 9).

To test calibration, techniques have been developed to check the calibration of WIM systems based on an extensive database of past results and physical characteristics of trucks (Southgate 2000).

Southgate (2000) used a logarithmic regression of axle spacing and weights to compare WIM calibration. The procedure is applied to Class 9, five axle, trucks since the properties of the steering axle are only related to the drive tractor, and not the payload. Further, Class 9 vehicles are the same used by most WIM systems for auto calibration. It is recommended to limit the sample size to a single day since seasonal temperature changes and drift will affect the data. The WIM quality control procedure is as follows:

(1)   Reduce the data such that only one day of data containing only class 9, five axle trucks remain

(2)   Consider each lane separately since the calibrations are independent by lane

(3)   Calculate the ratio of the steering axle weight (W1) divided by the first axle spacing (S1-2) for each truck record

(4)   Calculate the LOG (base 10) of the ratio (W1)/(S1-2), from Step 3

(5)   Find the LOG (base 10) of the first axle spacing (S1-2)

(6)   Plot the LOG(S1-2) on the x-axis vs. LOG((W1)/(S1-2)) on the y-axis, and perform a linear regression to obtain the slope, M, and the intercept, B

(7)   Calculate the LOG regression, R, of each data point such that R=10^(B+M*LOG(S1-2))

(8)   Calculate the reference regression E=10^(3.925361-0.952182*LOG(S1-2))

(9)   Find the upper bound of the regression as the maximum steering axle weight to spacing ratio (by manufacturers specifications) as MAX= 12,000lb/(S1-2)+50lb/ft.

(10)   Find the lower bound of the regression of the steering axle as MIN= 10^(3.942369-1.075085*LOG(S1-2))

(11)   Plot the following per lane: (W1)/(S1-2), the regression (R), the reference regression (E), the upper bound ratio (MAX), and the lower bound ratio (MIN) for each data point.

The following sections show the result of the WIM data quality control as applied to the NJDOT WIM and Doremus Avenue Bridge WIM data. Examples are given for site with good data quality and also poor data quality. Procedures are available to re-calibrate the marginally poor data. Refer to Section 4.3 for more detailed site information including lane designation, lane direction, and site locations.

5.1.2.1   WIM Data Quality Control: NJ WIM Site 78B

NJDOT WIM site 78B is located along Interstate 78 at Milepost 34.5 in Bernard

Township, Somerset County. The WIM layout as given is Table 5.4 is a Loop-Piezo-

Loop configuration. For best accuracy, WIM system manufacturers recommend

installing at least two axle sensors per lane. As vehicles pass over the axle sensors,

dynamic motion of the wheels or vehicle body leads to inaccurate weight readings. To

account for this error, WIM systems are installed with two axle sensors per lane. The

weight reading for each axle, is therefore, taken as the average of the two readings. Since

NJ Site 78B has an L-P-L configuration it has only a single axle sensor per lane. Another

problem with the single axle sensor relates to the measurement of axle spacings. Since

there is only one axle sensor, the vehicle speed must be determined by the inductive loop

sensors. Loops detect the vehicle by magnetic induction changes relating to the presence

of metal. The induction is not always definitive. There may be some error in the speed

measurement compared to using two piezo axle sensors. When the WIM system

calculates the axle spacing, the internal software uses the speed from the loop sensors and

the axle timings from the piezo sensors. Any error in the speed measurements will

therefore be propagated to the axle spacing measurements. This configuration reduces

installation costs, but introduces data quality problems.

Figure 5.2 gives the WIM quality control procedure results for Site 78B. The

plots of front axle spacing vs. the ratio of the first axle weight to the steering axle spacing

should produce a smooth logarithmic decay as given by the Reference Equation Curve.

The fit of the WIM data for lanes 1 and 2 show a divergence from the reference curve at

both small and large steering axle spacing. There is insufficient data to conclude on the

calibration of Lane 3. Since a significant majority of the data points fall within the upper

and lower thresholds, the weight calibration is satisfactory.

(a)

(b)

(c)
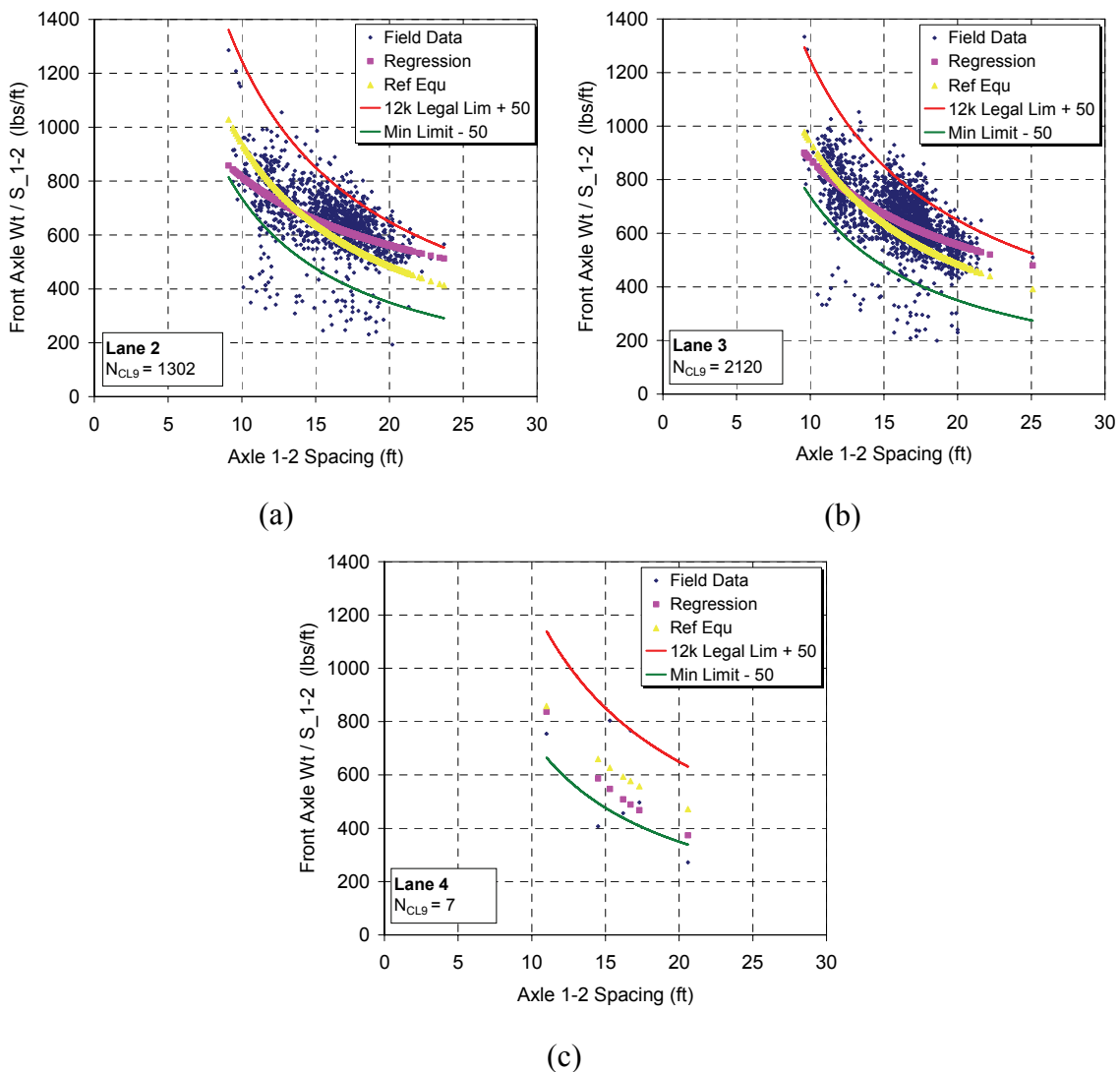
Figure 5.2 WIM Quality Control, logarithmic regressions of axle weight and spaces for NJ Site 78B on 9/20/06 for (a) Lane 1, (b) Lane 2, and (c) Lane 3. The poor data quality is due to having only one axle sensor.

Since the logarithmic regression does not differ from the reference curve by more

than ten percent and the divergence is symmetric, the data for Site 78B is acceptable for

general use for the load factor calibration study. However, regular filtering routines must

be applied to the data to eliminate gross errors and impractical measurements. Further,

extremely heavy vehicles from this site must be scrutinized since the sensor configuration is prone to errors.

5.1.2.2   WIM Data Quality Control: Doremus Avenue Bridge WIM Site

(a)

(b)

(c)

(d)
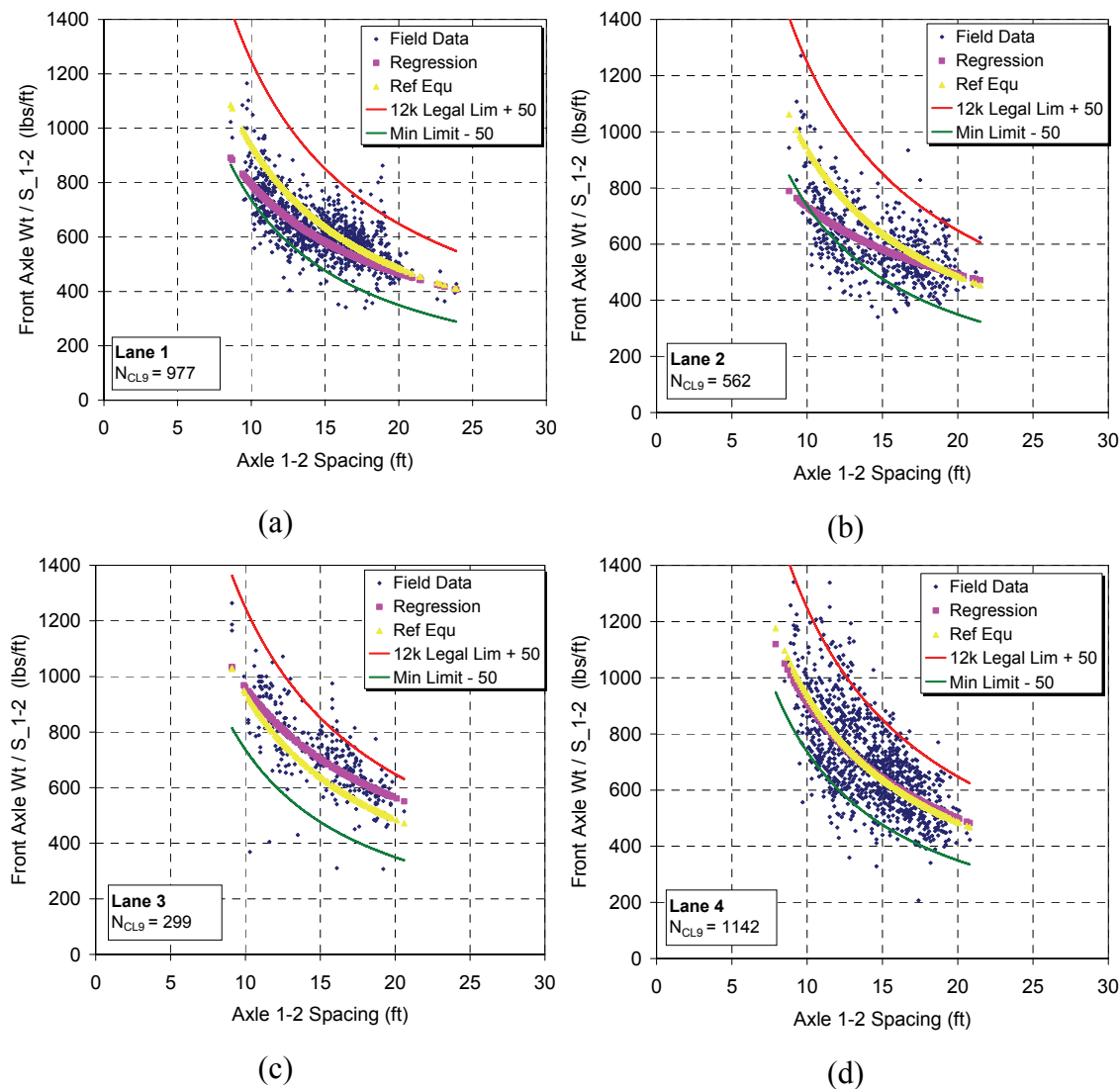
Figure 5.3 WIM Quality Control, logarithmic regressions of axle weight and spaces for Doremus Avenue Bridge WIM Site operated by Rutgers University for 6/1/05 for (a) Lane 1, (b) Lane 2, (c) Lane 3, and (d) Lane 4

5.1.2.3 WIM Data Quality Control: NJ WIM Site 78D
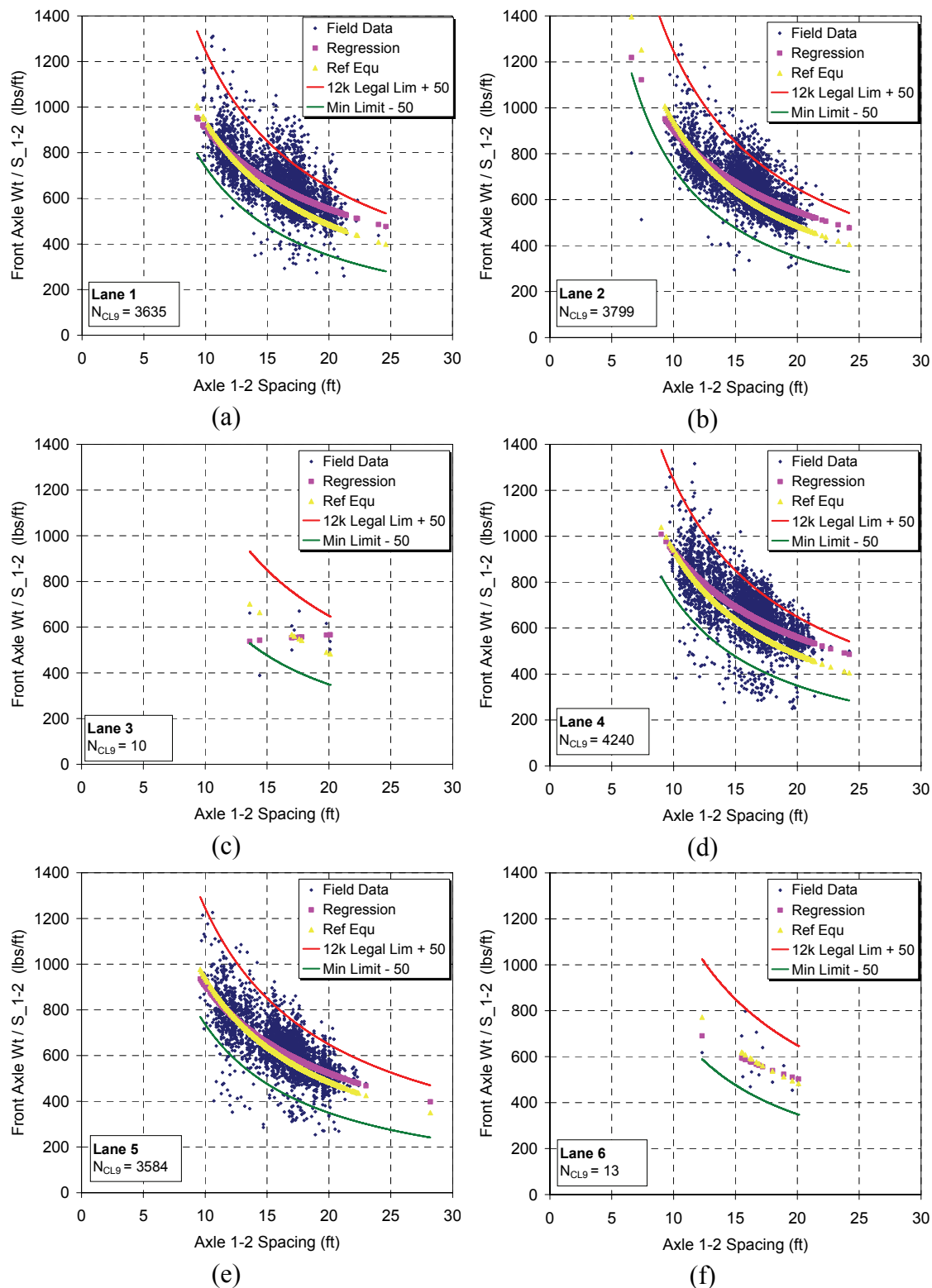
Figure 5.4 WIM Quality Control, logarithmic regressions of axle weight and spaces for NJ Site 78D
on 6/1/06 for (a) Lane 1, (b) Lane 2, (c) Lane 3, (d) Lane 4, (e) Lane 5, and (f) Lane 6

All data must be checked for quality and consistency. Using the procedures demonstrated, most of the data has been shown to be satisfactory. Data that was determined to be grossly out of calibration was excluded from this study. After passing the check for calibration, the data must be further scrutinized by applying filtering routines. The routines used for determining if the data is reasonable and practical are outlined in the next section.

5.1.3 WIM Data Filtering

After quality control checks have been complete there are further steps that need to be taken to reduce the amount of erroneous or otherwise insignificant data. Filters were developed to remove the known permit loads, insignificant data (such as trucks weighing less than 15k), and erroneous data (such as single axle weights over 40k or axle spaces less than 2 feet). A disqualification file was created for each of the filter criteria. Any data that was removed from the mainstream set was counted and placed into the respective disqualification file. The filter criteria are based on known trends, permit configurations furnished by a state transportation agency, or engineering judgment. The following filter criteria were developed and applied to the WIM data:

(1) <u>Criterion 1</u>. Minimum truck weight must be at least 15 kips. This is applied to eliminate inconsequential truck records or passenger vehicles that were classified as trucks. Additionally, piezo sensor technology may produce errors for vehicles with light axles (less than 5k).

(2) <u>Criterion 2</u>. Omit all Class 15 truck records. The IRD WIM system groups all unclassified vehicles as Class 15. These may include special configurations such as vehicles in tow. Class 15 also includes data errors as evident by low average gross weights and high standard deviations.

(3) <u>Criterion 3</u>. Eliminate all records with a pair of axles (tandem) totaling more than 60 kips. A tandem is defined as a pair of adjacent axles with a spacing of less than 5 feet (typical tandem spacing is 54 inches or 4.5 feet). This item is designed to screen data records that are unlikely due to limited tandem capacity. Although such weights can occur, they are likely due to errors or combining axles. Nonetheless, the omitted records are stored in a separate file for further review.

(4) <u>Criterion 4</u>. For any 9-axle vehicle the maximum gross weight is limited to 160 kips. This filter will omit any known permit vehicles from the mainstream data such as the permitted Demag Cranes. Permit vehicles include nine axles with axle weights ranging from 13.8 to 25.0 kips and a total gross vehicle weight of about 165.7 kips. An additional filter criteria was developed to look for the permit axle configuration. Refer to criterion 10 for an additional permit filter. (NJDOT 2005)

(5) <u>Criterion 5</u>. For any Class 9 (5 axle, 2 unit) truck the steering axle weight is limited to a maximum of 12k. Typical Class 9 steering axles weights range from 9 to 11 kips and are only influenced by the drive tractor, not by the load. Therefore, the first axle weight is an independent source of WIM verification (Southgate 2000).

(6) <u>Criterion 6</u>. For any class truck with a length equal or greater than 50 feet, the gross weight should be greater than 20 kips. This item serves to reduce data errors from unrealistic light and long vehicles or truck records that are erroneously appended to other vehicles.

(7) <u>Criterion 7</u>. The maximum gross weight any 10 axle truck is 170k. This is an additional filter for alternate permit configurations

(8) <u>Criterion 8</u>. No single axle can weigh more than 40k. There is a physical limit to how much load can be applied to a typical axle. While it may be possible to see axle loads in this range, they typically result from dynamic impact on the sensor or over calibration. For example, a record from the WIM data reported a three axle vehicle with axle weights of 11.6k, 13.8k, 127k.

The 127k axle is an obvious error. The results can be further screened within the disqualification file for possible legitimate trucks.

(9) <u>Criterion 9</u>. There can be no axle spacing less than 3 feet. Geometric constrains such as wheel diameter limit the minimum axle spacing for a tandem. Typical tandem spacing is about 54 inches or 4.5 feet. Additional axles with very short spacing may be reported if the truck is bouncing over the axle sensor. An axle spacing less than 3 feet, such as one measuring 0.6ft, was observed in WIM data. Unrealistically short axle spacing lead to over-estimates of bending moment and shears and therefore must be screened out.

(10)   <u>Criterion 10</u>. Remove all permit trucks that have 3 or more tandems. This filter looks for tandems, or pairs of axles, that are separated by a distance greater than seven feet. Permit vehicles have a distinct axle pattern consisting of a steering axle followed by a space of about 15 feet, a drive tandem with 4.5 ft spacing, a space of about 13.5 feet, a tandem with 4.5 ft spacing, a space of about 13.5 to 36 feet, and a tandem. Figure 5.10 shows the typical permit configuration. The axle weight restrictions for permits are given in Table 5.4 for CalTrans Purple load designation. For larger or longer payloads additional tandems up to a total of six are added such that only one tandem may exist within any 18 foot distance. The 18 foot restriction is in place to satisfy the FHWA Bridge Formula (FHWA 2001).

(11)   <u>Criterion 11</u>. Remove all permitted fixed load vehicles, specifically permitted cranes. Truck mounted cranes feature telescoping booms for easy transport to jobsites. The configuration and axle weight vary by manufacturer; however, the spacing of the last three axles is distinct to the cranes. In order to satisfy the permit specifications the boom of the crane is rotated 180 degrees to point toward the rear. A specialized three axle trailer, called a "boom dolly" (Manitowok 2006), is positioned under the boom to further distribute the load. A filter was designed to take advantage of this characteristic. The filter criteria are as follows: the gross weight must be greater than 140 kips, there must be 7 or more axles, the second to last axle spacing must be between 4 and 7 feet, and the last axle spacing must be

between 10 and 20 feet. The tolerances for axle spacing were chosen based on manufacturers' specifications and verified using the means of axle spacing from outlier points present in simple moment ratio plots. Figure 5.9 shows the average weights and spaces for the removed permitted cranes, the axle weights are in kips and the spacing is in feet.

(12)   Criterion 12. This parameter was introduced to identify and remove permitted cranes that do not fit the criteria of Criterion 11. It was found that cranes in the NJDOT WIM data occur as five, six, seven, or weight axle vehicles without the trailing dollies seen in the CalTrans data. The filter looks for gross weights greater than 100k, overall length less than 50 feet, and a first axle spacing less than 8 feet. Since most semi-trailer trucks have a front axle spacing between 12 and 15 feet and overall length greater than 50 feet, the chance of eliminating this type of truck is low. Cranes have the ability to raise and lower selected axles to conform to local DOT guidelines for axle loads. This feature makes detection of cranes by a single filter difficult. However, all cranes remain short with numerous axles closely spaced. A combination of filters is therefore needed to remove the spectrum of cranes in the truck population.

After filtering the data, a counter tallied these qualified trucks. Typically, approximately seventy-five percent of the raw data passed the filters and was included in the analysis. The qualifying percentage may be lower if the original data contained passenger cars and a high proportion of light trucks. The disqualified trucks were tallied according to the disqualification criteria and stored to a separate file. The most common disqualification occurred for gross vehicle weight under 15 kips. The next section details the permit configurations for the New Jersey Department of Transportation (NJDOT).

5.1.3.1   NJDOT Permit Loads

The NJDOT specifies a permit vehicle in the Bridge Design Manual (NJDOT 2002) that provides an envelope for the maximum expected load for design or evaluation. The 8-axle (200k) permit vehicle is shown in Figure 5.5. The configuration of the permit truck replicates a 4-axle single body Class 7 (dump truck) towing a 4-axle trailer. The first axle, weighing 16k, represents the steering axle. The second axle, weighing 16 kips, represents the auxiliary drop axle found on most single body dump trucks. The load effect envelope for simple moment is given in Figure 5.6. The maximum simple moment ratio for the NJDOT Permit truck was 2.43*HS20 for a span of 140 feet.

NJDOT requires commercial carriers to obtain authorizations when moving extra-legal loads or excessively large truck configurations. Each carrier submits a permit application that describes in detail the following: carrier information, proposed route, number of movements, number of axles, length, gross weight, individual axle weights, axle spacing, axle width, and number of tires per axle. A typical permit application is shown in Figure 5.7 with the name and contact information of the applicant removed. The example application shows five movements of a ten-axle 188 kip truck in the vicinity of Doremus Avenue, Newark, NJ. The number of permitted movements is important when considering damage due to overload such as concrete cracking and fatigue damage. Most permits are issued with a finite number of permitted movements to limit the damage to the structures along the route. The moment envelope of each permit application is check against the NJDOT permit vehicle. If the application truck causes moments or shears greater than the Permit Vehicle, permission is denied for a permit. Furthermore, the proposed route may be amended to avoid aging or deteriorating structures.
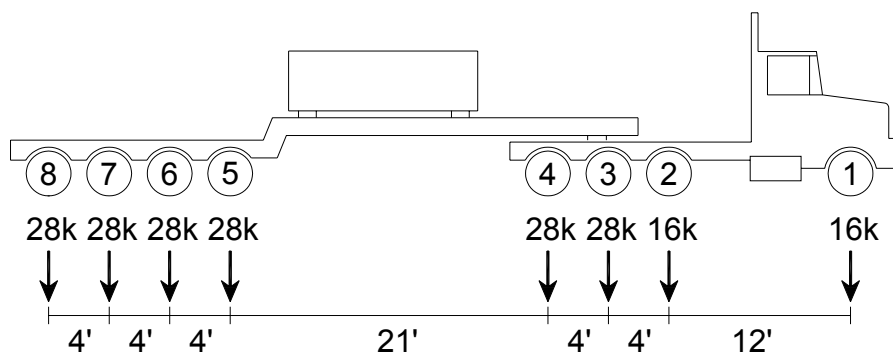
Figure 5.5 Permit Vehicle from NJDOT Bridge Design Manual (NJDOT 2002)
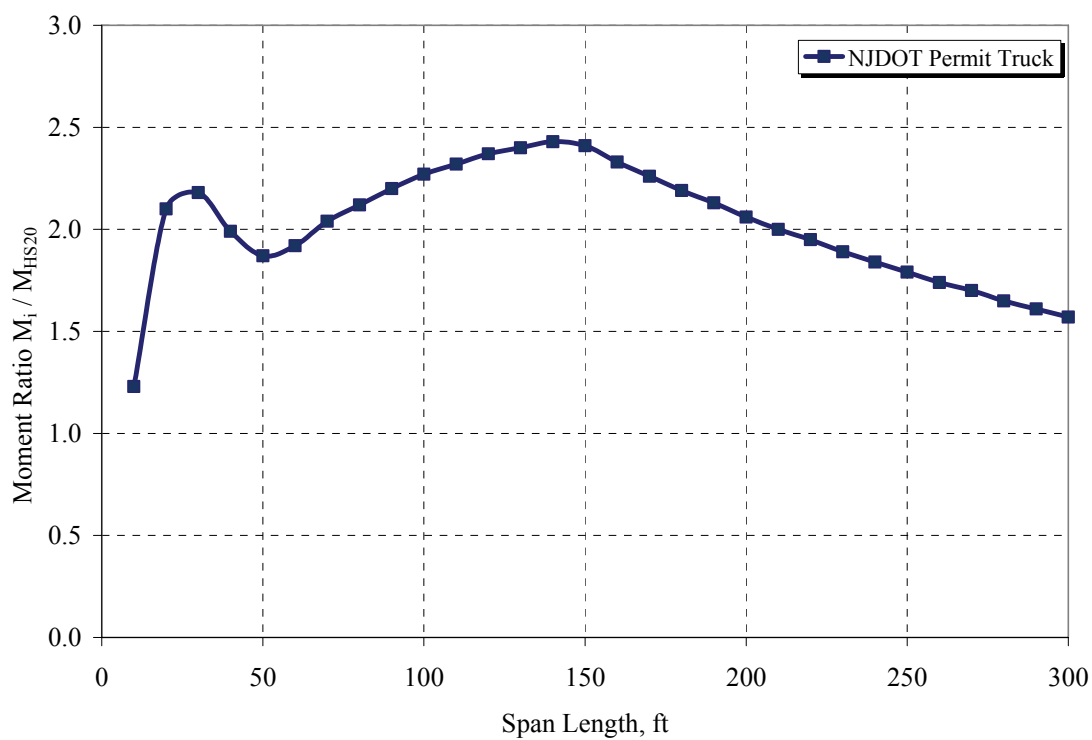
Figure 5.6 Simple moment envelope for NJDOT Permit Truck
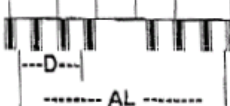
FAX REPORT – OVERLOAD REQUEST (REV 12/03)		PAGE 1 OF 1	DATE: 1/2/04
FROM		TO	

SWT TAG: NO
AXLES: 10
WEIGHT: 188,000

CARRIER:
STREET:
CITY/STATE:
PHONE:

4002
HA

| X = | 1 | | 2 | 3 | 4 | 5 | 6 | 7 | 8 | 9 | 10 | 11 | 12 | 13 | 14 | 15 | 16 | 17 | 18 | 19 | 20 | 21 | 22 | 23 |
| P = | 1 | | 2 | 3 | 4 | 5 | 6 | 7 | 8 | 9 | 10 | 11 | 12 | 13 | 14 | 15 | 16 | 17 | 18 | 19 | 20 | 21 | 22 | 23 | 24 |

AXLE LOADS (LBS)		AXLE SPACINGS (FEET/INCHES)		AXLE CONFIGURATION	OVERALL DIMENSIONS
P1 =	15,000	X1 =	17'00"		WIDTH: 12'04"
P2 =	13,000	X2 =	04'04"	ARE THERE ANY	LENGTH: 110'00"
P3 =	14,000	X3 =	04'04"	AXLES WITH	HEIGHT: 14'00"
P4 =	14,000	X4 =	13'06"	MORE THAN	APPROXIMATE
P5 =	22,000	X5 =	04'08"	FOUR WHEELS?	DISTANCE OF MOVE
P6 =	22,000	X6 =	37'08"	YES NO	50 MILES
P7 =	22,000	X7 =	04'06"		
P8 =	22,000	X8 =	13'06"		IF RECENT
P9 =	22,000	X9 =	04'06"	---D---	APPROVAL REFER
P10 =	22,000	X10 =		-------- AL --------	TO MEMO DATED:
P11 =		X11 =			
P12 =		X12 =			PROPOSED ROUTE
P13 =		X13 =		FROM: NEWARK	
P14 =		X14 =		TO: PA LINE RT 80	
P15 =		X15 =		VIA: NEWAR NJ-17 DOREMUS AVE. WELLENNS	
P16 =		X16 =		LINES BERTH-DOREMUS AVE S., E.PORT ST-W	
P17 =		X17 =		TO US-1 S TO SR 21 N, TO I-280 W TO I-80 W	
P18 =		X18 =			
P19 =		X19 =		5 MOVES BEING MADE	
P20 =		X20 =	Date of request:— 01/02/2004		
P21 =		X21 =	Axles & weight:— 10 axles & 188,000		
P22 =		X22 =			
P23 =		X23 =	Approved route:— Disapproved		
P24 =					
TOTAL =	188,000	TOTAL =			

Figure 5.7 Typical NJDOT Permit Application (NJDOT 2005)

Table 5.3 NJDOT Permit applications in the vicinity of Doremus Avenue between 2003 and 2004: (a) axle weights and (b) axle spacing

Ref No.	Permit Date	GVW (k)	Length (ft)	Axles	W1 (k)	W2 (k)	W3 (k)	W4 (k)	W5 (k)	W6 (k)	W7 (k)	W8 (k)	W9 (k)	W10 (k)	W11 (k)	W12 (k)
1	6/13/2003	172	105	9	12	20	20	20	20	20	20	20	20			
2	7/9/2003	180	110	10	12	16	16	16	20	20	20	20	20	20		
3	12/11/2003	164	110	9	12	19	19	19	19	19	19	19	19			
4	1/2/2004	188	110	10	15	13	14	14	22	22	22	22	22	22		
5	1/5/2004	197	110	9	13	23	23	23	23	23	23	23	23			
6	2/23/2004	199	110	11	12	16	16	16	23	23	17.7	17.7	17.7	20	20	
7	3/18/2004	172	106	9	12	20	20	20	20	20	20	20	20			
8	3/26/2004	173	110	9	13	20	20	20	20	20	20	20	20			
9	4/30/2004	181	110	9	13	21	21	21	21	21	21	21	21			
10	10/6/2004	172.5	110	9	12.5	20	20	20	20	20	20	20	20			

(a)

Ref No.	Permit Date	GVW (k)	Length (ft)	Axles	S1-2 (ft)	S2-3 (ft)	S3-4 (ft)	S4-5 (ft)	S5-6 (ft)	S6-7 (ft)	S7-8 (ft)	S8-9 (ft)	S9-10 (ft)	S10-11 (ft)	S11-12 (ft)
1	6/13/2003	172	105	9	19.0	4.5	14.1	4.5	36.0	4.5	14.0	4.5			
2	7/9/2003	180	110	10	17.7	4.3	4.3	13.8	4.5	38.8	4.5	14.1	4.5		
3	12/11/2003	164	110	9	21.2	4.5	13.5	4.5	35.0	4.5	13.5	4.5			
4	1/2/2004	188	110	10	17.0	4.3	4.3	13.5	4.5	37.7	4.5	13.5	4.5		
5	1/5/2004	197	110	9	22.1	5.1	14.5	4.5	34.5	4.5	14.1	4.5			
6	2/23/2004	199	110	11	17.1	5.1	5.1	16.5	5.1	27.7	5.1	5.1	14.1	5.1	
7	3/18/2004	172	106	9	17.5	4.5	15.4	4.1	32.4	4.2	12.8	4.2			
8	3/26/2004	173	110	9	21.8	4.5	13.5	4.5	38.2	4.5	13.5	4.5			
9	4/30/2004	181	110	9	21.2	4.5	14.3	4.5	35.3	4.5	14.0	4.5			
10	10/6/2004	172.5	110	9	17.3	4.6	14.5	4.5	34.3	4.5	13.6	4.5			

(b)

To predict the stress levels caused by these known permit trucks, the weight and spacing information was input and run with the semi-continuum model of Doremus Avenue (Figure 5.8). Since most of the approved routes from the permit applications indicate vehicles heading southbound on Doremus Avenue, all permit simulations are assumed to be in the southbound right lane (Lane D). The stress in the bottom flange of Girder 4 will be considered since the Lane D truck aligns over G4. A location at the maximum positive moment position of Span 3 is considered as the truck travels from Span 3 to Span 1 in Lane D.
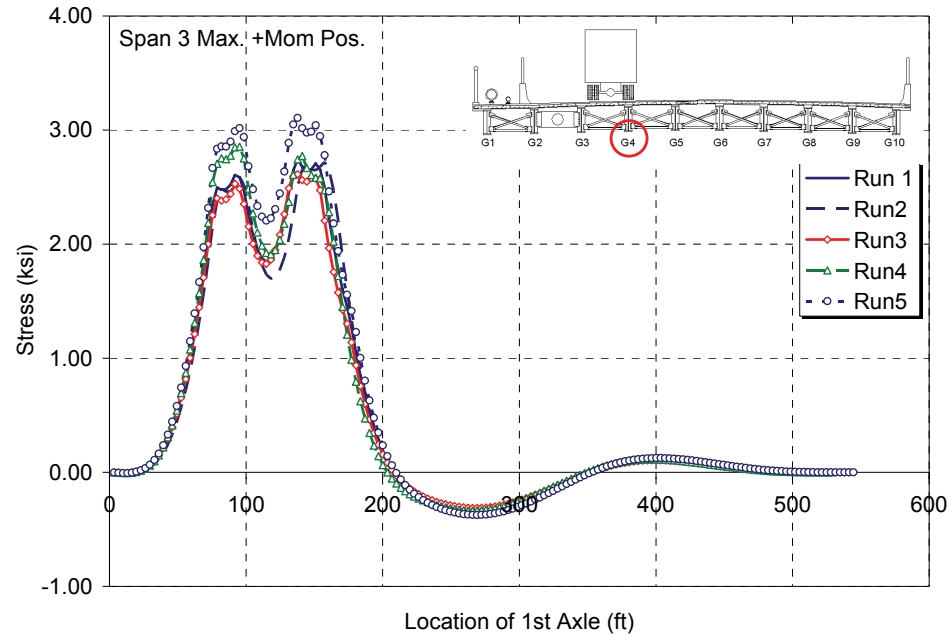
(a)
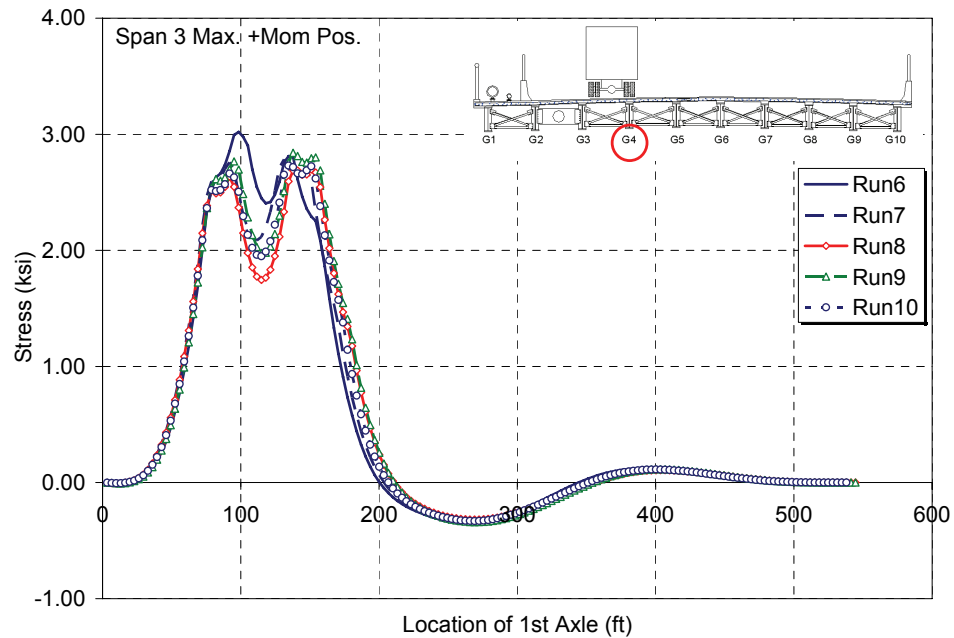
(b)

Figure 5.8 Semi-continuum Girder 4 stress predictions for Doremus Avenue permit trucks in Lane D

The plots in Figure 5.8a and Figure 5.8b show the semi-continuum stress

predictions for Girder 4 Span 3 given Permit Trucks 1 to 5 and 6 to 10, respectively. All

ten permit trucks exhibit similar twin peaked stress profiles during their passage. In

addition, the magnitude of G4 stress is similar for all known permit trucks with a
maximum stress of 3.11 ksi for Permit Number 5 in Figure 5.8a.

5.1.3.2   Crane Loads

(a) 7-axle crane observed from WIM data

(b) 8-axle crane observed from WIM data

(c) Grove GMK7550 crane manufacturers specification with 3-axle trailing dolly
(www.manitowoccranegroup.com)
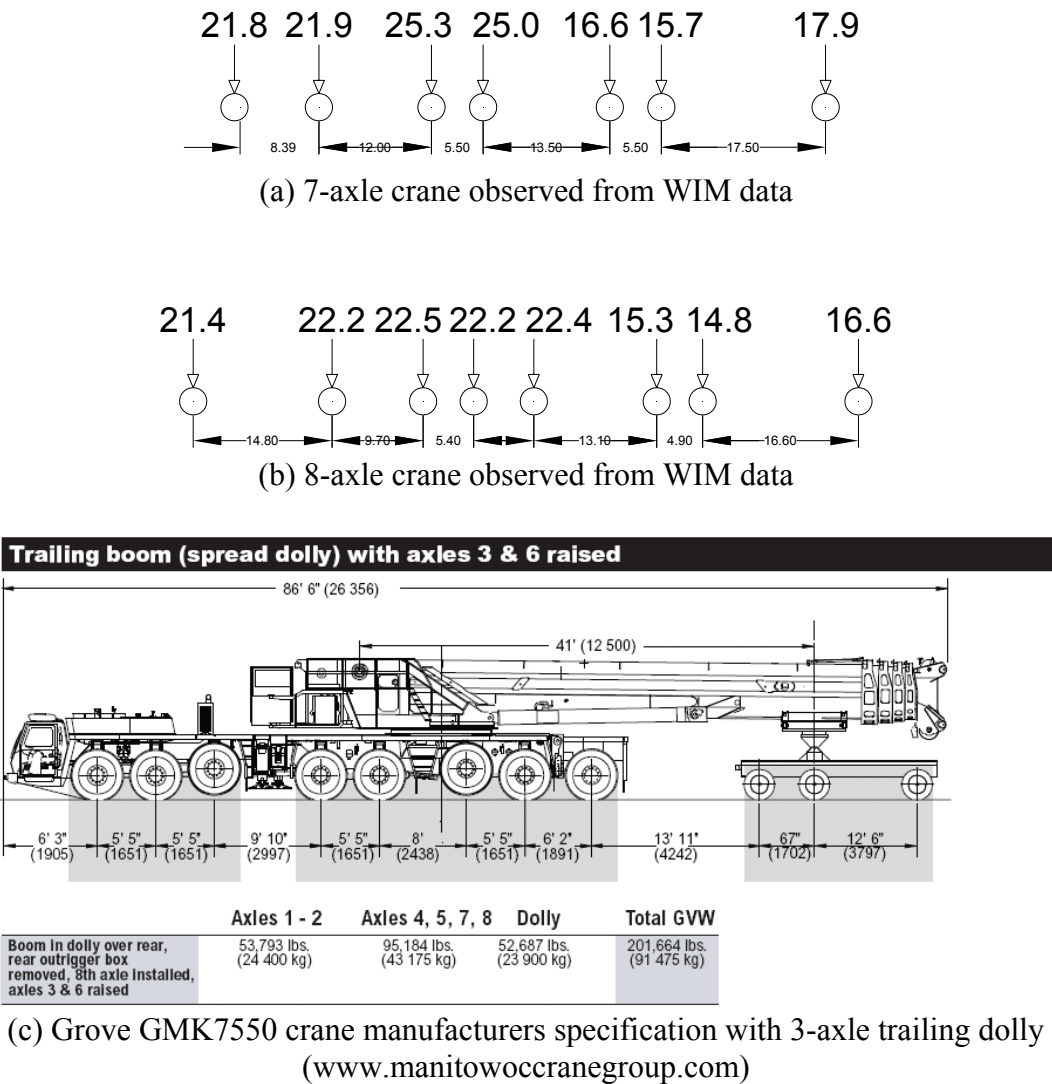
Figure 5.9 Configuration of permitted cranes from WIM data: (a) the 7-axle and (b) the 8-axle crane (units k & ft), the last three axles represent the "boom dolly", and (c) manufacturer specifications for Grove GMK7550 crane

(a)

(b)
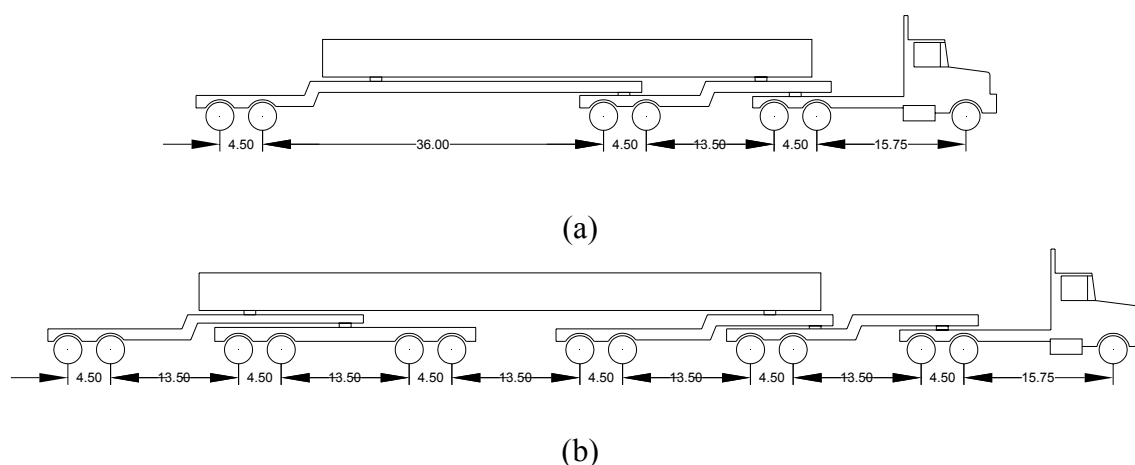
Figure 5.10 Typical permit configurations: (a) with seven axles and (b) with thirteen axles

Table 5.4 CalTrans permit umbrella loads (CalTrans 1995)

Name	Axle Purple Loads (unbonused), kips												
	W1	W2	W3	W4	W5	W6	W7	W8	W9	W10	W11	W12	W13
P5	26	24	24	24	24	---	---	---	---	---	---	---	---
P7	26	24	24	24	24	24	24	---	---	---	---	---	---
P9	26	24	24	24	24	24	24	24	24	---	---	---	---
P11	26	24	24	24	24	24	24	24	24	24	24	---	---
P13	26	24	24	24	24	24	24	24	24	24	24	24	24

5.1.3.3   Extreme Load Events (Rouge Trucks)

Permit information was requested for comparison with observed extreme heavy

loads at the Doremus Avenue WIM site at the south abutment of the bridge. If the

observed trucks are permitted, their information should be on record with NJDOT. The

loads and configurations of ten permit applications were obtained and reviewed for the

timeframe of the observed extreme trucks (Table 5.3) (NJDOT 2005). The reviewed

applications all proposed routes passing over the Doremus Avenue Bridge, but no vehicle

configurations could be found to match the observed extreme vehicles within the WIM

data. There are, however, open permits that allow certain fixed load vehicles to travel

freely. Fixed load and dimension vehicles include road capable truck mounted cranes and other moveable industrial machinery. The rouge vehicles not described in the permit applications or fitting the fixed load vehicle profile can therefore be deemed as illegal, since they exceed the legal gross weight of 80 kips and do not have approved permits to operate in the vicinity of Doremus Avenue.

The Fatigue system was programmed to automatically capture stress records for any trucks that weighed more than a specific threshold by class. If a vehicle was over the chosen threshold, a 14-second stress time history was captured. These trigger vehicles are then reviewed to determine if they fit the permit information or other fixed load vehicle profiles. The stress and displacement record for one such example is given in Figure 5.12 and Figure 5.13, respectively.
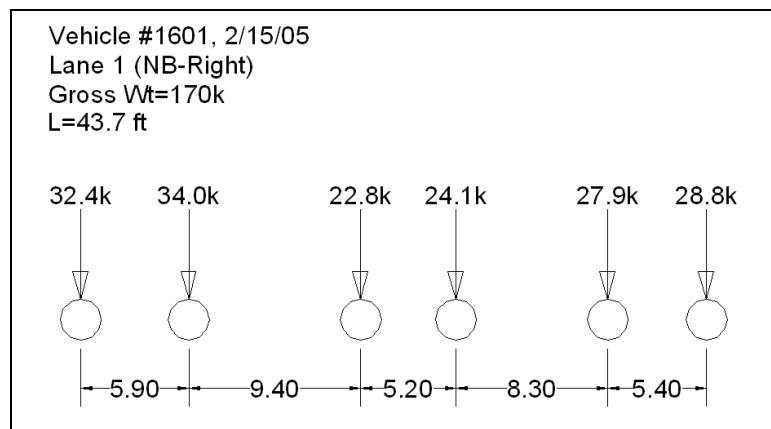
Figure 5.11 The axle spacing (ft) and weights(k) for trigger event 02/15/05-1601 resemble that of a mobile crane.
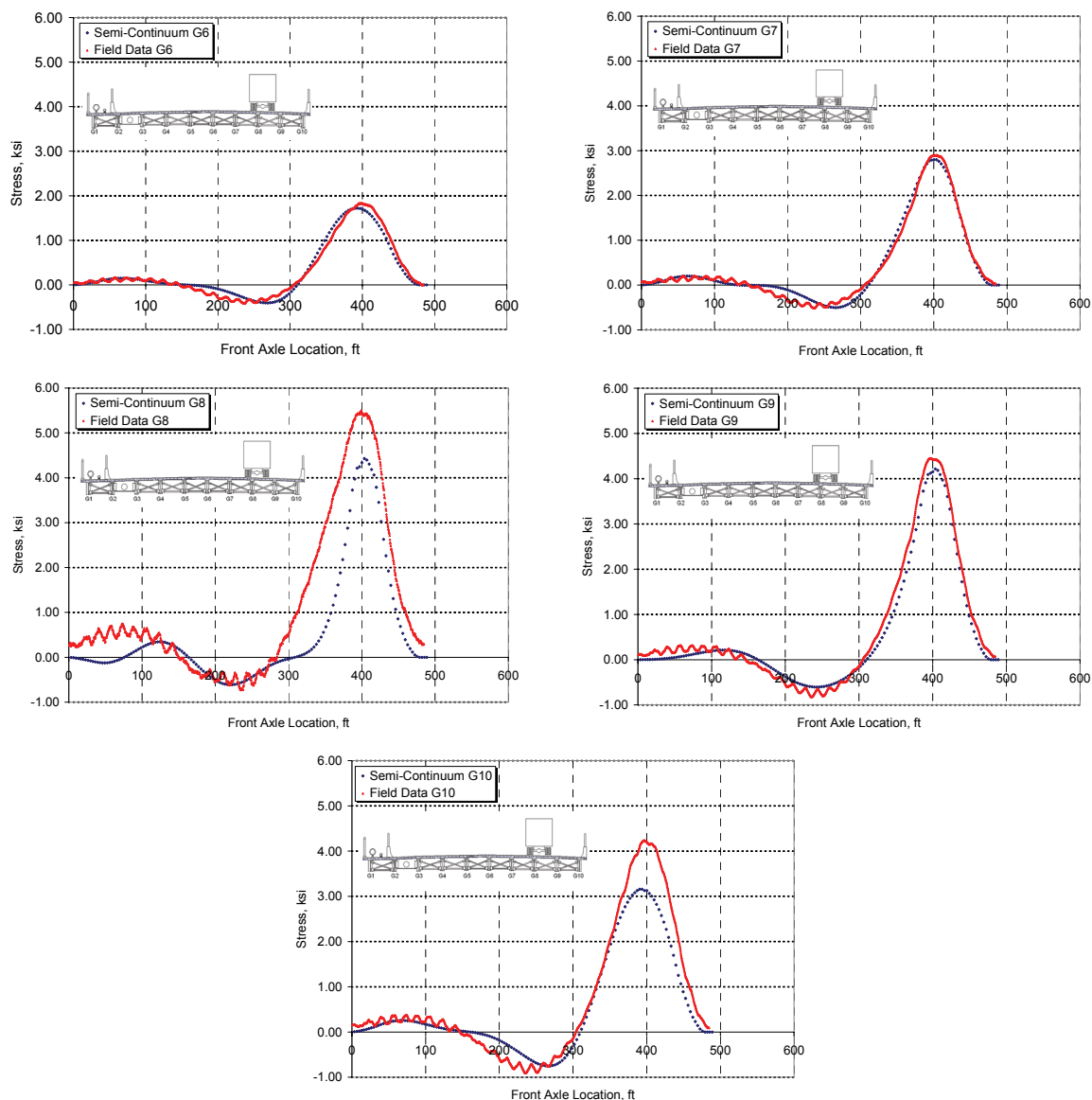
Figure 5.12 Comparison of observed and semi-continuum stresses for Span 3 during the passage of a trigger truck 02/12/05-1601
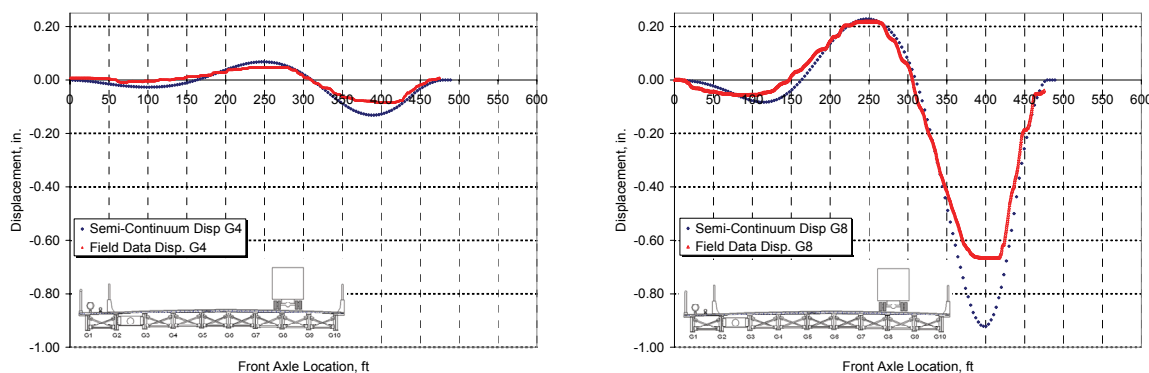
Figure 5.13 Comparison of observed and semi-continuum displacements for Span 3 during the passage of a trigger truck 02/12/05-1601

Stress and displacement records for the passage of truck 02/15/05-1601 are given in Figure 5.12 and Figure 5.13. Since the observed girder stresses were much higher than that of a typical test vehicle, further verification was needed. The truck was run using the semi-continuum model. The model output compared well with the observed stress, therefore, the WIM information is credible. The maximum observed stress in Span 3 Girder 9 was 4.45 ksi during this truck passage compared with a model stress of 4.22 ksi.

The trigger event identified as 02/15/05-1601 contains a 6-axle heavy vehicle (Figure 5.11) traveling northbound over Doremus Bridge in Lane A (rightmost lane). The vehicle was initially suspected of being a WIM error due to its designation as Class 15. Closer evaluation revealed that the axle weights and spacing resemble that of a truck mounted crane. Various crane manufacturers' specifications were reviewed (Manitowok 2006) and it was determined that event 02/15/05-1601 is, in fact, a truck mounted crane. These cranes are compact, road-legal vehicles with telescoping booms. Compact dimensions concentrate their weight over a smaller distance than a typical permit configuration, resulting in a greater load effects.

The truck configuration and corresponding bridge response for the heaviest observed truck at the Doremus Avenue Bridge is given in Figure 5.14 and Figure 5.15, respectively. The 7-axle truck crossed the bridge traveling northbound in Lane A on Tuesday 5/11/04 at 10:44 AM. The overall weight and length of the truck (as measured by the WIM system) were 227.5k and 73.6ft, respectively. Its speed, 18 MPH, is indicative of the extreme weight and uphill climb as it approached the bridge. The axle configuration is consistent with a 3-axle drive unit towing a 4-axle trailer. This trailer is known in the trucking industry as a "lowboy" (Atlantic 2004). A lowboy is a high capacity (50 to 100 ton) multi-axle trailer used to transport heavy equipment.

Further investigation into the validity of the axle weights was completed using the WIM data field for right and left wheel weighs. The bending plate system at Doremus Avenue Bridge contains two axle sensors per lane. The bending plate sensors are staggered about ten feet apart to measure each axle at different times. The per wheel weight measurements for truck #3465 show appropriate left-right correlation for all axles in Figure 5.14b.

The measured bridge response in terms of girder bottom flange stresses for Span 2 is given in Figure 5.15. The maximum observed stress was for Girder 9 at 5.76ksi (Girder 9 is located under the right wheel line for trucks in Lane A). The overall shape of the stress history confirms the measured axle configuration. Twin stress peaks are observed for Girders 8 and 9, corresponding to the two groups of axles (front three and last four axles).

Truck #3465 does not match any known permit configurations for Doremus Avenue as provided from NJDOT (2005). Therefore, the truck is considered an illegal

extreme load. The configuration does match the NJDOT Permit Vehicle in Figure 5.5,

but contains several axles that are over the 28k weight limit. It is possible that the

payload originated from the port and was being transported to a site nearby. Bridge

response data offers corroborating evidence to confirm extremely heavy trucks in the

WIM data. Truck #3465 may have been considered an error and discarded from the

WIM data for a typical site.

Vehicle #3465, 5/11/04 10:39A
Lane 1 (NB-Right)
Gross Wt=227.5k
Length=73.6ft

17.5k 41.2k 41.6k 37.4k 40.8k 37.7k 11.4k

15.60 4.80 39.10 4.00 4.20 4.80
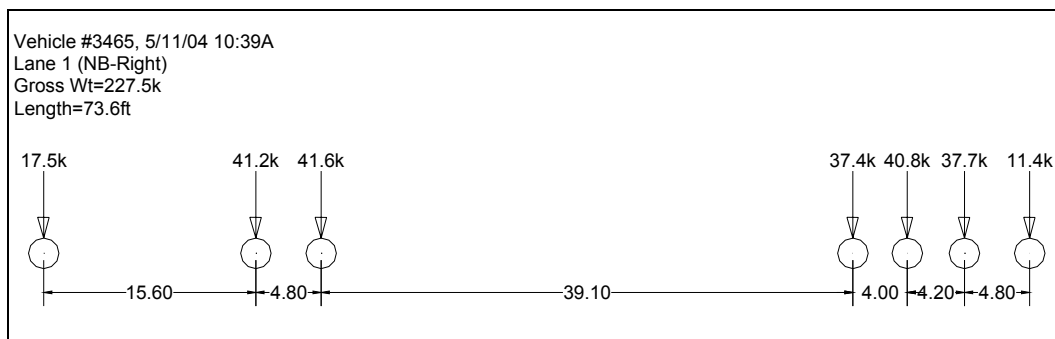
(a)

Truck #3465 5/11/04 Lane A				
	Right	Left		
W1,k	9.1	8.4	**S1, ft**	15.6
W2, k	22.3	18.8	**S2, ft**	4.8
W3, k	21.6	20	**S3, ft**	39.1
W4, k	20.4	17	**S4, ft**	4
W5, k	20.9	19.9	**S5, ft**	4.2
W6, k	17.9	19.8	**S6, ft**	4.8
W7, k	5.9	5.4		
Total W, k	227.4		**Total S, ft**	72.5

(b)

Figure 5.14 Extreme heavy truck observed at Doremus Avenue Bridge on 5/11/04 (a) axle configuration and (b) detailed WIM information (axle spacing in feet).
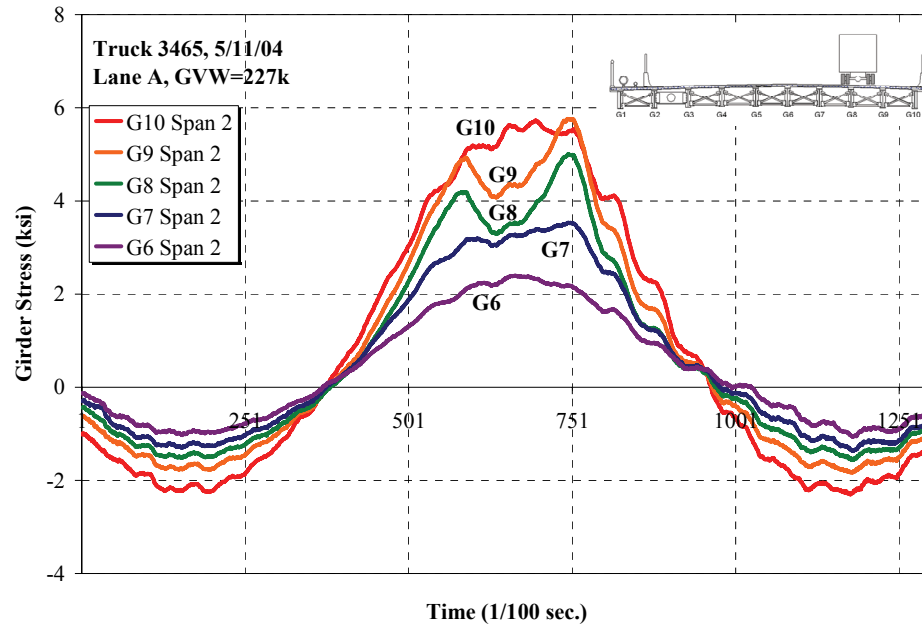
Figure 5.15 Measured stress history for Truck 3465 on 5/11/04 at Doremus Avenue Bridge

5.1.3.4   Filter Statistics by Site

In order to assure quality control of the data used to calibrate the load factors, various filters, described, earlier, were applied to the data. The filters were designed to eliminate erroneous and insignificant WIM records. For example, the most common disqualified records contain trucks weighing less than 15 kips. These light vehicles do not influence the overall load factors and may not be accurately weighed by the piezo axle sensors. Also, light vehicles may also include fragments from vehicles that were recorded as two separate trucks due to changes in lane or speed. Other code calibration procedures recommend removal of all light trucks (Moses 2001). Another filter seeks permit vehicles and cranes based on their axle weights and configurations. Permits and fixed load vehicles (cranes) represent extra-legal loads that should not be considered when calibrating load factors for general traffic. Cranes and permits have distinct axle configurations that allow filters to identify them. Cranes, for instance, typically have a

first axle spacing less than 10 feet, whereas all other semi-trailer trucks have first axle

spacing greater than 12 feet. Permits gain distinction over all other trucks by the number

and spacing between tandem axles. The FHWA Bridge Formula (FHWA 2006)

regulations, limit the number of axles and their combined weight that can occur within a

certain distance. Therefore, permits contain multiple (more than two) tandem axles

spaced at least 13 feet apart. No other legal truck configuration contains more than two

tandems with separations of 13 feet between tandems. The heaviest of the cranes travel

with their booms rotated pointing rearwards and supported on a three-axle specialized

trailer called a dolly. These heavy cranes must travel in this modified configuration to

distribute the load to additional axles. The dolly configuration is distinct and contains

three axles with axle spacings of 4 to 6 feet, and 8 to 10 feet, for the first two and last two

axles, respectively. Figure 5.9 shows the typical permitted cranes with the additional

dolly represented by the last three axles.

Filter statistics for NJWIM sites are given in Table 5.5. Over 22.5-million vehicle

records were analyzed, with about 14.5-million vehicles (64 percent) passing the filter

criteria. The most common disqualification was for gross weight less than 15kips. The

NJWIM data contained 284 permitted cranes (Filters 11 and 12) and 5687 known permit

configurations (Filters 4, 7, and 10).

Cranes represent a high intensity compact load that will cause significant moment,

shear, and negative moment compared to a typical truck. Cranes are considered as

permits and therefore should be excluded from load calibration. Furthermore, since

cranes are fixed-load vehicles, meaning their overall weight and weight distribution do

not change, there is no reason to extrapolate their load effects. The crane will cause the

same load effect now as it will in the future, whereas the converse is true of typical trucks with a random distribution of weights.

Additional filters are added to screen for data errors. For example, Filter 5 removes all Class 9 (5-axle semi-trailers) trucks with first axle weights greater than 12.5 kips. The first axle, or steering axle, is independent of the payload, and therefore is related only to the drive tractor configuration. The limit is chosen based on published reports of manufacturers maximum steering axle weights (Southgate 2000). In all likelihood, if the steering axle weight is incorrect, the entire record is erroneous. This may be due to excessive dynamic motion of the truck or lane/speed changes.

5.1.4 Volume Statistics by Site

In order to gain insight into the characteristics of truck traffic at each site, WIM data must be further processed into detailed parameters such as: average daily traffic (ADTT), volume per lane ($ADTT_{Lane}$), averages of speed, weight, etc., and maxima of speed, weight, etc. All truck volumes and other parameters (weight, speed, etc.) are based on qualified trucks that have passed the filter. Disqualified trucks, permits, and cranes are removed from the general data and not considered in any further analysis. Truck volume data alone does not represent the truck loading at a site. The volume must be normalized to make equivalent comparison across different sites with different amounts of available data. This is accomplished by calculating the annual average daily truck traffic (AADTT) for each site. The AADTT is the total number of observed qualified trucks divided by the duration of the observed data in days. This differs from the ADTT, which is calculated based on weekday traffic only. For simplicity, the AADTT will be used henceforth and referred to as the ADTT*. For large enough

Table 5.5 Filter Statistics by Site for NJ WIM Data

Location	Total Vehicles	Qualified Vehicles	Disqualified Trucks By Filter Number											
			F1	F2	F3	F4	F5	F6	F7	F8	F9	F10	F11	F12
18D	527072	349558	168692	0	198	1	3243	1829	1	3506	11	30	1	2
78B	1083930	342916	725204	0	30	0	13246	1614	0	874	20	17	0	9
78D	6234563	5218398	891924	0	108	6	112085	8971	0	1137	1681	201	1	51
80R	4627040	2056491	2309388	0	2851	15	184384	46247	1	23767	3644	123	5	124
195	1943664	1235127	554676	0	3494	0	104286	22295	0	23216	515	44	0	11
287	1690877	1257486	390015	0	553	0	34920	2123	0	2434	3297	37	2	10
A87	2145483	1153028	822745	0	1940	9	144509	11068	1	10799	1303	56	0	25
DOR 12	1083285	749709	242853	21362	108	0	7684	60934	0	32	0	597	0	6
DOR 34	1012736	659326	215772	99852	1406	0	14389	20977	0	475	45	473	0	21
DRM	2168920	1486783	485494	54896	1739	217	75334	41938	3646	12810	5833	212	9	7
TOTAL	22515570	14508822	6806763	176110	12427	248	694080	217996	3649	79050	16349	1790	18	266

Filter Description

1 Gross Wt <15k
2 Omit Class = 15
3 Tandems > 60k
4 NumAxles=9 & GrossWt>150k
5 Class = 9 & Wt1 > 12.5k
6 Length > 50ft & GrossWt < 20k
7 NumAxles=10 & GrossWt>170k
8 Any single axle over 40k
9 No axle spaces less than 2.5ft
10 3 or more tandems = Permit
11 GVW>140k, Numaxles>=7, 2nd last S=4..7ft, last spc=10..20ft for Permitted Cranes
12 Permitted Cranes with First Axle Spacing Less than 10.5ft, L<50ft, and GVW>100k

datasets, the ADTT* closely approximates the ADTT. Furthermore, when extrapolating

to the 75-year levels, each year contains 365 total days, not 260 weekdays. This

assumption is compatible with the definition of ADTT*.

5.1.4.1 Volume Statistics for NJ WIM Sites

The volume statistics for eight of the NJDOT WIM sites and Doremus Avenue

Bridge WIM site are summarized in Table 5.6 and Table 5.7. The following sites contain

bi-directional traffic: 18D, 78D, 80R, 195, 287, DOR. The following sites contain only a

single direction: 78B, A87, DRM. The layout of the lanes can be discerned from the

ADTT (lane) volumes. The lane with the lowest proportion of trucks is likely the

leftmost lane, or passing lane.

Table 5.6 Site statistics for NJ WIM Sites

Site	Route Name	Municipality	No. Lanes	Qualified Volume	Days of Data	ADTT*
18D	NJ Route 18, MP 44.6	Piscataway	5	349558	606	577
78B	I-78 MP 34.5	Bernards Twp.	4	342916	170	2017
78D	I-78 MP 25.7	Readington	6	5218398	353	14783
80R	I-80 MP 32.4 (a.k.a. 80B)	Roxbury	6	2056491	262	7849
195	I-195 MP 10.2	Upper Freehold	4	1235127	555	2225
287	I-287 MP 61.7	Franklin Lakes	4	1257486	193	6515
A87	I-287 MP 31.7	Harding Twp.	2	1153028	327	3526
DOR 12	Doremus Ave Bridge	Newark	2	749709	505	1485
DOR 34	Doremus Ave Bridge	Newark	2	659326	505	1306
DRM	Doremus Ave North	Newark	3	1486783	737	2017

* Annual Avg. Daily Truck Traffic

The information in Table 5.6 indicates that site 78D has the highest truck volume

of the sites shown. Further inspection of Table 5.7c reveals that site 78D also has the

highest single direction volume at 7401 trucks per day. Site 78D also has the highest

observed single lane volume of 4203 trucks per day of any of the NJ WIM sites. These

statistics are expected since Interstate 78 is a major truck route from the Pennsylvania

border in the west to the greater NY metropolitan area in the east. Site 78D is also located west of the interchange with Interstate 287; hence much of the regional traffic is maintained at this site.

Table 5.7 Detailed Site Statistics including lane information

(a) Route 18D

Lane	Qualified Count	ADTT (lane)*	Percent	Average Weight (k)	Max Weight (k)	Average Speed (MPH)
1	102168	169	29%	34.2	147.9	50.2
2	85083	140	24%	33.0	153.6	52.9
3	11947	20	3%	32.5	103.5	58.8
4	141080	233	40%	34.9	192.1	51.9
5	9280	15	3%	30.9	132.0	58.3

* Annual Avg. Daily Truck Traffic

(b) Site 78B

Lane	Qualified Count	ADTT (lane)*	Percent	Average Weight (k)	Max Weight (k)	Average Speed (MPH)
1	114	1	0%	29.6	58.4	40.4
2	146032	859	43%	45.2	154.5	60.3
3	194111	1142	57%	44.8	139.8	63.3
4	2659	16	1%	34.5	94.1	67.0

* Annual Avg. Daily Truck Traffic

(c) Site 78D

Lane	Qualified Count	ADTT (lane)*	Percent	Average Weight (k)	Max Weight (k)	Average Speed (MPH)
1	1368455	3877	26%	42.0	153.1	63.7
2	1226972	3476	24%	44.4	152.8	64.5
3	10072	29	0%	31.7	91.1	68.3
4	1483758	4203	28%	48.4	173.2	63.6
5	1119132	3170	21%	46.3	148.2	66.6
6	10009	28	0%	36.5	104.6	68.3

* Annual Avg. Daily Truck Traffic

(d) Site 80R

Lane	Qualified Count	ADTT (lane)*	Percent	Average Weight (k)	Max Weight (k)	Average Speed (MPH)
1	557305	2127	27%	42.8	175.6	55.0
2	540727	2064	26%	43.8	190.0	65.4
3	14439	55	1%	35.2	111.7	67.5
4	448197	1711	22%	37.1	178.8	57.6
5	482661	1842	23%	42.2	168.7	62.4
6	13162	50	1%	36.3	124.4	65.5

* Annual Avg. Daily Truck Traffic

(e) Site 195

Lane	Qualified Count	ADTT (lane)*	Percent	Average Weight (k)	Max Weight (k)	Average Speed (MPH)
1	537032	968	43%	36.6	177.5	62.6
2	83956	151	7%	37.5	129.2	70.9
3	95883	173	8%	40.5	155.8	69.1
4	518256	934	42%	41.0	175.5	63.8

* Annual Avg. Daily Truck Traffic

(f) Site 287

Lane	Qualified Count	ADTT (lane)*	Percent	Average Weight (k)	Max Weight (k)	Average Speed (MPH)
1	548307	2841	44%	46.9	189.1	63.8
2	73185	379	6%	39.9	129.4	67.9
3	114474	593	9%	44.2	107.4	68.2
4	521520	2702	41%	46.7	170.2	65.8

* Annual Avg. Daily Truck Traffic

(g) Site A87

Lane	Qualified Count	ADTT (lane)*	Percent	Average Weight (k)	Max Weight (k)	Average Speed (MPH)
1	761396	2328	66%	44.2	171.9	60.0
2	391632	1198	34%	45.5	171.9	60.9

* Annual Avg. Daily Truck Traffic

(h) Doremus Avenue Bridge Site

Lane	Qualified Count	ADTT (lane)*	Percent	Average Weight (k)	Max Weight (k)	Average Speed (MPH)
1	480063	951	34%	33.8	145.6	38.6
2	269646	534	19%	35.3	149.9	39.5
3	213613	423	15%	32.8	137.8	44.3
4	445713	883	32%	37.6	169.7	39.5

(i) Site DRM

Lane	Qualified Count	ADTT (lane)*	Percent	Average Weight (k)	Max Weight (k)	Average Speed (MPH)
1	433991	589	29%	33.1	178.6	33.3
2	726523	986	49%	34.8	149.0	33.3
3	326269	443	22%	23.5	143.1	21.9

* Annual Avg. Daily Truck Traffic

Table 5.8 Detailed site characteristics by vehicle classification for Doremus Avenue Bridge (a) Northbound Lanes 1 & 2 and (b) Southbound Lanes 3 & 4

(a)

Qualified Count	Class	RMC Wequ (k)	Average Weight (k)	Std.Dev. (k)	Max Weight (k)	Average Length (ft)	Average Speed (MPH)
0	1	0.0	0.0	0.0	0.0	0.0	0.0
0	2	0.0	0.0	0.0	0.0	0.0	0.0
0	3	0.0	0.0	0.0	0.0	0.0	0.0
14450	4	30.0	29.4	4.2	74.8	39.6	43.8
46994	5	25.1	22.5	7.4	74.3	24.4	38.2
138923	6	29.8	22.8	12.3	95.3	23.2	40.6
8386	7	64.8	56.3	24.5	108.1	28.2	38.0
68578	8	33.9	28.7	12.0	99.7	51.3	39.6
462259	9	48.7	39.2	20.1	130.9	52.5	38.4
6628	10	59.3	47.6	25.3	142.7	52.7	36.9
2608	11	53.2	49.1	12.4	90.1	113.1	36.0
80	12	54.3	52.0	11.9	92.3	72.6	33.2
803	13	67.2	54.2	27.8	149.9	102.1	35.1
0	14	0.0	0.0	0.0	0.0	0.0	0.0
0	15	0.0	0.0	0.0	0.0	0.0	0.0

749709 Total Qualified Vehciles   505 Days of Data

(b)

Qualified Count	Class	RMC Wequ (k)	Average Weight (k)	Std.Dev. (k)	Max Weight (k)	Average Length (ft)	Average Speed (MPH)
0	1	0.0	0.0	0.0	0.0	0.0	0.0
0	2	0.0	0.0	0.0	0.0	0.0	0.0
0	3	0.0	0.0	0.0	0.0	0.0	0.0
9109	4	33.2	31.2	7.9	77.0	47.6	42.8
50024	5	28.1	25.2	8.7	76.6	24.8	43.9
187067	6	31.2	25.5	12.0	96.8	24.4	41.1
5829	7	53.6	39.1	25.8	116.4	32.7	40.0
95858	8	34.1	28.8	11.8	111.8	51.3	41.2
296809	9	56.9	46.5	23.0	130.2	52.0	40.4
6706	10	52.6	43.5	20.1	148.0	52.4	39.7
2893	11	51.8	48.7	12.5	96.6	82.8	41.3
95	12	56.5	52.1	16.6	93.0	69.3	39.8
4936	13	61.9	49.8	24.7	169.7	138.3	40.8
0	14	0.0	0.0	0.0	0.0	0.0	0.0
0	15	0.0	0.0	0.0	0.0	0.0	0.0

659326 Total Qualified Vehciles   505 Days of Data

5.1.5   Vehicle Characteristics by Site

Vehicle characteristics, including counts by class, gross vehicle weights, vehicle types, length, speed, etc., are used to describe the truck population as a whole. Gross weight histograms show the distribution of trucks at different weight increments. Counts by class describe the makeup of the truck population. Typically, Class 9 (five-axle semi-trailers) dominates the truck population for interstate highways. Lower volume roadways

may be dominated by 2 or 3-axle (Class 5 and 6, respectively) single body trucks that are lighter than the Class 9 type. The dominant truck type is indicative of the function of the roadway. Major interstate routes service regional traffic while lower volume roads service local districts. Smaller and lighter trucks are more economical for local transportation, while larger five-axle semi-trailers are economical for long-haul regional routes.

The weight distribution within the dominant truck type also indicates the function of the roadway. Sites near ports or distribution centers are made up of a mixture of light empty and heavy loaded trucks. This mixture leads to a bi-modal truck weight distribution featuring two sub-distributions: one for empty and one for loaded trucks. Routes that constitute regional or interstate traffic exhibit a smoother single distribution. The reasons for the difference between distributions for local and regional traffic relate to the economics of truck movements. It is uneconomical to transport an empty truck over a long distance since the labor cost and tolls are fixed. Therefore, companies coordinate truck loads outbound and inbound such that the truck remains loaded.

5.1.5.1   Vehicle characteristics for NJ WIM Sites

The gross weight histograms for NJ WIM sites and Doremus Avenue Bridge are given in Figure 5.16 for the dominant Class 9 truck type. Note that Class 9 is the dominant truck type for all but Site 18D, where the dominant type is Class 6. The bi-modal weight distribution is evident at the following sites: 18D, 78B, 78D, 195, DRM, and DOR. These sites contain a mixture of loaded and unloaded trucks. It is possible that a distribution center is nearby the interstate sites. The bi-modal gross weight distribution for sites DOR (Figure 5.16i) and DRM (Figure 5.16h) is undoubtedly related

to their proximity to Port Newark. Near the port, trucks travel loaded with a container or empty without a container. Furthermore, Doremus Avenue is a short local connector where the economics of empty trucks are insignificant. Regional routes such as Interstate 80 (Site 80R, Figure 5.16d) and Interstate 287 (Site A87, Figure 5.16f) show a single continuous distribution of truck weights.

The percentage of overweight vehicles by site is given in Table 5.9. Since the legal gross weight limit without a permit is 80k, any filtered vehicle over 80k is considered to be overweight. Overweight vehicles make up most of the upper tail of the load effects used to determine the maximum 75-year levels in design. Therefore, the percentage of overweight vehicles and their trend dictates the load factors for each site. Table 5.9 shows that Doremus Avenue Bridge southbound at the bridge contains the highest proportion of overweight vehicles at 7%. Interstate sites such as 78B, 80R, 195, A87, and 287 have between 4 and 5 percent of vehicles overweight. The directionality of truck flow can be seen in the difference between northbound (DOR12) and southbound (DOR34) Doremus Avenue at the bridge. There are nearly three times more overweight vehicles traveling south (7%) over Doremus avenue bridge than traveling north (2%). The reason may be related to the proximity to the port. Southbound trucks (DOR34) are heading into the port carrying items for export which typically consist of bulk scrap metal and other materials. Northbound trucks (DOR12) exiting the port carry more highly regulated containers that are less likely to be overweight due to port oversight and controls.
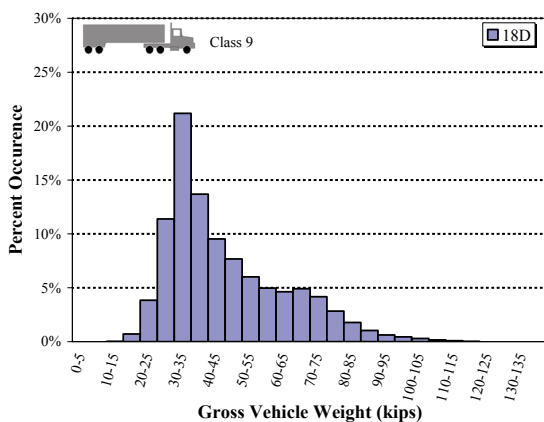
(a) Site 18D
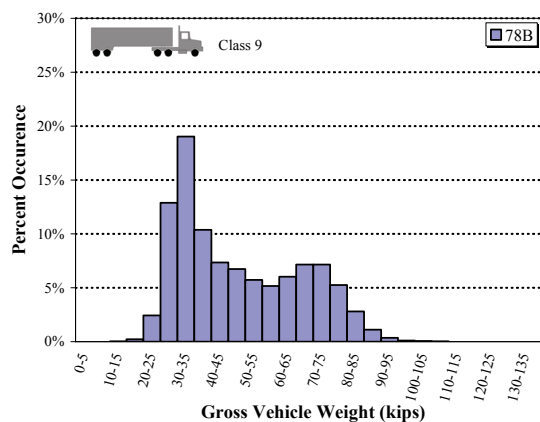
(b) Site 78B
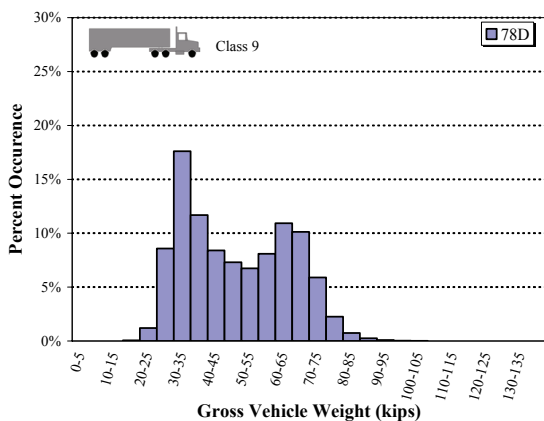
(c) Site 78D
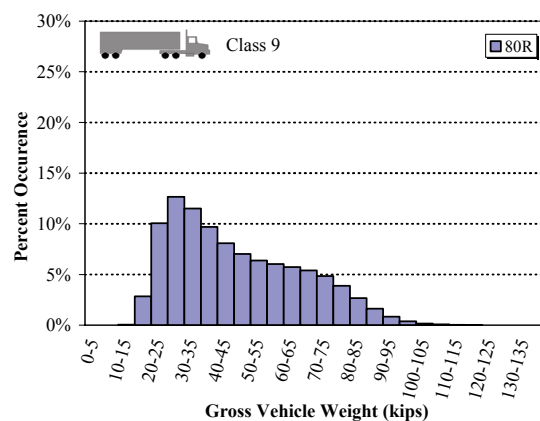
(d) Site 80R
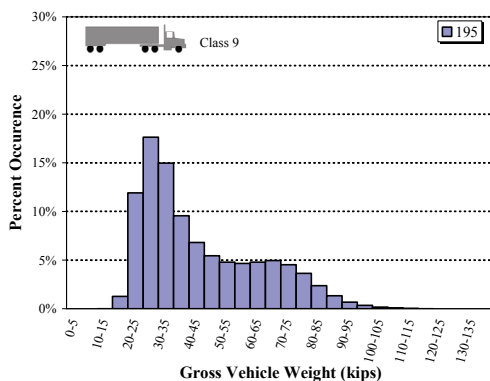
(e) Site 195
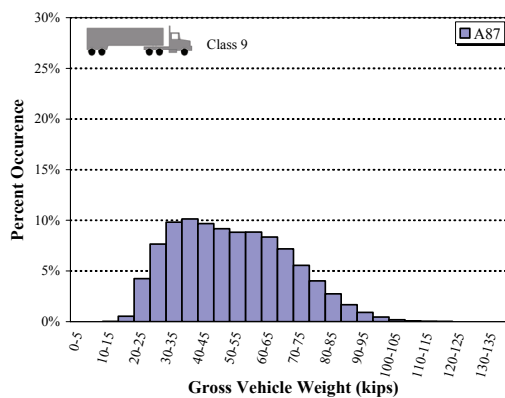
(f) Site A87

Figure 5.16 Class 9 gross vehicle weight histograms for NJ WIM Sites
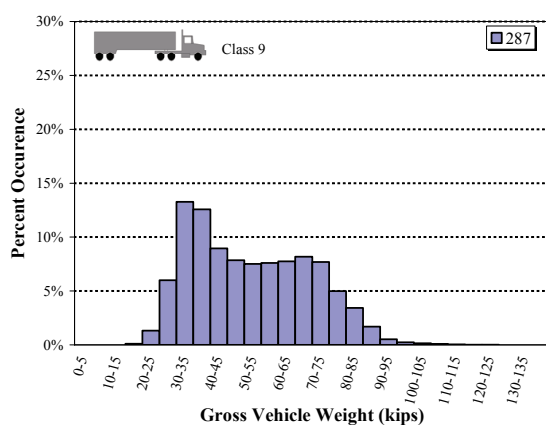
(g) Site 287
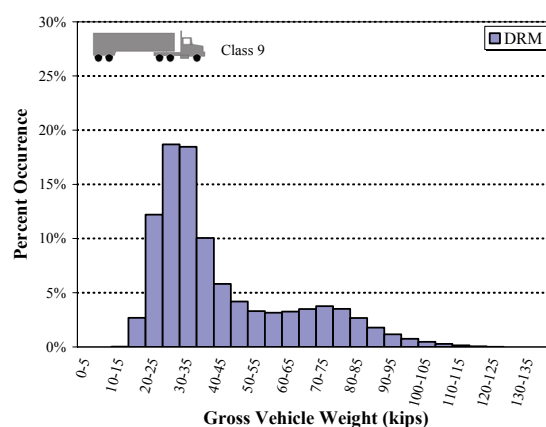
(h) Site DRM
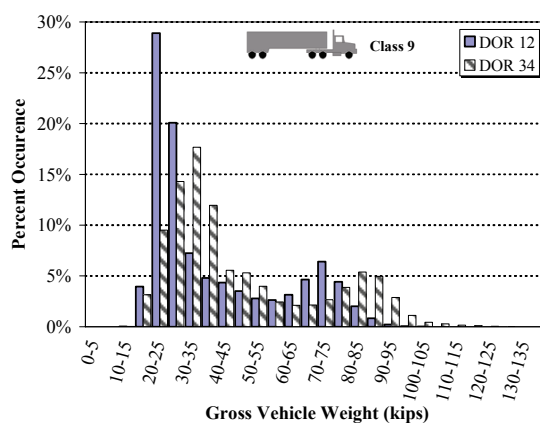
(i) Doremus Avenue Bridge (DOR)

Figure 5.16 (Continued)

Table 5.9 Truck volumes and percentage of overweight trucks for NJ WIM Sites

Site	Qualified ADTT	Percent Overweight
18D	577	2%
78B	2017	4%
78D	14783	1%
80R	7849	5%
195	2225	4%
287	6515	5%
A87	3526	5%
DOR 12	1485	2%
DOR 34	1306	7%
DRM	2017	4%

5.1.6   Truck Multiple Presence (Multipresence)

Truck superposition is defined as the presence of two or more trucks occurring simultaneously. The maximum load effect is often controlled by a truck superposition, such as the two-lanes loaded design case in the AASHTO LRFD. The multiple presence or multipresence is reported in terms of two main quantities: (1) the frequency of each type occurrence as a percentage of the total truck population and (2) the frequency of each type of occurrence with two trucks above a chosen "heavy" threshold. Truck superposition is site specific and is influenced by traffic density, speed, truck population and number of lanes. Multipresence statistics are reported only for qualified trucks and excludes all passenger vehicles, light truck, and erroneous records.

The configurations of multipresence are described by the following events: single, side-by-side, following, staggered, and other. The next sections describe in detail the criteria and significance of each truck superposition.

5.1.6.1   Single Event

A single event is defined as a truck occurring with no trucks in adjacent lanes such that the load effect on any particular girder results from one truck only. The basic case of a single event is one truck occurring on a span with no other traffic (Figure 5.17a). Since only one truck is acting on the span, any load effects are attributed to this truck. In multi-lane, multi-girder bridges the compounding effect of loading distant lanes is negligible due to the distribution of load to many girders. For example, consider a ten girder bridge where the moment is being considered at Girder 1, and a truck load is applied over Girder 10. The effect of the load applied over Girder 10 on the moment at Girder 1 is negligible since the distant load is distributed to Girders 10, 9, 8 and so on.

The residual moment leftover for Girder 1 is near zero. For a multi-lane bridge there may be several single events at a one time, provided that the loading is not in adjacent lanes. Figure 5.17b shows an example of two simultaneous single events on a four lane bridge. The truck in lane 1 (nearest the bottom), is nearly parallel with the truck in lane 3. This multipresence event would be considered a side-by-side event if the second truck occurred in lane 2. Since the loaded is not in the adjacent lane, this event would be classified as two single events. The single event is the simplest of all multipresence events, whereas the more severe case of loading, the side-by-side, is described next.

(a)

(b)
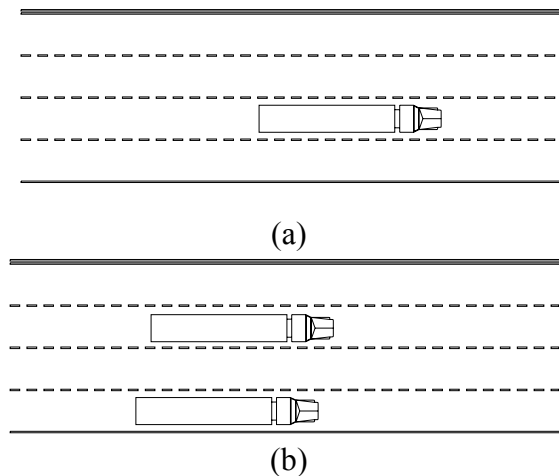
Figure 5.17 Typical truck configurations for the single event with one truck (a) and multiple single events (b) where the load effect on any one girder is equivalent to that due to one truck

5.1.6.2   Side-by-Side Event

The side-by-side event describes the case where two trucks are traveling parallel in adjacent lanes. To qualify, the second truck must overlap the leading truck by at least one-half of the leading truck's length. Therefore the range of acceptable for side-by-side starts with two trucks traveling perfectly parallel and ends with an allowable truck

overlap of less than one-half of the first trucks length. This tolerance allows for a range

over which side by side events may cause the same effect. Modeling of a long span

(about 150 feet) steel girder bridge has shown that two trucks positioned in adjacent lanes

with a longitudinal offset as much as one entire truck length produce the same moment as

two perfectly parallel side-by-side trucks (refer to Section 5.1.6.8).

The side-by-side event represents the two loaded lane design case in the

AASHTO-LRFD (AASHTO 2004). Two lanes loaded usually controls the girder design

for interior members. Therefore, quantification of the maximum expected side-by-side

load intensity is needed. In addition, the frequency of the side-by-side multi-presence

case must be found. The multipresence algorithm shown in Figure 5.22 also includes a

statement (not shown) that evaluates the weights of any identified side-by-side event and

tallies all cases which have two truck weights above a chosen "heavy" threshold. The

goal is to measure the frequency of side-by-side events, as well as, the weights associated

with those events.
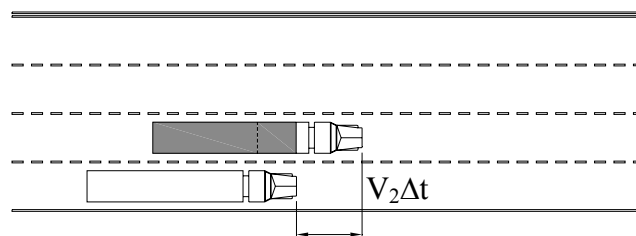
Figure 5.18 Typical truck configuration for the side-by-side event where two trucks travel in adjacent lanes within an overlap of one-half the first truck length

5.1.6.3   Staggered Event

Two trucks traveling in adjacent lanes such that both trucks are entirely on the

span and the overlap is less than one-half of the leading truck length is considered a

staggered event. Figure 5.19 shows the typical staggered truck configuration. The lower

bound for this case is an overlap of less than one half the leading truck lengths, and the

upper bound is that the entire length of both trucks must be within the span, but not

necessarily overlapping at all. Similar to the side-by-side, the effect of different degrees

of stagger have been modeled on the Doremus Avenue Bridge with a three spans at 147

feet each (SEE Section 5.1.6.8). The results show that the load effect for the lower bound

stagger case (overlap about one half length) generates the same moment as the perfect

side by side case. Furthermore, the stagger event where the clear distance is about one

half the leading truck lengths also generates nearly the same moment as the perfect side

by side case. Therefore, for long span bridges a portion of the staggered truck events

may be included in the side-by-side occurrences when calculating the maximum load

event. As in the side-by-side case, the weights of the staggered truck are evaluated and

compared to a chosen heavy threshold.

(a)

(b)
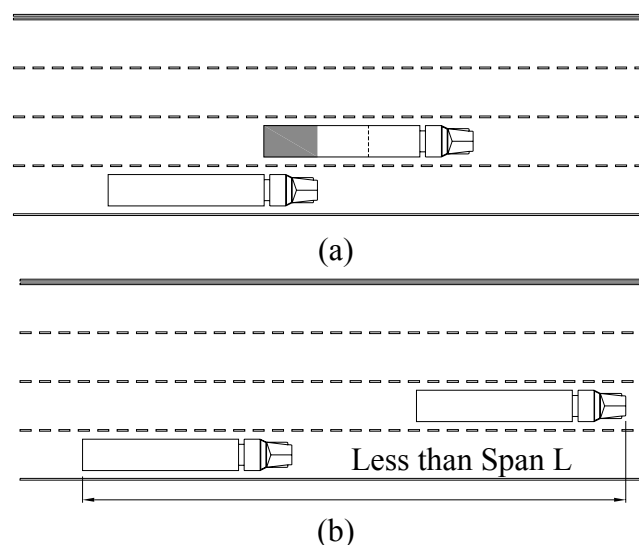
Figure 5.19 Typical truck configuration for the staggered event: (a) stagger with overlap and (b) stagger with clear distance

5.1.6.4 Following Event

When two trucks are traveling closely in the same lane they are said to be in a *following* configuration. The upper bound for the following event is when the distance from the front of the leading truck to the end of the following truck is less than the span length. The clear distance, as shown in Figure 5.20a, between two vehicles in the same lane is normally defined by transportation engineers as the headway distances. However, in terms of load effect, the headway is taken as the distance from the last axle of the leading truck to the first axle of the following truck as in Figure 5.20b (Nowak 1999). Truck parameters in terms of axle position are more relevant to the study of live load effects since this is where the forces are transferred to the structure. Further, many WIM systems measure the vehicle length based on the inductive loop sensors, which report the body length. The body of a truck will always overhang the first and last wheels. This contributes to error in the vehicle length, which is an important parameter to each MP case. Therefore, the vehicle length, for the purpose of evaluating truck multipresence, is taken as the summation of the axle spacing as shown in Figure 5.20b. As with all multipresence cases, the vehicle weights for the following events are compared to a selected heavy threshold. All following events where both vehicle weights are above the heavy threshold are tallied as heavy-following.

(a)

(b)
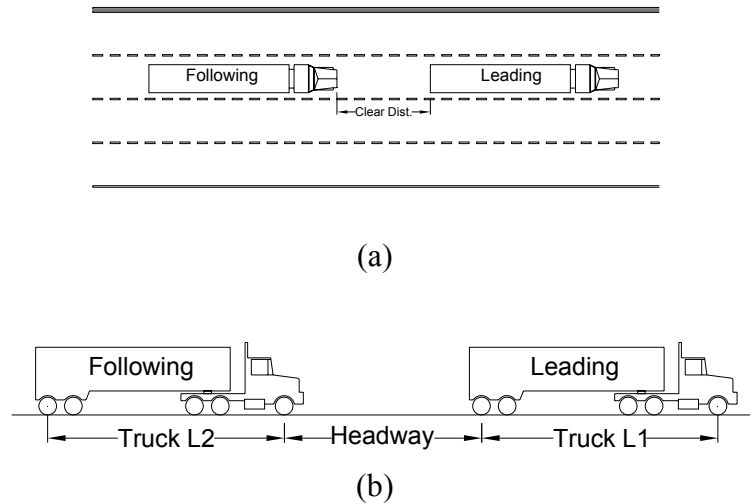
Figure 5.20 Example of clear distance between trucks (a). The headway (b) for the following event is defined as the distance between the last axle of the leading truck and the first axle of the following truck.

5.1.6.5   Other Events

The *other* event describes the case where more than one multipresence event occurs simultaneously over a given span length. The probabilities used to forecast the maximum load event for the design of bridges are based on two trucks occurring at the same time. Since the frequency of occurrence and the load effect (in terms of load distribution) for the common multipresence cases are known, approximation of the maximum lifetime load effect can be estimated. While more than two trucks may occur on a given span simultaneously, the probabilities for each of these events decrease because of the limited number of combinations that are possible. Estimating the load effect of each of the compound MP cases becomes difficult without the use of complex two-dimensional computer modeling. Examples of some of the other MP cases are given in Figure 5.21.
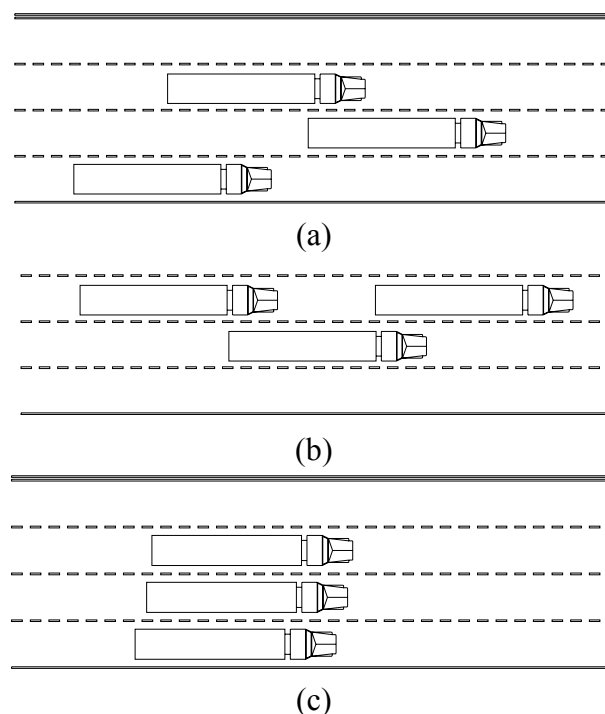
Figure 5.21 Examples of compound configurations classified as other: (a) double stagger, (b) following and stagger, and (c) triple side-by-side

5.1.6.6   Multipresence Detection Algorithm

A computer program was written to evaluate the WIM data for multipresence. As discussed earlier, a timestamp to the nearest one hundredth of a second resolution is needed to differentiate the cases of multipresence. The location of any vehicle can be described with the following information: (1) lane of travel, (2) time or arrival or timestamp to the nearest 1/100 second, and (3) speed of travel. Using these three parameters, the location of each vehicle relative to others can be established. Additional information such as gross weight and length are used to refine the qualifications for each event. A fictitious span length is chosen over which to consider the multipresence cases. The span comes into consideration when setting an upper bound for the event criteria.

For example, in the event where two trucks that are following such that the length from the first axle of the first truck to the last axle of the second truck is 190 feet, the event would be counted as a following event on a fictitious span length of 200 feet. However, the same two trucks would not qualify for following on a 100ft span since the two trucks would not fit entirely on the span.

The algorithm for the MP program is described by the flowchart in Figure 5.22. Basically, the program identifies trucks in the traffic stream and calculates their relative positions. Using a set of predefined criteria, the program identifies cases of multipresence. Refer to the preceding sections for specific event criteria.
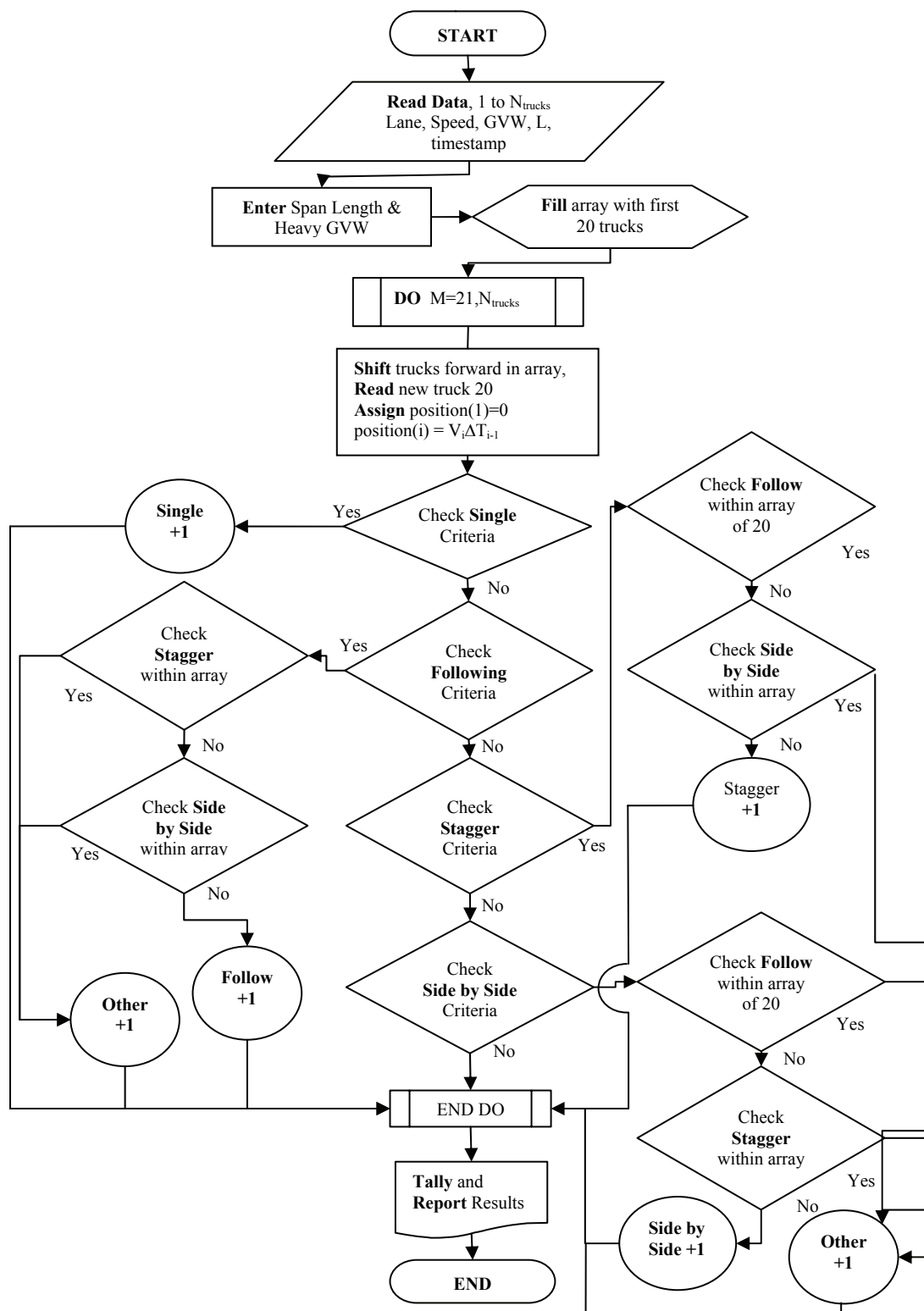
Figure 5.22 Flowchart of multipresence algorithm

5.1.6.7   Multipresence Verification

An important step in the development of any algorithm is the verification of its output by some independent means. The results of the MP program are verified in three ways: (1) the output for any MP event is stored to a file named for that event, i.e. "following.dat", and (2) a spreadsheet can be designed to replicate the MP criteria for each event, and (3) data can be synthesized to contain MP events and be processed with methods 1 and/or 2.

Verification by storing the events is done by saving the entire WIM data record for each truck involved in the event to a file named for each event. If Truck A and Truck B are found to be involved in a following event, the record in the "following.dat" will show the lane, timestamp, speed, length, etc. for each truck. To verify the MP event, one simply checks that the lanes are equal and that the timestamp allows both trucks to be within the given span length. Duplicate events are easy to identify using this method. The major limitation of this method is that events that were missed cannot be verified.

Verification by spreadsheet application is tedious and limited to a small amount of raw data, i.e. one day. Typically, only one day at a time can be evaluated using this method. A spreadsheet is created where each line represents the raw truck record from the WIM data.   A timestamp to the nearest 1/100 sec. is calculated from the hour, minute, second, and hundredth of a second. The vehicle speed is converted to feet per second as in the original MP program. The total vehicle length is computed as the summation of the individual axle spaces. Next, the criteria for each MP case: following, side-by-side, and staggered are entered using a series of embedded IF statements, similar to the methodology within the MP program. If an MP event is found, the cell result

contains a number 1, and if no event is found, the result is 0. The number of events is summed to find the total events for each case. The results of a single day of data were successfully verified using the spreadsheet method. However, it is important to note that the spreadsheet does not account for the cases of compound or other events. The MP program was run without consideration of the other cases in order to verify the basic criteria using the spreadsheet. The results were identical; therefore, the spreadsheet method is effective in verifying the basic MP events.

The last means of verification involves synthesizing or seeding specific MP events in a small dataset and running the MP program. This method has been found to be the most effective for verifying the basic and compound cases of MP. The major drawback is that the compound cases must be derived by hand, and fictitious trucks generated to match the same format as the original data.

5.1.6.8 2D Bridge Modeling for Multipresence

A two-dimensional Semi-continuum influence surface was generated to determine the effect of truck superposition in various configurations. The Doremus Avenue Bridge in Newark, NJ was chosen as the input for the influence surface model since instrumentation and field testing could provide model verification. Doremus Avenue was the first LRFD designed bridge in New Jersey and was designated for structural testing and monitoring. The bridge consists of a three span continuous unit with equal spans of 147 ft (45m). The bridge carries 4 lanes of traffic over a ten-girder cross-section with a composite reinforced concrete deck. To construct the influence surface a unit load was applied along the entire length of the bridge in each of the eight wheel lines. To find the

effect of superposition, one or more HS-20 trucks were applied to Span 3, shown in Figure 5.23. The stress was evaluated at the maximum positive moment position of Span 3 Girder 8, located between the adjacent travel lanes. This loading condition simulates the effect to two correlated trucks each weighing 72 kips. In the case of actual traffic conditions there may be events where both trucks are lighter, both trucks are heavier, or the weights are some combination of heavy and light. More sophisticated statistical simulation is needed to determine the best estimate of the actual loading conditions. However, the case of using two design trucks sufficiently illustrates the point.

The single, following, side-by-side, stagger, and quad configurations were considered. Furthermore, the stagger case was expanded to include three degrees of stagger: (1) overlap with half of the leading truck length, (2) back to front, and (3) no overlap but within given span length (Figure 5.23 d, e, and f, respectively). The results summarized in Table 5.10, suggest that the side-by-side (Figure 5.23b), stagger with overlap (d), and stagger back-to-front (e) generate similar stresses for the 147-foot span considered. The exact side by side case generates a stress of 3.5 ksi, while the stagger with overlap and stagger back to front cause stresses of 3.5 ksi and 3.4 ksi, respectively. This similarity may warrant the addition of the stagger multipresence percentages to the side-by-side cases for longer span bridges. There are important implications of including side-by-side and stagger cases for fatigue evaluation since the stagger multipresence percentages can reach four times that of side-by-side.

(a) Single Event

(b) Side by Side

(c) Following at one length

(d) Stagger – Within One-Half Length

(e) Stagger – Back to Front

(f) Stagger – No overlap but within span

(g) Double Side by Side (Quad) Event
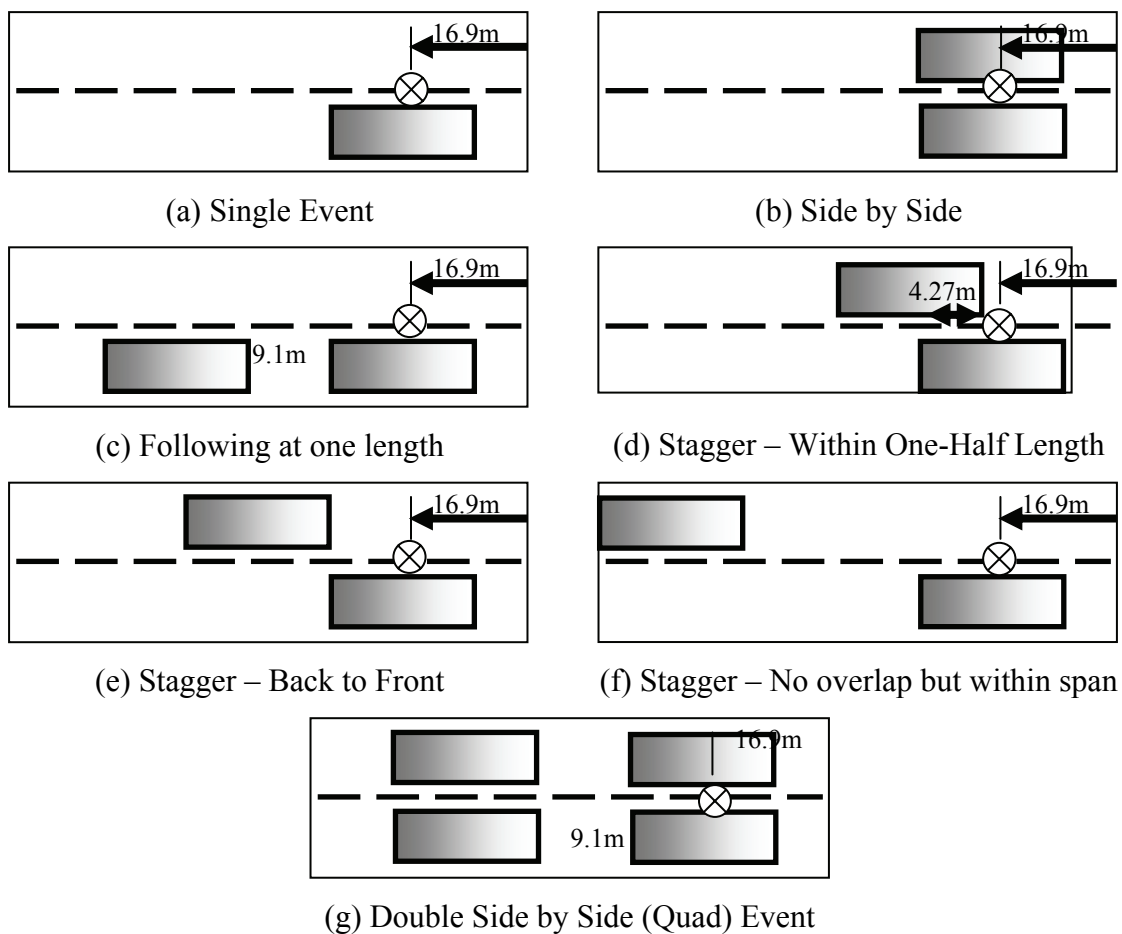
Figure 5.23 Various truck superposition configurations considered in the 2D Doremus Avenue Bridge model

Table 5.10 Effect of various truck superposition on the Doremus Avenue Bridge Model.

Truck Configuration	G8 Stress ksi	Ratio to Single
Single HS20 Lane A	2.22	87%
Side by Side HS20 Lane A+B	3.04	137%
Following HS20 Lane A	2.52	114%
Stagger HS20 Lane A+B w/Overlap	3.04	137%
Stagger HS20 Lane A+B Back to Front	2.96	133%
Stagger HS20 Lane A+B Max Distance	2.33	105%
Quad HS20 Lane A+B	3.60	162%

5.1.7   Multipresence Results by Site

A principle input into the forecast of future maximum live loads is the frequency of vehicle superposition or multipresence. Using the procedures and algorithms outlined previously, the frequency of multipresence for each site was determined. There are two main parameters to multipresence as outlined by Nowak (1999): frequency of each configuration and the weights (or degree of correlation) associated with each event. Again, the key modes of superposition are: side by side, staggered, and following. The frequency of each configuration can be determined from the relative positions of the vehicles in the traffic stream. The relationship of the vehicle weights is also determined from the data. For each occurrence of superposition, the weights of the vehicles involved are stored to an array, and the heaviest observed case for each type of multipresence is also stored. The frequency of the "heavy-heavy" multipresence has influence over the maximum expected load intensity during the service life of a bridge.

5.1.7.1   General Multipresence Statistics by Site

The multipresence statistics in terms of percentages of following, side-by-side, staggered, and other events are needed to quantify the amount of truck superposition on a given roadway. Multipresence is calculated based on incremental span lengths to gage the effect for different bridges. Events such as following, staggered, and other depend greatly on the span length considered. The percentages reported are the number of events divided by the total number of qualified trucks in the sample. Each event for following, side-by-side, and staggered contains only two trucks. Compound occurrences such as following with another truck in a stagger condition (involving three or more trucks) are classified as other. The number of other events is sensitive to span length since the

probability of seeing three or more trucks on a bridge increases with span length. The trends for the MP events by span take into account the losses due to compound occurrences. For example, the percentage of side-by-side events is greatest for shorter spans and decreases as the span length is increased. This is due to additional trucks being present on the bridge and causing a compound occurrence. The percentages of following and stagger are low for small spans by definition. For staggered or following events to occur, the entire length of both trucks must be within the span length. Given that trucks must maintain minimum headways at highway speeds, two following trucks typically occupy 150 feet from front of the first truck to rear of the following truck.

All MP results given are based on qualified trucks that have passed the filters. The percentages shown are calculated as total number of events divided by total qualified trucks. The case of other may include three or more trucks.

5.1.7.1.1 MP Statistics for NJ WIM Sites

The multipresence statistics for Doremus Avenue Bridge (DOR) and NJ WIM Sites 287 and 80R are given in Figure 5.24, Figure 5.25, and Figure 5.26, respectively. The MP statistics by span, shown in Figure 5.24, are given for northbound and southbound directions separately. The side-by-side event is the most common multipresence at 1.5% up to a span of 80 feet. Thereafter, the stagger event becomes more common. The MP statistics for side-by-side and stagger are greater in the northbound direction than the southbound direction. The northbound lanes approaching the Doremus Avenue Bridge are subject to an uphill grade of approximately 4% over a distance of about 1500 feet. The grade causes a reduction in truck speeds as they climb toward the bridge (northbound). The speed of loaded trucks is reduced more than the

speed for empty trucks. Therefore, an increase in the number of superposition events is expected as the number of passing events increases on the grade. The frequency of following events is greater for the southbound lanes than the northbound lanes. This is due to the traffic patterns near the end of Doremus Avenue. Doremus Avenue ends at Port Street approximately 3000 feet south of the bridge. At this intersection a majority of trucks turn right onto Port Street since all other directions have not outlet to other routes. This conclusion is supported by the truck lane proportions given in Table 5.7h, where the Lane 4 volumes and weights are greater than for Lane 3.

Since the Doremus Avenue is instrumented for both the applied loads (WIM) and bridge response (stresses and deflections), direct comparisons can be made between the frequency of MP events and the bridge response. Computer simulations evaluating the effect of MP on fatigue loading will be discussed in Chapter 6. The WIM data and calculated MP frequency correspond to an actual bridge with a span length of 147 feet (45m). Therefore, the MP statistics for the actual Doremus Avenue Bridge are given in Table 5.11. The overall MP statistics are low since Doremus Avenue is a local roadway with a relatively low ADTT* of 1485 and 1306 for northbound and southbound traffic, respectively.
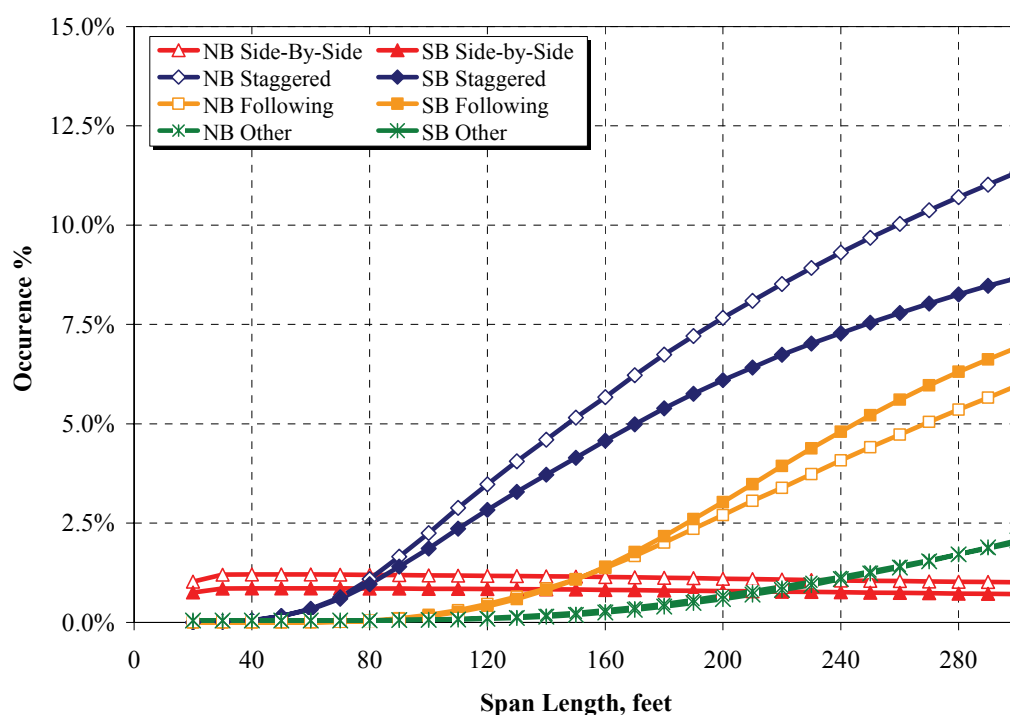
Figure 5.24 Doremus Avenue Bridge – MP Statistics by span for NB Lanes 1&2 and SB Lanes 3&4.

Table 5.11 Multipresence statistics for the Doremus Avenue Bridge for a span length of 147ft (45m)

Doremus Ave Bridge (DOR) Span L = 147ft (45m)	Follow Event %	Sideby Event %	Stagger Event %	Other Event %	Single Event %
Northbound Lanes (1&2)	1.1%	1.2%	5.2%	0.2%	92.4%
Southbound Lanes (3&4)	1.1%	0.8%	4.1%	0.2%	93.8%

Computer simulation using Doremus Avenue as a test case has shown that a portion of stagger events cause similar girder stresses as the side-by-side events (See Section 5.1.6.8). Therefore, a portion of the stagger events may be added to the side-by-side percentages when calculating the future load effects due to two trucks.

The MP statistics by span for Site 287 are given in Figure 5.25. The results are similar to Doremus Avenue in terms of percentages side-by-side and following. The stagger results are higher than those for Doremus Avenue. Since MP frequency is related

to traffic volume the higher stagger percentages are reasonable. The maximum single direction ADTT* for Site 287 is 3220 trucks/day, while Doremus Avenue has an ADTT* of 1485 trucks/day. Also the curves in Figure 5.25 indicate that the MP frequency is greater for northbound vs. southbound traffic in terms of stagger, following and other events. Multipresence frequency is related to traffic volume, grade, or other site-specific factors. The northbound ADTT* is 3295 trucks/day, while the southbound ADTT* is 3220 trucks/day. The difference is not significant enough to conclude that traffic volume is the sole factor contributing to MP events. Further investigation is needed to determine if other site specific factors such as grade, lane merge, exiting traffic, etc. are contributing to the increased MP.
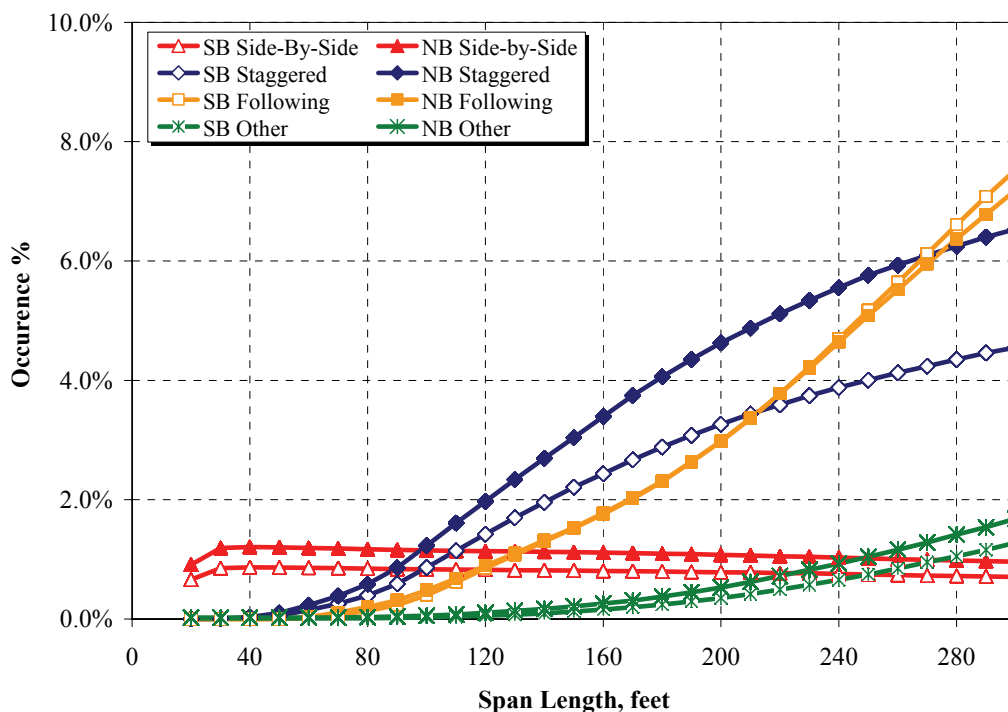
Figure 5.25 NJ WIM Site 287 – MP Statistics by span for NB and SB Lanes

NJ WIM site 80R has some of the highest MP statistics of any other NJ site. Figure 5.26 shows the MP frequency curves for the eastbound and westbound directions of Interstate 80. The maximum side-by-side percentage of 2.5% is larger than any other NJ WIM site studied. The MP frequency of the eastbound direction (lanes 1,2,3) is significantly greater than the westbound direction (lanes 4,5,6) for all types of MP events. This is due to a greater eastbound traffic volume of 4246 truck/day compared with a westbound volume of 3603. The high percentages of side-by-side, coupled with similarly high stagger percentages make Site 80R the most critical for multipresence of any other NJ WIM site.
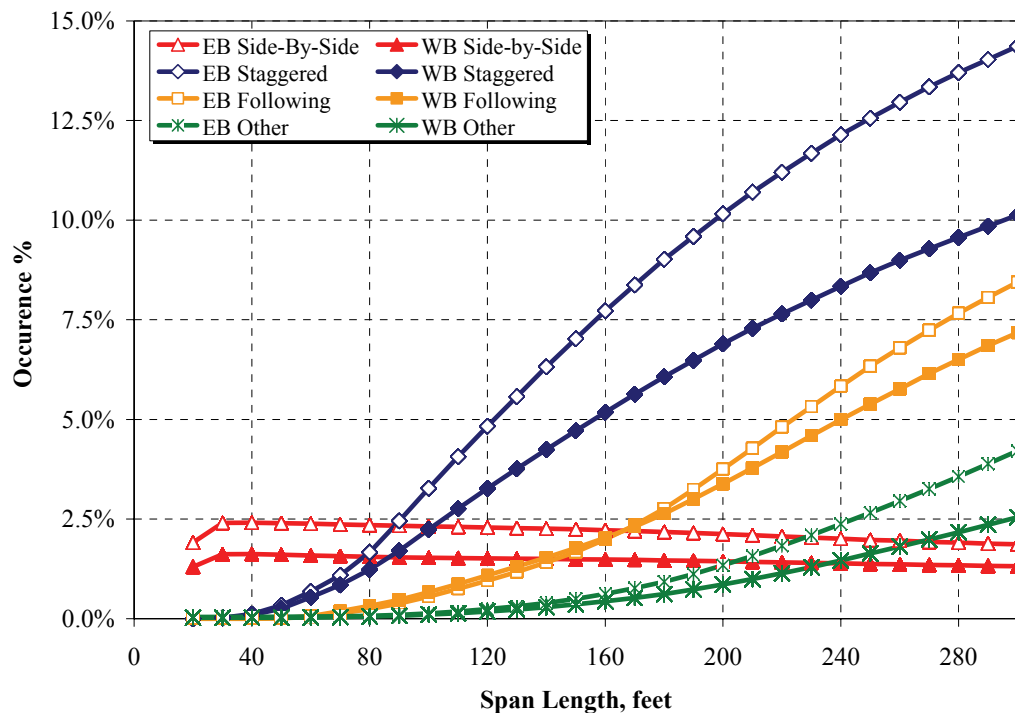
Figure 5.26 NJ WIM Site 80R – MP Statistics by span for EB and WB Lanes

5.1.7.2   Events Involving Two Heavy Trucks

The following analysis is a breakdown of the multipresence results in terms of the weights of each truck involved. These "heavy-heavy" plots represent the portion of the general MP results where each truck weight is equal to or greater than the given threshold weight. The majority of trucks involved in a multipresence event are light (weighing less than 60k each). In order to determine the maximum expected load event in 75 years, information is needed about the two heaviest trucks that are expected to occur together as two trucks following, side-by-side, or staggered. The percent occurrence for the heavy-heavy MP plots represents a subset of the MP events where each truck weight is equal to or greater than the threshold weight. Recall that the LRFD code assumption for overall side-by-side trucks was 1/15 or 6.67% (Nowak 1999). The assumptions further state that 1/30 or 3.3% of these side-by-side events involves two trucks that are 'heavy'. WIM data was analyzed to compare the frequency of two heavy trucks occurring in various MP configurations to verify the code assumptions.

5.1.7.2.1   Heavy MP Statistics for Doremus Avenue Bridge

The heavy-heavy statistics for side-by-side, staggered, and following are shown in Figure 5.27, Figure 5.28, and Figure 5.29, respectively. Each figure contains curves for each direction: northbound (Lanes 1 & 2) and southbound (Lanes 3 & 4). Figure 5.27 shows the proportion of side-by-side events where the gross vehicle weight of each truck involved is greater than or equal to the threshold weight. It is clear that the majority of side-by-side events, about 97%, involve two trucks each weighing less than 60 kips. The most extreme side-by-side event for the Doremus Avenue Bridge involved two trucks

each weighing 92 kips in the southbound lanes. Extreme side-by-side events are rare

considering that only 0.8% to 1.2% of trucks occurs side-by-side, and that less than 0.1%

of these cases involve two trucks weighing more than 90k. The heaviest occurrences of

side-by-side (Figure 5.27) and stagger (Figure 5.28) occurred in the southbound lanes.

As reported earlier in Table 5.8, the southbound lanes have a higher average weight or

the dominant class 9 trucks than the northbound lanes. Since the overall truck population

is heavier southbound, heavier MP events are expected in this direction.

The data in Figure 5.29 shows that very few heavy trucks are involved in

following events at Doremus Avenue Bridge. The most extreme following even involved

two northbound trucks each weighing at least 82 kips.

Detailed counts for each of the extreme MP cases are listed in Table 5.12. The

heavy-heavy counts listed are used along with the total number of base events to calculate

the percent occurrence of extreme MP events.
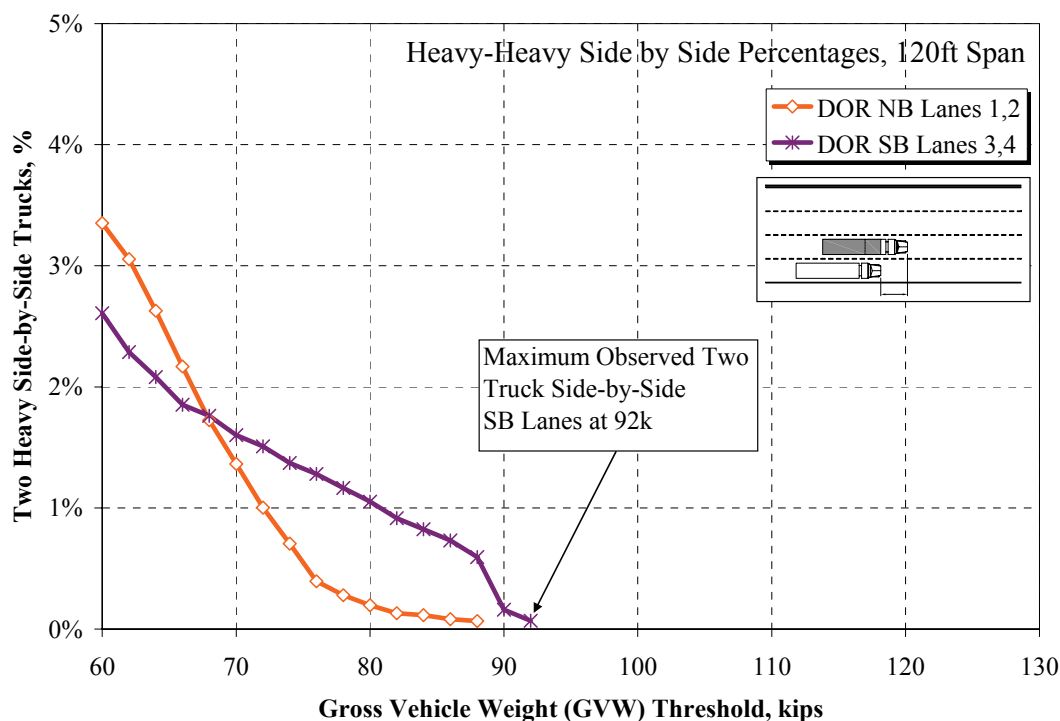
Figure 5.27 Doremus Ave. Bridge - Variation of side-by-side event statistics for two heavy trucks using different "heavy" weight thresholds for a Span of 120 feet
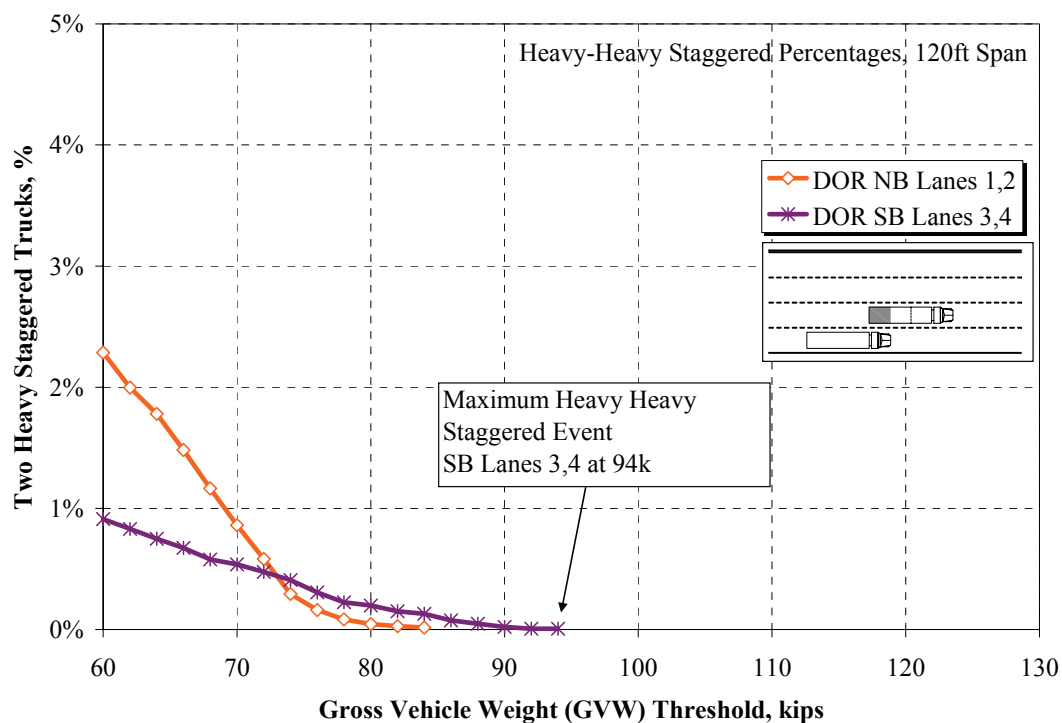
Figure 5.28 Doremus Ave. Bridge - Variation of staggered event statistics for two heavy trucks using different "heavy" weight thresholds for a Span of 120 feet
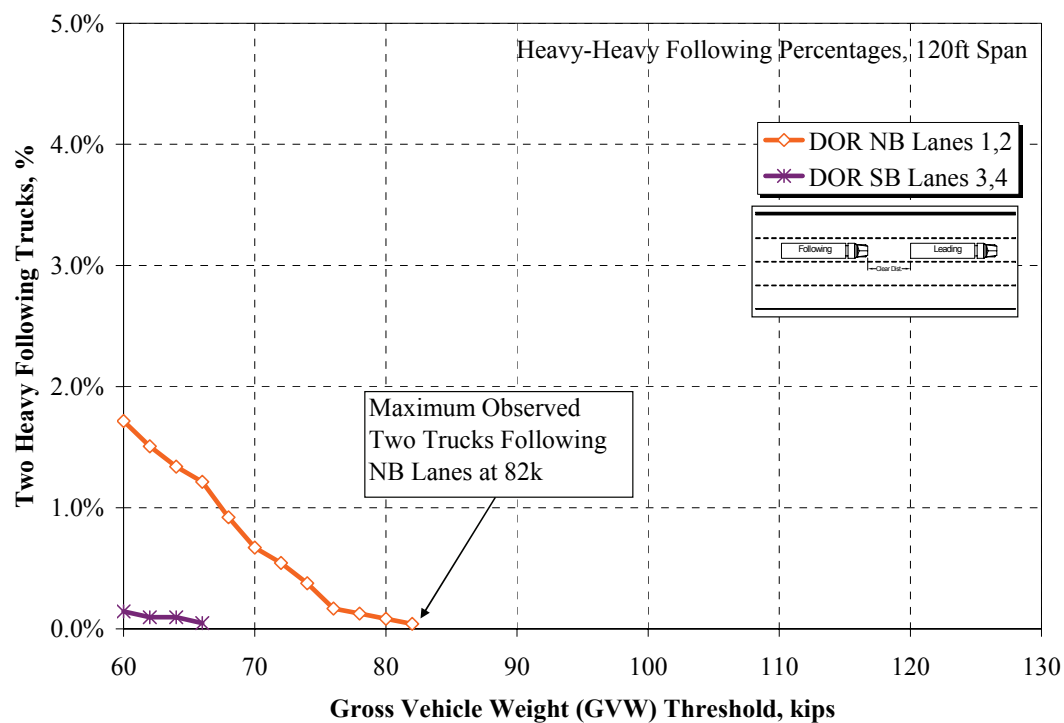
Figure 5.29 Doremus Ave. Bridge - Variation of following event statistics for two heavy trucks using different "heavy" weight thresholds for a Span of 120 feet

Table 5.12 Doremus Ave. Bridge – Summary of MP Events involving two heavy trucks of varying weight

120ft Span Threshold GVW, k	Heavy Side-by-Side		Heavy Staggered		Heavy Following	
	Doremus Lanes 1,2	Doremus Lanes 3,4	Doremus Lanes 1,2	Doremus Lanes 3,4	Doremus Lanes 1,2	Doremus Lanes 3,4
60	204	114	412	134	41	3
62	186	100	360	122	36	2
64	160	91	321	110	32	2
66	132	81	267	99	29	1
68	105	77	210	85	22	
70	83	70	155	79	16	
72	61	66	105	70	13	
74	43	60	53	60	9	
76	24	56	29	45	4	
78	17	51	15	33	3	
80	12	46	8	29	2	
82	8	40	5	22	1	
84	7	36	3	19		
86	5	32		11		
88	4	26		7		
90		7		3		
92		3		1		
94				1		
Total Base Events	**6087**	**4372**	**18027**	**14698**	**2389**	**2085**
Maximum Obs. Wt(k)	**88**	**92**	**84**	**94**	**82**	**66**

5.1.7.2.2   Heavy MP Statistics for NJ WIM Site 287
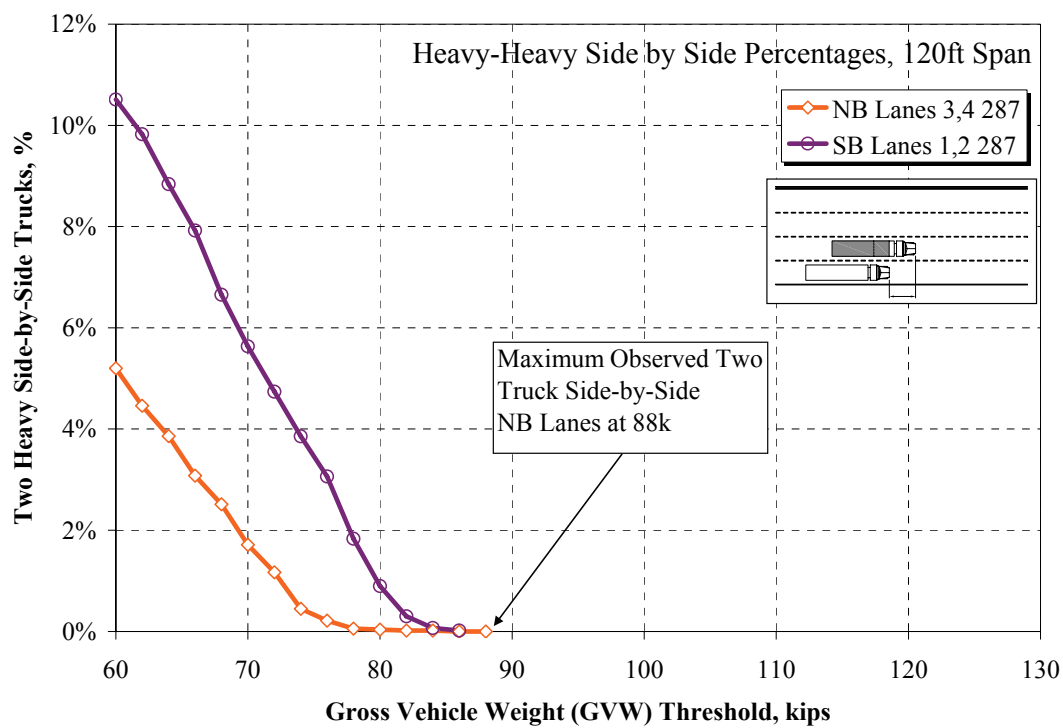
Figure 5.30 NJ WIM Site 287 - Variation of side-by-side event statistics for two heavy trucks using different "heavy" weight thresholds for a Span of 120 feet
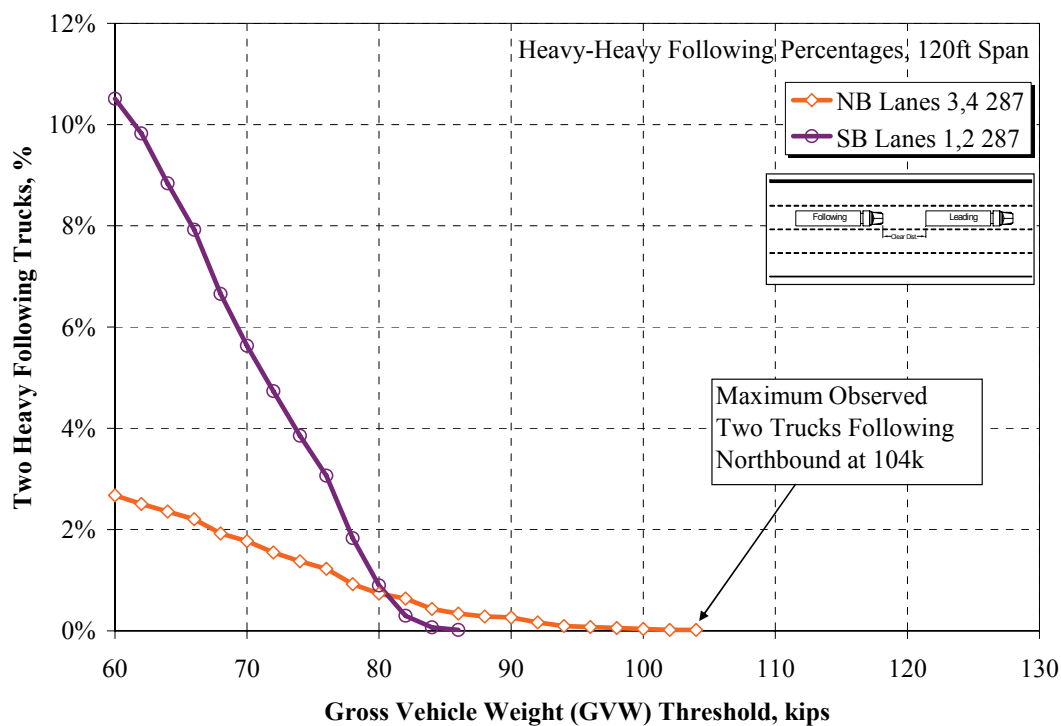
Figure 5.31 NJ WIM Site 287 - Variation of following event statistics for two heavy trucks using different "heavy" weight thresholds for a Span of 120 feet
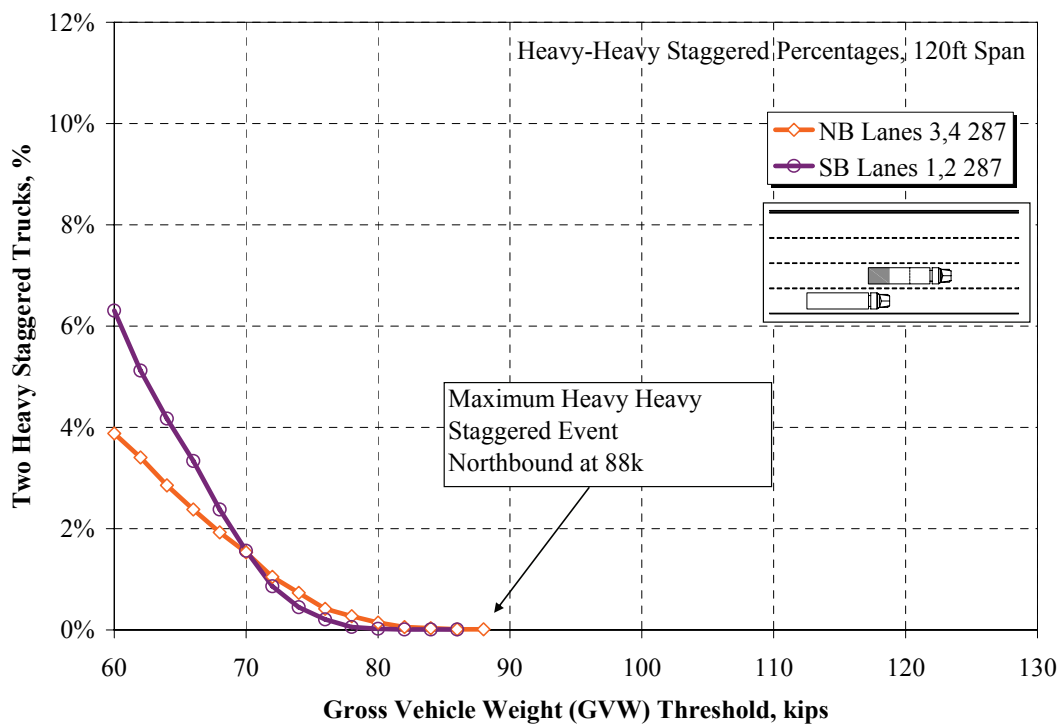
Figure 5.32 NJ WIM Site 287 - Variation of staggered event statistics for two heavy trucks using different "heavy" weight thresholds for a Span of 120 feet

Table 5.13 NJ WIM Site 287 - Summary of MP Events involving two heavy trucks at varying weight thresholds

120ft Span Threshold GVW, k	Heavy Side-by-Side Site 287		Heavy Staggered Site 287		Heavy Following Site 287	
	SB LN 1,2	NB LN 3,4	SB LN 1,2	NB LN 3,4	SB LN 1,2	NB LN 3,4
60	267	633	344	790	142	597
62	229	517	302	642	133	558
64	198	414	253	523	125	502
66	158	314	211	418	117	450
68	129	231	171	298	102	378
70	88	158	136	196	94	320
72	60	90	93	108	82	269
74	23	46	65	56	73	219
76	11	15	37	26	65	174
78	3	2	24	7	49	104
80	2	1	13	3	39	51
82	1	1	5	1	34	17
84	1		3	1	23	4
86			1	1	18	1
88			1		15	
90					14	
92					9	
94					5	
96					4	
98					3	
100					2	
102					1	
104					1	
106						
Total Base Events	**5132**	**7232**	**8867**	**12529**	**5304**	**5680**
Maximum Obs. Wt(k)	**84**	**82**	**88**	**86**	**104**	**86**

5.1.7.2.3   Heavy MP Statistics for NJ WIM Site 80R
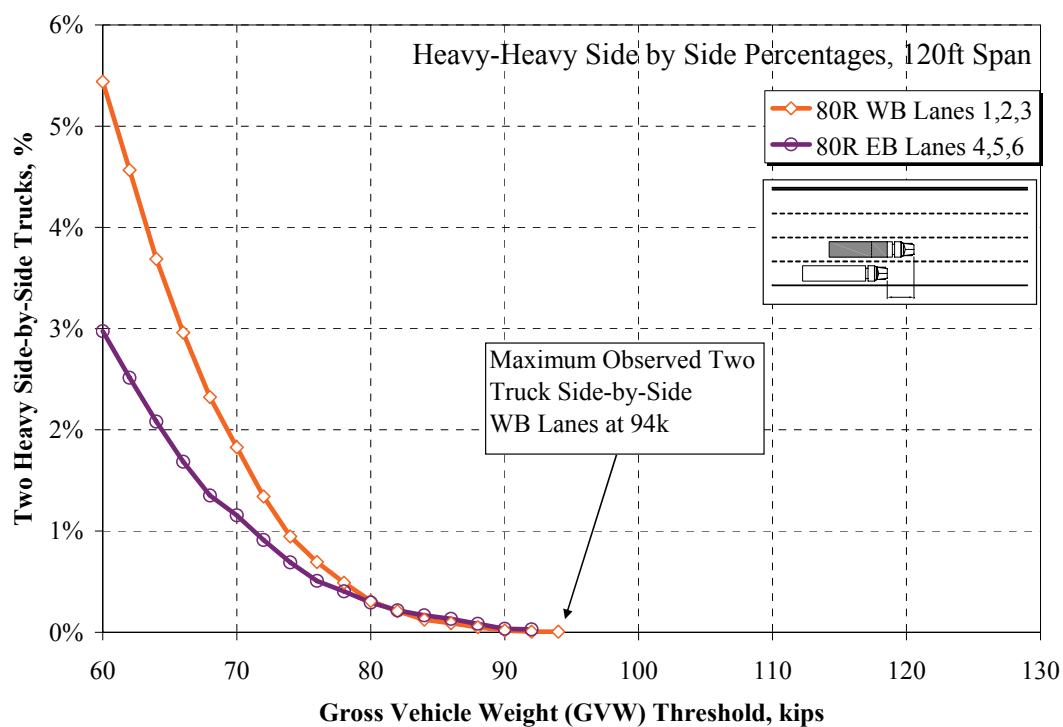
Figure 5.33 NJ WIM Site 80R - Variation of side-by-side event statistics for two heavy trucks using different "heavy" weight thresholds for a Span of 120 feet
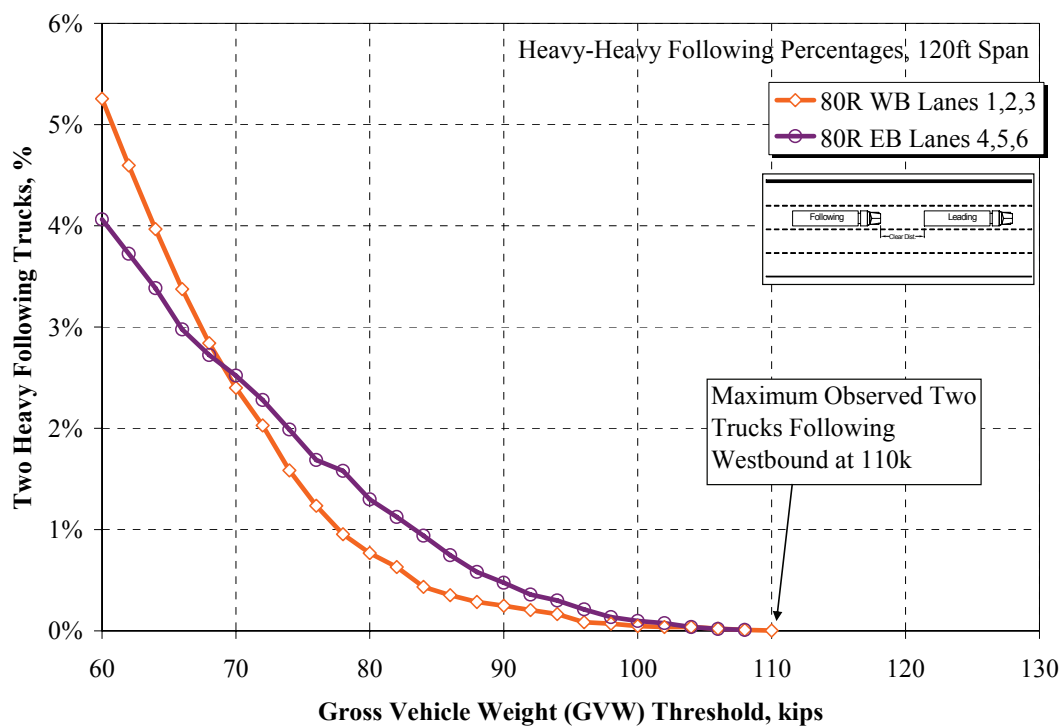
Figure 5.34 NJ WIM Site 80R - Variation of following event statistics for two heavy trucks using different "heavy" weight thresholds for a Span of 120 feet
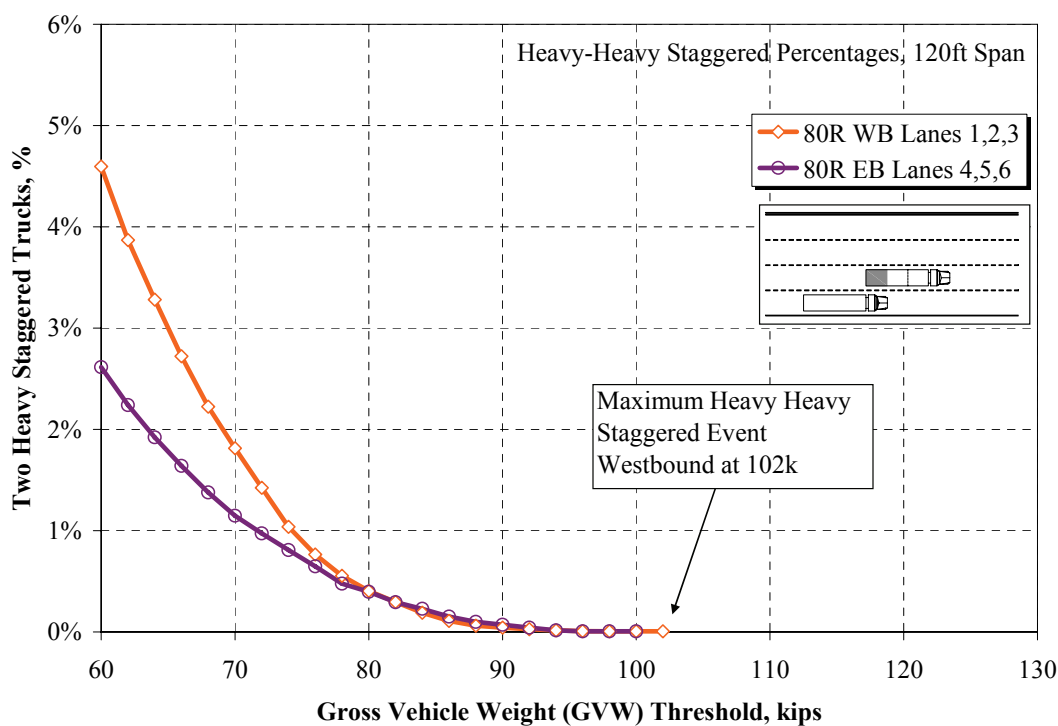
Figure 5.35 NJ WIM Site 80R - Variation of staggered event statistics for two heavy trucks using different "heavy" weight thresholds for a Span of 120 feet

Table 5.14 NJ WIM Site 80R - Summary of MP Events involving two heavy trucks at varying weight thresholds

120ft Span Threshold GVW, k	Heavy Side-by-Side Site 80R		Heavy Staggered Site 80R		Heavy Following Site 80R	
	WB LN 1,2,3	EB LN 4,5,6	WB LN 1,2,3	EB LN 4,5,6	WB LN 1,2,3	EB LN 4,5,6
60	965	427	1727	811	1101	419
62	810	361	1454	695	963	384
64	654	299	1233	596	831	349
66	525	242	1023	509	707	307
68	412	194	836	427	595	281
70	324	166	682	356	503	260
72	238	131	535	302	425	235
74	168	99	390	251	332	205
76	123	73	287	201	259	174
78	87	58	208	148	200	163
80	55	42	152	123	161	134
82	37	31	111	91	132	116
84	22	24	71	71	91	97
86	16	19	41	47	74	77
88	9	12	23	31	60	60
90	3	5	16	22	52	49
92	1	4	10	13	43	37
94	1		6	5	35	31
96			3	2	18	22
98			2	2	15	14
100			2	2	10	10
102			2		8	8
104					8	4
106					5	2
108					2	1
110					1	
Total Base Events	**17735**	**14361**	**37574**	**31022**	**20950**	**10312**
Max Obs Wts (k)	**94**	**92**	**102**	**100**	**110**	**108**

5.2   Live Load Effects due to a Single Truck

When designing or evaluating structures the loads are first identified, and then their effects are quantified. In live load calibration, the bridge response is the underlying design factor, i.e. moments, shears, stresses, and deflections, rather than truck weight. Since every truck is unique in terms of configuration and axle loads, weight alone does not accurately describe the demand on a structure. The distribution of the weight must also be taken into account. Consider two trucks of equal gross weight, W. One truck has five axles and an overall length, L. The other has five axles and an overall length of 1.5L. The two trucks have identical weights, however, it is clear that the shorter truck will cause a higher moment and shear on a given span than the longer truck. This point is evident when considering permit loads. A typical permit truck weighs much more than a legal truck. The main differentiation is that a permit configuration distributes the load over more axles and a longer distance. The opposite is true of certain fixed load vehicles or mobile cranes. The crane configuration is often compact with heavy axles causing a higher moment than similar regular configurations of similar weight. Nonetheless, permits and crane configurations are removed from the general truck data for calibration. When evaluating the effect of live load, the moment or shear demand of each truck must be considered. The load effects, specifically the moment or shears acting on specific members are of the utmost interest.

The next sections present the moment and shear demands caused by the site specific WIM data. The load effects are given in terms of a design load bias. Data from the Doremus Avenue Bridge WIM site operated by Rutgers University and NJ WIM stations, owned and operated by the New Jersey Department of Transportation were

analyzed for their effect on the LRFD load factors. The following sections present the results of the load effect analysis using these site specific WIM datasets. The observed and predicted data for simple moment based on the NJ WIM data are presented for the following NJ Sites: 78B, 78D, 80R, 195, 287, A87, DOR12, DOR34, and DRM. A complete description, indulging the site location and sensor configuration, are given in Chapter 4. More detail information in terms of truck volumes, average weights, counts by class, etc. are given in Section 0. These sites were selected for detailed analysis based on their proximity to the Port of Newark and their function as major truck routes in the greater NY metropolitan area.

5.2.1 Simple Moment - NJ WIM Data

The mean of the upper tail observed simple moments by span length based on the NJ WIM data subset are given in Figure 5.37. The upper tail is defined as the uppermost linear portion of the load effect data as plotted on the Normal Probability Paper, NPP. The upper tail mean simple moment for all of the NJ WIM sites follow a similar trend. This is expected as each of the sites are part of the same regional highway network and contain much of the same truck traffic. A common characteristic of the upper tail mean moments is that there are higher moment ratios for shorter spans. This is due to heavy single or groups of closely spaced axles acting on a short span. The HS20 design moment for short spans is governed by the design tandem pair of axles. The remaining shape of the plot is dictated by the truck configuration relative to the span length. For spans above 140 feet, the HS20 distributed lane loading controls. The upper tail moments decrease linearly with larger spans above 140 feet because the lane load moment is significantly greater than the single truck moment.

The plot in Figure 5.37 shows very large value simple moment on the 20 foot span for the Doremus Avenue Bridge site. Initially, this aberration was thought to be an error in the WIM data. All processed WIM data was filtered to remove obvious data errors and impractical values of weights and axle spacings, as well as permits. Further investigation revealed that the southbound lanes contain a number of overweight four-axle single unit trucks (Figure 5.36) with axle weights of 14k, 16k, 38k, and 38k for axles 1, 2, 3 and 4, respectively. The axle spacings for a typical truck are: 17ft, 3.7ft, and 4ft. This truck configuration contains three axles totaling over 92k within a distance of 7.7 feet. The resulting moment on a 20 ft simple span is nearly equivalent to a single point load of 92k. When compared to the design values for the HS20, the moment ratio becomes 2.35*HS20. Since these short heavy vehicles are not permits and do not contain obvious errors in weight or configuration, they must be included in the analysis. Their effect is most pronounced in the shorter spans due to the closely spaced heavy axles. In longer spans their distinction is lost to longer heavier semi-trailer trucks. Heavy single axles are of special concern for pavement design, where a high concentration of load will cause severe rutting and cracking.
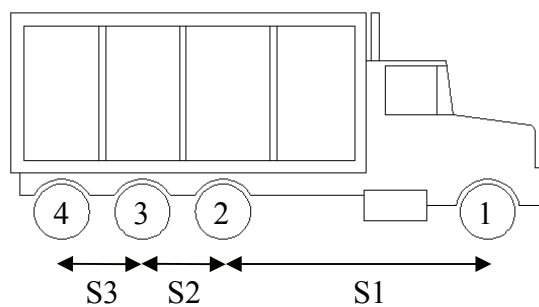
4-axle Single Unit Heavy Trucks			
W1, k	13.4	**S1, ft**	15.3
W2, k	20.8	**S2, ft**	3.6
W3, k	39.8	**S3, ft**	4.1
W4, k	37.6		
Total W, k	111.6		

Figure 5.36 Characteristics of short heavy truck observed at the Doremus Avenue Bridge WIM site
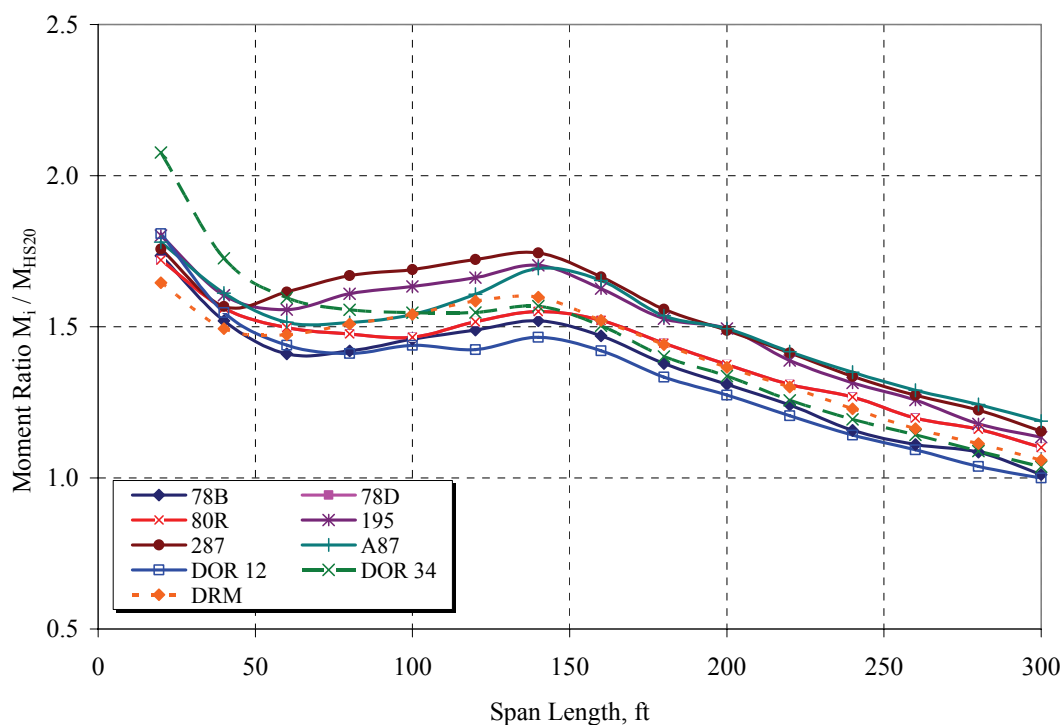
Figure 5.37 Upper tail mean moment ratio by simple span length for NJ WIM sites
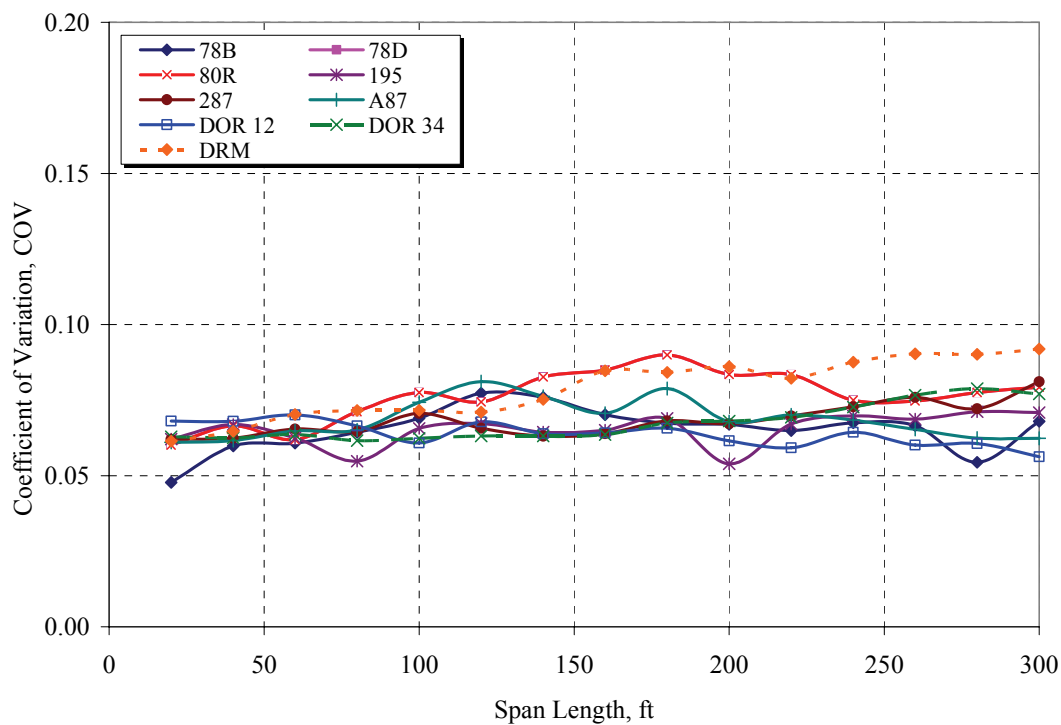
Figure 5.38 Coefficient of variation of upper tail moment by simple span for NJ WIM Sites
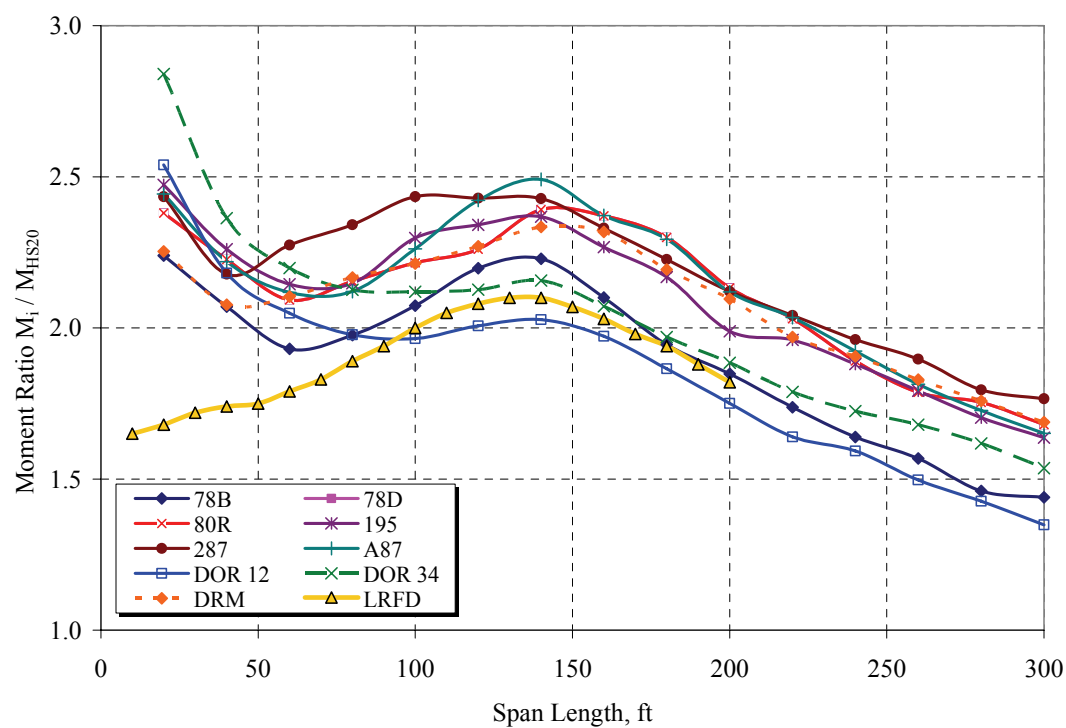
Figure 5.39 75-year predicted moment ratio by simple span for NJ WIM Sites

5.2.2   Simple Shear - NJ WIM Data
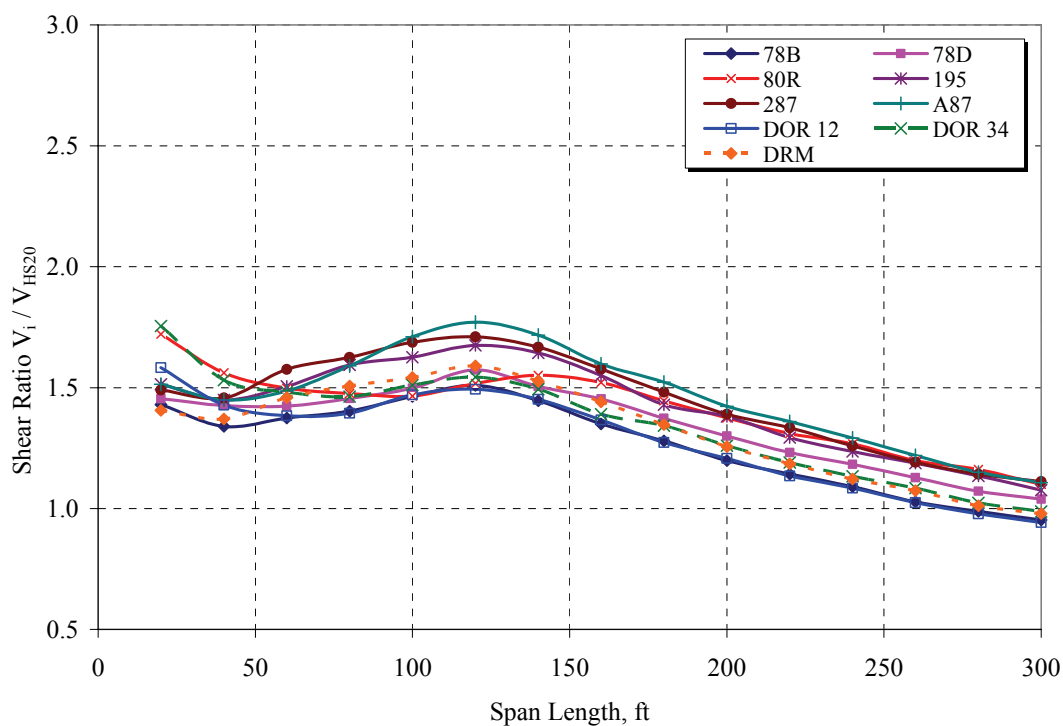
Figure 5.40 Upper tail mean shear ratio by simple span length for NJ WIM sites
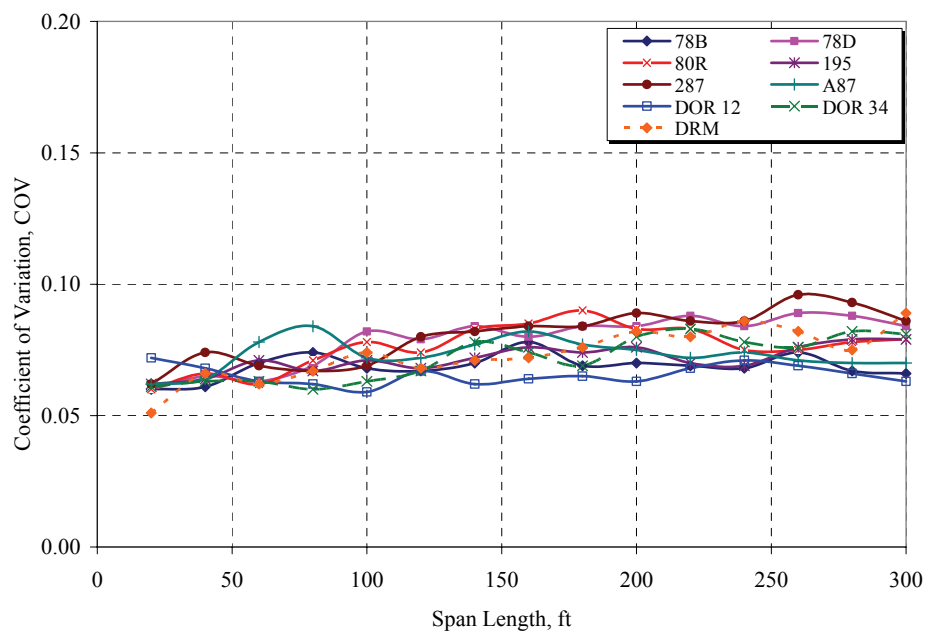
Figure 5.41 Coefficient of variation of upper tail shear by simple span for NJ WIM Sites
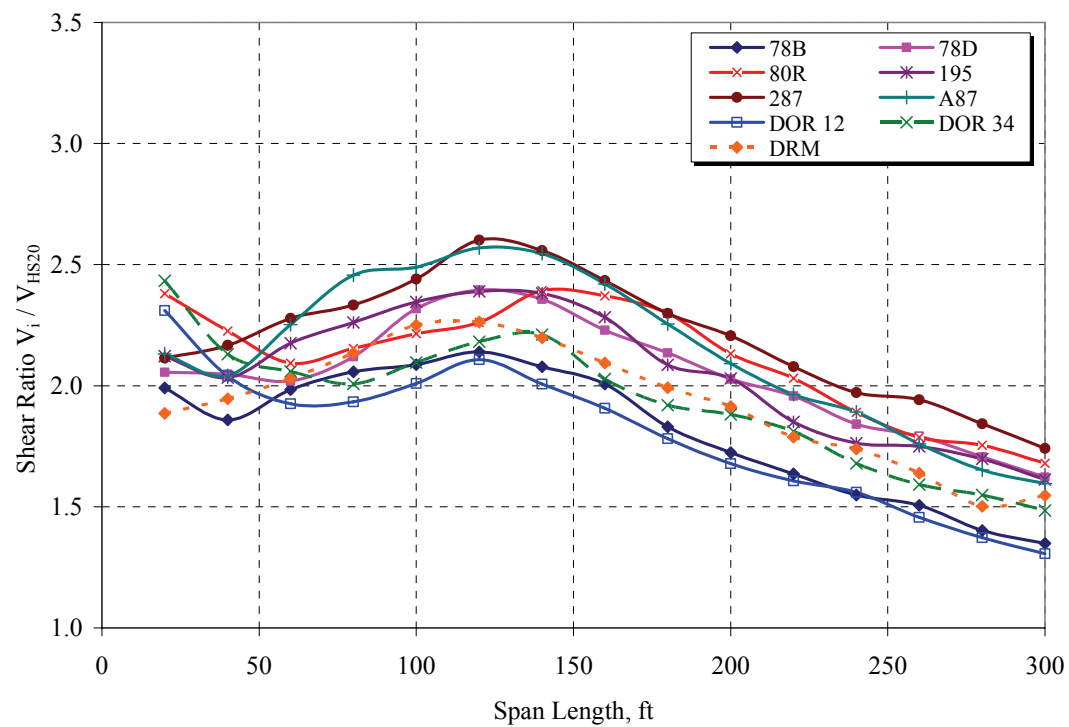
Figure 5.42 75-year predicted shear ratio by simple span for NJ WIM Sites

5.2.3   Maximum Negative Moment on Two Continuous Spans - NJ WIM Data
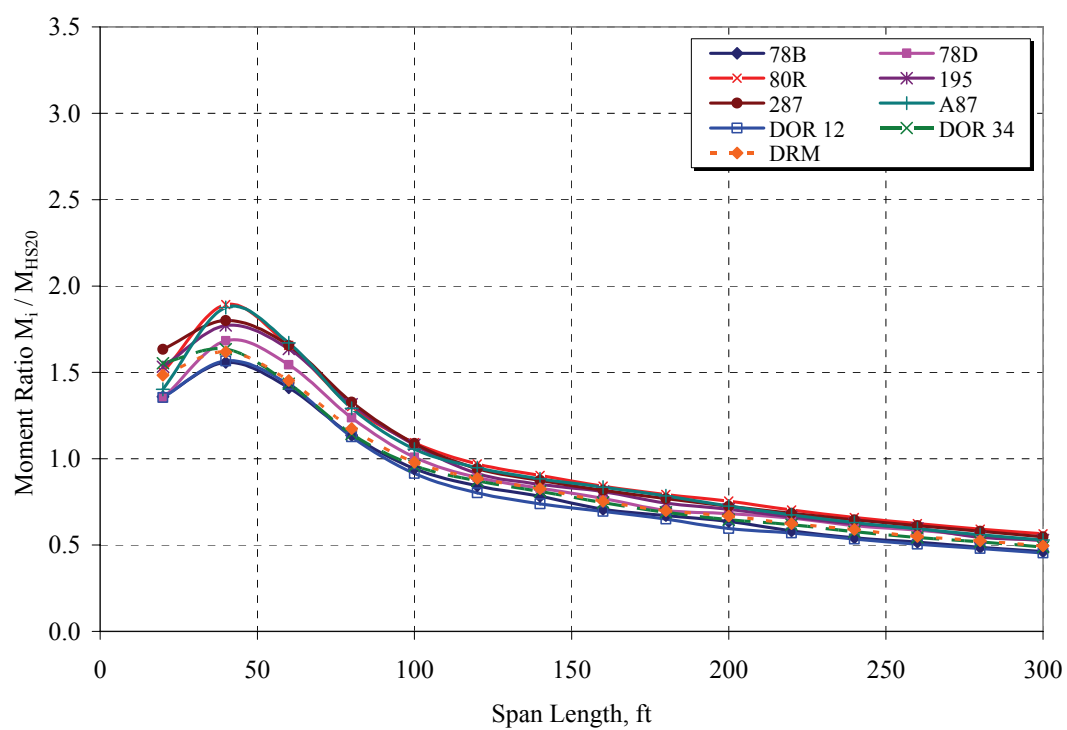
Figure 5.43 Upper tail mean maximum negative moment ratio by span length for NJ WIM sites
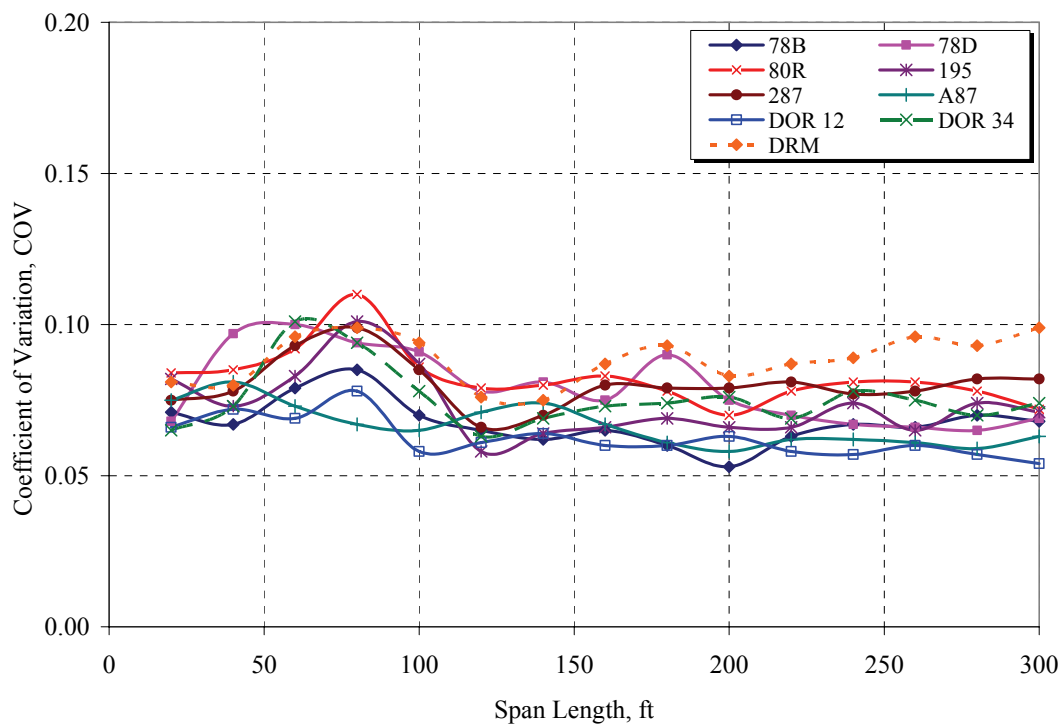
Figure 5.44 Coefficient of variation of upper tail negative moment by span for NJ WIM Sites
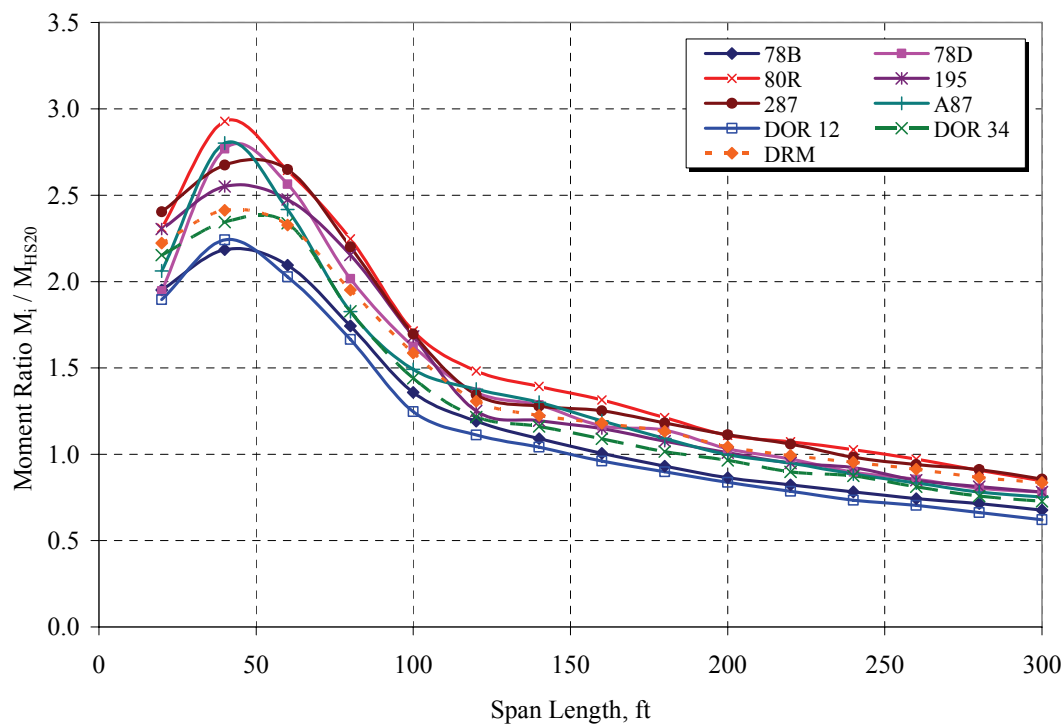
Figure 5.45 75-year predicted negative moment ratio by span for NJ WIM Sites

5.3   Parametric Study

A number of different methods for extrapolating future effects are available. The statistical distribution of the sample data will define which method of extrapolation is most appropriate. To determine the effect of the model on the predicted load values several distributions were considered: Normal, Extreme Type II (Gumbel) and the Generalized Pareto Distribution (GPD). For the Normal and Gumbel models the upper tail was extrapolated within the respective probability paper. The GPD extrapolation was done by choosing a threshold above which to consider the exceedence.

The effect of including permit vehicles and cranes was also studied. This demonstrates the need for proper filtering of raw WIM data. The reliability analysis of the load factor calibration assumes that the sample includes only ambient truck data. Permits and cranes are special cases where the loads are controlled or constant. The exclusion of cranes and permits is only warranted when these vehicles account for a very small proportion of the overall data.

The effect of the sample duration was also studied. The assumption is that longer measurement durations will produce more determinant design values with lower variation. The duration of measurement is a major factor in load factor calibration. A representative sample is needed to describe the truck population. The question is what duration of data is required to attain an accurate and consistent prediction of the live load effects. The address this issue different sample sizes are drawn from the larger overall dataset and extrapolation performed.

5.3.1   Effect of Extrapolation Methods

5.3.1.1   Normal Probability Paper

To extrapolate the load effects using normal probability paper (NPP), the load

effects are plotted against the standard normal variate, Z, as shown in Figure 5.46. More

details on the NPP extrapolation technique are given in Chapter 3. Basically, each data

point is assigned an order, or probability, from zero to one. The inverse of the standard

normal distribution is used to obtain the standard normal variate, Z. The intersection of

the plotted data and the ordinate represents the mean of the distribution. A plot

representing a straight line indicates a good fit to the normal distribution. Overall, the

plotted data in Figure 5.46 does not fit a straight line, and therefore is not normal.

However, the upper tail of the distribution, typically the top 20%, does exhibit a normal

fit. The exact location of the upper tail within the data varies for each sample.

However, a general procedure to locate the upper tail is as follows: (1) locate the

uppermost linear portion of the cumulative density function, CDF, typically within the

upper 20% of the data, (2) fit a linear trend line to this portion, (3) adjust the lower

bound of the linear trend line to maximize the correlation coefficient, R^2 to a value

greater than 0.90, and (4) extend the trend line to the corresponding future variate, Z.

The slope of the upper tail (defined as the standard deviation of the normal) is

used along with the future variate to determine the predicted load levels at some future

duration. Since the normal variate varies as an exponential function, the linear extension

of the observed data is minimal. The extrapolation shown in Figure 5.46 represents the

extension of the simple moment effects from an observed 238 days ($Z = 4.957$) to a full

75-year design life ($Z = 5.820$).
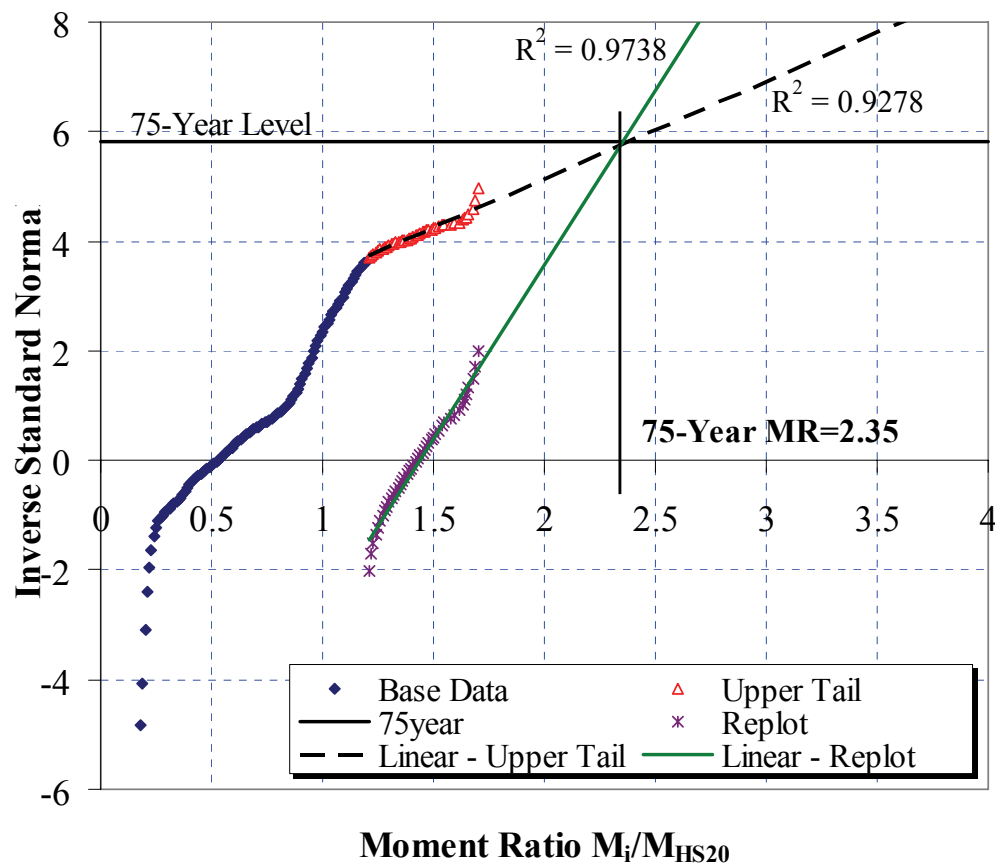
Figure 5.46 Normal probability paper upper tail extrapolation for simple moment on a 140ft span showing both the upper tail extension (dashed line) and replot approach (solid trend line) for Site 060

5.3.1.2   Extreme Type II – Gumbel Distribution

A procedure similar to the normal probability paper extrapolation given in the previous section was conducted using the Gumbel distribution. The Gumbel, specifically, the Extreme Type II (largest), has been shown to describe events that are extreme in nature or have very long return periods (Ang and Tang 1975). The procedure involves plotting the moment or shear ratio data versus the Standard Gumbel Variate, S. The Gumbel Variate is given as:

$$ s = \ln\left(\frac{1}{\ln\left(\frac{1}{p} \right)} \right) $$

Eq. 5.1

Where, p is the order statistic of probability of the data point given as $p=N_i/(1+M)$, where N_i is the index of the value within the sorted data and M is the total number of data points. The process of Gumbel Probability Paper, GPP, may be similar to the NPP, however, a review of the standard variate of the Gumbel reveals that it tends to increase an order of magnitude more than the standard normal variate. Therefore, the Gumbel is better suited for describing very extreme events or very rare events.
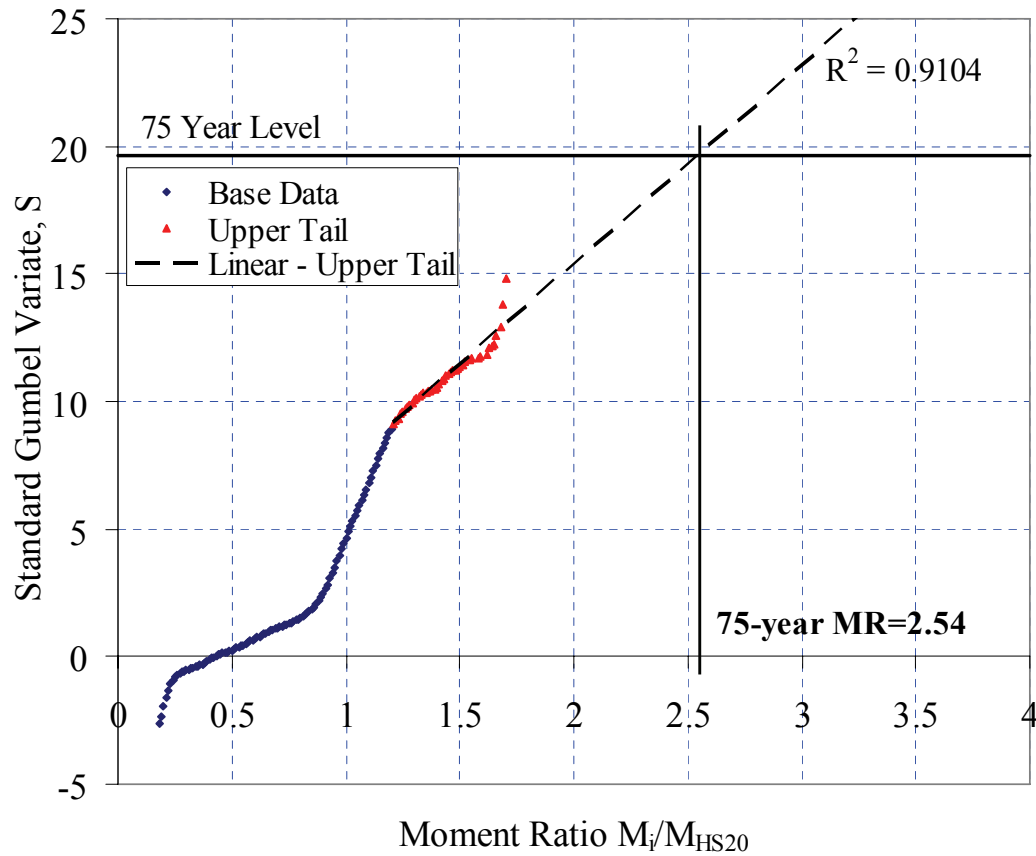
Figure 5.47 Upper tail extrapolation using Gumbel Probability Paper

Extrapolation for future load levels using the GPP involves the following steps: (1) sort the data from least to greatest, (2) assign an index to each data point starting with 1 for the first point and ending at **M** for the last, (3) calculate the order statistic, **p**, for each index, (4) calculate the standard Gumbel variate, **S**, for each value using the order statistic, (5) determine the bounds of the upper tail, (6) fit a linear trend to the upper tail and extend to the future return level.

The GPP extrapolation is conducted in much the same manner as with the NPP. The upper tail is identified as the upper most linear portion of the cumulative density function, CDF. A linear trend line is applied, and the upper tail is modified to maximize the correlation coefficient, R^2. When a R^2 value is maximized and is greater than 0.9, the tail has been located.

The GPP plot (Figure 5.47) often provides a much larger and clearly defined upper tail than the NPP plot (Figure 5.46). This is due to the most extreme nature of the Gumbel Distribution. Therefore, the upper tail of the plotted data for the Gumbel extends further than the for the Normal. As with the Normal, one-half of the data falls below the variate value of zero. However, the Gumbel provides a larger and more easily identifiable tail. The number of trucks used for both the Normal and Gumbel extrapolation in Figure 5.46 is 334. The x-values of load effect are the same for both extrapolations, only the value of the standard variate depends on the distribution.

A comparison of the Gumbel and Normal extrapolations for the Doremus Avenue Bridge site is given in Figure 5.48. Both distributions provide similar results for the 75-year predicted simple moments. The Gumbel exceeds the Normal in the short spans by

15% in the case of Lanes 3 and 4 (Southbound). The extreme moment ratios at the

shorter spans are due to short heavy vehicles, some weighing over 100 kips with a length

of less than 25 feet. These extreme moment ratios were investigated to determine their

authenticity. All WIM data used for these predictions was subject to the same filtering

routines and contains the same number of data points. The extreme moment values were

found to be plausible and therefore remain in the results. Since the Gumbel distribution

is more sensitive to these extreme, the predicted 75-year moment ratios for the shorter

spans are greater than the Normal prediction.
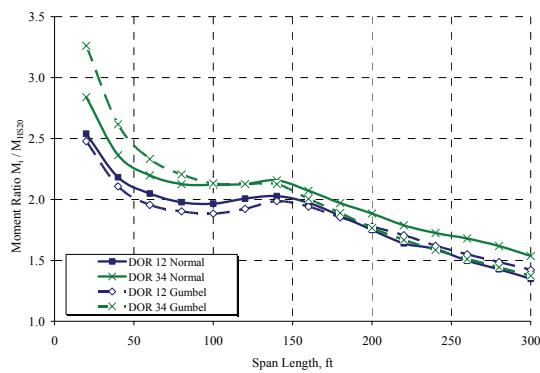
(a) Doremus Avenue Bridge
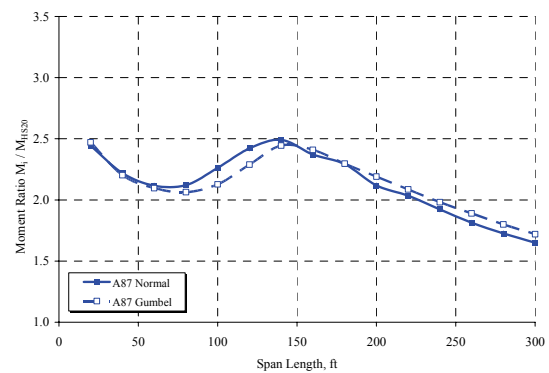
(b) Site A87

(c) Site 80R

(d) Site 195

(e) Site 287   (f) Site DRM

(g) Site 78B   (h) Site 78D
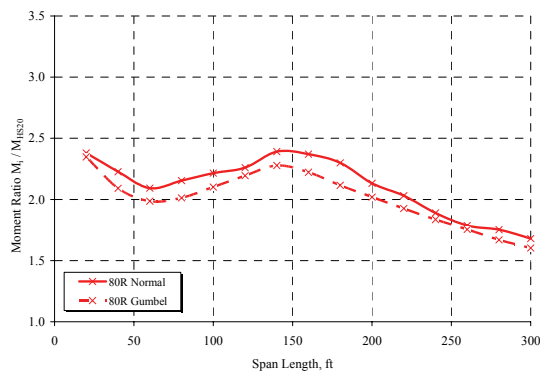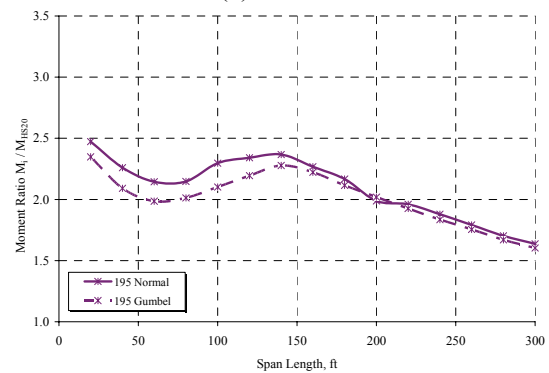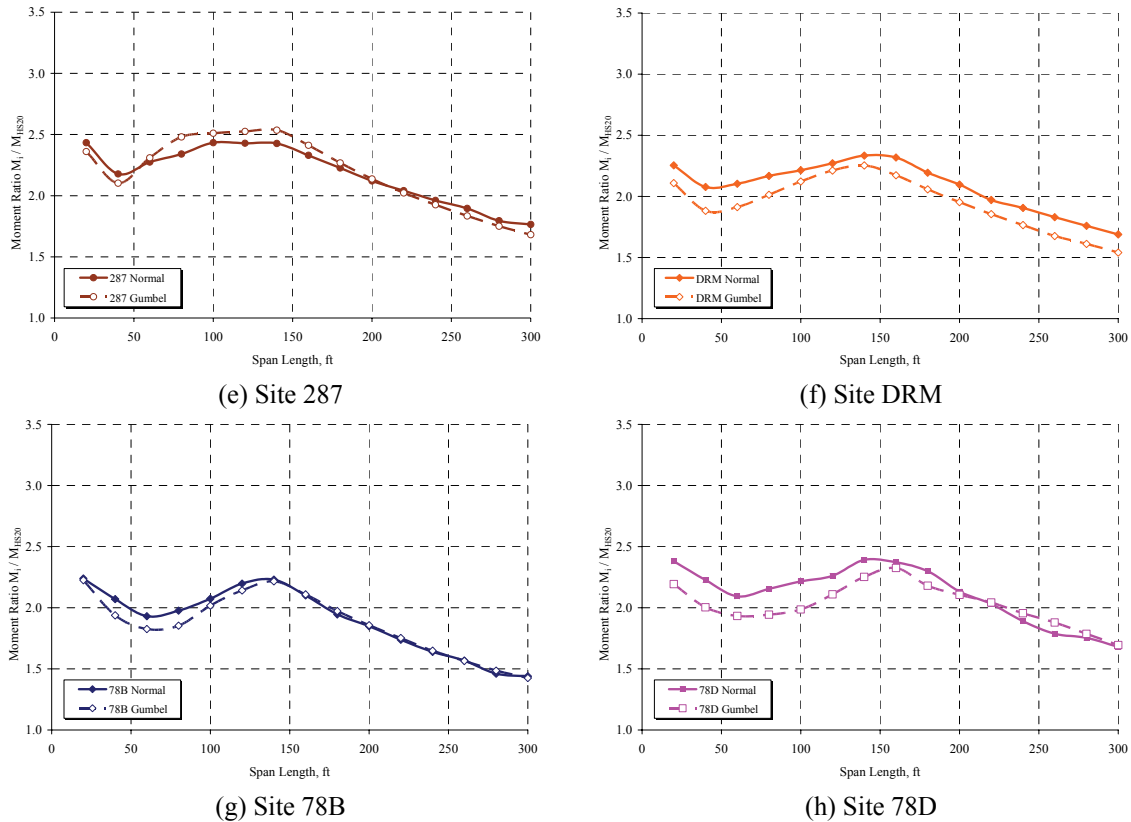
Figure 5.48 Comparison of 75-year simple moment predictions for Doremus Ave. Bridge (a), A87 (b), 80R (c), 195 (d), 287 (e), DRM (f), 78B (g), and 78D (h) using Normal and Gumbel distributions.

Based on the comparisons in Figure 5.48, the 75-year extrapolation is not sensitive to the choice of distribution. Both the Normal and Gumbel distributions give similar prediction results. However, since the Normal distribution was used in the original LFRD calibration procedure and the upper tail of the data fits a normal distribution, there is no need to utilize other distributions for load effect extrapolation.

5.3.2 Effect of Including Permits and Cranes

As discussed earlier, when calibrating load factors for normal traffic all known permits and cranes must be purged from the data. Permits represent special load events that have different assumptions governing their treatment. For superposition, permits are assumed to occur independently on a bridge. The weights of many permits are fixed,

meaning that there is no justification to extrapolate their weights to future levels. The frequency of permits and cranes in the data is low compared with mainstream trucks; however, they strongly influence the mean of the upper tail of load effects. Since permits and cranes have high gross vehicle weights, when included, they readily populate the upper tail of the load effects and increase the mean and COV.

An example of the normal probability plots for simple moment on a 140 ft span for Site 80R is shown in Figure 5.49. For each case the data was filtered to remove insignificant and erroneous records. Additional filters were included to remove all known permit and crane configurations (Figure 5.49a). To include the permits and cranes, these additional filters were omitted (Figure 5.49b). The shape and extent of the upper tail changes with the inclusion of permit vehicles. The upper tail is shifted and extended due to the higher moment ratios of these typically heavy permit vehicles. The mean of the upper tail in Figure 5.49a and Figure 5.49b are 1.55 and 1.77, respectively. Likewise, the maximum observed moment ratios were 1.89 and 2.15 HS20 for the exclusion and inclusion of permits, respectively. The assumption that the upper tail is normal is verified by the linear trend when plotted on the NPP scale for both inclusion and exclusion of permits.

(a) Simple Moment without Permits or Cranes

(b) Simple Moment including permits and Cranes
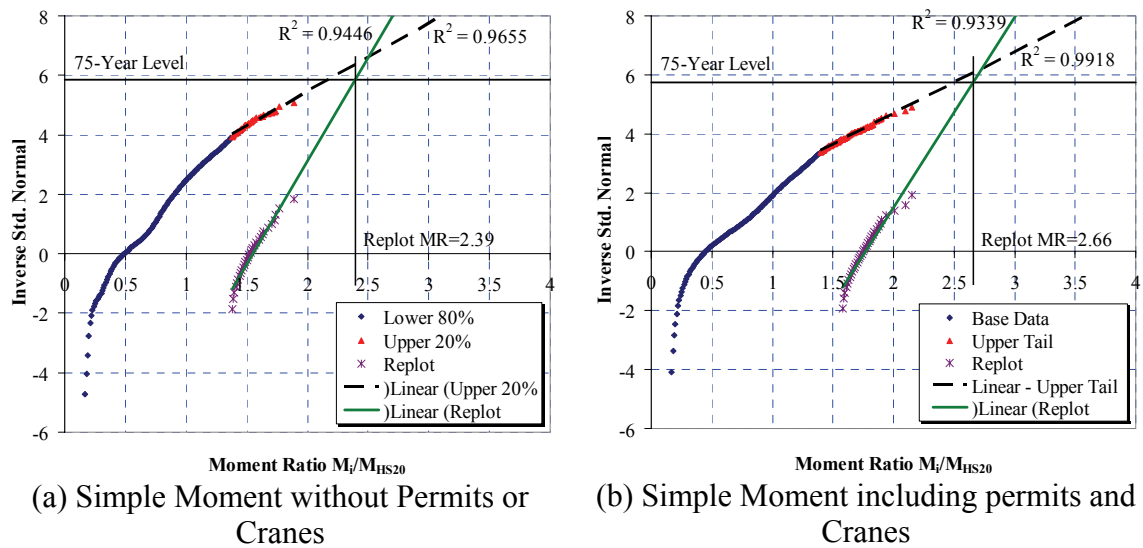
Parameter	Without Permits	With Permits
Upper Tail Mean MR	1.55	1.77
Upper Tail COV	0.083	0.078
Predicted 75-yr MR	2.39	2.66

Figure 5.49 Normal probability scale plots of simple moment (Site 80R) for 140ft span - (a) without permits and (b) including permits.

The inclusion of permits and cranes to a dataset of nearly 5 million trucks has a dramatic effect of the upper tail of the load effects as well as the 75-year predictions. Figure 5.50 gives a comparison of the 75-year predicted simple moment ratios for the case of excluding permits (solid lines), and including permits (dashed lines) for select New Jersey WIM sites. Sites 80R, DOR 12, and DOR 34 were chosen for detailed permit sensitivity since a longer period of data were available for these sites. The inclusion of permit vehicles clearly increases the predicted 75-year moment ratios as seen in Figure 5.50. For example, consider Site 80R for a span of 140 feet. The moment ratios are 2.39 and 2.66 HS20 for inclusion and exclusion of permits, respectively. This constitutes an increase of 11% simply by including permit vehicles.
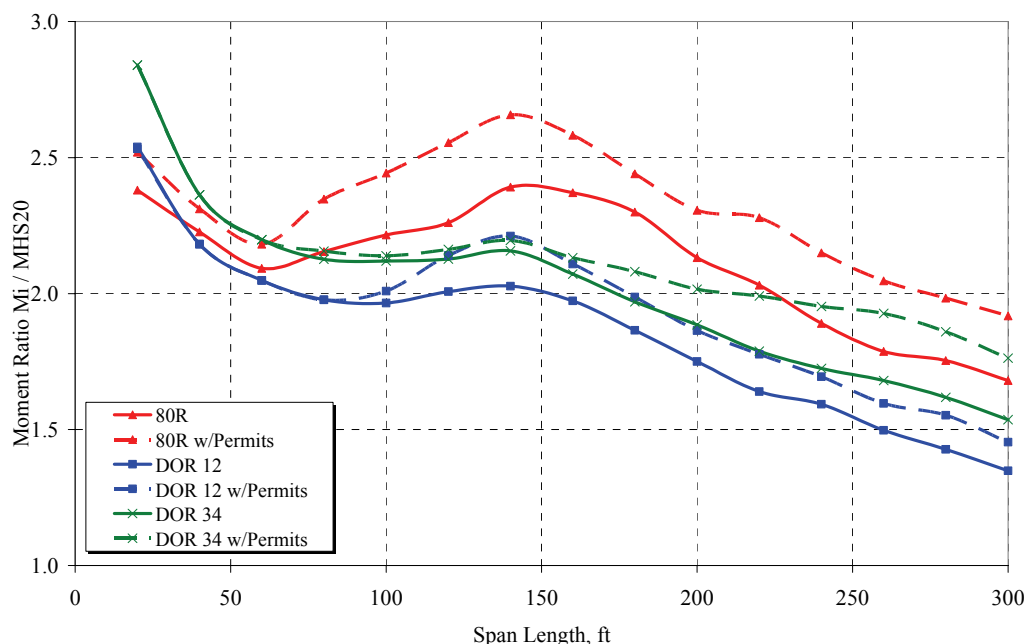
Figure 5.50 Comparison of 75-year simple moments for select NJWIM sites including and excluding permits.

5.3.3   Effect of Sample Duration on Predictions

The basic questions in any extrapolation is: "How much data is needed to achieve an accurate prediction?" The simplest answer is: "As much data as possible." As with any resource, data is limited. Therefore, predictions must be made based on limited data. This was the case for the AASHTO LRFD calibration work done by Nowak (1995, 1999). Faced with limited weigh-in-motion, Nowak made the assumption that the Ontario Truck Survey Data (Agarwal and Wolkowicz 1976) represented the heavy upper tail of a typical interstate highway site with an ADTT of 1000 trucks per day. Fortunately, WIM technology has become more ubiquitous. State and federal transportation agencies now have large databases of WIM data, with some dating back more than ten years.

To address the effect of duration on the 75-year load effect predictions, a series of data samples were taken from an overall dataset of two years. The data sample durations range from three days to the full extent of the data. The sample durations included: (1) four samples at three days each, (2) four samples at 7 days each, (3) eight samples at 14 days each, (4) four samples at 30 days each, (5) three at 60 days each, (6) four at six months, (7) two at one year each, (8) one at 18 months, and (9) and one at 2 years. The samples were chosen throughout the whole dataset to be representative. For example, each of the samples was selected at consistent intervals throughout the two years.

For each sample size the Normal Probability extrapolation techniques were used. It is clear that a longer duration of data will produce a more reliable prediction (closest to the 75-year maximum effect), as indicated by a decrease in the coefficient of variation (Figure 5.52) and asymptotic behavior of the moment ratios in Figure 5.51. The shortest sample durations, i.e. 3, 7, 14 days, have low upper tail mean moment ratios when compared to the longer sample durations, 18 months to 2 years. Additionally, the scatter from the fitted trend line is greater for the shorter duration samples as indicated by larger COV in Figure 5.52. Figure 5.51 indicates that the mean of the upper tail of moment ratios within the observed data increases with longer sample durations. The upper tail is defined as the upper most linear portion of the normal probability plot of the load effects. The upper tail includes the highest load effects within the observed data. It should be noted that the number of truck comprising the upper tail changes with the sample size (number of qualified trucks). The proportion of the overall data (in percent of total qualified trucks) remains constant for all spans of a particular site. The descriptive characteristics of the upper tail vary by site and include: start point, mean, COV,

maximum, and proportion of overall data. Typically, the upper tail contains 0.01% of all trucks. These trucks represent the heaviest, in terms of load effect, acting on the bridge.

For a short duration sample, such as 3 days, there may not be many heavy trucks observed. The mean of the upper tail will, therefore, be low. As the observation duration is extended more and more heavy trucks populate the upper tail and the mean rises. The rise in mean is not linear, rather asymptotic, rising rapidly initially, then tapering off (Figure 5.51). As the sample duration becomes longer, a greater portion of the truck population is sampled. At some point, additional samples do not influence the mean, signifying that the sampled heavy trucks are approaching the maximum of the truck population. The COV (Figure 5.52) of the upper tail exhibits are greater degree of scatter in the short durations, transitioning and stabilizing at about 0.07 for the 2-year sample. The sudden transition in slope of the upper tail mean in Figure 5.51 from short to long duration is attributed to the formation and refinement of the upper tail. Further evidence of this property can be seen in Figure 5.52, where the values of COV converge toward the trend line. At short durations the upper tail contains trucks that are not heavy relative to larger sample durations. In other words, the trucks in the low end of the tail will be quickly replaced by heavier trucks as more data is sampled. As these lighter trucks are forced out, the mean of the upper tail increases. The rate of this increase in mean is reduced as the tail is populated by the heaviest trucks. The trucks within the tail become less differentiated for larger samples, as indicated by the stabilization of the COV in Figure 5.52.

Theoretically, if the entire 75 years of trucks are sampled, the upper tail would include only contain the most extreme of all trucks that the site has experienced. The

maximum of the 75-year upper tail would be the target truck that is being estimated in

Figure 5.53, or approximately 2.4*HS20.
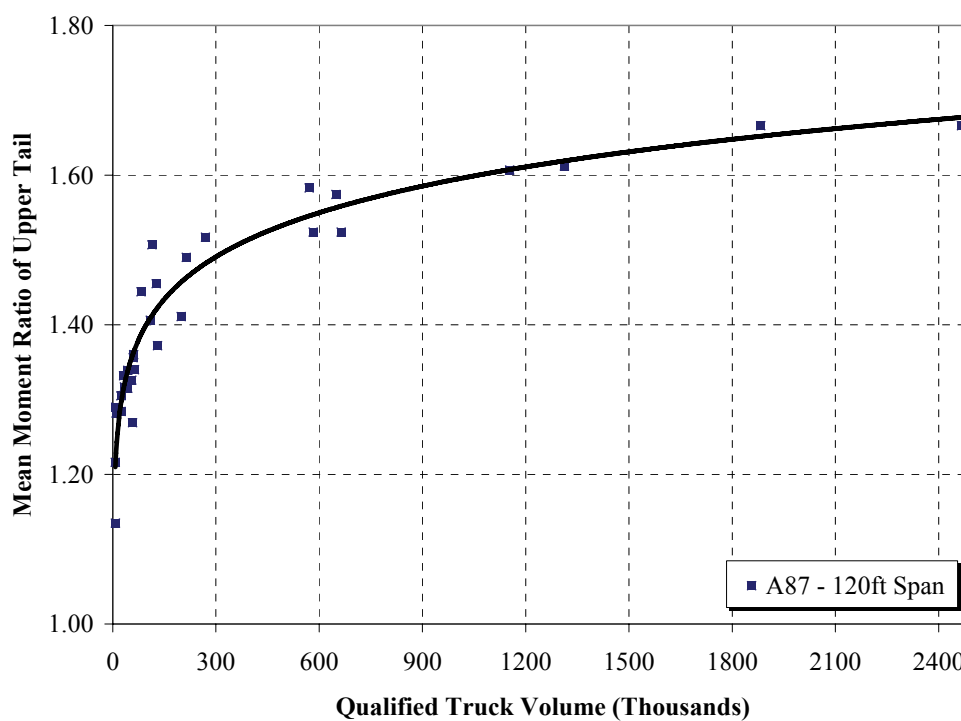
Figure 5.51 Effect of sample size (qualified trucks) on the mean of the upper tail of simple moment ratios for Site A87
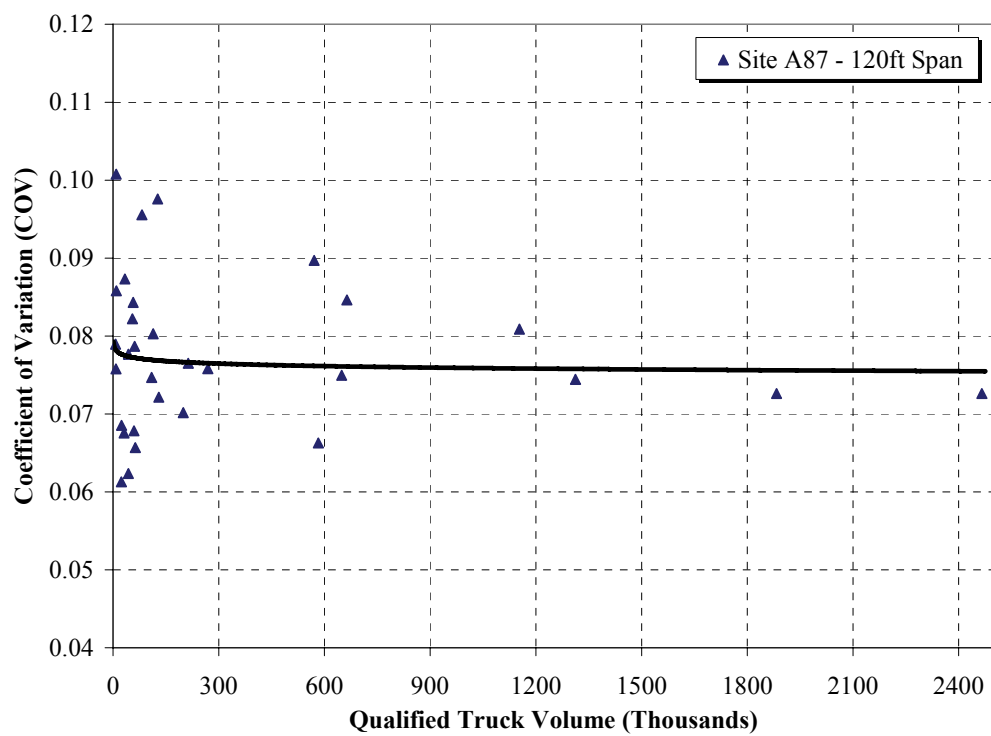
Figure 5.52 Effect of sample size (qualified trucks) on the coefficient of variation of the upper tail of simple moment
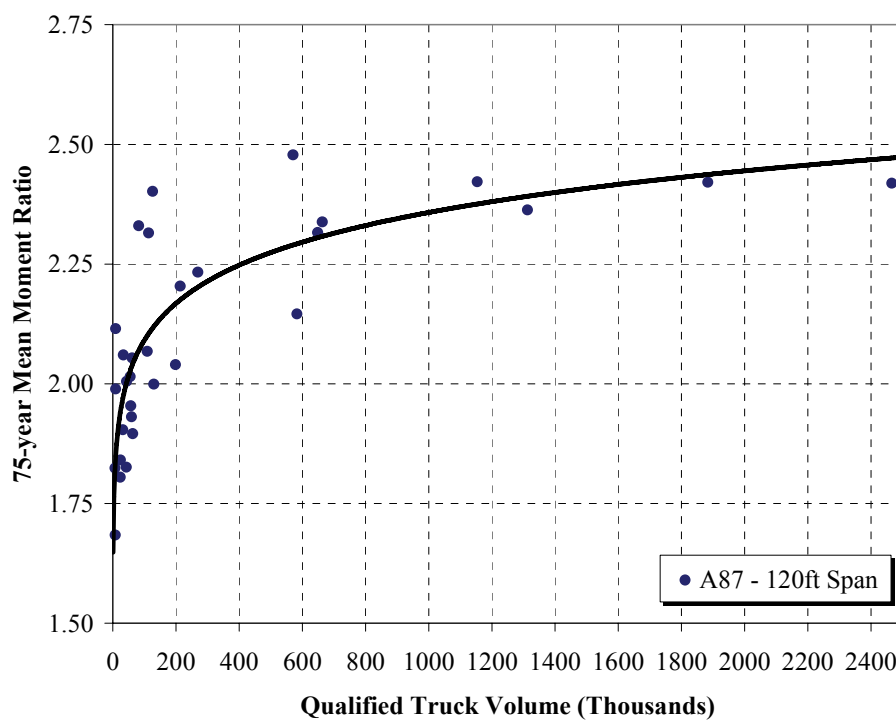
Figure 5.53 Effect of sample size (qualified trucks) on the 75-year prediction of simple moment ratios

CHAPTER 6

FATIGUE LOAD MODEL

Fatigue is defined as the process that causes premature failure or damage of a component subject to repetitive loading (Bannantine 1990). Fatigue cracking occurs at levels well below the ultimate design loads. Unlike, the strength limit state that is defined by the maximum load event in the entire service life of a structure, fatigue damage accumulates over time, sometimes decades. Recent research has led to a better understanding of the phenomena in steel highway structures (Fisher and Dexter 1999). However, fatigue load spectra remains a difficult quantity to determine. Truck gross and individual axle weights contain a great degree of scatter due to the random nature of truck traffic. Furthermore, laboratory tests for fatigue strength are done under constant amplitude conditions, whereas, highway structures are subject to variable amplitude loading. This difference is rectified using cumulative damage assumptions, such as the Palmgren-Miner Rule.

This chapter outlines techniques for quantifying the fatigue load spectra. WIM data is analyzed to determine equivalent load models to represent the truck population. The truck information is fed into structural models to determine nominal member stresses.

The effect of multipresence (truck superposition) is also studied in relation to the fatigue loading.

6.1   Comparison of Observed Truck data to Nominal Fatigue Truck

The current AASHTO LRFD fatigue truck is essentially a three-axle HS20 truck (AASHTO 2004) with a load factor of 0.75. By comparison, the HS20 truck used for strength analysis has a load factor of 1.0. The front axle has a weight of 6k, while the last two axles have a weight of 24k each. The two rear axles of the HS20 actually represent pairs of tandem axles. This assumption makes load analysis simpler without losing accuracy for general member stresses. For deck components such as modular expansion joints or orthotropic deck panels, the individual axles should be considered (Dexter and Fisher 1999). The weight and configuration of the fatigue design truck was meant to resemble the 3S2 vehicle type (Class 9) five-axle semi-trailer (Figure 6.1). The 3S2 truck type is typically the dominant truck type and accounts for a majority of the fatigue damage to bridge elements.

The configuration and weight of the AASHTO fatigue truck is based on weigh in motion studies conducted as part of NCHRP 299 (Moses 1987). The rear axle spacing of 30 feet compares well with the 3S2 rear axle spacing from the data used in the study.

The WIM data for New Jersey sites was analyzed with respect to Class 9 (5-axle semi-trailers) to compare the weights and dimensions to the nominal Fatigue Truck. As shown in Figure 6.2 and Figure 6.3 the axle spacing and gross weight of the dominant Class 9 truck type for various sites resembles the nominal Fatigue Truck. Following the methodology of Moses et al. 1987, the root-mean-cube (RMC) effect gross weight was

calculated for the Class 9 trucks at each site and is presented in Figure 6.2. The overall

effective RMC gross weight observed for the NJ sites was 53.8 kips. The nominal

fatigue truck weight is given as 54k (AASHTO 2004). Therefore, the AASHTO LRFD

nominal Fatigue truck is adequate to represent the weight and configuration of the

dominant truck type in New Jersey.
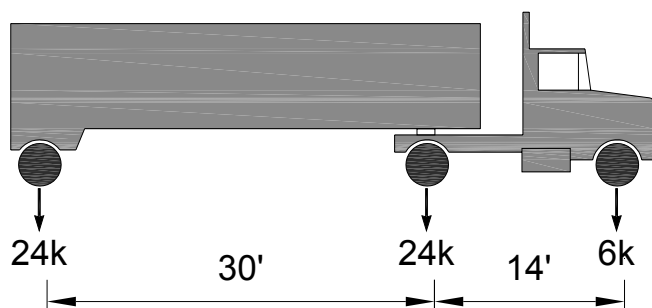
Figure 6.1 AASHTO LRFD Fatigue Truck (AASHTO 2004)

Site	Dom. Class	Dominant W_{equ} (k)	Average Axle Weights					Axle Spacings			
			W1 (k)	W2 (k)	W3 (k)	W4 (k)	W5 (k)	S1 (ft)	S2 (ft)	S3 (ft)	S4 (ft)
78B	9	54.5	9.9	10.1	9.9	9.1	9.2	16.2	4.4	30.8	4.5
78D	9	53.4	10.1	9.9	9.7	9.6	9.6	16.2	4.3	31.4	4.6
80R	9	53.5	9.3	9.9	9.6	9.0	9.0	15.3	4.2	29.4	4.5
195	9	51.6	9.3	9.1	8.8	8.5	8.2	15.3	4.4	30.6	4.6
287	9	57.6	9.9	11.1	10.8	10.1	10.2	16.5	4.4	32.3	4.8
A87	9	56.6	9.2	10.6	10.3	10.3	10.5	15.6	4.2	30.8	4.6
DOR 12	9	48.7	9.1	8.2	8.0	7.3	6.9	15.0	4.3	26.3	4.2
DOR 34	9	56.9	9.6	10.2	9.8	9.3	8.8	15.0	4.3	26.3	4.2
DRM	9	51.5	9.0	9.1	8.8	7.7	7.8	15.4	4.5	28.5	4.3
Average		53.8	9.5	9.8	9.5	9.0	8.9	15.6	4.3	29.6	4.5
COV		0.05	0.04	0.09	0.09	0.11	0.13	0.04	0.02	0.07	0.04
Weight Distribution			20%	21%	20%	19%	19%				

Figure 6.2 Characteristics of Class 9 (3S2) vehicles for NJ WIM Sites, where Wequ is the root-mean-cube equivalent truck weight.

Site	Dom. Class	Dominant W_{equ} (k)	Dominant W_{avg} (k)	Dominant W_{max} (k)	Ratio W_{equ}/W_{max}	Ratio W_{equ}/W_{avg}
78B	9	54.5	48.2	118.0	0.46	1.13
78D	9	53.4	48.8	125.7	0.42	1.09
80R	9	53.5	46.0	126.5	0.42	1.16
195	9	51.6	43.7	126.1	0.41	1.18
287	9	57.6	52.1	127.7	0.45	1.11
A87	9	56.6	50.9	126.5	0.45	1.11
DOR 12	9	48.7	39.2	130.9	0.37	1.24
DOR 34	9	56.9	46.5	130.2	0.44	1.22
DRM	9	51.5	42.4	128.2	0.40	1.21
Average		53.8	46.4	126.6	0.4	1.2
COV		0.05	0.09	0.03	0.07	0.05

Figure 6.3 Characteristics of Class 9 vehicles for NJ WIM sites including equivalent, average, and maximum observed weights.

6.2   Fatigue Load Spectra and Rainflow Extrapolation

Evaluation of existing bridges for fatigue performance is important in the effort to deal with the deteriorating infrastructure. The effort to prioritize bridge repair and rehabilitation options will highly depend on the identification of live loads and their effects. Bridge live load effects vary for different components and structural details. In many cases, analytical methods do not allow for an accurate estimation of load, in particular the load distribution and actual stress ranges. Structural health monitoring and field testing can be very effective in the evaluation of bridge performance at the serviceability limits.

Field measurement of in-service structures is expensive in terms of time and money. It is not practical to dedicate testing equipment to a single bridge for a long period of time. However, longer measurement periods yield a more complete picture of the load spectra. The ever-present question is: "How long does one need to measure to accurately predict the future fatigue damage?" Moreover, prediction methods can be misleading if they are not based on rational and tested procedures. Therefore, there is a

need to establish procedures for data collection and methods for reliable prediction of the remaining fatigue life of an existing bridge.

Knowing the complete load spectra for a bridge is an important aspect in fatigue prediction. To achieve the best description of the loading, one could monitor the structure for an extended period of time. The time-history data recorded would contain the complete loading profile: stress ranges, number of cycles, times of occurrence, and mean cycle stresses. With the response of multiple sensors being recorded, the memory capacity of most data acquisition systems would be quickly exhausted. Afterward, the time-history data collected is analyzed using a rainflow counting algorithm to extract discreet stress cycles (ASTM E1049-85). Although the complete time-history record is very useful, it is impractical and not necessary for fatigue evaluation. Fatigue damage depends only on the magnitude (stress range), number of respective cycles (at each range), and the fatigue category for the detail in question (Fisher 1998). For complicated load histories a representative means to convert variable amplitude signals to a count of closed loop hysteresis was developed, termed rainflow cycle counting. The rainflow method of cycle counting was originally proposed by Matsuishi and Endo in 1968 (Matsuishi and Endo 1968) which was analogous to rain falling down a pagoda roof. More recent cycle counting mechanisms are more efficient for real-time cycle counting (Socie and Downing 1982). Typically, rainflow data is stored in the stress range histograms. The cycles are classified into a discreet number of categories, or bins, along with the number of cycles for each stress range. The stress range-only format is the most compact in terms of data storage while maintaining all of the necessary parameters for describing the fatigue load spectra.

6.2.1   Load and Response Measurement for Doremus Avenue Bridge

The layout of the Fatigue Monitoring system as installed on the Doremus Avenue Bridge is shown in Figure 6.4. Vehicle information including: arrival time, travel lane, speed, axle weights, axle spacing, length, and class are generated by the WIM system for each truck passage and relayed to the Fatigue System via the data link. The complete load history in terms of individual trucks and the corresponding bridge response in terms of strains and cycle counts are stored.
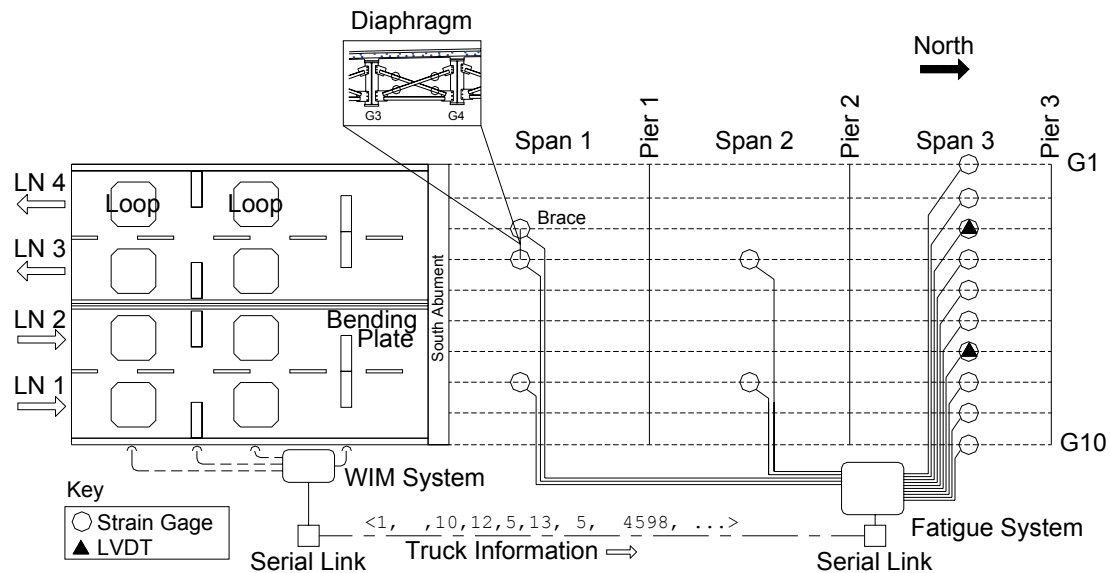
Figure 6.4 Fatigue monitoring system layout for Doremus Avenue Bridge showing the WIM system and Fatigue Monitoring System connected by data link.

Two data collection modes were used to gather load and response information at Doremus Avenue: (1) triggered time-history and (2) continuous rainflow histograms. The triggered time history data contained full snapshots of the bridge response due to the passage of a truck weighing more than a set threshold. The complete truck information

was attached to the response record for later review. Information from these snapshots is used to verify very large stress cycles. Occasionally, electromagnetic interference may produce false strain readings in the strain transducers. The truck information would later be used as input for calibrated bridge models to verify the observed response. Furthermore, the snapshot data could be used to determine other bridge loading parameters such as girder distribution factor and dynamic load amplification. The sensor layout as shown in Figure 6.4 contains one complete 10-girder cross section instrumented for girder strains. The triggered stress history snapshot contains the strain data for gages throughout the cross section allowing for girder distribution calculation. The snapshot contains the real-time stress history allowing for dynamic amplification calculation for each truck passage.

6.2.2   Rainflow Data for Doremus Avenue

Fatigue damage to bridge structures accumulates over many years. Structural monitoring cannot be done for extended periods of time due to cost. A compromise must be found whereby short field measurements produce a reasonable estimate of the remaining fatigue life of a bridge structure. The load spectra of a bridge can be represented the form of an effective stress that produces the same damage as the entire variable amplitude load spectrum. Fatigue is not an extreme load phenomena. Its rather the opposite. The primary contribution to fatigue damage comes from typical trucks. A typical truck is defined by the root-mean-cube truck weight from the WIM data histrogram of weights. Unlike heavy trucks, typical trucks occur regularly. For heavy trucks, a short observation is unlikely to capture an extreme truck. Typical trucks are

readily measured from durations as small as one day. Figure 6.5 shows the shape of the measured rainflow matrix for different measurement durations ranging from 1 hour to 1 year. At 1 hour the RFM is not fully developed, at 1 day the RFM takes on a familiar shape with a dominant core near the origin at the center of the plot. After 1 day, the shape of the RFM remains the same; however, additional scattered cycles are added away from the central core. This scatter is the result of differences in the cycle mean stress.

The effect of measurement duration on the observed and limiting RFM is given in Figure 6.6. A trend of decreasing effective stress is observed for both observed and extrapolated RFM. The effective stress is stable at about 1 day of measurement, suggesting that this is the minimum amount of data needed to make fatigue damage predictions. Despite this finding, a week is recommended to account for daily variations and the effect of low activity on weekends.
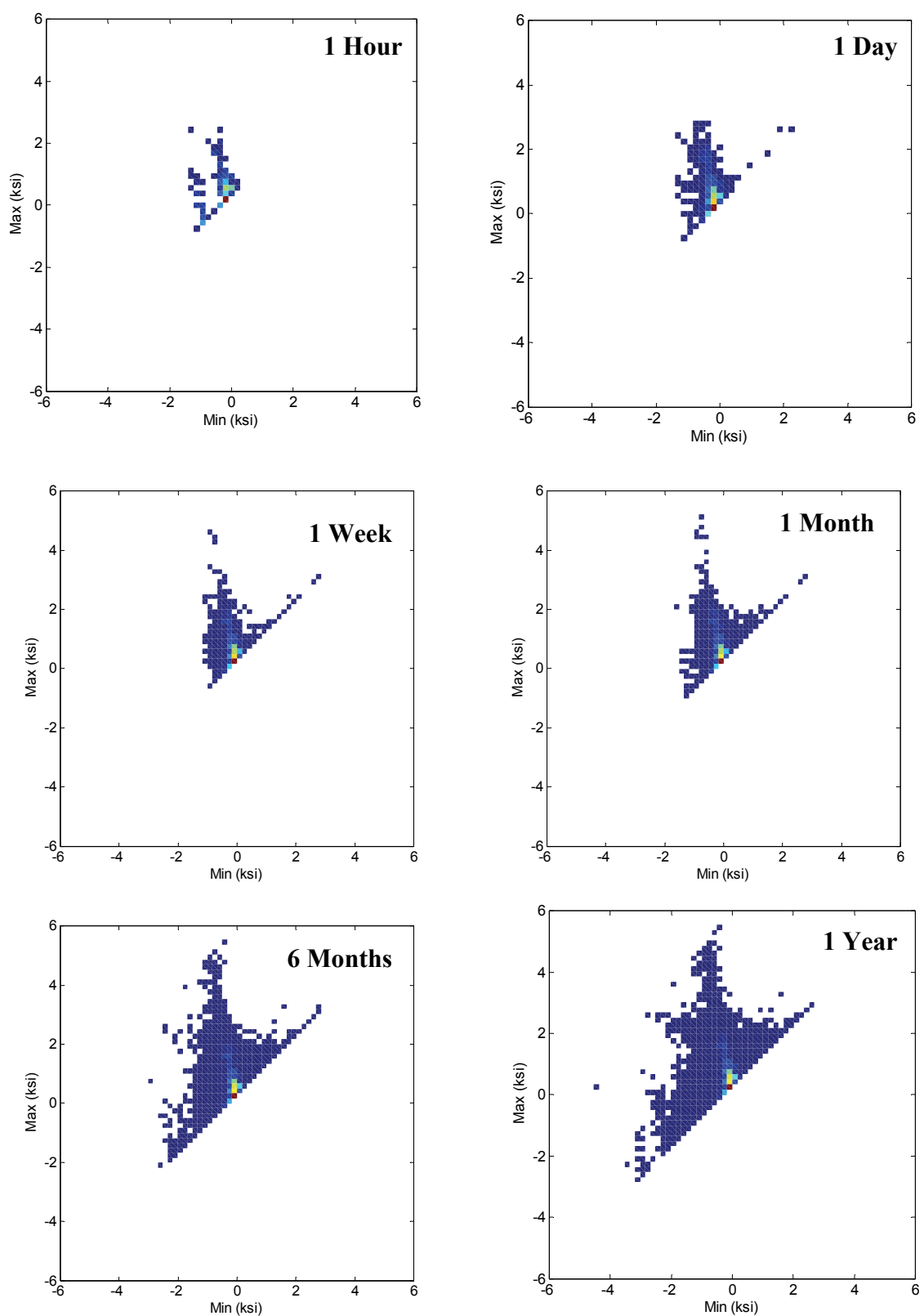
Figure 6.5 Observed rainflow matrices for different durations at Doremus Avenue S3G9.
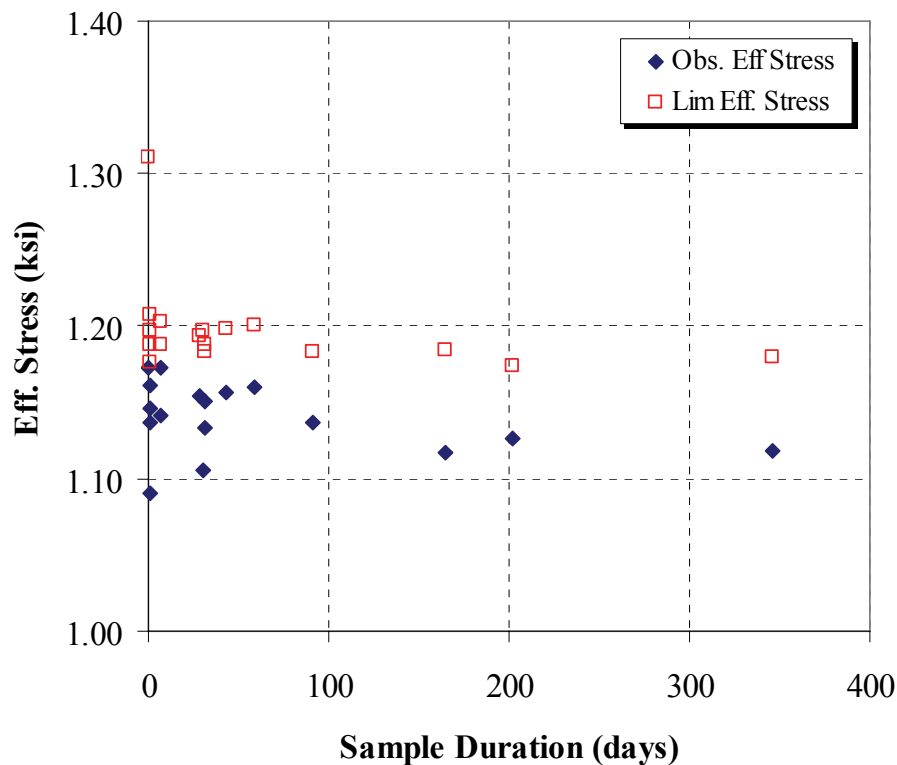
Figure 6.6 Effect of measurement duration on observed and extrapolated RFM (Doremus Avenue Br.)

6.2.3   Rainflow Data for Turnpike Delaware River Bridge

Rainflow data observed from the longitudinal stringers of the NJ Turnpike's

Delaware Memorial Bridge is shown in Figure 6.7 and Figure 6.8. Data was collected

from a strain gage positioned on the bottom flange underneath a bolted diaphragm at the

midpoint of a stringer underneath the right wheel line of traffic. A total of 1 week of data

was collected. The measured rainflow histogram (Figure 6.7) indicates that there is no

clear bimodal truck weight distribution as in the case of the Doremus Avenue Bridge.

Single mode histograms are common for interstate highway sites where trucks tend to be

loaded as opposed to a mixture of empty and loaded trucks. The effective RMC stress for

the observed data was 1.35ksi. The maximum observed stress cycle was 5.81ksi. A

lower stress cutoff of 0.5ksi was imposed to eliminate insignificant cycles due to sensor noise of high frequency vibration.
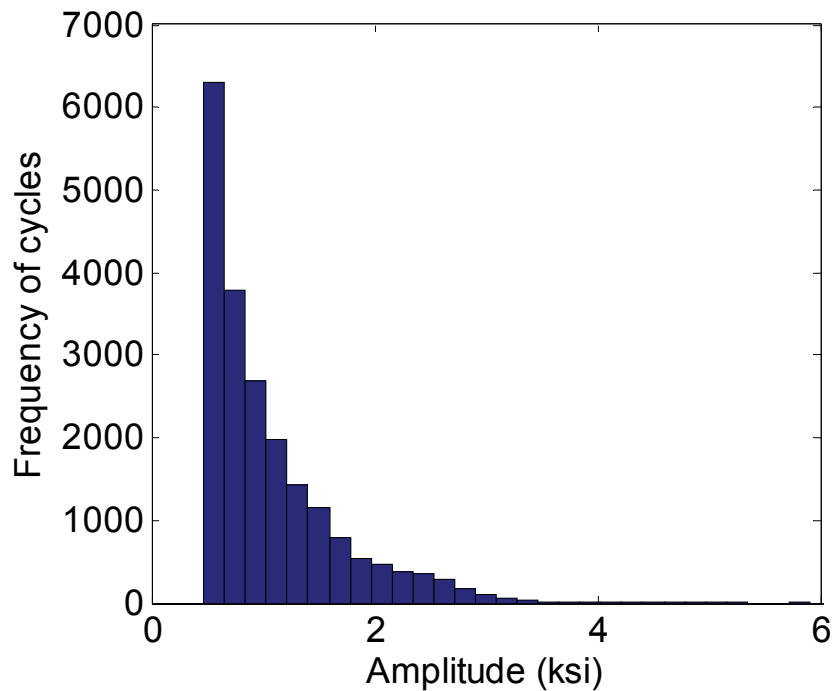
Figure 6.7 Rainflow histogram for longitudinal stringer at Turnpike Delaware River Br.

The rainflow matrix for stress cycles of the Turnpike Bridge stringer is given in Figure 6.8. The shape is typical with a positive mean shift. In other words for increasing magnitude of stress cycles, the mean of the stress cycle also increases at the same rate. This is typical of bridge elements subject to bending. Other structures such as aircraft wings may have negative mean shifts if the wings are in overall compression during flight.
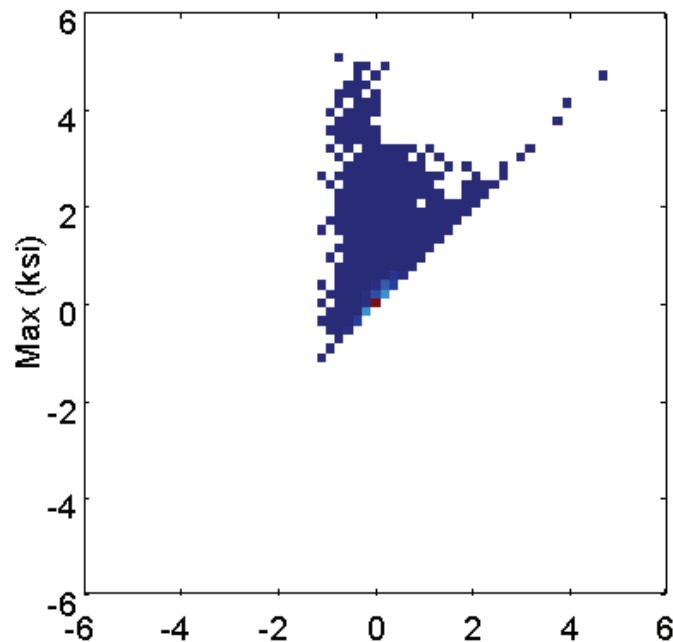
Figure 6.8 Rainflow matrix for longitudinal stringer at Turnpike Delaware River Br.

6.2.4   Rainflow Data for Route 18 Over River Road

Route 18 over River Road was instrumented in the summer of 2005 as part of a

pilot run of a new load and response measurement program. The live-load was measured

using a portable WIM system, while the bridge response was measured using a field data

acquisition system. Data was collected over a two-month period. Construction was

completed just one year before testing was conducted.

For the purpose of fatigue evaluation and long-term data efficiency, stresses were

tabulated in rainflow histograms for each channel. Additionally, burst records were taken

for sufficiently heavy load events. The burst trigger was specified as a stress level above

which a full time-history of the response was recorded. Rainflow histograms of girder

stresses for two locations observed over 4.7 days are given in Figure 6.9. Both

northbound and southbound structures of Route 18 over River Road were instrumented

for bridge response. However, since much of the northbound traffic was slowing and

exiting just after the bridge, weigh-in-motion could not be installed. Therefore, only the

southbound lanes are instrumented to measure both live-load and bridge response.
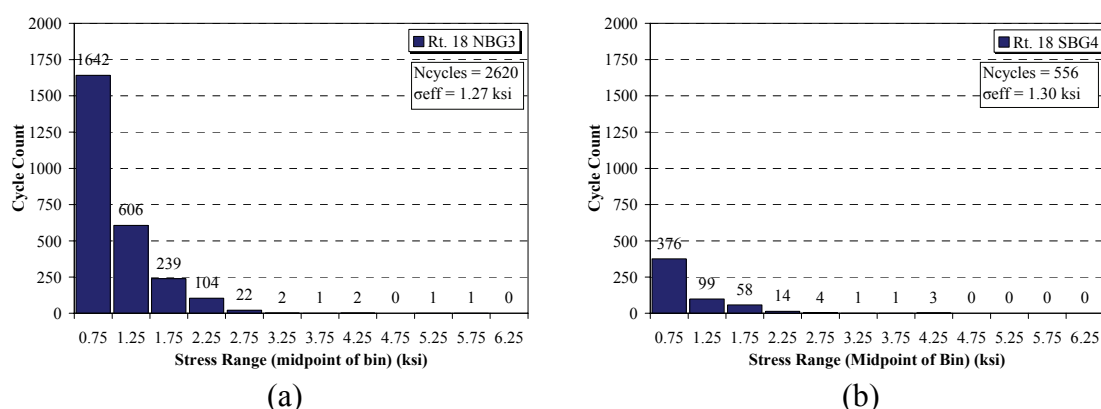
Figure 6.9 Rainflow histograms for Route 18 girder stresses: (a) Northbound Girder 3 and (b) Southbound Girder 4.

As shown in Figure 6.9, the effective stress for Route 18 northbound and

southbound is 1.27 and 1.30ksi, respectively. The total overall number of cycles for the

northbound and southbound directions is: 2620 and 559 cycles, respectively. Since the

effective stresses are nearly equal, the northbound structures is subject to a higher fatigue

loading due to nearly five times more stress cycles than the southbound structure. There

is no danger of fatigue damage for either structure. The AASHTO fatigue details for this

bridge are Category C with a Constant Amplitude Fatigue Limit (CAFL) of 12 ksi. The

effective stress observed was 1.30 ksi; well below the level that would lead to damage.

Additionally, the maximum observed stress cycle, at 5.75 ksi, is less than half of the

CAFL of Category C. Therefore, the bridge is expected to have an infinite fatigue life.

6.2.5   Simulation of Bridge Response for Fatigue

Many methods are available for bridge modeling: finite element, grillage, semi-continuum (Jaeger and Bakht 1989), or a simple beam-line analogy. For the application of simultaneously loaded lanes, an influence surface offers accuracy coupled with computational efficiency. The influence surfaces used to model the Doremus Avenue Bridge were generated using the semi-continuum method (Chapter 4). The semi-continuum model has been widely used in previous truck load simulations (Laman and Ashbaugh 2000). Since the Doremus Avenue Bridge is composed of variable section plate girders, a weighted average method was used to arrive at an effective moment of inertia for each girder. Unit loads were then applied to the semi-continuum model to generate an influence surface for strain gage locations. To model bridge response a time-lapse was employed recreate the truck traffic on the bridge as it occurred. Using the timestamp and speed information contained in the WIM data, the axle loads are applied, and the stresses are calculated for each 0.01 second time interval. This procedure can be visualized as a truck animation where time is advanced in very small increments. A rainflow filter was applied to the output according to ASTM E1049-85 to extract stress cycles.

The field data and semi-continuum time-lapse model results are shown in Figure 6.10. The data set constitutes one week of WIM truck information and rainflow stress response data for Span 3, girder 9 (maximum positive moment location).   Additionally, a welded stiffener and attached cross frame are coincident at this location. The right wheels of trucks traveling in the northbound right lane pass directly over this location. The rainflow histogram shape and cycle counts are similar in Figure 6.10 for both the

actual (left histogram) and simulated data (right histogram). A lower threshold stress of

4.64 MPa (0.67 ksi) was imposed to eliminate erroneous and insignificant low-damage

cycles. Relevant fatigue parameters for the rainflow histograms are presented in Table 4.

The accumulated damage was calculated using the Palmgren-Miner Linear Damage Rule

with an AASHTO LRFD fatigue detail of category C using a detail constant, A, of

14.4E11 MPa3 (4.4E9 ksi3). A total damage of or exceeding 1.0 represents the fatigue

limit and therefore the structural detail is considered deficient or in need of repair.
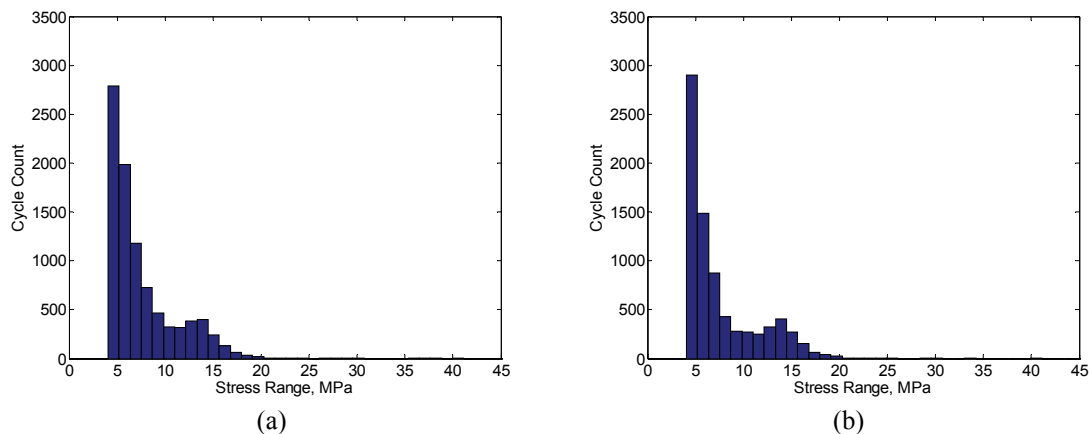
Figure 6.10 One week rainflow histograms for observed field data (left) and semi-continuum model output (right)

To estimate the effect of truck superposition on fatigue, each truck in the WIM

data was applied to the model independently. Figure 6.11 shows the effect of no truck

superposition on the rainflow histogram.   A reduction in the maximum stress range,

RMC effective stress range, and overall cumulative damage was observed (Table 6.1).

Furthermore, the number of cycles above 4.64 MPa (0.67 ksi) was increased compared to

the time-lapse model.   By neglecting truck superposition, events that were coincident are

taken as independent, increasing the overall number of cycles. Other studies of

multipresence effect on fatigue loading have shown similar results (Moses et. Al. 1987).

Fatigue damage accumulates over millions of truck passages. If the percentage of truck

superposition is low, such as in the case of Doremus Avenue, there is no appreciable

increase in fatigue damage due to multipresence.
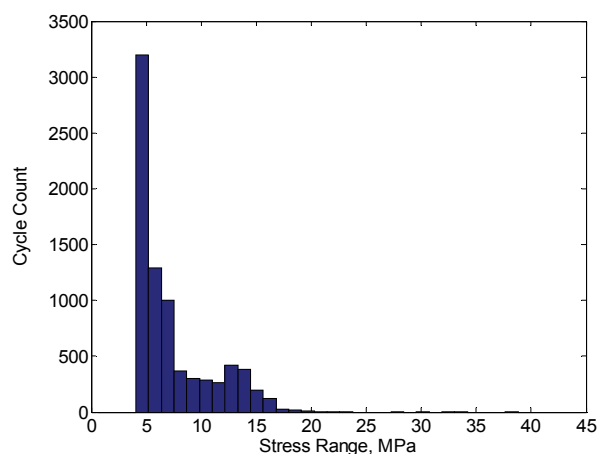
Figure 6.11 Results of semi-continuum simulation neglecting truck superposition

Table 6.1 Fatigue parameters of one week of field and model data observed at location F-9, category C, detail constant, A=14.4E11 MPa3

Parameter	Field Data	Time-Lapse Model	Model w/o Superposition
N cycles > 4.64 MPa	9083	7794	7896
Max Stress, MPa	40.56	40.56	38.24
(ksi)	(5.88)	(5.88)	(5.55)
RMC Stress, MPa	9.22	9.42	9.01
(ksi)	(1.34)	(1.37)	(1.31)
Miner's Total Damage	4.94E-06	4.53E-06	4.01E-06

6.2.6   Damage Prediction

The monitoring of truck loads (WIM data) and bridge response (rainflow histograms) at Doremus Avenue has been ongoing for more than 2 years. Over this time, seasonal variations in daily fatigue damage are evident, as shown in Figure 6.12. It should be noted that the effective stress and observed maximum stress during this period are 1.34 ksi (9.22 MPa) and 9.86 ksi (68 MPa), respectively. Since both the effective RMC stress and maximum stress are below the constant amplitude fatigue limit for the category C detail, 10 ksi (69 MPa), infinite life is expected (Fisher 1998). Nonetheless, as a comparative exercise, damage estimates are done to evaluate the collected data over time.   The daily damage fraction was calculated from rainflow data using the Palmgren-Miner damage rule. The data shown covers a time span of 18 months beginning in mid-February 2004 and extending through August 2005. A seasonal variation in the fatigue damage can be seen in Figure 6.12 where the damage surges in June 2004 and diminishes in December 2004. Two distinct groups of data are also evident: a high damage cluster and a low damage cluster. These low damage periods correspond to weekend days of low truck volume. Since the weekdays account for the most fatigue damage, linear scaling of weekday stress ranges would result in a highly conservative remaining life prediction. For this reason, the minimum monitoring duration for fatigue damage should be a typical seven day week. Further investigation shows that the truck volume at Doremus Avenue Bridge tends to peak on Wednesdays as shown in Figure 6.13. Fatigue damage also varies weekly and seasonally, however, one week can be considered as the minimum duration needed for measurement.
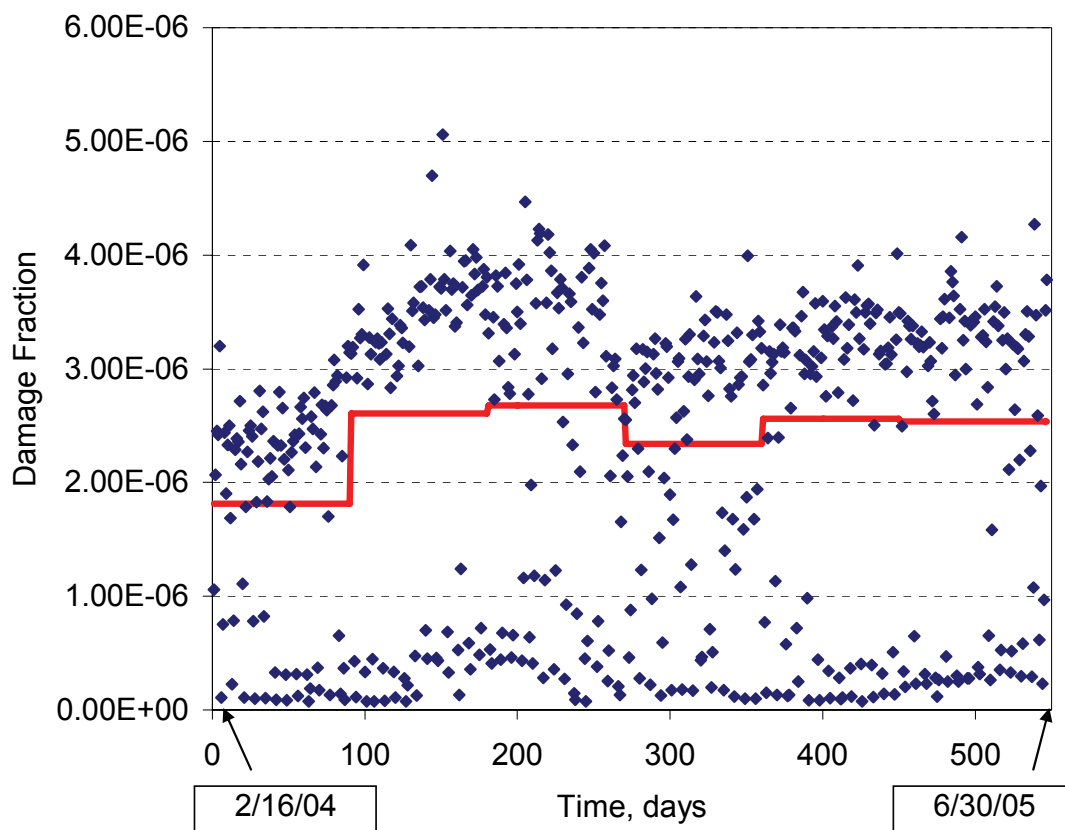
Figure 6.12 Daily fatigue damage for Doremus Bridge, Location F-9 (data points) shown with 3-month equivalent blocks (solid line).

Table 6.2 . Simple linear extrapolation of damage fractions given different data durations for Doremus Avenue Bridge (Span 3 Girder 9).

		Observation Period					
		1 week	1 month	3 months	6 months	12 mon.	18 mon.
	Observed Damage	0.00002	0.00006	0.00017	0.00041	0.00082	0.00125
Prediction	In 5 years	0.00436	0.00385	0.00342	0.00408	0.00410	0.00416
	In 25 years	0.02182	0.01923	0.01712	0.02039	0.02050	0.02078
	In 75 years	0.06546	0.05770	0.05137	0.06118	0.06150	0.06233
	In 75 years using one week equivalent blocks	---	---	---	---	0.06375	0.06544
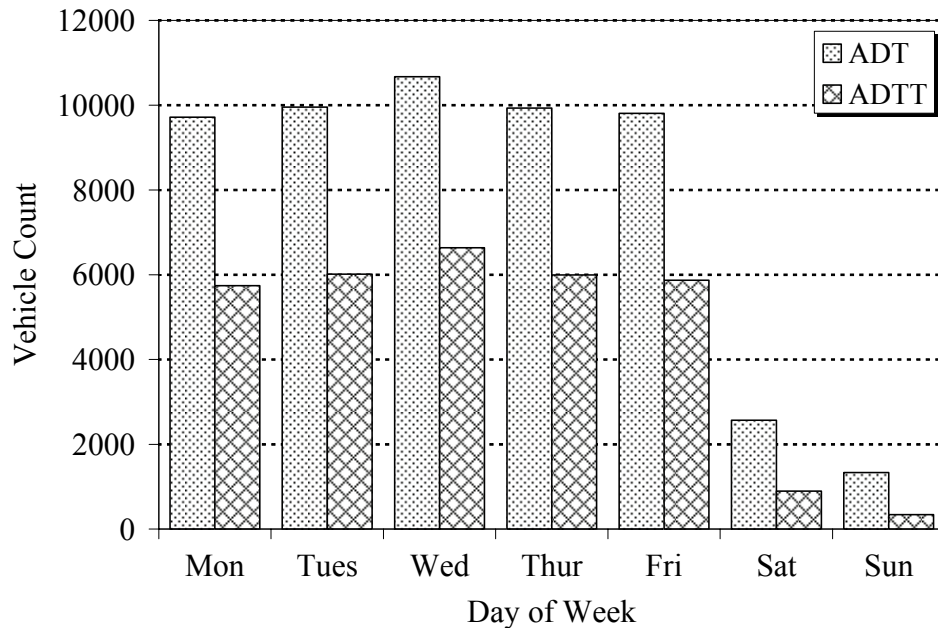
Figure 6.13 Traffic information for all vehicles (ADT) and trucks (ADTT) for all four lanes of Doremus Avenue Bridge for a typical week.

Given the short term data, a methodology is needed to predict the future fatigue damage that the structure will endure. Linear scaling is the simplest way to scale a current damage quantity to some future time. Linear scaling has been demonstrated by Hahin, et al. (1993), where brief strain readings are taken at locations of critical fatigue details. The strain readings are stored as a rainflow histogram. To determine the fatigue damage at some future time the engineer needs the following: (1) the rainflow histograms of stress range, (2) the fatigue detail constant, (3) a linear damage rule (such as Palmgren-Miner), and (4) the present age of the bridge. Additional growth rates may be incorporated to account for an increase in the truck volume. Hahin et al, sampled multiple bridges in Illinois for very brief periods, some as short as 8 hours. The future fatigue damage was estimated by linearly scaling to one day and then to 25 or more years. Growth rates for volume and truck weight increase were also included. A similar

methodology was applied to the Doremus Avenue data. The linear damage from different durations of field measurement and linear estimates for Doremus Avenue are given in Table 6.2.

To account for the seasonality of the fatigue damage, sampling could be done at intervals throughout the year. For example, given the periodic fluctuation shown in Figure 6.12, monitoring for one week every three months would be effective in capturing the seasonality. An example of one week measurements that represent the fatigue damage over a 3 month period is shown by the stepped solid line in Figure 6.12. The 75-year damage estimate using different sample intervals is shown in Table 5. The damage fraction by observed data duration are given across the top ranging from 1 week to 18 months. Prediction of the future accumulated damage is accomplished by linearly scaling the observed damage fraction to the future time period. For example, the damage fraction observed over 1 month was 0.0000641. To determine the accumulated damage over 75-years the observed value is multiplied by the number of months in 75 years (75x12), or 900 months. Therefore the estimated damage in 75 years based on 1 month of observed data is 0.0000641 x 900, or 0.0577. Since the fatigue life is said to be exhausted at a cumulative damage fraction of 1.00, the values observed are trivial. This is expected since Doremus Avenue is a newly constructed bridge which was designed for high truck volumes.

The expected truck volume growth rate was also considered for future damage estimation. Figure 6.14 shows the fatigue damage estimates for the bottom flange location of Span 3 Girder 9 of Doremus Avenue Bridge. The simple linear damage estimate is shown in the solid line, whereas, the extrapolation with 4% growth is shown

in the dashed curve. Despite the large increase in damage due to traffic growth, the detail

is in little danger of expending its fatigue life within 75 years. This is not surprising since

the Doremus Avenue bridge was designed according to the LRFD fatigue specifications

with consideration for the high volume of port traffic. Rapid growth is expected for the

Port Newark Container Terminal (PNCT). The PNCT container traffic in 2001 was 2.5

million twenty foot (6.1m) equivalent units and is expected to reach 5.3 million TEUs by

2015 (Nassif et al. 2002). Such rapid growth must be considered when making fatigue

damage estimates for bridges in the surround region. For comparison, the daily fatigue

damage fraction was plotted along with Port Newark container volumes (PANYNJ 2006)

for the observation period (Figure 6.15).   The port volumes are reported in twenty-foot

equivalent units, TEU. A standard twenty foot long container would count as 1 TEU.

Most containers are fourth feet in length and would count as 2 TEU. As seen in Figure

6.15, the daily fatigue damage fraction closely follows the TEU port volume. This is

expected since the fatigue damage is most sensitive to the number of trucks. Expected

future port container volumes in the form of TEUs can be used to periodically update the

fatigue damage predictions. Expansion of the port and increased truck movements also

has implications on the fatigue performance of bridges surrounding the port. Many of

these surrounding structures are reaching the end of their expected service lives and were

not designed for the increased truck volumes and weights. A systematic fatigue

performance study utilizing WIM data, traffic route modeling, and bridge characteristics

is needed in the vicinity of the port.

Other factors, such as section loss due to corrosion, may accelerate the damage. Periodically updating the prediction with traffic volume and inspection report data will give a more accurate fatigue damage estimate.
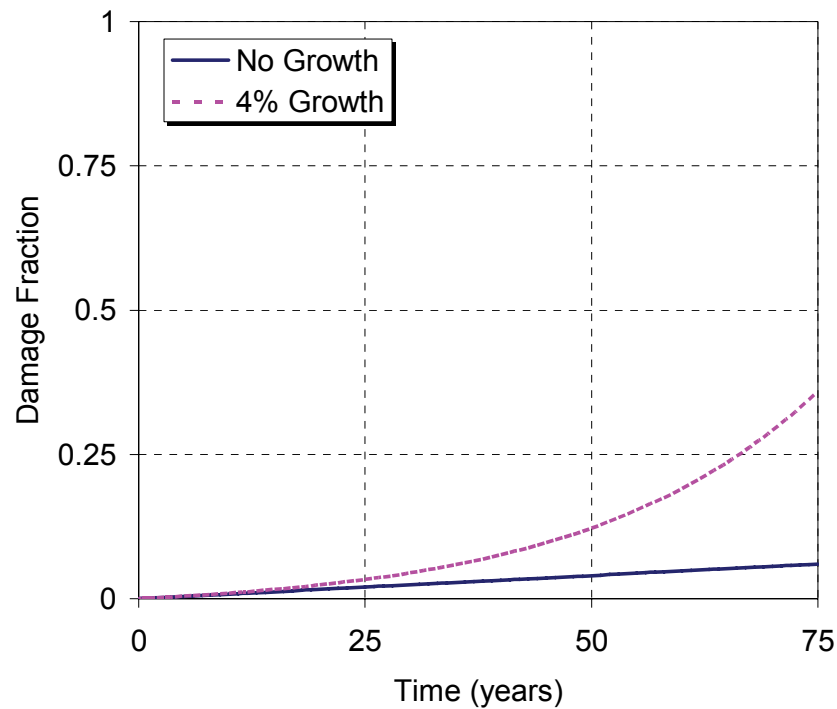
Figure 6.14 Cumulative fatigue damage fraction over time for Doremus Ave. Bridge, Span 3 Girder 9 including 4% traffic growth annually.

The analysis of lifetime fatigue damage accumulation herein does not consider the effects of vehicle dynamic load amplification or traffic growth. Dynamic amplification or vehicle impact for the Doremus Avenue Bridge is minimal since it was recently constructed and the road surface is smooth. Roadway and deck deterioration will contribute to dynamic load amplification in the future. Weigh-in-motion traffic data collection and rainflow stress histograms should be periodically collected at the site after the current monitoring is concluded. The WIM system at Doremus Avenue has been

operating since the opening of the bridge. The loading history of the bridge has been

well documented to date. In the future, fatigue predictions can be updated to include the

past loading history, the effects of traffic volume growth, weight increases, and structural

deterioration.
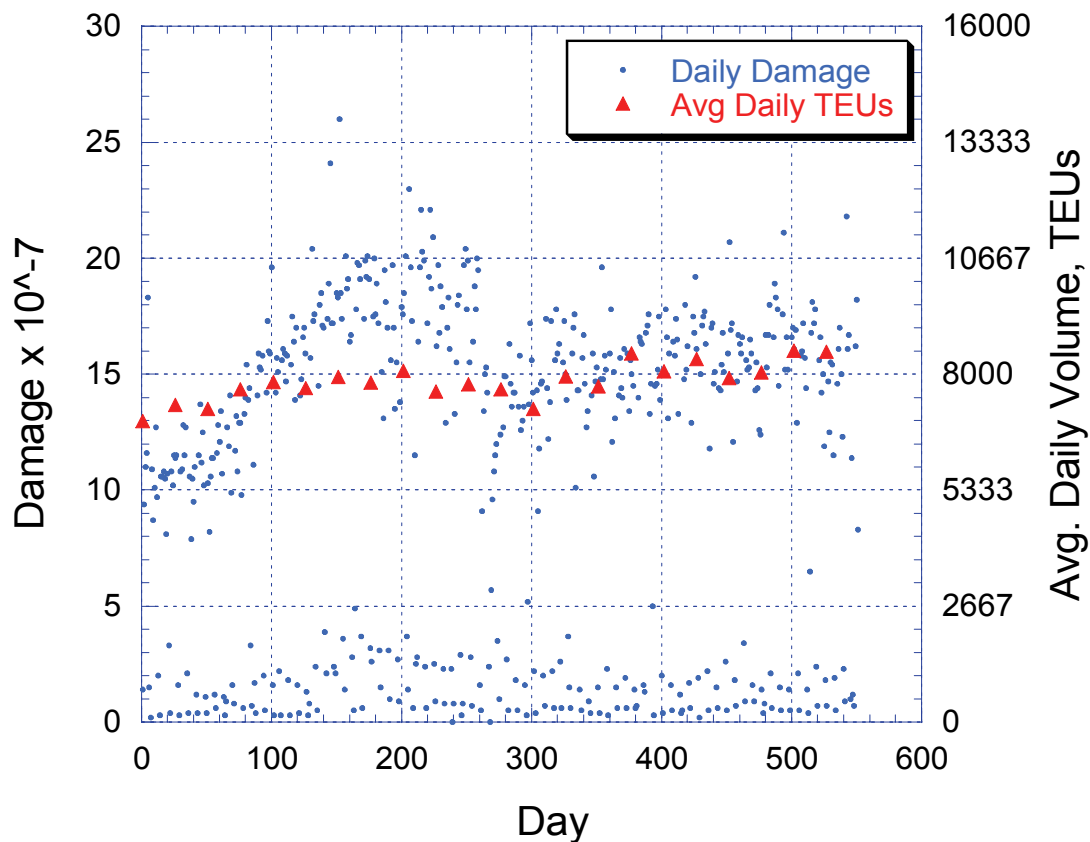
Figure 6.15 Daily fatigue damage fraction plotted with port activity
(TEU = Twenty Foot Equivalent Unit (20ft = 6.1m), www.panynj.gov

The most reliable method of determining fatigue load spectra is to directly collect

bridge stress responses. Direct measurement eliminates the need for modeling

assumptions such as impact, section properties, and girder distribution factors. As shown

in Figure 6.12, the fatigue load demand fluctuates over time. Without prior information,

determining when to sample the bridge response is difficult. One simple solution is to

obtain WIM data at sites nearby the structure of interest. Since fatigue damage greatly

depends on truck volume and weight, the WIM data is an indispensable resource. The New Jersey Department of Transportation (NJDOT), for example, maintains over 80 strategic highway research project (SHRP) WIM sites throughout the state. Given the WIM data, the researcher has only to determine the truck volumes and equivalent root-mean-cube (RMC) truck weights at intervals throughout a typical year to determine when to sample the stresses. Alternatively, the WIM data itself can be used as input for computer simulations to determine stress ranges and cycle counts for fatigue evaluation of specific bridges. A more detailed procedure for incorporating WIM data in fatigue evaluation will be introduced in the next section.

6.3   Systematic Fatigue Evaluation

Evaluation of existing bridges for fatigue performance is important in the effort to deal with an aging infrastructure. The effort to prioritize bridge repair and rehabilitation options will highly depend on the identification of live loads and their effects. Bridge live load is highly site specific and varies for different roadways and regions (Laman and Nowak 1996). To monitor the effect of truck loads and volumes, New Jersey DOT operates more than 80 weigh-in-motion (WIM) sites throughout the state. The WIM data, to this point, is mainly used for pavement design in terms of equivalent single axle loads (ESAL) and freight volume monitoring. This data offers a great deal of valuable site-specific information about truck loads and long term growth patterns. Truck loads vary greatly by region and by roadway type (local, urban arterial, interstate, etc.). Therefore, the current fatigue rating truck may not be sufficient to describe the actual loading experienced by the structure.

A large percentage of the infrastructure is reaching the end of its design life in the next decade. Furthermore, truck weights and volumes are ever increasing. A fast and accurate procedure is needed to identify fatigue prone bridges and track the future increase in the number and magnitude of truck loads.

Knowing the complete load spectra for a bridge is an important aspect in fatigue evaluation. Weigh-in-motion data provides valuable site specific truck load information including: (1) volume by truck classification, (2) gross and individual axle weights, (3) axle spacing, and (4) lane and time of arrival. The truck volumes by class are used to identify the dominant truck class. Typically, five-axle Class 9 semi-trailer trucks are the dominant truck. Vehicle class, axle weight, and axle spacing data can be used to further subdivide the vehicle classes into thirty-seven body types. WIM data may be used on a more general basis to locate highways or regions that are fatigue "hot-spots". Since fatigue damage is a result of stress range magnitude, number of cycles, and structural details; there is no single answer as in strength limit state design. A bridge with a high volume of mid-range trucks may be more fatigue prone than a bridge carrying a few very heavy trucks. The following is a tiered approach to simplify the fatigue analysis for an owner/agency managing hundreds of structures with different regional truck load characteristics. Similar approaches have been proposed using simulation of bridge stresses (Schilling, 1977).

6.3.1   Level 1: Regional truck load information

Truck load and volume information can provide an overview of the fatigue load spectra of highway bridges. Based on WIM data a cursory fatigue screening can be accomplished. For example, New Jersey DOT maintains more than 80 permanent weigh-

in-motion sites throughout the state (Chapter 4). Currently, NJDOT has more than fifteen

years of WIM at selected sites.   Description of the WIM sites are given in Chapter 4.

The truck volume and effective weights for dominant classes is given in Table 6.3. Also

given is the count for the dominant truck type, and the root-mean-cube (RMC) equivalent

weight of the dominant type. Assuming that the number of cycles per truck is one, the

fatigue damage is related to the effective root-mean-cube (RMC) truck weight and the

volume for the site. The detail category is also critical for any fatigue evaluation;

however, at this stage it is enough to compute a performance table showing all categories

independent of any structure. Following this basic procedure will help an owner/operator

identify routes or regions with high fatigue potential as well as enable simple tracking of

truck weight and volume trends.

A new factor is introduced, called Fatigue Potential, defined as the RMC W_{equ}

multiplied by the dominant truck count. This factor can be used to quickly identify sites

that have the highest fatigue loading as defined by the truck weight and volume. The

Fatigue Potential is meant only for relative comparison between sites and has no direct

relation to fatigue evaluation. The fatigue potential for fifteen NJ WIM sites and

Doremus Avenue Bridge are given in Table 6.3.

The current fatigue evaluation vehicle is an HS20 truck with a load factor of 0.75

(AASHTO LRFD 2004). The fatigue truck has a gross weight of 54 kips and has three

axles with weights of 24k, 24k, and 6k. The axle spacing between the two 24k axles is

30 feet and the spacing between the 24k and 6k axle is 14 feet. The fatigue truck was

made to resemble a typical five axle Class 9 semi-trailer truck, which is the dominant

type at most sites. The 24k axles of the fatigue truck actually represent a pair of axles

closely spaced (tandem). The weight of the fatigue truck was chosen to represent the

RMC W_{equ} of the dominant truck types for a large national WIM database (Moses

Shilling Raju 1986 NCHRP 299).

Table 6.3 Characteristics of 15 NJ WIM sites and Doremus Avenue.

Site Name	All Trucks	Dominant Class	N_dom.	Dominant Wequ, k	Tr. Fatigue Potential
Doremus, NB (June 2004)	51961	9	22509	46.96	1057023
I-295 Cherry Hill	70415	9	21051	79.78	1679449
Route 130, Salem	21196	5	5044	43.02	216993
Route 552, Gloucester	72385	9	15005	67.60	1014338
US-130, Burlington, MP57	32994	9	9073	71.34	647268
Route 72 Burlington	34658	9	4441	82.22	365139
Route 18, Monmouth, MP26	89967	9	19881	66.95	1331033
I-287, Bergen	212550	9	75666	59.57	4507424
I-295 Burlington MP39	100371	9	50810	61.85	3142599
I-287 NB, Morris	173006	9	109834	64.88	**7126030**
Route 18, Monmouth, MP16	45160	9	11423	61.64	704114
NJ-31, Warren, MP40	49925	9	10190	66.56	678246
I-78, Hunterdon	108843	9	47003	57.22	2689512
NJ-31, Hunterdon, MP13	85627	9	27434	55.61	1525605
US-1&9,Local, Essex MP48	69924	9	24414	50.00	1220700
NJ Turnpike, Salem	101535	9	55536	44.53	2473018

6.3.2   Level 2: Beam-Line analysis with girder distribution factors

Finite element analysis and other structural models are too complex and time

consuming for widespread implementation. Therefore, to achieve an efficient inventory-

wide fatigue screening tool, a more simplified structural model is needed. A beam-line

analysis coupled with LRFD girder distribution factors accomplishes this task (Schilling,

1982). The current LRFD girder distribution factor equations have been shown to be

accurate; however, cumbersome (Table 1).   The procedure requires the following: WIM

data, influence lines, and a program to loop the trucks and record output. A loop program

is preferred over a typical spreadsheet due to the large volume of data to be processed

(more than five million records per year). Additionally, the loop program will record a

more complete stress history which can be used later to extract stress range cycles using a

rainflow algorithm (ASTM E1802). The stress history of a typical truck passage using the beam model is given in Figure 6.16. Note there is a greater than 30% difference in the modeled stress by the simplified beam model. This over estimate is likely due to the nature of the GDF equations for design purposes. Results for WIM data simulation from the 15 WIM sites on the Doremus beam and semi-continuum model is given in Table 6.4.
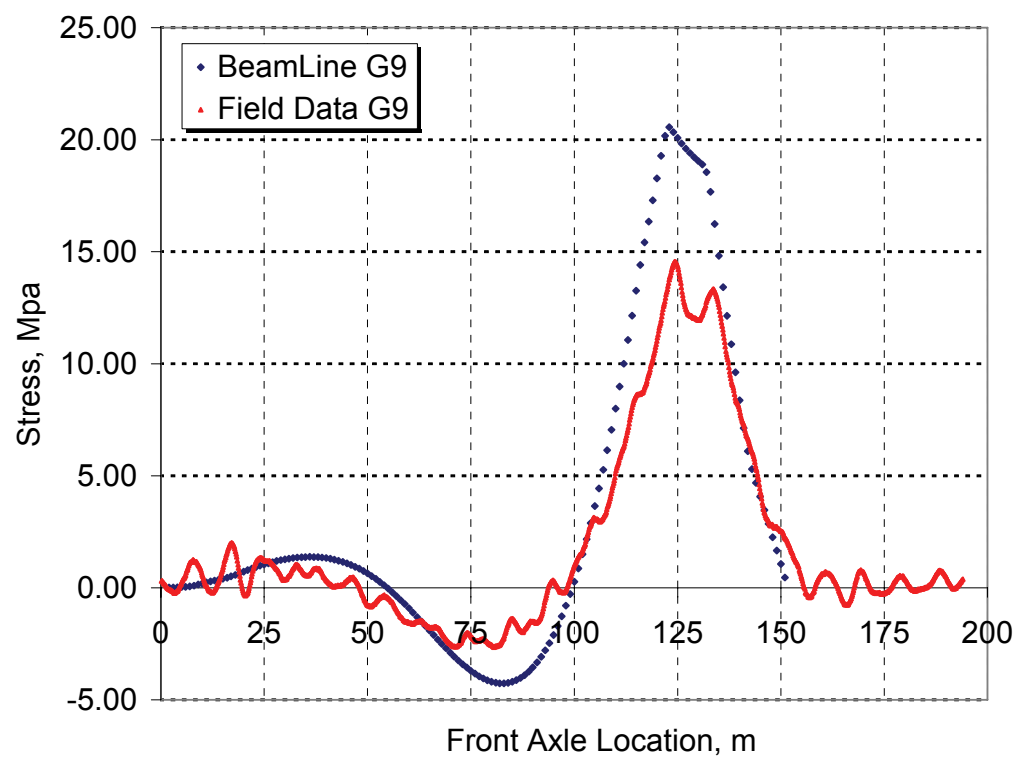

Figure 6.16 Beam-line model and field data comparison for span 3 girder 9 of Doremus Avenue.

Table 6.4 Doremus beam-line and semi-continuum model results comparing 15 NJ WIM sites.

Site Name	Site ID	Lanes*	SC Model Ncycles	SC Model S_eff, ksi	Beam-Line S_eff, ksi	Beam/SC Ratio
Doremus, NB (June 2004)	001	2	14034	1.25	1.64	1.31
I-295 Cherry Hill	I2C	3	33763	2.16	2.85	1.32
Route 130, Salem	130	2	9760	1.85	2.41	1.30
Route 552, Gloucester	552	2	33745	1.83	2.33	1.27
US-130, Burlington, MP57	13B	2	16991	1.81	2.37	1.31
Route 72 Burlington	072	2	14196	1.77	2.51	1.42
Route 18, Monmouth, MP26	018	2	52809	1.77	2.28	1.29
I-287, Bergen	287	2	98197	1.63	2.13	1.31
I-295 Burlington MP39	295	3	61681	1.62	2.03	1.26
I-287 NB, Morris	A87	3	128735	1.59	2.31	1.45
Route 18, Monmouth, MP16	18B	2	29300	1.56	2.00	1.28
NJ-31, Warren, MP40	31C	2	21219	1.53	2.19	1.44
I-78, Hunterdon	78B	3	63556	1.51	2.17	1.43
NJ-31, Hunterdon, MP13	31B	2	35454	1.39	1.89	1.36
US-1&9,Local, Essex MP48	01C	2	22237	1.33	1.88	1.41
NJ Turnpike, Salem	NJT	2	67695	1.20	1.66	1.39

* Lanes being considered in the evaluation.

6.3.3   Level 3: Computer Bridge Models

Computer models, specifically, semi-continuum can be used to generate an influence surface for bridges at fatigue critical locations.   A main advantage of the influence surface is the ability to superimpose multiple trucks on the bridge. The aggregate effect of multiple trucks will lead to higher stress cycles. The model was run using a time-lapse method to recreate the truck traffic on the bridge as it occurred. Using the timestamp and speed information contained in the WIM data, the axle loads are applied, and the stresses are calculated for each 0.01 second time split. This procedure can be visualized as a truck animation where time is advanced at very small increments. A rainflow filter was applied to the output according to ASTM E1049-85 to extract stress cycles.

The beam-line and semi-continuum time-lapse model results are given in Table 6.4. The data set constitutes one month of WIM truck information for the fifteen NJ WIM

sites and Doremus Avenue. The location studied is the bottom flange of Girder 9 of Span 3. Additionally, a welded stiffener and attached cross frame are coincident at this location. The right wheels of trucks traveling in the northbound right lane pass directly over this location.

6.3.4   Level 4: Field measurement

Verification of the WIM data simulated stresses should be done periodically using quality control techniques as demonstrated in Chapter 5. WIM data can become unreliable as sensors deteriorate under repeated truck loading. Calibration can drift or auto-calibration functions could be faulty. Field measurement may also be warranted for special bridge configurations. Girder connections with floor beam have been found to act as moment connections, though they are modeled as simple pins (Nowak, et al. 1993). Field testing will serve to verify true in-service stresses and distribution of loads.

In addition to strain measurement, truck weights can also be measured using portable weigh-in-motion systems. Theses systems connect to Piezo electric sensor strips embedded permanently or affixed to the roadway temporarily. Inductive loops are also affixed to the roadway to enhance vehicle recognition. The goal of field testing is not to examine every bridge. Rather, provide a spot measurement to verify the accuracy of the evaluation procedure. Truck traffic is highly site and route specific (Laman, 1996). Permanent WIM data may not be available in the vicinity of the study bridge. A portable WIM can be installed at the study bridge. The system captures the actual loads affecting the structure, while the strain data is used to verify the output of WIM data simulations.

Obviously it is not practical to instrument and monitor every candidate bridge. Typically, managing agencies have a list of fatigue critical bridges that require further investigation. A testing or research organization cannot dedicate monitoring resources to one location for extended periods of time. Therefore, a compromise is needed between brief and exhaustive monitoring. One solution is to monitor the bridge stresses at seasonal intervals. The sampling interval could be obtained from regional WIM data. For the case of the Doremus Avenue Bridge the minimum monitoring duration was shown to be one week due to daily variations in truck volume. Furthermore, equivalent fatigue damage estimates can be made by sampling for one week every 3 months. Given the structural dimensions and properties of the study bridge and WIM data in the surrounding vicinity, a bridge model could be used to simulate stresses. Simulation using a structural model and WIM data has been shown to closely replicate the actual stress cycles. The implications of using bridge models with WIM data are tremendous: the ability to forecast the future fatigue damage more efficiently and spread monitoring resources over a larger population of structures. Simply input the properties of the structure and apply the known site specific weigh-in-motion truck information to the model to generate a rainflow histogram of stresses. Quality control testing is obligatory. However, the testing required to verify the procedure is far less extensive than instrumenting the entire bridge inventory. In this manner, most if not all, of the bridges under a state or local jurisdiction could be evaluated and re-evaluated for fatigue by updating the WIM truck information for each site. Certain site characteristics such as traffic volume increase, truck weight increase, and girder section loss will accelerate

 fatigue damage. Site inspection data should be referenced to determine the extent of corrosion.

6.4   Exceedences of the Constant Amplitude Fatigue Limit, CAFL (Periodic Overloads)

Design for infinite fatigue life requires that the effective stress be below the Constant Amplitude Fatigue Limit (CAFL) of the structural detail. Full scale laboratory testing of steel connection details has shown that if as few as 0.01% of stress cycles exceed the Constant Amplitude Fatigue Limit (CAFL), fatigue damage will result, regardless if the effective stress is below the CAFL (Fisher et al. 1983, 1995). This criterion is especially relevant for highway bridges with very high truck traffic, where the level of stress at 0.01% exceedence if high.

The truck load effect (simple moment) corresponding to 0.01% exceedence for Doremus Avenue was found to be 1.39 times HS20. The HS20 causes a stress range of 2.18 ksi at Span 3 Girder 9 for passage in the right northbound lane. Therefore, the 0.01% exceedence stress range for Doremus Avenue is 1.39*2.18ksi, or 3.03 ksi. Doremus Avenue contains Category C details as defined by AASHTO LRFD at the Span 3 Girder 9 location. The CAFL for a Category C detail is 12 ksi. The effective stress and 0.01% exceedence stress range are below the critical levels; therefore, Doremus Avenue is in no danger of fatigue damage due to this effect.

CHAPTER 7

SUMMARY AND CONCLUSIONS

7.1 SUMMARY

Over twenty-two million truck records from nine New Jersey weigh-in-motion stations and the Doremus Avenue Bridge have been analyzed with regard to strength limit state design and fatigue limit state evaluation. The current study represents a comprehensive and detailed study of live-load data beyond the scale used to calibrate the current design specifications. WIM data was processed and filtered to reduce errors, light vehicles, and eliminate permit vehicles. Live-load information was analyzed with regard to load effects (moments and shears) and extrapolated to the 75-year design levels consistent with the LRFD code methodology. The available data was plotted using Normal Probability paper. A clear upper tail was observed and was used to extrapolate to future levels. Additional statistical distributions were considered; however, the normal distribution was found to be adequate for extrapolation.

The data was then analyzed with regard to fatigue. Consistent with the current LRFD fatigue methodology the dominant truck types and equivalent weight were determined for each site. Bridge response from the newly constructed Doremus Avenue Bridge was analyzed in terms of effective stress and number of cycles. The

corresponding WIM information was used to perform simulations on the effect of truck

multiple presence. Finally, new extreme value techniques were utilized to extrapolate the

observed stress cycle records to future levels. The rainflow extrapolation techniques used

account for inherent statistical variation and predict stresses that one would expect to

observe if measurement were extended to a much longer duration. The effect of

measurement duration and truck multiple presence was also studied.

7.2   PROPOSED LOAD MODEL FOR SHORT SPANS

The following load model is proposed to account for short heavy vehicles and

heavy tridem axles that are observed at many NJ WIM sites. The current model consists

of two 25k axles separated by 4 feet. The proposed 3-axle tridem represents the short

heavy dump truck vehicles observed at sites like Doremus Avenue (Fig).

The new load model is shown in Figure 3.6.
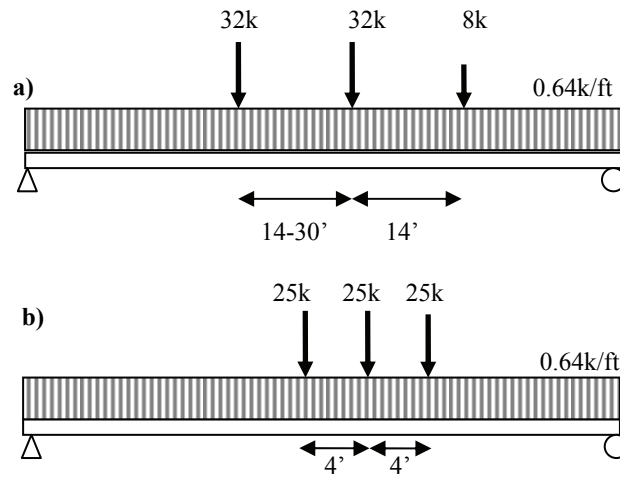
Figure 7.1 Proposed bridge load model with new design tridem (b).

7.3   CONCLUSIONS

The following conclusions are based on the findings of this work:

(1)   Site specific weigh-in-motion data provides the best information on the live loads for bridge design and evaluation. Truck data from weigh stations may be biased as heavier trucks tend to avoid these locations.

(2)   WIM data must be filtered to remove light vehicles, erroneous records, and known permit configurations when performing site-specific load factor calibration.

(3)   The Semi-Continuum Model provides an excellent representation of slab-on-girder bridges. The computational efficiency and accuracy are easily verified using load test data

(4)   The percentage of overweight trucks in New Jersey was found to be between 1 and 7% depending on the site studied. The implications for

design are real with regard to a reduced level of safety for bridges of particular span lengths since these extreme trucks constitute the majority of the upper tail used to predict future load levels.

(5)   The New Jersey permit vehicle was found to provide a sufficient envelope for all NJ WIM sites with respect to the maximum observed load effects.

(6)   The inclusion of permit vehicles in load factor calibration increases load effects by 10-15% for the New Jersey WIM data studied.   Permit and crane configurations should be removed before processing since the extrapolation of permit vehicle weights is not logical and leads to unreasonable or impossible vehicle weights.

(7)   The LRFD load factors for New Jersey must be increased by 20% to maintain the same intended level of safety specified in the code. The load factors must be re-evaluated in the event of a future shift in truck weights or a change in regulatory policy that would allow heavier truck loads

(8)   A new notional load model was proposed to account for heavy tridem axles and short extremely heavy vehicles. The new load model follows the previous design tandem, but replaces the tandem of two-25k loads with a tridem of three-25k loads to better represent the observed 4-axle dump trucks observed in the NJ WIM data.

(9)   The Normal distribution adequately models the upper tail of truck live-load effects for future level extrapolation. Consistency must be maintained when determining the extent of the upper tail for each site

(10) Two months of data was found to be the minimum duration of observation needed to reliably predict the 75-year load effects.

(11) Multiple presence has little effect on strength or fatigue limit state as observed. Site with greater truck volume may exhibit greater sensitivity to multiple presence frequency. The frequency of two correlated trucks occurring simultaneously was observed to be much less than the code assumption of 1/450 with each truck weighing 130k. The most extreme event observed involved two trucks each weighing at least 94k. The frequency of this event was 1/1million trucks.

(12) The current AASHTO LRFD Fatigue Truck sufficiently describes the gross weight and dimensions of the dominant trucks in New Jersey. It may be necessary to periodically adjust the weight as truck weights increase or regulatory changes permit increased legal loads.

(13) Rainflow extrapolation provides a rational means to predict fatigue damage from short observations. The extrapolation shows reduced scatter than the observed RFM in terms of effective stress. Additionally, extrapolation results in larger stress cycles than were observed in the original RFM.

REFERENCES

AASHTO (2004). "LRFD bridge design specifications", American Society of State Highway and Transportation Officials (AASHTO), Washington, D.C.

Agarwal, A. C. and Wolkowicz, M. (1976). "Interim Report on 1975 Commercial Vehicle Survey," Res. and Dev. Div., Ministry of Transportation, Downsview, Ontario, Canada.

American Society for Testing and Materials, ASTM (1985). "E1049-85, Standard practices for cycle counting in fatigue analysis."

American Society for Testing and Materials, ASTM (2002). "E1318-02, Standard Specification for Highway Weigh-in-Motion (WIM) Systems with User Requirements and Test Methods."

Ang, A. H.-S., and Tang, W.H. (1975). *Probability Concepts in Engineering Planning and Design: Volume I. Basic Principles.* New York: Wiley.

Ang, A. H.-S., and Tang, W.H. (1984). *Probability Concepts in Engineering Planning and Design: Volume II. Decision, Risk, and Reliability.* New York: Wiley.

Atlantic Trailer Company (2004), website: http://www.atlantictrailers.com

Bannantine, J.A., Comer, J.J., and Handrock, J.L. (1990). *Fundamentals of Metal Fatigue Analysis.* Prentice Hall, Englewood Cliffs, NJ.

Bakht, B. and Jaeger, L. G. (1985). *Bridge Analysis Simplified*. McGraw-Hill:New York

Barker, R. M., J. M. Duncan, K.B. Rojiani, P. S. K. Ooi, C. K. Tan, and S. G. Kim (1991). *Manual for the Design of Bridge Foundations*, *NCHRP Report 343*, Transportation Research Board, Washington, DC, 308 pp.

Barker, R.M. and Puckett, J.A. (1997). *Design of highway bridges: based on AASHTO LRFD Bridge Design Specifications*. New York: Wiley.

Bridge Diagnosits Inc. (2001). *Strucutral Testing System: User Manual.* Bridge Diagnostis Inc., Boulder, Colorado. http://www.bridgetest.com.

Brodtkorb, P.A., Johannesson, P., Lindgren, G., Rychlik, I., Ryden, J., and Sjo, E. (2000). "WAFO – A Matlab toolbox for analysis of random waves and loads." Norwegian University of Science and Technology, Lund Institute of Technology.

Chen, Y. (1994). "Modeling Bridges Subjected to Moving Loads," Mathematical Modeling and Scientific Computing, Vol. 4, pp 567-572.

Coles, S. (2001). "An Introduction to Statistical Modeling of Extreme Values". Springer-Verlag, London.

Dressler, K., Hack, M., Krueger, W. (1997). "Stochastic reconstruction of loading histories from a rainflow matrix." *Zeit. F. ang. Math. U. Mech.* 77(3), pp 217-226.

Dressler, K., Gründer, B., Hack, M., and Köttgen, V.B. (1996). "Extrapolation of Rainflow Matrices." SAE Technical Paper 960569.

Downing, S.D. and Socie, D.F. (1982). "Simple rainflow counting algorithms." *International Journal of Fatigue,* 4(1), pp 31-40.

Federal Highway Administration, FHWA (2001). "FHWA Vehicle Types," USDOT online: http://www.fhwa.dot.gov/policy/ohpi/vehclass.htm

Federal Highway Administration, FHWA (2006). "Bridge Formula," USDOT online: http://www.fhwa.dot.gov/policy/ohpi/vehclass.htm

Fisher, J.W., Mertz, D.R., and Zhong, A. (1983) "Steel bridge members under variable amplitude long life fatigue loading." National Cooperative Highway Research Program Report 267.

Fisher, J.W., Jian, J., Wagner, D.C., and Yen, B.T. (1990). "Distortion-induced fatigue cracking in steel bridges." National Cooperative Highway Research Program Report 336.

Fisher, J.W., G.L Kulak, and I.F. Smith (1998) "A Faitgue Primer for Structural Engineers." National Steel Bridge Alliance, American Institute of Steel Construction.

Fu, G., Feng, J., Dekelbab, W., Moses, F., Cohen, H., Mertz, D., and Thompson, P. Effect of Truck Weight on Bridge Network Costs. NCHRP Report 495. Transportation Research Board. Washington D.C., 2003.

Hahin, C., South, J.M., Mohammadi, J., and Polpeddi, R.K. (1993). "Accurate and Rapid Determination of Fatigue Damage in Steel Bridges." *Journal of Structural Engineering.* ASCE, 119(1), 150-168.

International Road Dynamics Inc. (1999), "Software User's Manual: IRD Weigh-In-Motion Data Collection System," Version 7.5.0, December.

International Road Dynamics Inc., IRD, (2005), "Operator's Manual-TC/C 540," Revision C, Part No. 69004801, January.

Jaeger, L. G. and Bakht, B. (1982). "The Grillage Analogy in Bridge Analysis," Canadian Journal of Civil Engineering, Vol. 9, pp. 224-235.

Jaeger, L.G. and Bahkt, B. (1989). *Bridge Analysis by Microcomputer.* McGraw-Hill Co., New York.

Johannesson, P., Thomas, J-J. (2001). "Extrapolation of rainflow matrices." *Extremes,* 4(3), 241-262.

Khosrovaneh, A.K. and Dowling, N.E. (1990). "Fatigue loading history reconstruction based on the rainflow technique." *International Journal of Fatigue*, 12(2), pp 99-106.

Laman, J. and Nowak, A. (1996). "Fatigue-load model for girder bridges." *Journal of Structural Engineering*, ASCE, 122(7), pp726-733.

Liu, M. (1996). "A Three-Dimensional Dynamic Model for Bridge-Road-Vehicle System," Master's Thesis, Bradley University, Peoria, IL.

Manitowok Crane Group (2006). "Specifications for Grove portable cranes" online: http://www.manitowokcranegroup.com

MATLAB (2000), The Language of Technical Computing, Version 6.0, Release 12, The MathWorks, Inc., MA.

Matsuishi, M. and Endo, T. (1968). "Fatigue of metals subjected to varying stress-fatigue lives under random loading." *Preliminary Proceedings of the Kyushu District Meeting*, pages 37-40. The Japan Society of Mechanical Engineers. In Japanese, March 1968.

Microsoft Terraserver Aerial Photographs (2005), http://terraserver.microsoft.com

Microsoft Virtual Earth (2007). http://live.local.com

Mohammadi, J., and Shah, N. (1992). "Statistical evaluation of truck overloads." *Journal of Transportation Engineering.* ASCE, 118(5), 651-665.

Mohammadi, J. Guralnick, S.A. and Polepeddi, R. (1992). "Effect of increased truck weight upon Illinois highway bridges." *Report Number FHWA/IL/RC-013*, Dept. of Civ. Engrg., Illinois Inst. of Technology, Chicago, Ill.

Mohammadi, J., Guralnick, S.A., and Polepeddi, R. (1998). "Bridge fatigue life estimation from field data." *Practice Periodical on Structural Design and Construction*, 3(3), 128-133.

Mohammadi, J., and Polepeddi, R. (2000). "Bridge rating with consideration for fatigue damage from overloads." *Journal of Bridge Engineering*, ASCE, 5(3), 259-265.

Moses, F. (2001) "Calibration of Load Factors for LRFR Bridge Evaluation," *NCHRP Report 454*, Transportation Research Board, National Research Council, Washington, D.C.

Moses, F., Schilling, C.G., and Raju, K.S. (1987) "Fatigue evaluation procedures for steel bridges." National Cooperative Highway Research Program Report 299.

Munse, W.H. (1990). "Fatigue, brittle fracture, and lamellar tearing." *Structural engineering handbook, 3rd Ed.* E.H. Gaylord Jr. and C.N. Gaylord, eds., McGraw-Hill Inc., N.Y., 4.1-4.24.

Nassif, H.H. (1993). "Live Load Spectra for Girder Bridges." Ph.D. Thesis, Department of Civil Engineering, University of Michigan, Ann Arbor, MI.

Nassif, H. H., Gindy, M. and Davis, J. (2005). "Monitoring of Bridge Girder Deflection Using Laser Doppler Vibrometer," *Journal of Non-Destructive Testing and Evaluation*, 38,

Nassif, H. H. and Liu, M. (2004). "Analytical Modeling of Bridge-Road-Vehicle Dynamic Interaction System," Journal of Vibration and Control, Vol. 10, pp. 215-241.

Nassif, H. H., Liu, M. and Ertekin, O. (2003). "Model Validation for Bridge-Road-Vehicle Dynamic Interaction System," Journal of Bridge Engineering, Vol. 8, No. 2, pp.112-120.

New Jersey Department of Transportation, NJDOT (2002), *Bridges and Structures Design Manual*, 2002 available online at http://www.state.nj.us/transportation/

New Jersey Department of Transportation, NJDOT (2005), email correspondence with Research Bureau, Dec 2005.

Nowak, A. S. and Lind, N. C. (1979). "Practical bridge code calibration." *Journal of the Structural Division*, ASCE, 105(12), 2497-2510, Dec.

Nowak, A.S., Nassif, H.N., and DeFrain, L. (1993). "Effect of truck loads on bridges." *Journal of Transportation Engineering.* 119(6), 853-867.

Nowak, A.S., Nassif, N., and Frank, K.H. (1993). "Fatigue Load Spectra for a Steel Girder Bridge." *Transportation Research Record 1393,* pp. 154-161.

Nowak, A.S., Nassif, H., and Frank, K.H. (1993). "Fatigue load spectra for a steel girder bridge." *Transportation Research Record 1393*, Transportation Research Board, Washington, D.C.

Nowak, A.S. (1995). "Calibration of the LRFD bridge code." *Journal of Structural Engineering.* ASCE, 121(8), 1245-1251

Nowak, A.S. (1999). "Calibration of the LRFD Bridge Design Code." *NCHRP Report 368*, Transportation Research Board, National Research Council, Washington, D.C.

Nowak, A. S. and Collins, K. R. (2000). "Reliability of Structures". McGraw Hill Companies, Inc.

Nowak, A. S. and Hong, Y. K. (1991). "Bridge Live-Load Models," *Journal of Structural Engineering*, ASCE, 117(9), pp. 2757-2767.

Phuvoravan, K., W. Chung, J. Liu, and E.D. Sotelino, (2004). "Simplified Live-Load Distribution Factor Equations for Steel Girder Bridges," *Transportation Research Record: Journal of the Transportation Research Board,* No. 1892, National Research Council, Washington, D.C., pp. 88-97.
Port Authority of New York and New Jersey, PANYNJ (2005). "Freight volumes study 2005" available online: htpp://www.panynj.gov

Schilling, C.G., et al. (1978). "Fatigue of welded steel bridge members under variable-amplitude loadings." NCHRP Report 188.

Shenton, H.W., M. J. Chajes, C. P. Chasten, C. M. Chu (2006) "Field Test/Fatigue Evaluation of the Summit Bridge," Proceedings of the Transportation Research Board (TRB) Annual Meeting, Washington D.C.

Socie, D. (2001). "Modeling expected service usage from short term loading measurements." *International Journal of Materials & Product Technology*, 16(4/5).

Socie, D.F. and Pompetzki, M.A. (2004). "Modeling variability in service loading spectra." *Journal of ASTM International*, 1(2), Paper ID JAI11561, Feb. 2004.

Southgate, H. (2000). "Quality Assurance of Weigh-in-motion Data" FHWA Contract No. DTFH61-P-00724. Federal Highway Administration USDOT, Washington D.C.

Thoft-Christensen, P. and Baker, M. J., *Structural Reliability Theory and Its Applications*. Springer-Verlag, 1982.

West, R. (1973). "Recommendations on the Use of Grillage Analysis for Slab and Pseudo-slab Bridge Decks," Cement and Concrete Association and Construction Industry Research and Information Association, London, UK.

Zokaie, T., T.A. Osterkamp, and R.A. Imbsen (1991). *Distribution of Wheel Loads on Highway Bridges*, Final Report Project 12-26/1, National Cooperative Highway Research Program, Transportation Research Board, National Research Council, Washington, DC.

BIBLIOGRAPHY

Agerskov, H., and Nielsen, J.A. (1999). "Fatigue in steel highway bridges under random loading." *Journal of Structural Engineering*, ASCE, 125(2), 152-162.

Byers, W.G., Marley, M.J., Mohammadi, J., Nielsen, R.J., and Sarkani, S. (1997). "Fatigue reliability reassessment applications: state-of-the-art paper." *Journal of Structural Engineering,* ASCE, 123(3), 277-285.

Dicleci, M., and Bruneau, M. (1995). "Fatigue-based methodology for managing impact of heavy permit trucks on steel highway bridges." *Journal of Structural Engineering*, ASCE, 121(11), pp. 1651-1659.

Downing, S.D. and Socie, D.F. (1982) "Simple Rainflow Counting Algorithms." *International Journal of Fatigue*, Butterworth and Co., Ltd., 4(1), pp. 31-40

Fekpe, E.S.K., and Clayton, A.M. (1995). "Prediction of heavy vehicle weight distributions." *Journal of Transportation Engineering.* ASCE, 121(2), pp. 158-168.

Jajich, D., and Schultz, A.E. (2003). "Measurement and Analysis of Distortion-Induced Fatigue in Multigirder Steel Bridges." *Journal of Bridge Engineering*, ASCE, 8(2), 84-91.

Moses, F. and Snyder, R. (1985). "Application of in-motion weighing using instrumented bridges." Transportation Research Record 1048. *Transportation Research Board, National Research Council*, Washington, DC.

Nagode, M., and Fajdija, M.A. (1998) "On a new method for prediction of the scatter of loading spectra." *International Journal of Fatigue*, 20(4), pp.271-277.

Nagode, M., and Fajdija, M.A. (1998) "A general multi-modal probability density function suitable for the rainflow ranges of stationary random processes." *International Journal of Fatigue*, 20(3), pp. 211-223.

Socie, D., and Downing, S. (1996). "Statistical strain-life fatigue analysis." *SAE Technical Paper No. 960566*, Warrendale, PA.

USDOT (1998) "Comprehensive truck size and weight study." Draft Volume III, Scenario Analysis, Dec. 30, 1998.

Wang, T.L , Liu, C., Huang, D., and Shahawy, M. (2005). "Truck Loading and Fatigue Damage Analysis for Girder Bridges Based on Weigh-in-Motion Data." *Journal of Bridge Engineering*, ASCE, 10(1), 12-20

Zhao, Z., Halder, A., and Breen, F.L. Jr. (1994) "Fatigue reliability evaluation of steel bridges." *Journal of Structural Engineering*, ASCE, 120(5), pp. 1608-1623.

Zwernman, F.J. and Frank, K.H. "Fatigue Damage Under Variable Amplitude Loads." *Journal of Structural Engineering.* Vol. 114, No. 1, 1988, pp. 76-83.

APPENDIX A

DETAILED BRIDGE INFORMATION

Detailed parameters are needed to construct computer models of highway bridges. These include but are not limited to: girder dimensions and spacing, girder material properties (Elastic Modulus, Shear Modulus, yield strength), bridge span, deck thickness, deck material properties, and extent of composite action with deck.

A semi-continuum model was constructed for the Doremus Avenue Bridge in Newark, NJ. The bridge is three-span continuous with a 10-girder cross section. There are three equal spans of about 147 feet (45m) each that carry four travel lanes, two shoulders, and a utility bay over a large railroad yard. Each plate girder is built-up with a constant depth web between flanges of variable top and bottom thicknesses. Each girder line was divided in to 11 subsections of contact dimensions. Spreadsheets were used to input detailed section properties to calculate the moments of inertia for each subsection of the girder. A weighted average was taken to determine an equivalent girder moment of inertia over the entire bridge length. The section properties in the transverse direction also varied girder to girder. Exterior girders, girders underneath barriers, and two

different girder spacings required six different girder profiles for calculating the section properties.

Table 0.1 Weighted average moments of inertia for Doremus Avenue Bridge

Moment of Inertia, I m4, from geometry, no funny business

Method	G1	G2	G3	G4	G5	G6	G7	G8	G9	G10
Calculated Wt Average	0.0284	0.0405	0.0381	0.0381	0.0379	0.0377	0.0377	0.0377	0.0377	0.0351
Calc + 15% Calibration	0.0327	0.0466	0.0439	0.0439	0.0436	0.0433	0.0433	0.0433	0.0433	0.0404
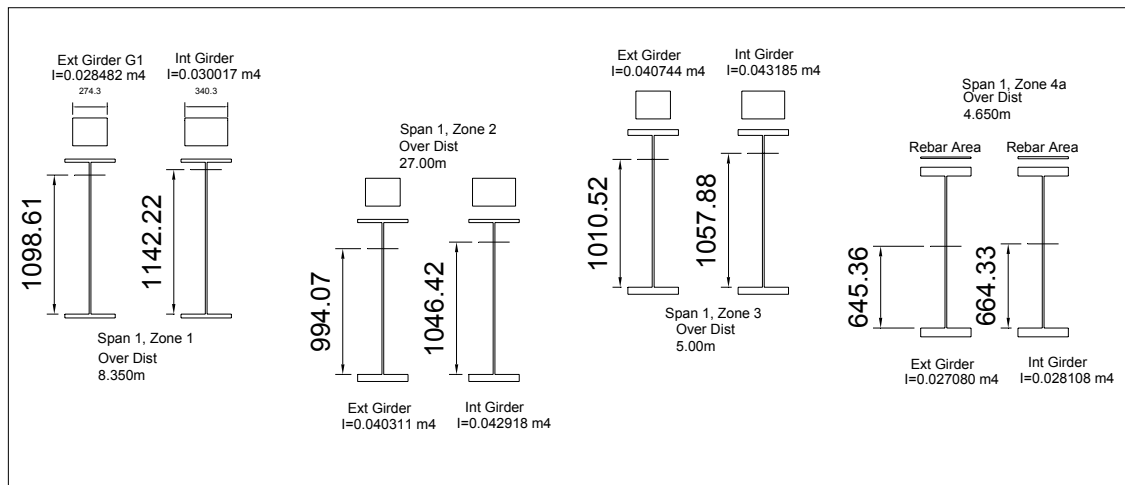
Figure 0.1 Verification of composite section properties in CADD program showing different effective composite sections for different zones

Doremus Effective Flange Width

LRFD 4.6.2.6.1

Interior Beams   **Exterior Beams**

Min of $\quad$ L_eff / 4 $\qquad\qquad\qquad\qquad$ Min of $\quad$ L_eff / 8

$\qquad\qquad$ 12 hs + max(b_w, 0.5b_fl) $\qquad\qquad\qquad$ 6 hs + max(0.5b_w, 0.25b_fl)

$\qquad\qquad$ S $\qquad\qquad\qquad\qquad\qquad\qquad\qquad$ Overhang

Girder Spacing (mm)

1-2	2-3	3-4	4-5	5-6	6-7	7-8	8-9	9-10
2450	2450	2450	2450	2300	2300	2300	2300	2300

Parameter	**All girders**		**Other Parameters**	
L_eff (mm) Span1,3	35100		Barrier Area (mm2)	408428
Slab hs (mm)	220			
Top Fl width (mm)	400			
Web Width (mm)	14			
Overhang (mm)	750			
Modular Ratio, Es/Ec	5.69			

Effective Width b_eff (mm), no barrier

1	2	3	4	5	6	7	8	9	10
750.0	2450.0	2450.0	2450.0	2375.0	2300.0	2300.0	2300.0	2300.0	750.0

Effective Width b_eff (mm), with comp. barrier

1	2	3	4	5	6	7	8	9	10
750.0	3378.2	2450.0	2450.0	2375.0	2300.0	2300.0	2300.0	2300.0	1678.2

References

LRFD 4.5.1

"Unless otherwise permitted, consideration of continuous composite barriers shall be limited to service and fatigue limit states and to structural evaluation."

"The stiffness of structurally discontinuous railings, curbs, elevated medians, and barriers shall not be considered in structural analysis"

LRFD C4.6.2.6.1

"Where a structurally continuous concrete barrier is present and is included in the models for analysis as permitted by Article 4.5.1, the width of the overhang for the purpose of this article may be extended by:

$\quad$ delta_w=A_b / 2t_s

where: A_b = cross sectional area of barrier (in2)
$\qquad\quad$ t_s = depth of deck slab (in)

G1 Exterior

b_eff	750.0 mm	
b_trans	131.8 mm	

Rebar Area	6880 mm2	
Rebar Dist	145 mm, center to web top	

AASHTO LRFD Section Properties, Barrier = extra b_eff

Zone b_eff (m)	Clear Haunch, mm	Centroid from bot fl mm c_bottom	Flange top to CG mm CG Location	Components Bottom Flange I mm4	Web I mm4	Top FL I mm4	Slab I mm4	Rebar for Neg Mom I mm4	Distance Over m	Total I m4	Cumulative Dist m
									0	0	0
Span 1											
1	105	970.8	284.2	1.1E+10	3.97E+09	7.388E+08	7.34E+09	0.000E+00	8.35	0.0230	8.35
2	105	869.4	410.6	1.56E+10	2.79E+09	1.585E+09	1.15E+10	0.000E+00	27.00	0.0314	35.35
3	85	908.6	391.4	1.71E+10	3.1E+09	2.452E+09	1.01E+10	0.000E+00	5.00	0.0327	40.35
4a	60	734.3	605.7	1.37E+10	2.09E+09	9.130E+09	0	3.188E+09	4.65	0.0281	45.00
Span 2											
Zone											
4b	60	734.3	605.7	1.37E+10	2.09E+09	9.130E+09	8.64E+09	3.188E+09	7.85	0.0281	52.85
5	85	942.8	347.2	1.52E+10	3.51E+09	1.901E+09	8.64E+09	0.000E+00	7.00	0.0293	59.85
6	105	995.2	254.8	9.66E+09	4.32E+09	5.875E+08	6.52E+09	0.000E+00	16.00	0.0211	75.85
7	85	942.8	347.2	1.52E+10	3.51E+09	1.901E+09	8.64E+09	0.000E+00	7.00	0.0293	82.85
8a	60	734.3	605.7	1.37E+10	2.09E+09	9.130E+09	0	3.188E+09	7.15	0.0281	90.00
Span 3											
Zone											
8b	60	734.3	605.7	1.37E+10	2.09E+09	9.130E+09	0	3.188E+09	5.35	0.0281	95.35
9	85	908.6	391.4	1.71E+10	3.1E+09	2.452E+09	1.01E+10	0.000E+00	5.00	0.0327	100.35
10	105	869.4	410.6	1.56E+10	2.79E+09	1.585E+09	1.15E+10	0.000E+00	27.00	0.0314	127.35
11	105	970.8	284.2	1.1E+10	3.97E+09	7.388E+08	7.34E+09	0.000E+00	8.14	0.0230	135.49
Avg C_bot	882.2 mm							Weighted Average I		0.0284 m4	

Figure 0.2 Doremus Avenue detailed Girder 1 properties for semi-continuum model

G2 Interior

b_eff	2450	mm
b_trans	430.6	mm

Barrier trans b	0 mm		Rebar Area	6880 mm2
Barrier h	0 mm		Rebar Dist	145 mm, center to web top

AASHTO LRFD Section Properties, Barrier =extra b_eff

Zone / b_eff (m)	Clear Haunch, mm	Centroid from bot fl, mm (c_bottom)	Flange top to CG, mm	CG Location	Bottom Flange I, mm4	Web I, mm4	Top FL I, mm4	Slab I, mm4	Rebar for Neg Mom I, mm4	Total Barrier, mm4	Distance Over, m	Total I, m4	Cumulative Dist, m
							(Components)						
											0	0	0
Span 1													
1	105	1216.5	38.5		1.73E+10	7.8E+09	7.264E+06	6.47E+09	0.000E+00		8.35	0.0316	8.35
2	105	1155.9	124.1		2.8E+10	6.23E+09	1.251E+08	1.13E+10	0.000E+00		27.00	0.0456	35.35
3	85	1163.0	137.0		2.84E+10	6.35E+09	2.391E+08	1.08E+10	0.000E+00		5.00	0.0458	40.35
4a	60	734.3	605.7		1.37E+10	2.09E+09	9.130E+09	0.00E+00	3.188E+09		4.65	0.0281	45.00
Span 2													
Zone													
4b	60	734.3	605.7		1.37E+10	2.09E+09	9.130E+09		3.188E+09		7.85	0.0281	52.85
5	85	1184.4	105.6		2.43E+10	6.9E+09	1.274E+08	8.94E+09	0.000E+00		7.00	0.0403	59.85
6	105	1230.0	20.0		1.48E+10	8.17E+09	1.085E+08	5.61E+09	0.000E+00		16.00	0.0286	75.85
7	85	1184.4	105.6		2.43E+10	6.9E+09	1.274E+08	8.94E+09	0.000E+00		7.00	0.0403	82.85
8a	60	734.3	605.7		1.37E+10	2.09E+09	9.130E+09	0	3.188E+09		7.15	0.0281	90.00
Span 3													
Zone													
8b	60	734.3	605.7		1.37E+10	2.09E+09	9.130E+09	0	3.188E+09		5.35	0.0281	95.35
9	85	1163.0	137.0		2.84E+10	6.35E+09	2.391E+08	1.08E+10	0.000E+00		5.00	0.0458	100.35
10	105	1155.9	124.1		2.8E+10	6.23E+09	1.251E+08	1.13E+10	0.000E+00		27.00	0.0456	127.35
11	105	1216.5	38.5		1.73E+10	7.8E+09	7.264E+06	6.47E+09	0.000E+00		8.14	0.0316	135.49
Avg C_bot		1097.7 mm								Weighted Average I		0.0381 m4	

Figure 0.3 Doremus Avenue detailed Girder 2 properties for semi-continuum model

G3-4 Interior

b_eff	2450	mm
b_trans	430.6	mm

Rebar Area	6880	mm2
Rebar Dist	145	mm, center to web top

AASHTO LRFD Section Properties, Barrier =extra b_eff

Zone b_eff (m)	Clear Haunch, mm	Centroid from bot fl mm c_bottom	Flange top to CG mm	CG Location	Bottom Flange I mm4	Web I mm4	Top FL I mm4	Slab I mm4	Rebar for Neg Mom I mm4	Distance Over m	Total I m4	Cumulative Dist m
								Components				
1	105	1216.5	38.5		1.73E+10	7.8E+09	7.264E+06	6.47E+00	0.000E+00	8.35	0.0316	8.35
2	105	1155.9	124.1		2.8E+10	6.23E+09	1.251E+08	1.13E+10	0.000E+00	27.00	0.0456	35.35
3	85	1163.0	137.0		2.84E+10	6.35E+09	2.391E+08	1.08E+10	0.000E+00	5.00	0.0458	40.35
4a	60	734.3	605.7		1.37E+10	2.09E+09	9.130E+09	0.00E+00	3.188E+09	4.65	0.0281	45.00
Span 2												
Zone												
4b	60	734.3	605.7		1.37E+10	2.09E+09	9.130E+09	0.00E+00	3.188E+09	7.85	0.0281	52.85
5	85	1184.4	105.6		2.43E+10	6.9E+09	1.274E+08	8.94E+09	0.000E+00	7.00	0.0403	59.85
6	105	1230.0	20.0		1.48E+10	8.17E+09	1.085E+06	5.61E+09	0.000E+00	16.00	0.0286	75.85
7	85	1184.4	105.6		2.43E+10	6.9E+09	1.274E+08	8.94E+09	0.000E+00	7.00	0.0403	82.85
8a	60	734.3	-605.7		1.37E+10	2.09E+09	9.130E+09	0.00E+00	3.188E+09	7.15	0.0281	90.00
Span 3												
Zone												
8b	60	734.3	605.7		1.37E+10	2.09E+09	9.130E+09	0.00E+00	3.188E+09	5.35	0.0281	95.35
9	85	1163.0	137.0		2.8E+10	6.35E+09	2.391E+08	1.08E+10	0.000E+00	5.00	0.0458	100.35
10	105	1155.9	124.1		2.8E+10	6.23E+09	1.251E+08	1.13E+10	0.000E+00	27.00	0.0456	127.35
11	105	1216.5	38.5		1.73E+10	7.8E+09	7.264E+06	6.47E+09	0.000E+00	8.14	0.0316	135.49

Avg C_bot	1097.7	mm
Weighted Average I	0.0381	m4

Figure 0.4 Doremus Avenue detailed Girder 3 & 4 properties for semi-continuum model

G5 Interior

b_eff	2375	mm
b_trans	417.4	mm

Rebar Area	6880	mm2
Rebar Dist	145	mm, center to web top

AASHTO LRFD Section Properties, Barrier =extra b_eff

Zone b_eff (m)	Clear Haunch, mm	Centroid from bot fl, mm c_bottom	Flange top to CG, mm CG Location	Bottom Flange I mm4	Web I mm4	Top FL I mm4	Slab I mm4	Rebar for Neg Mom I mm4	Distance Over m	Total I m4	Cumulative Dist m
						Components					
									0	0	0
1	105	1210.9	44.1	1.72E+10	7.69E+09	1.050E+07	6.54E+09	0.000E+00	8.35	0.0314	8.35
2	105	1148.9	131.1	2.77E+10	6.11E+09	1.411E+08	1.14E+10	0.000E+00	27.00	0.0453	35.35
3	85	1156.5	143.5	2.8E+10	6.24E+09	2.665E+08	1.09E+10	0.000E+00	5.00	0.0454	40.35
4a	60	734.3	605.7	1.37E+10	2.09E+09	9.130E+09	0.00E+00	3.188E+09	4.65	0.0281	45.00
Span 2											
Zone											
4b	60	734.3	605.7	1.37E+10	2.09E+09	9.130E+09	0.00E+00	3.188E+09	7.85	0.0281	52.85
5	85	1178.4	111.6	2.41E+10	6.8E+09	1.461E+08	9.01E+09	0.000E+00	7.00	0.0400	59.85
6	105	1224.7	25.3	1.47E+10	8.06E+09	2.161E+06	5.67E+09	0.000E+00	16.00	0.0284	75.85
7	85	1178.4	111.6	2.41E+10	6.8E+09	1.461E+08	9.01E+09	0.000E+00	7.00	0.0400	82.85
8a	60	734.3	605.7	1.37E+10	2.09E+09	9.130E+09	0.00E+00	3.188E+09	7.15	0.0281	90.00
Span 3											
Zone											
8b	60	734.3	605.7	1.37E+10	2.09E+09	9.130E+09	0.00E+00	3.188E+09	5.35	0.0281	95.35
9	85	1156.5	143.5	2.8E+10	6.24E+09	2.665E+08	1.09E+10	0.000E+00	5.00	0.0454	100.35
10	105	1148.9	131.1	2.77E+10	6.11E+09	1.411E+08	1.14E+10	0.000E+00	27.00	0.0453	127.35
11	105	1210.9	44.1	1.72E+10	7.69E+09	1.050E+07	6.54E+09	0.000E+00	8.14	0.0314	135.49
Avg C_bot	1092.5 mm							Weighted Average I		0.0379 m4	

Figure 0.5 Doremus Avenue detailed Girder 5 properties for semi-continuum model

G6-9 Interior

b_eff	2300	mm
b_trans	404.3	mm
Rebar Area	6880	mm2
Rebar Dist	145	mm, center to web top

AASHTO LRFD Section Properties, Barrier=extra b_eff

Zone b_eff (m)	Haunch, m	Centroid from bot fl mm (c_bottom)	Flange top to CG mm (CG Location)	Bottom Flange I mm4	Web I mm4	Top FL I mm4	Slab I mm4	Rebar for Neg Mom I mm4	Total Barrier mm4	Distance Over m	I m4	Cumulative Dist m
										0	0	0
1	105	1205.0	50.0	1.7E+10	7.57E+09	1.457E+07	6.60E+07	0.000E+00		8.35	0.0312	8.35
2	105	1141.6	138.4	2.73E+10	5.99E+09	1.590E+08	1.15E+10	0.000E+00		27.00	0.0449	35.35
3	85	1149.8	150.2	2.77E+10	6.13E+09	2.967E+08	1.10E+10	0.000E+00		5.00	0.0451	40.35
4a	60	734.3	605.7	1.37E+10	2.09E+09	9.130E+09	0	3.188E+09		4.65	0.0281	45.00
Span 2												
Zone												
4b	60	734.3	605.7	1.37E+10	2.09E+09	9.130E+09	0	3.188E+09		7.85	0.0281	52.85
5	85	1172.1	117.9	2.38E+10	6.68E+09	1.669E+08	9.07E+09	0.000E+00		7.00	0.0397	59.85
6	105	1219.2	30.8	1.46E+10	7.95E+09	3.888E+06	5.73E+09	0.000E+00		16.00	0.0282	75.85
7	85	1172.1	117.9	2.38E+10	6.68E+09	1.669E+08	9.07E+09	0.000E+00		7.00	0.0397	82.85
8a	60	734.3	605.7	1.37E+10	2.09E+09	9.130E+09	0	3.188E+09		7.15	0.0281	90.00
Span 3												
Zone												
8b	60	734.3	605.7	1.37E+10	2.09E+09	9.130E+09	0	3.188E+09		5.35	0.0281	95.35
9	85	1149.8	150.2	2.77E+10	6.13E+09	2.967E+08	1.10E+10	0.000E+00		5.00	0.0451	100.35
10	105	1141.6	138.4	2.73E+10	5.99E+09	1.590E+08	1.15E+10	0.000E+00		27.00	0.0449	127.35
11	105	1205.0	50.0	1.7E+10	7.57E+09	1.457E+07	6.60E+09	0.000E+00		8.14	0.0312	135.49

Components header spans: Bottom Flange | Web | Top FL | Slab

Avg C_bot	1087.1 mm	Weighted Average I	0.0377 m4

Figure 0.6 Doremus Avenue detailed Girders 6-9 properties for semi-continuum model

G10 Exterior

b_eff	750.0 mm	Barrier trans b	0 mm
b_trans	131.8 mm	Barrier h	0 mm
		Rebar Area	6880 mm2
		Rebar Dist	145 mm, center to web top

AASHTO LRFD Section Properties, Barrier = extra b_eff

Zone / b_eff (m)	Haunch, m	Centroid from bot fl (mm) c_bottom	Flange top to CG (mm)	CG Location / Bottom Flange I (mm4)	Web I (mm4)	Top FL I (mm4)	Slab I (mm4)	Rebar for Neg Mom I (mm4)	Total Barrier I (mm4)	Distance Over (m)	Total I (m4)	Cumulative Dist (m)
										0	0	0
1	105	970.8	284.2	1.1E+10	3.97E+09	7.388E+08	7.34E+09	0.000E+00		8.35	0.0230	8.35
2	105	869.4	410.6	1.56E+10	2.79E+09	1.585E+09	1.15E+10	0.000E+00		27.00	0.0314	35.35
3	85	908.6	391.4	1.71E+10	3.1E+09	2.452E+09	1.01E+10	0.000E+00		5.00	0.0327	40.35
4a	60	734.3	605.7	1.37E+10	2.09E+09	9.130E+09	0	3.188E+09		4.65	0.0281	45.00
Span 2												
Zone												
4b	60	734.3	605.7	1.37E+10	2.09E+09	9.130E+09	0	3.188E+09		7.85	0.0281	52.85
5	85	942.8	347.2	1.52E+10	3.51E+09	1.901E+09	8.64E+09	0.000E+00		7.00	0.0293	59.85
6	105	995.2	254.8	9.66E+09	4.32E+09	5.875E+08	6.52E+09	0.000E+00		16.00	0.0211	75.85
7	85	942.8	347.2	1.52E+10	3.51E+09	1.901E+09	8.64E+09	0.000E+00		7.00	0.0293	82.85
8a	60	734.3	605.7	1.37E+10	2.09E+09	9.130E+09	0	3.188E+09		7.15	0.0281	90.00
Span 3												
Zone												
8b	60	734.3	605.7	1.37E+10	2.09E+09	9.130E+09	0	3.188E+09		5.35	0.0281	95.35
9	85	908.6	391.4	1.71E+10	3.1E+09	2.452E+09	1.01E+10	0.000E+00		5.00	0.0327	100.35
10	105	869.4	410.6	1.56E+10	2.79E+09	1.585E+09	1.15E+10	0.000E+00		27.00	0.0314	127.35
11	105	970.8	284.2	1.1E+10	3.97E+09	7.388E+08	7.34E+09	0.000E+00		8.14	0.0230	135.49
Avg C_bot		881.3 mm					Weighted Average I				0.0284 m4	

Components

Figure 0.7 Doremus Avenue detailed Girder 10 properties for semi-continuum model

APPENDIX B

DETAILED WIM INFORMATION BY SITE

This appendix contains detailed WIM information for NJ Sites and Doremus Avenue Bridge. The data given have been processed with a filter to remove all light, erroneous, and permit vehicles.

Data By Truck Class for Each Site

18D

Qualified Count	Class	RMC Wequ (k)	Average Weight (k)	Std.Dev. (k)	Max Weight (k)	Average Length (ft)	Average Speed (MPH)
0	1	0.0	0.0	0.0	0.0	0.0	0.0
0	2	0.0	0.0	0.0	0.0	0.0	0.0
220	3	9.6	9.1	2.0	38.0	7.4	24.7
65407	4	32.8	30.7	8.0	77.8	24.0	51.4
85418	5	22.3	21.1	5.1	50.5	18.5	52.5
74011	6	41.8	36.8	14.0	88.5	21.0	51.7
8079	7	69.7	66.1	16.2	114.3	21.8	50.8
36869	8	34.2	30.5	10.7	90.3	40.4	51.0
75807	9	51.9	45.3	17.4	123.2	54.3	53.1
3264	10	73.4	63.8	25.4	192.1	61.6	52.3
290	11	46.0	41.4	14.0	98.5	49.8	48.4
47	12	66.1	59.9	20.1	123.4	64.9	52.9
146	13	107.5	99.0	30.3	167.8	66.8	48.1
0	14	0.0	0.0	0.0	0.0	0.0	0.0
0	15	0.0	0.0	0.0	0.0	0.0	0.0

349558 Total Qualified Vehciles

78B

Qualified Count	Class	RMC Wequ (k)	Average Weight (k)	Std.Dev. (k)	Max Weight (k)	Average Length (ft)	Average Speed (MPH)
0	1	0.0	0.0	0.0	0.0	0.0	0.0
0	2	0.0	0.0	0.0	0.0	0.0	0.0
0	3	0.0	0.0	0.0	0.0	0.0	0.0
13226	4	30.3	27.1	9.4	76.0	24.1	62.5
22628	5	20.8	19.8	4.4	46.7	17.9	60.1
25795	6	37.5	32.5	13.0	84.6	23.5	62.6
16312	7	71.7	70.0	11.5	102.3	21.5	61.3
16925	8	35.0	32.1	9.8	84.9	46.1	61.1
235784	9	54.5	48.2	18.1	118.0	55.4	62.4
3738	10	72.1	64.1	23.7	146.8	54.8	60.8
6761	11	54.3	51.9	11.7	91.9	64.9	60.4
1662	12	58.5	55.4	13.4	121.5	68.5	61.6
85	13	103.8	98.9	22.7	154.5	59.4	57.2
0	14	0.0	0.0	0.0	0.0	0.0	0.0
0	15	0.0	0.0	0.0	0.0	0.0	0.0

342916 Total Qualified Vehciles

78D

Qualified Count	Class	RMC Wequ (k)	Average Weight (k)	Std.Dev. (k)	Max Weight (k)	Average Length (ft)	Average Speed (MPH)
0	1	0.0	0.0	0.0	0.0	0.0	0.0
0	2	0.0	0.0	0.0	0.0	0.0	0.0
0	3	0.0	0.0	0.0	0.0	0.0	0.0
130495	4	29.6	26.6	9.1	82.2	23.9	63.8
235697	5	20.3	19.5	3.9	48.4	18.7	62.6
260275	6	33.3	29.2	10.9	84.2	22.6	64.2
79676	7	65.1	62.6	13.1	115.6	22.2	61.1
321563	8	34.3	31.6	9.4	84.2	45.6	63.6
3925803	9	53.4	48.8	15.5	125.7	56.1	64.9
31930	10	65.7	59.4	20.1	173.2	54.6	64.5
176588	11	52.0	50.4	9.3	103.2	64.7	62.8
55113	12	55.4	53.5	10.3	129.9	69.8	65.2
1258	13	86.8	79.7	24.6	160.5	61.2	63.7
0	14	0.0	0.0	0.0	0.0	0.0	0.0
0	15	0.0	0.0	0.0	0.0	0.0	0.0

5218398 Total Qualified Vehciles

80R

Qualified Count	Class	RMC Wequ (k)	Average Weight (k)	Std.Dev. (k)	Max Weight (k)	Average Length (ft)	Average Speed (MPH)
0	1	0.0	0.0	0.0	0.0	0.0	0.0
0	2	0.0	0.0	0.0	0.0	0.0	0.0
18882	3	22.4	20.4	6.1	59.1	13.6	57.6
78187	4	34.5	31.6	9.7	84.6	25.2	62.8
154409	5	23.5	21.5	6.3	59.2	17.5	59.0
166595	6	38.5	33.0	13.8	88.4	21.4	60.2
23045	7	68.8	63.9	18.9	111.2	21.6	57.3
160079	8	36.2	31.3	12.3	112.2	41.3	57.7
1385130	9	53.5	46.0	19.3	126.5	52.7	60.9
19459	10	68.9	59.2	24.9	190.0	51.2	60.6
45725	11	56.3	51.7	15.7	131.6	58.9	57.6
4540	12	61.7	55.9	17.9	153.1	64.0	61.0
440	13	95.9	84.7	32.0	168.7	65.1	58.1
0	14	0.0	0.0	0.0	0.0	0.0	0.0
0	15	0.0	0.0	0.0	0.0	0.0	0.0

2056491 Total Qualified Vehciles

195

Qualified Count	Class	RMC Wequ (k)	Average Weight (k)	Std.Dev. (k)	Max Weight (k)	Average Length (ft)	Average Speed (MPH)
0	1	0.0	0.0	0.0	0.0	0.0	0.0
0	2	0.0	0.0	0.0	0.0	0.0	0.0
0	3	0.0	0.0	0.0	0.0	0.0	0.0
108422	4	31.9	28.0	10.5	85.8	23.7	65.0
163337	5	22.8	21.2	5.7	59.4	17.8	63.0
127412	6	37.2	31.7	13.3	88.4	22.0	64.1
98973	7	70.1	66.9	15.4	115.2	22.0	65.3
122249	8	34.1	30.3	10.6	105.4	44.3	63.3
591884	9	51.6	43.7	19.1	126.1	54.4	64.5
10916	10	69.6	58.5	26.3	177.5	57.6	64.1
10359	11	53.4	49.2	14.6	117.7	64.2	60.9
1144	12	62.1	57.2	16.8	143.6	66.1	61.6
431	13	102.2	92.0	32.2	173.5	64.1	63.2
0	14	0.0	0.0	0.0	0.0	0.0	0.0
0	15	0.0	0.0	0.0	0.0	0.0	0.0

1235127 Total Qualified Vehciles

287

Qualified Count	Class	RMC Wequ (k)	Average Weight (k)	Std.Dev. (k)	Max Weight (k)	Average Length (ft)	Average Speed (MPH)
0	1	0.0	0.0	0.0	0.0	0.0	0.0
0	2	0.0	0.0	0.0	0.0	0.0	0.0
0	3	0.0	0.0	0.0	0.0	0.0	0.0
47109	4	28.8	25.7	8.8	81.2	23.5	66.0
84758	5	21.2	20.1	4.5	51.4	18.5	63.9
100235	6	35.6	31.4	11.6	82.9	21.0	64.6
17939	7	71.1	69.0	12.6	110.8	22.0	62.6
104104	8	35.0	31.8	10.3	95.5	45.0	64.1
839218	9	57.6	52.1	17.5	127.7	57.6	65.7
12664	10	81.7	73.5	25.6	189.1	55.8	65.7
38978	11	55.3	52.7	11.8	120.7	65.2	63.1
11958	12	58.4	54.7	14.3	141.2	67.6	65.0
523	13	103.0	96.2	26.5	156.2	61.3	63.7
0	14	0.0	0.0	0.0	0.0	0.0	0.0
0	15	0.0	0.0	0.0	0.0	0.0	0.0

1257486 Total Qualified Vehciles

A87

Qualified Count	Class	RMC Wequ (k)	Average Weight (k)	Std.Dev. (k)	Max Weight (k)	Average Length (ft)	Average Speed (MPH)
0	1	0.0	0.0	0.0	0.0	0.0	0.0
0	2	0.0	0.0	0.0	0.0	0.0	0.0
0	3	0.0	0.0	0.0	0.0	0.0	0.0
30452	4	32.2	28.2	10.6	83.3	23.4	60.7
123867	5	22.7	21.1	5.6	59.2	17.4	59.9
73867	6	35.6	30.6	12.4	89.0	20.5	59.4
16739	7	62.8	56.3	20.2	115.8	25.1	58.5
98088	8	38.1	33.8	12.1	108.1	44.7	60.0
748577	9	56.6	50.9	17.7	126.5	54.8	60.6
9627	10	73.8	64.2	25.6	171.9	57.4	59.5
41985	11	56.8	52.7	14.8	139.4	63.0	59.9
9225	12	62.1	57.4	16.5	144.9	66.7	61.1
601	13	107.6	99.5	29.6	171.3	62.6	57.2
0	14	0.0	0.0	0.0	0.0	0.0	0.0
0	15	0.0	0.0	0.0	0.0	0.0	0.0

1153028 Total Qualified Vehciles

DOR 12

Qualified Count	Class	RMC Wequ (k)	Average Weight (k)	Std.Dev. (k)	Max Weight (k)	Average Length (ft)	Average Speed (MPH)
0	1	0.0	0.0	0.0	0.0	0.0	0.0
0	2	0.0	0.0	0.0	0.0	0.0	0.0
0	3	0.0	0.0	0.0	0.0	0.0	0.0
14450	4	30.0	29.4	4.2	74.8	39.6	43.8
46994	5	25.1	22.5	7.4	74.3	24.4	38.2
138923	6	29.8	22.8	12.3	95.3	23.2	40.6
8386	7	64.8	56.3	24.5	108.1	28.2	38.0
68578	8	33.9	28.7	12.0	99.7	51.3	39.6
462259	9	48.7	39.2	20.1	130.9	52.5	38.4
6628	10	59.3	47.6	25.3	142.7	52.7	36.9
2608	11	53.2	49.1	12.4	90.1	113.1	36.0
80	12	54.3	52.0	11.9	92.3	72.6	33.2
803	13	67.2	54.2	27.8	149.9	102.1	35.1
0	14	0.0	0.0	0.0	0.0	0.0	0.0
0	15	0.0	0.0	0.0	0.0	0.0	0.0

749709 Total Qualified Vehciles   505 Days of Data

DOR 34

Qualified Count	Class	RMC Wequ (k)	Average Weight (k)	Std.Dev. (k)	Max Weight (k)	Average Length (ft)	Average Speed (MPH)
0	1	0.0	0.0	0.0	0.0	0.0	0.0
0	2	0.0	0.0	0.0	0.0	0.0	0.0
0	3	0.0	0.0	0.0	0.0	0.0	0.0
9109	4	33.2	31.2	7.9	77.0	47.6	42.8
50024	5	28.1	25.2	8.7	76.6	24.8	43.9
187067	6	31.2	25.5	12.0	96.8	24.4	41.1
5829	7	53.6	39.1	25.8	116.4	32.7	40.0
95858	8	34.1	28.8	11.8	111.8	51.3	41.2
296809	9	56.9	46.5	23.0	130.2	52.0	40.4
6706	10	52.6	43.5	20.1	148.0	52.4	39.7
2893	11	51.8	48.7	12.5	96.6	82.8	41.3
95	12	56.5	52.1	16.6	93.0	69.3	39.8
4936	13	61.9	49.8	24.7	169.7	138.3	40.8
0	14	0.0	0.0	0.0	0.0	0.0	0.0
0	15	0.0	0.0	0.0	0.0	0.0	0.0

659326 Total Qualified Vehciles   505 Days of Data

DRM

Qualified Count	Class	RMC Wequ (k)	Average Weight (k)	Std.Dev. (k)	Max Weight (k)	Average Length (ft)	Average Speed (MPH)
0	1	0.0	0.0	0.0	0.0	0.0	0.0
0	2	0.0	0.0	0.0	0.0	0.0	0.0
2749	3	14.3	13.2	3.7	44.0	7.7	21.8
118493	4	32.7	28.7	10.5	88.4	25.2	39.0
122463	5	26.3	23.8	7.6	59.8	18.8	38.2
351649	6	30.7	25.3	11.4	87.9	20.2	32.0
35704	7	55.6	47.1	21.3	115.0	33.9	30.1
168902	8	35.5	30.6	12.0	101.8	45.4	32.9
674805	9	51.5	42.4	20.1	128.2	52.2	32.3
9095	10	58.6	46.8	24.3	149.0	52.3	30.8
2475	11	50.9	45.9	15.0	122.5	59.5	32.9
399	12	61.6	54.4	19.6	145.0	66.4	35.1
49	13	99.8	89.8	31.5	178.6	68.5	31.5
0	14	0.0	0.0	0.0	0.0	0.0	0.0
0	15	0.0	0.0	0.0	0.0	0.0	0.0

1486783 Total Qualified Vehciles

CURRICULUM VITA

JOSEPH C. DAVIS

EDUCATION

October 2007   **Ph.D. in Structural Engineering**, Rutgers University
Dissertation Title: "Live-Load Models for Strength Limit State Design and Fatigue Evaluation of Highway Bridges"

2003   **M.S. in Structural Engineering**, Rutgers University
Thesis: "Development of Scour Monitoring Systems for New Jersey"

2001   **B.S. in Civil Engineering**, Rutgers University, Highest Honors

TEACHING AND RESEARCH EXPERIENCE

Fall Semesters 2003-2006   **Teaching Assistant, Reinforced Concrete Laboratory**
Department of Civil and Environmental Engineering, Rutgers University

Spring Semesters 2004-2007   **Teaching Assistant, Mechanical Properties of Materials Laboratory**
Department of Civil and Environmental Engineering, Rutgers University

Spring 2006   **Substitute Lecturer, Bridge Design II Graduate Course**
Department of Civil and Environmental Engineering, Rutgers University

Spring 2003   **Teaching Assistant, Structural Design Capstone**
Department of Civil and Environmental Engineering, Rutgers University

2001 - 2002   **Graduate Assistant**
Center for Advanced Infrastructure and Transportation

2002-2003   **Research Fellow**
University Transportation Research Center (UTRC) Region II

2002   **Textbook Revisions,** "Prestressed Concrete - A Fundamental Approach, Solutions Manual," Nawy, E. (2002)

Fall 2001 & 2002	**Teaching Assistant, Mechanics of Solids** *Department of Civil and Environmental Engineering, Rutgers University*
Summers 2001 & 2002	**Instructor, Civil Engineering Elective** *Governor's School of Engineering, Rutgers University*
Fall 1998 to May 2001	**Undergraduate Assistant** *Department of Civil and Environmental Engineering, Rutgers University*

REFEREED PUBLICATIONS

- Nassif, H.H., Gindy, M., **Davis, J.** (2006), "Comparison of Laser Doppler Vibrometer with Contact Sensors for Monitoring Bridge Deflection and Vibration," NDT&E International (38) 2005, pp. 213-218